Universitat Politècnica de Catalunya

Programa de Doctorat:

Automàtica, Robòtica i Visió

Tesi Doctoral

ON THE FAULT DIAGNOSIS OF DYNAMIC SYSTEMS USING SET-BASED APPROACHES

Masoud Pourasghar-Lafmejani

Directors: Prof. Vicenç Puig Cayuela i Prof. Carlos Ocampo-Martinez

Març de 2019

To my parents,
to my brother and sister,
to my girlfriend.

Acknowledgement

Reaching to the end of Ph.D. research is an exciting moment. During the Ph.D. journey, I have experienced failure, depression and hope to learn the pattern of success. While doing research, there are a number of people with whom I always received support and encouragement. I do want to express my gratitude to those who participated in this moment of my life.

First, I would like to deeply thank my supervisors, Prof. Vicenç Puig Cayuela and Prof. Carlos Ocampo-Martinez from Universitat Politécnica de Catalunya (UPC) whom I received many supports during this research journey. During the process of doing the Ph.D., I have learned plenty of things from their critiques and persistent questioning. I am also grateful to them for being always available for academic discussions.

Second, I want to thank Prof. Christophe Combastel from Université de Bordeaux to accept me as a visitor researcher in Laboratoire de I'Intégration du Matériau au Système (IMS-Lab) and for giving me the opportunity to interact with excellent researchers.

Third, I sincerely thank Agència de Gestió d'Ajust Universitaris i de Recerca AGAUR for having granted the FI scholarship for me to study the doctoral degree at Universitat Politécnica de Catalunya (UPC). I would also like to thank the projects DEOCS (ref. DPI2016-76493-C3-3-R) and HARCRICS (ref. DPI2014-58104-R) for partially supporting me.

Fourth, I want to thank all the people at Institut de Robòtica i Informàtica Industria (IRI), especially office No. 7, to provide me a friendly atmosphere, which allows me to focus on my research and enjoy my life in Barcelona.

Finally, loving thanks to my parents, Mohammadreza Pourasghar, Jamileh Hatami, my brother, Saeed Pourasghar, and my sister, Mahboobeh Poursghar, who played such important roles along my life journey. They have taught me the essential aspects that

are not learned in the academic environment. I also express my thankfulness to Fatemeh Karimi Pour for her eternal support and understanding.

My final world is to unpack the poem from Rumi (13^{th}-century) that always inspires me

Seek that science that will untie your knot
Seek that path that demands your whole being
Leave that which is not, but appears to be
Seek that which is, but is not apparent

Masoud Pourasghar-Lafmejani
Barcelona, Spain, 2018

Abstract

Model-based Fault Detection and Isolation (FDI) is a major theoretical topic that is becoming increasingly to one of the most significant key features to increase safety and reliability of complex automatic control systems. Basically, model-based FDI relies on the use of a mathematical model to describe the system behavior. However, uncertainty remains always present when modelling a system since its effect is non-negligible even if there are no process faults. One way to deal with uncertainty is to assume its unknown-but-bounded description. Generally speaking, the uncertainty in so-called *set-based approaches* is represented by a set that is unknown-but-bounded at each time instant. Set-based approaches can be classified into three main paradigms: interval observer approach, set-membership approach and set-invariance approach. In this thesis, the influence of the uncertainty is addressed using the set-based approaches considering a zonotopic representation. Moreover, this thesis presents both analysis and comparison of the set-based approaches for the state estimation and FDI frameworks with the goal of establishing the advantages and disadvantages of each approach, and also, to find out their relationship in a formal mathematical framework. However, the mentioned set-based approaches implicitly assume time-varying uncertainty. In the set-based approach, the propagation of the state set is affected by several problems such as the wrapping effect, temporal variance on uncertain parameters (or uncertain parameter time dependency) and range evaluation of an interval function, especially in the case of using the interval hull of the set at each iteration. Therefore, conservative and unstable results may be obtained (for even a stable system) when using the set-based approach in the simulation of the system with parametric time-invariant uncertainties. On the other hand, the approximated state set can be computed based on a set of point-wise trajectories. This type of approach is called *trajectory-based approach*. Therefore, the uncertain parameter time dependency is preserved if the set of point-wise trajectories is generated using the mentioned trajectory-based approach.

This thesis includes six parts. The first part addresses the state of the art and provides an introduction of the research tools. The second part proposes the mathematical relationship between interval observer and set-membership approaches. The third part focuses on the integration of the observer-based and set-invariance approaches in FDI framework by means of computing both the minimum detectable and the minimum isolable faults. The fourth part presents the design of an interval observer approach enhancing the sensitivity to faults with respect to disturbances. The fifth part proposes the robust interval observer design for uncertain systems subject to both time-invariant and time-varying uncertainties. The last part draws some conclusions, summarizes this research and gives clues for the future work.

Keywords: Uncertain systems, interval observer approach, set-membership approach, set set-invariance approach, fault detection, bounded uncertainties, zonotopes, sensitivity analysis, minimum detectable/isolable fault, time-invariant and time-varying uncertainties

Resumen

La detección y el aislamiento de fallos (DAF) basado en modelos es un problema teórico importante que se está convirtiendo cada vez más en una de las características clave para aumentar la seguridad y fiabilidad de los sistemas de control automático complejos. Básicamente, la DAF basada en modelos utiliza un modelo matemático para describir el comportamiento del sistema. Sin embargo, la incertidumbre permanece siempre presente cuando se modela un sistema, ya que su efecto no es despreciable, incluso si no hay fallos que afecten al sistema. Una forma de tener en cuenta la incertidumbre es asumir una descripción desconocida pero acotada. En términos generales, la incertidumbre en los llamados *enfoques basados en conjuntos* se representa mediante un conjunto que es desconocido pero acotado en cada instante de tiempo. Los enfoques basados en conjuntos se pueden clasificar en tres paradigmas principales: enfoque basado en observadores intervalares, enfoque de pertenencia al conjunto y enfoque basados en conjuntos invariante. En esta tesis, la influencia de la incertidumbre se aborda utilizando los enfoques basados en conjuntos y representaciones zonotópicas de los mismos. Además, esta tesis presenta tanto el análisis como la comparación de los enfoques basados en conjuntos para la estimación de estado con el objetivo de establecer las ventajas y desventajas de cada enfoque, y también, para descubrir su relación en un marco matemático formal. Sin embargo, los mencionados enfoques basados en conjuntos suponen implícitamente una incertidumbre variante en el tiempo. En el enfoque basado en pertenencia a conjuntos, la propagación del conjunto de estados se ve afectada por varios problemas, como el efecto de del aumento de incertidumbre, la varianza temporal de los parámetros inciertos (o la dependencia temporal de los parámetros inciertos) y la evaluación de rango de una función de intervalo, especialmente cundo se usa el "Interval Hull" en cada iteración. Por lo tanto, se pueden obtener resultados conservadores (incluso para un sistema estable) en la simulación del sistema con incertidumbres paramétricas invariantes en el tiempo con el uso del enfoque basado en pertenencia a conjuntos. Por otro lado, el conjunto

de estados aproximados se puede calcular con base en un conjunto de trayectorias puntuales. Este tipo de enfoque se denomina *enfoque basado en trayectorias*. Por lo tanto, la dependencia temporal del parámetro incierto se conserva si el conjunto de trayectorias puntuales se genera utilizando el mencionado enfoque basado en trayectorias.

Esta tesis incluye seis partes. La primera parte aborda el estado del arte y ofrece una introducción de las herramientas de investigación. La segunda parte propone la relación matemática entre los enfoques basados en observadores intervalares y de pertenencia a conjunto. La tercera parte se centra en la integración de los enfoques basados en observadores intervalares y conjuntos invariantes en el marco de la DAF mediante el cálculo de los mínimos fallos detectables y aislables. La cuarta parte presenta el diseño de un enfoque de observador intervalar que mejora la sensibilidad a fallos respecto a las perturbaciones. La quinta parte propone el diseño robusto del observador intervalar para sistemas inciertos sujetos a incertidumbres invariantes en el tiempo y variantes en el tiempo. La última parte extrae algunas conclusiones, resume la investigación desarollada y sienta las bases para el trabajo futuro.

Palabras clave: Sistemas inciertos, enfoque basados en observadores intervalares, enfoque de pertenencia a conjunto, enfoque basado en conjuntos invariantes, detección de fallos, incertidumbres acotadas, zonotopos, análisis de sensibilidad, fallos mínimos detectables/aislables, incertidumbres invariantes en el tiempo y variantes en el tiempo

Resum

La detecció i aïllament de fallades basada en models (DAF) és un problema teòric important que està esdevenint cada cop més una de les característiques clau per augmentar la seguretat i la fiabilitat dels sistemes de control automàtic complexos. Bàsicament, la DAF basada en models es basa en l'ús d'un model matemàtic per descriure el comportament del sistema. Tanmateix, la incertesa roman sempre present quan es modelitza un sistema ja que el seu efecte no és insignificant, fins i tot si no hi ha fallades en el procés. Una forma de fer front a la incertesa és assumir una descripció desconeguda però acotada. En termes generals, la incertesa en els anomenats *enfocaments basats en conjunts* està representada per un conjunt desconegut però acotat en cada instant. Els enfocaments basats en conjunts es poden classificar en tres paradigmes principals: l'enfocament d'observadors d'intervals, l'enfocament de pertinença a conjunts i l'enfocament d'invariància. En aquesta tesi, s'aborda la influència de la incertesa mitjançant els enfocaments basats en conjounts fent servir una representació zonotòpica. A més, aquesta tesi presenta tant l'anàlisi com la comparació dels enfocaments basats en conjounts per a l'estimació de l'estat i la seva aplicació a DAF amb l'objectiu d'establir els avantatges i desavantatges de cada enfocament i, a més, conèixer la seva relació en un marc matemàtic formal. Tanmateix, els esmentats enfocaments basats en conjunts assumeixen implícitament una incertesa variable en el temps. En l'enfocament basat en conjounts, la propagació del conjunt d'estats es veu afectada per diversos problemes com l'efecte d'embolcall, la variació temporal dels paràmetres incerts (o la dependència en el temps dels paràmetres incerts) i l'avaluació del rang d'una funció intervalar, especialment en el cas d'utilitzar el "Interval Hull" del conjunt a cada iteració. Per tant, es poden obtenir resultats conservadors i inestables (fins i tot per a un sistema estable) en la simulació del sistema amb incerteses temporals invariants paramètriques amb l'ús del mètode basat en conjunts. D'altra banda, el conjunt d'estats aproximat es pot calcular a partir d'un conjunt de trajectòries puntuals. Aquest tipus d'enfocament s'anomena *enfocament basat en trajectòries*. Per tant, la dependència en el temps del paràmetres es

conserva si el conjunt de trajectòries puntuals es generen utilitzant l'enfocament basat en trajectòries esmentat.

Aquesta tesi inclou sis parts. La primera part, presenta l'estat de la tècnica i fa una introducció de les eines de recerca. La segona part proposa la relació matemàtica entre l'observador intervalar i els enfocaments de pertinença. La tercera part se centra en la integració dels enfocaments basats en observadors i d'invariància de conjunts en la seva aplicació a DAF caracteritzant la mínima fallada detectable i aïllable. La quarta part presenta el disseny d'un observador intervalar que millora la sensibilitat a les fallades respecte les perturbacions. La cinquena part proposa el disseny robust d'observadors d'intervals per a sistemes incerts, subjectes a incerteses tant temporals com variables es el temps. L'última part presenta algunes conclusions, resumeix la investigació realtizada i estableix les bases per al treball futur.

Paraules clau: Sistemes incerts, enfocament d'observador d'intervals, enfocament de pertinença a conjuntos, enfocament de conjunts invariants, detecció de fallades, incerteses limitades, zonotopes, anàlisi de sensibilitat, fallades mínima detectable/aïllable, incerteses temporals i variable

Notation

Throughout the thesis

$\mathbb{R}$	Set of real numbers
$\mathbb{Z}_+$	Set of non-negative integer numbers
$\mathbb{R}^n$	Set of n-dimensional real vectors
$\mathbb{R}^{n\times m}$	Set of real $n \times m$ matrices
$\mathbf{B}^r$	Unitary box composed of r unitary intervals
$\lvert\cdot\rvert$	Absolute value
$\lVert\cdot\rVert_s$	Euclidean s-norm
$\lVert\cdot\rVert_F$	Frobenius norm
$\lVert\cdot\rVert_\infty$	Infinity norm
$\bigoplus$	Minkowski sum
$\bigotimes$	Kronecker product
I_n	$n \times n$ identity matrix.
$O_{n\times m}$	$n \times m$ matrix with zero entries.
$diag(\cdot)$	Diagonal matrix with appropriate dimensions
$\alpha^\top$	Transpose of a vector/matrix α
$[\underline{x},\ \overline{x}]$	Interval with lower bound $\underline{x}$ and upper bound $\overline{x}$
$\{\cdot\}$	Set
$\langle c,\ R\rangle$	Zonotope with the center c and the shape matrix R
$\square\mathcal{X}$	Interval hull of a set $\mathcal{X}$
$\in$	It belongs to
$\subset$	Subset
$\cap$	Intersection
x_i	i^{th} element of the vector $x \in \mathbb{R}^n$
a_{ij}	i^{th} Element in the i^{th} row and j^{th} column of the matrix $A \in \mathbb{R}^{n\times m}$
$X > 0\ (< 0)$	X is a positive (negative) definite matrix

$X \geq 0$ (≤ 0)	X is a positive (negative) semidefinite matrix
x_k	The subindex k indicates the discrete time
$\min$ / $\max$	Minimum / maximum
X^{-1}	Inverse of the matrix $X \in \mathbb{R}^{n \times n}$
$cov(\mathcal{Z})$	Covariation of the zonotope $\mathcal{Z}$
$det(A)$	Determinant of the matrix A
$tr(A)$	Trace of the matrix A
$\downarrow_q$	Reduction operator

Acronyms

FD	Fault Detection
FDI	Fault Detection and Isolation
FTC	Fault-tolerant Control
IOA	Interval Observer Approach
SMA	Set-membership Approach
SIA	Set-invariance Approach
MDF	Minimum Detectable Fault
MIF	Minimum Isolable Fault
RPI	Robust Positively Invariant
mRPI	Minimal Robust Positively Invariant
LTI	Linear time-invariant
LTV	Linear time-varying
TIU	Time-invariant Uncertainty
TVU	Time-varying Uncertainty
LMI	Linear Matrix Inequality
KF	Kalman Filter
ZKF	Zonotopic Kalman Filter
ZF	Zonotopic Filter

Contents

List of Tables

List of Figures

Part I

Background

Chapter 1

Introduction

This chapter corresponds to the introduction of this PhD thesis document in which all the work carried out to achieve the planned objectives is detailed. Thereby, the aim of this chapter is to first describe the main motivations of this PhD thesis in Section 1.1. Then, the thesis objectives are presented in Section 1.2. Finally, in Section 1.3, a brief outline of the structure of this dissertation is presented, which provides a summary of every chapter.

1.1 Motivation

In order to produce efficient and high-quality products, modern processes and systems must satisfy their function correctly. Consequently, there are some important issues as safety operation, cost efficiency or environmental protection that must be considered in engineering applications.

In this context, faults can be the cause for unsatisfactory performance or even instability of the system. There are several possible explanations for occurrence of the faults, e.g., design errors, implementation errors, human operator errors. Therefore, Fault Detection and Isolation (FDI) has been an active research topic for the scientific community since 1970's. Generally speaking, the goal of FDI theory is devoted to assess the effect of the fault occurrence on the system in order to detect its presence as quick as possible, to avoid an unexpected performance. After detecting the fault, maintaining the overall system stability and having an acceptable performance will be the next target to be achieved. Therefore, Fault-tolerant Control (FTC) is the name used to describe

all techniques capable of maintaining desirable performance of the system. Since 1980's, there has been an increasing interest in FTC for improving the safety and reliability of the system from academic and industrial communities. In this regard, the first concern of the FTC techniques is fault diagnosis that includes detection and isolation, and then designing the suitable controller for the system. Generally speaking, the right state estimation is required for both Fault Detection (FD) and FTC techniques. Moreover, FD and FDI rely on the quality of the state estimation. However, there is always the unavoidable effect of the uncertainties in the system that should be distinguished from the effect of the fault.

The motivation of this PhD thesis is to design methods for FDI of complex systems for increasing their performance since even a small fault can have an important influence on the performance of the system. Set-theoretical approaches, which are quite well established tools in automatic control, are chosen due to their abilities dealing with the non-negligible effect of the uncertainties. To evaluate the fault diagnosis performance, the characterization of the Minimum Detectable Fault (MDF) and Minimum Isolable Fault (MIF) is done considering different type of actuator and sensor faults. Therefore, the aim of this dissertation is to be focused on designing novel set-based FDI approaches by integrating all available ones that can improve their performance. On the other hand, enhancing the sensitivity to faults with respect to uncertainties, rather than optimizing the precision of the state estimation is another motivation of this thesis.

1.2 Thesis objectives

Keeping the mentioned issues in previous section in mind, the general objective of this PhD thesis is to study the advantages and disadvantages of the existing FDI approaches to design novel set-based algorithms in order to improve their performance. In this regard, this thesis is divided into different parts to fulfill this general objective. The roadmap of this dissertation is presented in Figure 1.1.

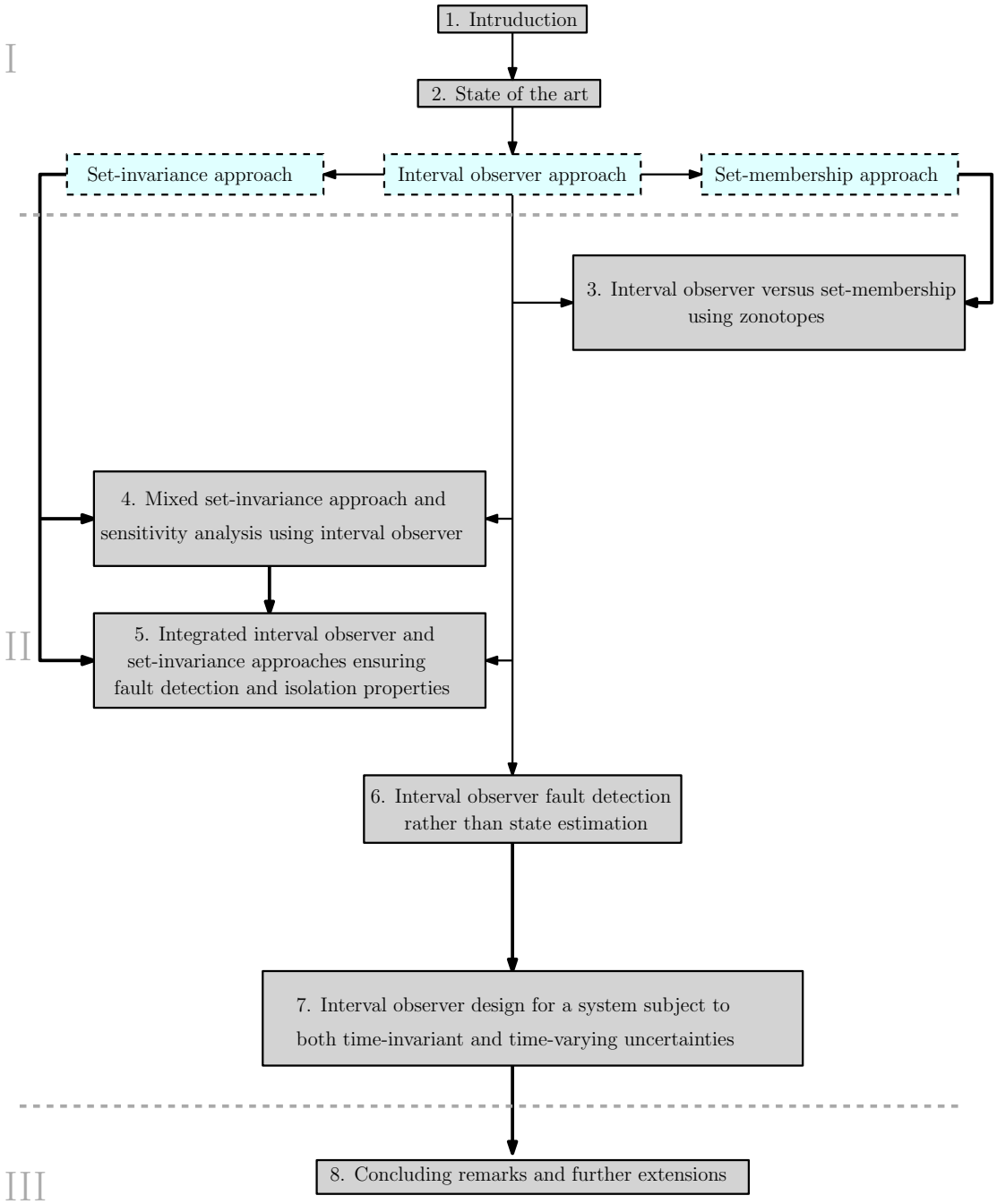

Figure 1.1: Roadmap of the thesis.

Furthermore, a sequence of specific objectives were accomplished as well, which are outlined next:

Objective I Revise and study the advantages and disadvantages of current existing interval observer approach (IOA) and set-membership approach (SMA) for combining them under specific conditions and figure out under which conditions they provide better or equivalent FD performance.

Objective II The same objective as in the previous case but now considering the set-invariance approach (SIA) in order to provide the connection between SIA and IOA.

Objective III To apply the developed method in characterization of MDF using sensitivity analysis.

Objective IV To complement the developed SMA with set-theoretic methods in order to provide fault detectability and isolability properties to the FDI approach proposed.

Objective V To provide the connection of IOA and SIA in estimating the magnitude of MDF and MIF.

Objective VI To provide a method to optimize the FD performance rather than the state estimation one.

Objective VII Revise and study the advantages and disadvantages of set-based and trajectory-based interval observers in order to provide the condition between them under some specific conditions.

Objective VIII Design an IOA for the dynamic system with time-invariant parameter uncertainty.

Objective IX Complement the developed method in previous objective for the system subjected to both time-invariant and time-varying uncertainties.

Objective X Apply the obtained results to a real case study to assess their performance and effectiveness.

1.3 Thesis structure

The structure of this dissertation is described in this section introducing the different parts and chapters. Thereby, a short description of contents and its related published papers are provided for each chapter.

Apart from Chapter 1, where the motivation and general objectives of the thesis and Chapter 2, where the state of the art of the main topics considered in this dissertation are described, this PhD thesis is divided into two parts related to different mentioned objectives as follow:

Part I entitled ***Contributions*** contains the following chapters:

- *Chapter 3: IOA versus SMA using zonotopes.*
- *Chapter 4: Mixed SIA and sensitivity analysis using IOA.*
- *Chapter 5: Integrated IOA and SIA ensuring FDI properties.*
- *Chapter 6: Interval observer FD rather than state estimation.*
- *Chapter 7: Interval observer design for a system subject to both time invariant and varying uncertainties.*

Part II entitled ***Conclusions and future research*** contains the following chapter:

- *Chapter 8: Concluding remarks and further extensions.*

Moreover, a short description of contents and the related published papers are provided for every chapter in the following subsections.

1.3.1 Chapter 3: IOA versus SMA using zonotopes

This chapter mainly focuses on the analysis and comparison of the IOA and SMA from both state estimation and FD point of view for the case of uncertain linear systems. Both state disturbance and measurement noise are assumed unknown-but-bounded through a zonotopic set representation. Both approaches have been mathematically related and compared in state estimation and FD tasks. A case study based on a two-tanks system is used to show the relationship between both approaches while comparing their performance.

This chapter is based on the following papers:

M. Pourasghar, V. Puig and C. Ocampo-Martinez. Comparison of Set-membership and Interval Observer Approaches for State Estimation of Uncertain Systems. *European Control Conference (ECC)*, (pp. 1111-1116), Denmark, 2016.

M. Pourasghar, V. Puig and C. Ocampo-Martinez. Interval Observer versus Set-membership Approaches for FD in Uncertain Systems using Zonotope. *International Journal of Robust and Nonlinear Control*, Accepted.

1.3.2 Chapter 4: Mixed SIA and sensitivity analysis using IOA

This chapter focuses on the characterization of the MDF by means of residual sensitivity integrated with the SIA when using an IOA. Modelling of the uncertainties propagation is carried out by using zonotopic representation of the set and assuming unknown-but-bounded nature (i.e., in the set-membership framework). Finally, a quadruple-tank system is employed to both illustrate and discuss the effectiveness of the proposed approach.

This chapter is based on the following papers:

M. Pourasghar, V. Puig and C. Ocampo-Martinez. Characterization of the Minimum Detectable Fault of Interval Observers by using Set-invariance Theory. 3^{rd} *Conference on Control and Fault-Tolerant Systems (SysTol)*, (pp. 79-86), Spain, 2016.

A. R. Kodakkadan, M. Pourasghar, V. Puig, S. Olaru, C. Ocampo-Martinez and V. Reppa. Observer-based Sensor Fault Detectability: About Robust Positive Invariance Approach and Residual Sensitivity. *IFAC World Congress*, 50(1): 5041-5046, France, 2017.

M. Pourasghar, V. Puig and C. Ocampo-Martinez. Interval observer-based fault detectability analysis using mixed set-invariance theory and sensitivity analysis approach. *International Journal of System and Science*, (pp. 1-22), 2019.

1.3.3 Chapter 5: Integrated IOA and SIA ensuring FDI properties

This chapter focuses on the design of an on-line interval observer-based FDI algorithm using SIA. In SIA, FDI can be done during the steady-state operation of the system. The effect of the uncertainties is modeled by considering zonotopes. The MDF and the MIF are characterized for a given type of faults using the integration of sensitivity analysis and SIA. Finally, a simulation example based on a two-tanks system is used to show the effectiveness of the proposed approaches.

This chapter is based on the following papers:

M. Pourasghar, V. Puig and C. Ocampo-Martinez. Interval observer fault detection ensuring detectability and isolability by using a set-invariance approach. 10^{th} *IFAC Symposium on Fault Detection, Supervision and Safety for Technical Processes (SAFEPROCESS)*, Poland, 2018.

M. Pourasghar, V. Puig and C. Ocampo-Martinez. Integrated interval-observer set-invariance approach ensuring FDI properties. *Journal of Franklin Institute*, Under review.

1.3.4 Chapter 6: Interval observer FD rather than state estimation

This chapter focuses on enhancing the sensitivity to faults with respect to disturbances in the context of the bounded-error paradigm using Zonotopic Kalman Filters (ZKF). The proposed on-line maximization provides an optimal time-varying observer gain leading to the so-called FD-ZKF filter that allows enhancing the FD properties. The characterization of MDF magnitude is done based on a sensitivity analysis. The effect of the uncertainty is modeled utilizing a zonotopic representation of the involved sets. A case study based on a quadruple-tank system is used both to illustrate and compare the effectiveness of the results obtained from the FD-ZKF approach compared to a pure ZKF approach.

This chapter is based on the following paper:

M. Pourasghar, C. Combastel, V. Puig and C. Ocampo-Martinez. FD-ZKF : A Zonotopic Kalman Filter Optimizing Fault Detection rather than State Estimation. *Journal of Process Control*, 73, (pp. 89-102), 2019.

1.3.5 Chapter 7: Interval observer design for a system subject to both TIU and TVU

This chapter addresses the design of an IOA for linear dynamic systems affected by both time-invariant uncertainty (TIU) and time-varying uncertainty (TVU). First, the comparison of set-based IOA and trajectory-based IOA is done. Then, an integrated set-based and trajectory-based observer is proposed in order to overcome the drawbacks of using the set-based approach. Furthermore, H_∞ performance is considered in order

to compute the observer gain by using an LMI technique. Finally, a numerical example and a real case study based on a two-tank system are used to show the effectiveness of the proposed approach.

This chapter is based on the following papers:

M. Pourasghar, V. Puig, C. Ocampo-Martinez and Q. Zhang. Reduced-order Interval-observer Design for Dynamic Systems with Time-invariant Uncertainty. *IFAC World Congress*, 50(1): 6271-6276, France, 2017.

M. Pourasghar, V. Puig and C. Ocampo-Martinez. On robust interval observer design for uncertain systems subject to both time-invariant and time-varying uncertainties. *International Journal of Control*, Special issue on interval estimation applied to diagnosis and control of uncertain systems, Under review.

Chapter 2

State of the art

This chapter introduces the main sources of inspiration in this PhD dissertation. A brief discussion on the different fault diagnosis approaches is given focusing on the passive robust FD methods based on the available set-based approaches.

2.1 Introduction to fault diagnosis

Over the past century, there has been increased application of control systems. Also, the control systems are being more and more sensitive to the faults because of their higher complexity. Therefore, considerably more work will need to be done to determine the effect of a fault on the systems. Recent developments in control theory have highlighted the need of working on the FD field for developing methods to allow the system to achieve the desire performance even in faulty situation. In this regard, researchers have shown an increased interest in the FD concept since the beginning of 1970's [BKL+06], [PC97]. This topic is still an interesting field of research in control theory community and in the industry.

According to [BKL+06], fault is identified as a deviation of the system structure or the system parameters from the nominal system. Hence, the fault is known as an unexpected change of the system behaviour. Generally speaking, the procedure of monitoring the system to detect the fault and finding its locations is called *fault diagnosis*. In order to monitor the system, three steps should be done with the following tasks:

- FD that is used to test whether or not a fault has occurred,

- Fault isolation that is used to determine the location of the fault occurrence,
- Fault identification and estimation that is use to estimate the size and type or nature of the fault.

Moreover, fault diagnosis is often considered as *fault detection and isolation*, abbreviated FDI, in the literature [Pat94, FD97]. Traditionally, fault diagnosis in the application context is based on *hardware redundancy* methods. In this context, multiple sensors, actuators, computers and software are used to measure and/or control a particular variable. Mainly, a voting scheme is applied to the hardware redundant system to decide whether and when a fault has occurred and its likely location amongst redundant system components. However, extra equipment and the additional space required for the equipments and their maintenance costs are known as the major problem with this approach. Moreover, considering the conflict between the reliability and the cost of adding more hardware, it is reasonable to use the dissimilar measured values together to cross check each other, rather than replicating each hardware individually. This concept is known as *analytical redundancy* [Fav94].

2.2 FDI approaches

Different methodologies have been studied for FDI that include a great variety of techniques. However, there are two major classifications of FDI methods: those based on the analytic model of the system [Ger98], called *Model-based methods*, and the methods that do not use the model of the system [BN93], called *Data-based methods*. This thesis is focused on the study of the Model-based methods, however the techniques that do not use the system model will be reviewed shortly next.

2.2.1 Data-based methods

Data-based FDI methods include those methods that do not use the mathematical model for detecting the occurrence of the fault. These methods include hardware redundancy, limit checking, frequency spectrum analysis and logical reasoning techniques [ZJ08].

- *Hardware redundancy*: This technique requires to install multiple sensors to measure the physical quantity. Any significant difference between the measurements

known as sensor fault. This physical redundancy consists extra cost of hardware and an additional weight that can represent serious concerns in some applications.

- *Limit confirmation*: This method is based on comparing the system measurements with fixed thresholds (limits). Exceeding the threshold indicates a faulty operation. Since the plant variables can vary widely due to the normal input variations, the major drawback of this approach is related to the selection of the detection thresholds in a conservative way. Moreover, the fault isolation is extremely difficult since the effect of a single fault in a component can spread to many variables and activate the fault alarms.
- *Spectrum analysis*: Since most of the plant variables exhibit a typical spectrum of frequency under normal operation conditions, any deviation, is an indication of a fault occurrence.
- *Statistical process control*: In this approach, a large amount of data is required to find appropriate operation to monitor. Then, specific features of signals are extracted and compared with the measurements.

2.2.2 Model-based methods

The use of mathematical models to describe the system behaviour is known as the fundamental concept of model-based FD approaches [Ger98, CP99, CFS16, Com15b]. Therefore, to improve performance of FD is directly related with the quality of the mathematical model [CP99, BKL+06]. But, in practice, a mismatch between the actual process and its mathematical model is non-negligible even if there are no process faults because of the presence of model uncertainty, unknown disturbances and noises [PMdOB13]. Thus, dealing with uncertainty and noise/disturbance is an important issue that implies developing robust model-based FD approaches [CP99]. In recent years, several methods have been developed and introduced to explicitly consider such uncertainties in the models [REZ12, Pui10, ULHM15]. See [Kal60], [May82], [Sch68], [Pui10] and [ULHM15] for more information related to different available ways for modeling the effect of uncertainties in model-based FDI framework.

FD in model-based approaches relies on checking the consistency of the observed behavior from measured outputs using sensors and the estimated behavior that is computed by using the system model [Ger98]. This consistency test is based on generating the residual by computing the difference between the output predicted values from the

model and the real measured values obtained from the sensors [CP99, Ger15]. Then, the fault can be detected by comparing that residual with a threshold value that takes into account the uncertainty associated with measurement noise, disturbances, and the model mismatch between the real and modeled system behavior [PQES03]. If the residual is larger than such threshold, the existence of the fault can be proved [Pui10, FPG04]. Otherwise, the system is assumed to be still in healthy operation and working properly.

Moreover, model-based FD can be categorized considering how residuals are generated: observers (as e.g., KF or unknown input observers), parity equations and parameter estimation [CP12, Ger98]. Then, the decision of the FD module can be made based on evaluating the residual generated by using the output estimation error [CP12, PQES03]. In particular, in the KF-based approach, the innovation is considered as a residual to detect the fault (i.e., in the presence of faults, the prediction error is not null). In this framework, KF, extended KF and unscented KF are different techniques for state estimation of linear/nonlinear systems where the uncertainties are taken into account stochastically [Kal60, KB61]. In the set-membership approach, the uncertainties are assumed unknown but bounded [Pui10, Com13, LSA+13b, PPOM16a]. In the case of the set-membership-based state estimation [ABC05, NPH12, Jau09], the estimation characterizes a set of possible states [ABC05, PCQ01, BAC06, Com03].

As in the observer-based approaches, FD using parity equations is based on checking possible inconsistencies of the measured outputs with suitable analytical redundancy relations derived from the system model [PA06, FD94, Din08]. On the other hand, it is possible to detect the fault based on the parameter estimation where the plant is firstly identified in fault-free scenario (called reference model). Then, the existence of the fault is proved by checking the reference model with the parameters that are repeatedly re-identified on-line [Ise05, IBPA05, LC06a]. Some works have explored the relation between different approaches regarding FD performance [Ger98, Ger97, KPP+17]: for example, if the residual generators have been designed for the same specification, parity relation and observer-based approaches can produce identical residuals.

Furthermore, methods that explicitly consider uncertainty in the FD task are known as robust approaches. Most robust approaches try to maximize the fault sensitivity while minimizing the sensitivity to uncertainty at the residual generation phase, following the *active robust approach* [CP99, Din08, ZDLW03] [1]. On the other hand, the *passive robust*

[1] In the book [CP12], there is an excellent survey of the active approach.

approach tries to bound the effect of uncertainty in the residual evaluation phase by generating adaptive thresholds [Pui10]. In the former class, the main idea is to decouple the effect of the uncertainty [CP12], and the latter approach is based on enhancing the robustness of the FD system at the decision-making stage [PQEdlH02]. The main purpose of the passive FD approach is to determine whether or not there is any member in the uncertainty set that can explain the measurements. Then, any inconsistency between the measurement and this set is considered as fault occurrence. Therefore, it is not necessary to know the exact model of as a fault. In recent years, there has been an increasing interest in using the passive approach since its main advantage over the corresponding active approach is to achieve robustness in the FD procedure in spite of the number of uncertain parameters in the model by using the underlying parameter representation without any simplification [XTW+17, CQ14, Tab15, TCRZ15, SRHS17].

Moreover, based on [PC97] and [CPZ96], several techniques can be used to model the noises and disturbances affecting the system. For example, KF is one of the useful techniques addressing this issue, but in these methods, the knowledge about the statistical distribution of the disturbances and noises should be available. Therefore, the set-based methods were proposed as an alternative approach to characterize the uncertainties in the system. In these methods, only the bounds of disturbances and noises are required. Taking into account the research presented in [Sto11], [ODDSS10], [ABC05], [Com03], [OMDDS10] and [FTF12], the set-based methods can be classified into the following categories:

- interval observer approach (IOA) [Pui10, Com15b, XSP+13],
- set-membership approach (SMA) [ABC05, LSA+13b, LSA+13a], and
- set-invariance approach (SIA) [Kof05, KHS07, SDD10, XSP+13, RKKM05].

Then, the FD decision is done using some of the methods in these three categories. On the other hand, the state estimation problem has become one of the significant issues in control theory since knowing the state of a system is crucial for solving many problems in both control and FD frameworks. There are several approaches in the literature for representing the uncertainties. These approaches can be classified in two main categories: stochastic and deterministic. According to [Kal60], the differences between these two main families are related to the way of how noises and perturbations are modeled. In stochastic approaches, noises and perturbations are assumed to be described by

some known statistical distributions (typically Gaussian) while deterministic approaches consider noises and disturbances as unknown variables with known bounds. Within the family of deterministic approaches, the IOA and SMA have been introduced separately [PSQ03, ERCZ13, MB11]. The state estimation provided by both approaches is given in a form of a set of states at each time instant.

IOA is one of the most common approaches in FD methods. This approach has appeared in the last decade for systems with uncertainties [BG04], allowing to estimate the state set one time instant ahead based on the set estimated in the previous time instant [PAR99, ABC05]. Generally speaking, the FD test is done by means of generating the residual signal by comparing actual measurements with the output predicted by using the IOA at each time instant, i.e., the FD decision is done by checking the consistency of threshold (zero in ideal case) with the observations obtained from some sensors. On the other hand, the SMA state estimation is an alternative approach for estimating the state of the system including the measured output and bounded noises [LSA+13c]. Furthermore, the SMA algorithm has been already applied to the FD framework (see [ABC05], [Com03], [LAC+11] and [Pui10]). In order to compute the set of states using both families of approaches, there are several geometrical structures considered in the literature, e.g., polytopes [VZ96], ellipsoids [PNDW04], [Com05] and zonotopes [PSQ03, LAC+11, LSA+13c, Com03]. In these approaches, the set is approximated by using the outer bounds of the exact uncertain state set at time instant $k-1$ and measured output set at time instant k, where $k \in \mathbb{Z}$ denotes the discrete time.

In addition, set invariance is another approach that can be used in the FDI context. This approach obtains the residual set in the healthy mode considering unknown-but-bounded uncertainties. This invariant set can be used for showing the healthy operation of the system. Therefore, the fault will be detected if the residual in faulty mode is outside of the healthy invariant set. Thus, as long as both healthy and faulty sets are separated, the FDI test can be performed.

Moreover, considering a discrete linear time-invariant (LTI) interval model, the approximated state set can be computed based on a set of point-wise trajectories following the so-called *trajectory-based approach* [PSQ05a, Tib93]. In the set-based approach, the propagation of the state set is affected by several problems such as the wrapping effect, temporal variance on uncertain parameters (or uncertain parameter time dependency) and the range evaluation of an interval function, especially in the case of using the interval hull of the set at each iteration. Therefore, conservative and unstable results may be

obtained (for even a stable system) when using the set-based approach for the simulation of the system with parametric time-invariant uncertain. The advantage of trajectory-based approach in comparison with the set-based approach is that allow overcoming the wrapping effect because uses real trajectories based on selecting a particular value of the uncertain parameters. Meanwhile, the uncertain parameter time dependency can be preserved if the set of point-wise trajectories are generated [PSQ05a].

2.3 Set-based state estimation and FD approaches

As it is mentioned, model-based FD relies on the use of a model describing the system behavior in order to check the consistency with the observations obtained from some sensors. Therefore, the performance of FD depends on the quality of the mathematical model and it is vital to obtain a simple mathematical model as proper as possible representing the behavior of the system to be monitored. The class of systems addressed in this thesis is that of a discrete-time invariant linear uncertain system with the following state-space form:

$$x_{k+1} = Ax_k + Bu_k + E_\omega \omega_k, \tag{2.1a}$$

$$y_k = Cx_k + E_\upsilon \upsilon_k, \tag{2.1b}$$

where $u \in \mathbb{R}^{n_u}$, $y \in \mathbb{R}^{n_y}$ and $x \in \mathbb{R}^{n_x}$ are the input, the output and the state vectors, respectively. Moreover, $A \in \mathbb{R}^{n_x \times n_x}$, $B \in \mathbb{R}^{n_x \times n_u}$ and $C \in \mathbb{R}^{n_y \times n_x}$ are the state-space matrices. Both state disturbance and process noise vectors are defined by $\omega \in \mathbb{R}^{n_x}$ and $\upsilon \in \mathbb{R}^{n_y}$, respectively. Besides, E_ω and E_υ are the associated distribution matrices with appropriate dimensions while $k \in \mathbb{N}$ indicates the discrete time.

Moreover, the measurement noise and process disturbances are assumed to be unknown but bounded, i.e.,

$$\mathcal{W} = \{\omega_k \in \mathbb{R}^{n_x} : |\omega_k - c_\omega| \leq \bar{\omega}, c_\omega \in \mathbb{R}^{n_x}, \bar{\omega} \in \mathbb{R}^{n_x}\}, \tag{2.2a}$$

$$\mathcal{V} = \{\upsilon_k \in \mathbb{R}^{n_y} : |\upsilon_k - c_\upsilon| \leq \bar{\upsilon}, c_\upsilon \in \mathbb{R}^{n_y}, \bar{\upsilon} \in \mathbb{R}^{n_y}\}, \tag{2.2b}$$

where c_ω, $\bar{\omega}$, c_υ and $\bar{\upsilon}$ are constant vectors. Noticed that the inequalities associated to $|\omega_k - c_\omega|$ and $|\upsilon_k - c_\upsilon|$ in (2.2) are considered component-wise.

Furthermore, (2.2) can be rewritten as a zonotopic representation of the set as

$$\mathcal{W} = \langle c_\omega,\ R_\omega \rangle\,, \tag{2.3a}$$

$$\mathcal{V} = \langle c_\upsilon,\ R_\upsilon \rangle\,, \tag{2.3b}$$

where c_ω and c_υ denote the centers of the disturbance and noise bounding zonotopes, respectively, with their generator matrices $R_\omega \in \mathbb{R}^{n_x \times n_x}$ and $R_\upsilon \in \mathbb{R}^{n_y \times n_y}$, respectively.

Assumption 2.1. *The pair $\{A, C\}$ of the dynamical model (2.1) is detectable.* □

Assumption 2.2. *Disturbance and noise bounds represented in (2.3) are assumed to be bounded by a unitary hypercube zonotopes centered at the origin, i.e., $\forall\ k \geq 0,\ \omega \in [-1,\ 1]^{n_\omega} = \langle 0,\ I_{n_\omega} \rangle$ and $\upsilon \in [-1,\ 1]^{n_\upsilon} = \langle 0,\ I_{n_\upsilon} \rangle$ where $I_{n_\omega} \in \mathbb{R}^{n_\omega \times n_\omega}$ and $I_{n_\upsilon} \in \mathbb{R}^{n_\upsilon \times n_\upsilon}$ denote the identity matrices.* □

Henceforth, the index $k+1$ will be replaced by $+$ and k will be omitted for the sake of simplified notations. Then, the dynamical model (2.1) is simply rewritten as

$$x_+ = Ax + Bu + E_\omega \omega, \tag{2.4a}$$

$$y = Cx + E_\upsilon \upsilon. \tag{2.4b}$$

Consequently, the index $k-1$ will be replaced by $-$ when it will be needed throughout the thesis.

2.3.1 IOA

FD test in the IOA consists in testing whether the system measurements are consistent with the behavior described by the model in healthy operation. The existence of the fault is demonstrated in the case that measurements are inconsistent with the behavior of the model. Monitoring the dynamical model (2.4) can be done by designing a Luenberger observer of the form

$$\hat{x}_+ = A\hat{x} + Bu + L(y - \hat{y}), \tag{2.5}$$

where $\hat{x}$ is the state estimation. Moreover, the observer gain L should be computed such that $(A - LC)$ was a Schur matrix.

Assumption 2.3. *The initial state x_0 belongs to the set $\mathcal{X}_0^{io} = \langle c_{x,0}^{io},\ R_{x,0}^{io} \rangle$, where*

$c^{io}_{x,0} \in \mathbb{R}^{n_x}$ *denotes the center and* $R^{io}_{x,0} \in \mathbb{R}^{n_x \times n_{R^{io}_{x,0}}}$ *is a non-empty matrix containing the generators matrix of the initial zonotope* $\mathcal{X}^{io}_0$. □

Therefore, according to [XPOM+15], the resulting interval observation of the dynamical model (2.4) can be defined by using Proposition 2.1.

Proposition 2.1. *(Zonotopic-observer structure) Considering the dynamical model (2.4), observer (2.5) and Assumptions 2.2 and 2.3, the center* c^{io}_x *and the segment (shape) matrix* R^{io}_x *of the state bounding zonotope* $\hat{\mathcal{X}}^{io}$*, i.e.,*

$$\hat{\mathcal{X}}^{io} = \left\langle c^{io}_x,\ R^{io}_x \right\rangle, \tag{2.6}$$

can be recursively computed using

$$c^{io}_{x,+} = (A - L^{io}C)c^{io}_x + Bu + L^{io}y, \tag{2.7a}$$

$$R^{io}_{x,+} = \left[(A - L^{io}C)\bar{R}^{io}_x \quad E_\omega \quad -L^{io}E_\upsilon\right], \tag{2.7b}$$

where $\bar{R}^{io}_x = \downarrow_q \left\{R^{io}_x\right\}$ *and* L^{io} *is the observer gain that provides degrees of freedom to tune the system monitoring with respect to its aim, e.g., with the goal of optimizing the state estimation or FD according to some given criterion. Moreover, the state inclusion property* $x \in \left\langle c^{io}_x, R^{io}_x \right\rangle$ *holds for all* $k \geq 0$ *(see Properties B.2 and B.3).*

Proof. Assume $x \in \left\langle c^{io}_x,\ R^{io}_x \right\rangle$, $\omega \in \langle 0,\ I_{n_\omega} \rangle$ and $\upsilon \in \langle 0,\ I_{n_\upsilon} \rangle$ where the inclusion property (see Property B.2) is preserved by using the reduction operator, which means $x_k \in \left\langle c^{io}_x,\ \bar{R}^{io}_x \right\rangle$. Thus, the set-based interval observation can be written using (2.5) as

$$\begin{aligned} x_+ \in \left\langle c^{io}_{x,+},\ R^{io}_{x,+} \right\rangle = &\left\langle (A - L^{io}C)c^{io}_x,\ (A - L^{io}C)\bar{R}^{io}_x \right\rangle \oplus \langle B_u u,\ 0 \rangle \\ &\oplus \langle 0,\ E_\omega \rangle \oplus \left\langle L^{io}y,\ 0 \right\rangle \oplus \left\langle 0,\ -L^{io}E_\upsilon \right\rangle. \end{aligned} \tag{2.8}$$

Thus, based on Definitions B.22 and B.24, $c^{io}_{x,+}$ and $R^{io}_{x,+}$ in (2.8) can be derived as in (2.7). □

In [Com15b], an special type of IOA named Zonotopic Filter (ZF) is proposed. This approach can be viewed as the deterministic counterpart of the stochastic KF when uncertainties (noise and disturbance) are assumed to be unknown but bounded. The

ZF yields the same zonotopic representations for the set in (2.5) for the state estimation of (2.4) but using the optimal observer gain given by Theorem 2.1.

Theorem 2.1. *Considering $x \in \hat{\mathcal{X}}^{\text{io}}$ at time k, the optimal observer gain $L^{io,*}$ that minimizes the F-radius of the state bounding zonotope (2.7) at time instant $k+1$ is computed as*

$$L^{io,*} = \left(AR_x^{io}R_x^{io^\top}C^\top\right)\left(CR_x^{io}R_x^{io^\top}C^\top + E_\upsilon E_\upsilon^\top\right)^{-1}. \tag{2.9}$$

Proof. According to [Com15b], minimizing the F-radius and F_W-radius of a zonotope is equivalent to minimize the trace of its covariance. Therefore, the proof is based on the minimization of the F-radius and the F_W-radius of the zonotope that is computed by the observer. The F-radius of the zonotope in (2.7) can be obtained as

$$J = \left\|R_{x,+}^{io}\right\|_F^2 = tr(R_{x,+}^{io}R_{x,+}^{io^\top}) = tr(P_+), \tag{2.10}$$

where J denotes the Frobenius radius and P is the covariance of the zonotope matrix $R_{x,+}^{io}$. Likewise, the F_W-radius of the zonotope in (2.7) will lead to

$$J_W = \left\|R_{x,+}^{io}\right\|_{F,W}^2 = tr(R_{x,+}^{io}R_{x,+}^{io^\top}) = tr(WP_+), \tag{2.11}$$

where J_W denotes weighted Frobenius radius and WP is the weighted-function covariance of the zonotope matrix R_x^{io}. Hence, the Frobenius radius in (2.10) can be written as

$$J = tr(\begin{bmatrix}(A-LC)\bar{R}_x^{io} & E_\omega & -L^{io}E_\upsilon\end{bmatrix}\begin{bmatrix}(A-LC)\bar{R}_x^{io} & E_\omega & -L^{io}E_\upsilon\end{bmatrix}^\top).$$

Then, by considering $Q_\omega = E_\omega E_\omega^\top$ and $Q_\upsilon = E_\upsilon E_\upsilon^\top$, (2.10) can be rewritten as

$$J = tr\left((A-L^{io}C)P(A-L_k^{io}C)^\top + L^{io}Q_\eta L^{io^\top} + Q_\omega\right).$$

Similarly, the weighted Frobenius radius J_w in (2.11) satisfies

$$J_w = tr\left(W(A-L^{io}C)P(A-L^{io}C)^\top + WL^{io}Q_\eta L^{io^\top} + WQ_\omega\right).$$

Therefore, the minimum L^{io} is obtained when $\dfrac{\partial J_w}{\partial L^{io}} = 0$, then using the definition of matrix trace in Definition B.7 yields

$$\partial_{L^{io}}\, tr(WL^{io}(CPC^T + Q_\upsilon)) = 2\partial_{L^{io}}\, tr(WAL^{io}L^{io^\top}),$$

where $\partial_{L^{io}}\, tr(\cdot)$ is a short notation for $\dfrac{\partial tr(\cdot)}{\partial_{L^{io}}}$. If W is an SPD matrix (see Definition B.1) and $W = W^T \succ 0$, by transposition and left multiplication of W^{-1} and considering Definition B.7, it can be written that $-APC^\top + L^{io}(CPC^\top + Q_v) = 0$. Then, the optimal gain $L^{io,*}$ will be computed as it is written in (2.9) [2]. If W is an SPD matrix (see Definition B.1) and $W = W^T \succ 0$, by transposition and left multiplication of W^{-1}, the optimal gain $L^{io,*}$ will be computed as it is written in (2.9). □

Moreover, the system output can be predicted using Proposition 2.2.

Proposition 2.2. *Considering the dynamical model (2.4) and Proposition 2.1, c_y^{io} and R_y^{io} defining the output-bounding zonotopic set $\langle c_y^{io},\ R_y^{io} \rangle$ can be computed as*

$$c_y^{io} = C c_x^{io} \tag{2.12a}$$

$$R_y^{io} = \begin{bmatrix} C\bar{R}_x^{io} & E_v \end{bmatrix}. \tag{2.12b}$$

Proof. Assume that $x \in \langle c_x^{io},\ R_x^{io} \rangle$ and $v \in \langle 0,\ I_{n_v} \rangle$ for all $k \geq 0$, where the inclusion is preserved by using the reduction operator, which means $x \in \langle c_x^{io},\ \bar{R}_x^{io} \rangle$. Thus, (2.4b) can be written as

$$y_k \in \langle c_y^{io},\ R_y^{io} \rangle = \langle C c_x^{io},\ C\bar{R}_x^{io} \rangle \oplus \langle 0,\ E_v \rangle. \tag{2.13}$$

Therefore, based on Definitions B.22 and B.24, c_y^{io} and R_y^{io} in (2.13) can be expressed as (2.12). This gives the proof of Proposition 2.2. □

Now, the difference between the measurement and the predicted system output, called residual, can be generated using the Proposition 2.3.

Proposition 2.3. *(Residual generation using IOA) Considering Proposition 2.2 and the measurement equation in (2.4b), the center c_r^{io} and the generator matrix R_r^{io} of the residual zonotopic set are generated as*

$$c_r^{io} = y_k - C c_x^{io}, \tag{2.14a}$$

$$R_r^{io} = \begin{bmatrix} -C\bar{R}_x^{io} & -E_v \end{bmatrix}. \tag{2.14b}$$

Proof. The output (2.4b) can be written as

$$0 = y - Cx - E_v v_k. \tag{2.15}$$

[2] The proof follows from the results available in [Com15b].

Algorithm 2.1 FD test based on IOA

$k \longleftarrow 0$
$\mathcal{X}_0 = \langle c^{io}_{x,0},\ R^{io}_{x,0} \rangle$
while 1 **do**
  Computing the center $c^{io}_{x,k+1}$ and shape matrix $R^{io}_{x,k+1}$ of the state observer using (2.7)
  Computing the center $c^{io}_{y,k}$ and shape matrix $R^{io}_{y,k}$ of the output prediction using (2.12)
  Computing the center $c^{io}_{r,k}$ and shape matrix $R^{io}_{r,k}$ of the residual using (2.14)
  if $0 \notin \left\langle c^{io}_{r,k},\ b(R^{io}_{r,k}) \right\rangle$ **then**
    $Fault \leftarrow true$
  else
    $Fault \leftarrow false$
  end if
  $k \longleftarrow k+1$
end while

Now, considering $x \in \langle c^{io}_x,\ R^{io}_x \rangle$ and $\upsilon \in \langle 0,\ I_{n_\upsilon} \rangle$, (2.15) becomes

$$0 \in \langle y,\ 0 \rangle \oplus \langle -Cc^{io}_x,\ -CR^{io}_x \rangle \oplus \langle 0,\ -E_\upsilon \rangle\,, \tag{2.16}$$

where c^{io}_x is known using observer (2.7). Thus, considering Definitions B.22 and B.24, c^{io}_r and R^{io}_r in (2.16) can be expressed as in (2.14). This gives the proof of Proposition 2.3. □

Hence, the FD test can be done by checking the satisfaction of $0 \notin \langle c^{io}_r,\ R^{io}_r \rangle$. A computationally efficient way to implement the detection test without increasing the false alarm rate consists in testing whether or not 0 belongs to an aligned box enclosing the zonotope $\langle c^{io}_r,\ R^{io}_r \rangle$, i.e.,

$$0 \notin \langle c^{io}_r,\ b(R^{io}_r) \rangle\,, \tag{2.17}$$

where $\langle c^{io}_r,\ b(R^{io}_r) \rangle$ is enclosed by an aligned box denoted by $b(R^{io}_r)$.

Algorithm 2.1 summarizes the FD test procedure using IOA in this thesis. The FD test in Algorithm 2.1 is based on checking if 0 is inside the residual zonotopic set. This set is propagated online to detect the existence of the fault.

2.3.2 SMA

Alternatively, one possible way for detecting the fault is to make use of the SMA that is carried out based on [ABC05] and Proposition 2.4.

Proposition 2.4. *Considering the dynamical model (2.4), the center c_x^{sm} and the segment (shape) matrix R_x^{sm} of the state bounding zonotope $\hat{\mathcal{X}}^{sm}$ corrected by the i^{th} output, i.e.,*

$$\hat{\mathcal{X}}_i^{sm} = \langle c_x^{sm},\ R_x^{sm} \rangle\,, \tag{2.18}$$

can be obtained by intersecting the prediction state set $\mathcal{P}^{sm} = \langle c_p^{sm},\ R_p^{sm} \rangle$, where c_p^{sm} and R_p^{sm} denote the center and segments of the zonotope $\mathcal{P}_k^{sm}$, respectively, and the set of states consistent with each output strip $\mathcal{S}_y$ as

$$c_x^{sm} = c_p^{sm} + \lambda_i(y_i - C_i c_p^{sm}), \tag{2.19a}$$

$$R_x^{sm} = \begin{bmatrix} (I - \lambda_i C_i) R_p^{sm} & -\lambda_i E_{v_i} \end{bmatrix}, \tag{2.19b}$$

with

$$c_p^{sm} = A c_{x,-}^{sm} + B u_-, \tag{2.20a}$$

$$R_p^{sm} = \begin{bmatrix} A R_{x,-}^{sm} & E_\omega \end{bmatrix}, \tag{2.20b}$$

where λ is a vector that provides degrees of freedom to tune the system monitoring, e.g., optimizing the state bounding zonotope to be as robust as possible with respect to effect of uncertainties.

Proof. Considering the dynamical model (2.4), the prediction state set can be computed as a zonotope, i.e.,

$$\mathcal{P}^{sm} = \langle c_p^{sm},\ R_p^{sm} \rangle\,, \tag{2.21}$$

Furthermore, c_p^{sm} and R_p^{sm} can be calculated using (2.20) at time instant k. Additionally, a strip $\mathcal{S}_y$ is computed by considering each measurement component y as

$$\mathcal{S}_{y_i} = \{x \in \mathbb{R}^{n_x} : |C_i x - y_i| \leq E_{v_i}\}\,. \tag{2.22}$$

According to [ABC05], intersection between the zonotope in (2.21) and the obtained strip in (2.22) provides the state estimation using SMA. In order to compute the intersection between a zonotope and a strip, the Property B.4 can be used. Therefore, using Property B.4 to compute the intersection of (2.21) and (2.22), the time evolution of the center and the segments of state bounding zonotope (2.18) are given as it is derived in (2.19). □

Based on (2.19), the obtained state bounding zonotope using SMA is parametrized by means of a vector λ. Computing the parameter λ can be done using several methods, e.g., singular value decomposition, segments minimization, volume minimization and the P-radius minimization [ABC05, LSA+13c].

In this thesis, the optimal value of λ is explicitly computed by using Theorem 2.2.

Theorem 2.2. *Considering the dynamical model (2.4) and the state bounding zonotope (2.19) at time instant k, the optimal value of λ that minimizes the F-radius of the zonotope (2.19) to be robust with respect to effect of uncertainties at time instant $k+1$ is computed as*

$$\lambda_i^* = \left(R_x^{sm} R_x^{sm^\top} C_i^\top\right) \left(C_i R_x^{sm} R_x^{sm^\top} C_i^\top + E_{v_i} E_{v_i}^\top\right)^{-1}, \tag{2.23}$$

where the superscript $*$ denotes the optimal value.

Proof. Based on [ABC05], the obtained zonotopic set can be minimized according to its generator matrix. Considering Property B.4, the intersection of the zonotope $\mathcal{P}^{sm} = \langle c_p^{sm},\ R_p^{sm} \rangle$ in (2.21) and the strip $\mathcal{S}_{y_i} = \{x \in \mathbb{R}^{n_x} : |C_i x - y_i| \leq E_{v_i}\}$ in (2.22) creates the zonotope $\hat{\mathcal{X}}^{sm}$ with the generator matrix $R_x^{sm} = \begin{bmatrix}(I - \lambda_i C_i) R_p^{sm} & -\lambda E_{v_i}\end{bmatrix}$. The size of this zonotope depends on the Frobenius norm of its generator. Therefore, minimizing the predicted zonotope is equal to minimizing the Frobenius norm of matrix R_x^{sm}. Moreover, for simplification of the computation procedure, R_x^{sm} is considered as

$$R_x^{sm} = M + \lambda_i b^\top,$$

where $M = \begin{bmatrix}R_p & 0\end{bmatrix}$ and $b^T = \begin{bmatrix}-CR_p & E_{v_i}\end{bmatrix}$. Then, using Definition B.8, R_x^{sm} can be derived as

$$\|R_x^{sm}\|_F^2 = \left\|M + \lambda_i b^\top\right\|_F^2 = tr(M^\top + b\lambda_i^\top)(M + \lambda_i b^\top). \tag{2.24}$$

Furthermore, (2.24) can be rewritten as

$$\|R_x^{sm}\|_F^2 = tr(M^\top M) + tr(M^\top \lambda_i b^\top) + tr(b\lambda_i^\top M) + tr(b\lambda_i^\top \lambda_i b^\top).$$

Thus, the Frobenius norm of matrix R_x^{sm} can be modified as

$$\|R_x^{sm}\|_F^2 = 2\lambda_i^\top M b + b^\top b \lambda_i^\top \lambda_i + tr(M^\top M).$$

Algorithm 2.2 FD using the SMA

1: $k \longleftarrow 0$
2: $\mathcal{P}_0^{sm} = \langle c_{p,0}^{sm},\ R_{p,0}^{sm} \rangle$
3: **while** 1 **do**
4: Obtain and store input-output data $\{u_k, y_k\}$
5: Compute the approximate set of estimated states $\mathcal{P}_k^{sm}$ using (2.20)
6: Compute the strip from the measured output $\mathcal{S}_{y,k}$ using (2.22)
7: **if** $\mathcal{P}_k^{sm} \cap \mathcal{S}_{y,k} = \emptyset$ **then**
8: $Fault \leftarrow true$
9: **else**
10: $Fault \leftarrow false$
11: **end if**
12: $k \longleftarrow k + 1$
13: **end while**

Moreover, the minimization of matrix $\|R_x^{sm}\|_F^2$ is achieved by imposing $\dfrac{d\,\|R_x^{sm}\|_F^2}{d\lambda} = 0$. Thus,

$$\frac{d(2\lambda_i^\top M b + b^\top b \lambda_i^\top \lambda_i + tr(M^\top M))}{d\lambda_i} = 0. \tag{2.25}$$

At the end, after computing the derivative of (2.25), the optimal value of vector λ is computed as

$$2Mb + 2b^\top b \lambda_i^* = 0,$$

and hence

$$\lambda_i^* = \frac{-Mb}{b^T b}. \tag{2.26}$$

Now, substituting M and b into (2.26) yields the optimal λ in (2.23). □

Remark 2.1. *According to [LSA+13a], in order to apply the SMA to the multi-output case, i.e., $n_y > 1$, the system can be considered as several single-output systems based on the dimension of the outputs n_y. Considering the system as several single-output systems lead to use Property B.4 and compute the vectors $\lambda_1, \lambda_2, \ldots, \lambda_{n_y}$, independently.*

In general, the FD test using SMA is based on checking the intersection between the obtained zonotope $\mathcal{P}^{sm}$ in (2.21) and the strip $\mathcal{S}_y$ in (2.22). In the case that the intersection is empty, the existence of the fault will be proved, i.e., if

$$\mathcal{P}^{sm} \cap \mathcal{S}_y = \emptyset, \tag{2.27}$$

the fault will be detected. Otherwise, the system is considered working in an healthy operation. Following the FD test based on the SMA, Algorithm 2.2 can be used.

Remark 2.2. *According to [LSA+13a], in order to apply the state estimation using SMA to multi-measurement cases, i.e., $n_y > 1$, the system can be considered as several single-measurement systems based on the dimension of the measurement n_y. Considering the system as several single-measurement systems leads to use Property B.4 towards computing the optimal vectors $\lambda_1, \lambda_2, \ldots, \lambda_{n_y}$, independently* [3].

2.3.3 SIA

Generally speaking, the RPI set defined as a bounded region in state-space that the system state can be confined, despite of considering the bounded system uncertainties [SDD10, XSP+13]. Furthermore, the mRPI set is a unique and compact RPI set that contained in any closed RPI set [SZDDM08, RKKM05].

Given the system (2.4) and considering the observer (2.5), the trajectories of the residual will ultimately converge to an invariant set. Then, based on [SZDDM08] and [SODDS11], the constructed RPI set in state space can be projected to the residual space and whenever the corresponding residual is inside this set, it will remain inside. Furthermore, the residual can be generated as

$$r = y - \hat{y} = C\tilde{x} + E_\upsilon \upsilon, \tag{2.28}$$

where $\tilde{x} = (x - \hat{x})$ is the state estimation error whose dynamics can be described using (2.4) and (2.5) as

$$\tilde{x}_+ = (A - LC)\tilde{x} + E_d d, \tag{2.29}$$

where $d = \begin{bmatrix} \omega & \upsilon \end{bmatrix}^\top$.

According to [Bla99], the set $\Phi^{\tilde{x}}$ is an RPI set for (2.29) if and only if for all $\omega \in \mathcal{W}$ and $\upsilon \in \mathcal{V}$,

$$(A - LC)\tilde{x} + E_d d \ \in \Phi^{\tilde{x}}. \tag{2.30}$$

There is a large amount of reported results describing the construction of $\Phi^{\tilde{x}}$ [Kof05]. In this thesis, the Ultimate Bound (UB) method reported in [KHS07] will be used in order to obtain the RPI set. Therefore, $\Phi^{\tilde{x}}$ can be computed using Theorem 2.3.

Theorem 2.3. *[KHS07] Consider the Jordan Conical form of matrix $(A - LC)$ as*

[3] This approach called equivalent single-measurement approach in [LSA+13a].

$J = V(A - LC)V^{-1}$, where J is a diagonal matrix corresponding to the Jordan-normal form of $(A - LC)$ and V is a non-singular transformation matrix. Thus, the state estimation error $\tilde{x}$ in (2.29) will ultimately converge within the polyhedral RPI set that is constructed as

$$\Phi^{\tilde{x}} = \left\{ \tilde{x} \in \mathbb{R}^{n_x} : |V^{-1}\tilde{x}| \leq (I - |J|)^{-1}|V^{-1}|\overline{d} + \varepsilon \right\}, \tag{2.31}$$

where ε can be any arbitrary small vector with strictly positive components.

Therefore, $\Phi^{\tilde{x}}$ can be computed straightaway using Theorem 2.3. Then, considering $\tilde{x} \in \Phi^{\tilde{x}}$ and $v \in \mathcal{V}$, the projection of $\tilde{x}$ to a residual space, i.e., invariant set for the residual in (2.28) denoted by Φ^r, can be computed as

$$\Phi^r = C\Phi^{\tilde{x}} \oplus \mathcal{V}. \tag{2.32}$$

According to [XSP+13], if $\tilde{x} \in \Phi^{\tilde{x}}$, then $r \in \Phi^r$. Therefore, the existence of the fault will be detected based on the SIA whenever

$$r \notin \Phi^r. \tag{2.33}$$

2.4 Summary

This chapter presents the state of art regarding FD with a special emphasis in robust approaches. It is worth mentioning that the main idea of this chapter is to give the general picture of the research area. Then, some of the existing set-based FD approaches related to this research are also reviewed. Therefore, not all details of these knowledge are presented in this chapter. More details and discussions regarding the advantages and drawbacks of each mentioned approaches, which can be undrestood as motivations for the thesis, will be reported in the introduction section at the beginning of each chapter. After introducing the main background and the required tools for this thesis, the main objective of the next chapters is to focus on each approach to investigate the advantages and drawbacks of each mentioned approaches in order to provide new method that improve the performances in both state estimation and FD frameworks.

Part II

Contributions

Chapter 3

IOA versus SMA using zonotopes

This chapter presents both analysis and comparison of the IOA and SMA for the state estimation and FD in uncertain linear systems. The considered approaches assume that both state disturbance and measurement noise are modeled in a deterministic context following the unknown but bounded approach. The propagation of uncertainty in the state estimation is bounded through a zonotopic set representation. Both approaches have been mathematically related and compared when used for state estimation and FD. A case study based on a two-tanks system is employed for showing the relationship between both approaches while comparing their performance.

3.1 Introduction

IOA and SMA estimators have been introduced separately [ERCZ13, MB11]. IOA has appeared during the last decade as an attractive approach for the state estimation of uncertain dynamical systems [PSE+06, BRPN14, RC13]. In this approach, the state set can be estimated at time instant k based on the state estimation set at time instant $k-1$ [REZ12, ABC05]. IOA is also nowadays one of the ways for dealing with uncertainty in FD applications. The fault can be detected using an IOA by generating an adaptive threshold for the residual signal that allow checking the consistency of the measurements with the estimated output. Likewise, SMA is an alternative approach that allows to estimate the system state including the measured output and bounded noises [LSA+13c,

MNPLW13] by means of the intersection between the prediction state set and the set[1] of states consistent with the output measurements (as it will be further explained in the following part of the thesis) [ABC05].

Furthermore, several model-based FD methods have been developed for computing the minimum magnitude of the fault that can be detected through the use of IOA and SMA. The difference between the model-based approaches regarding the MDF is related to the different ways of modeling the fault. A fault in a state estimation scheme can be modeled as a state or as an unknown input [TB14]. Additionally, the effect of observer gain and its influence on the computation of the the minimum detectable fault (MDF) has already been studied in [MPES10].

However, to the best of the authors knowledge, both IOA and SMA are still considered as two different approaches. Therefore, the main contribution of this chapter is to analyze and compare both state estimation approaches in order to establish the advantages and disadvantages of each approach, and also, to find out their relationship in a formal mathematical framework. Moreover, the comparison is also performed in the context of FD application by means of proposing a novel FD test to connect the approaches for the characterization of the MDF. Finally, the relationship between both approaches when applied to both the state estimation and FD is illustrated by using a two-tanks case study

The remainder of this chapter is organized as follows: first, the problem formulation regarding state estimation for each approach and the way to relate them is discussed in Section 3.2. Then, the approaches are compared into the FD application context in Section 3.3. In Section 3.4, a case study based on a two-tanks system is proposed in order to show the aforementioned relationships and present the comparison results. Finally, in Section 3.5 the main conclusions of the chapter are drawn.

[1] As it was mentioned in Chapter 2, the set enclosing the state estimation considering uncertainty can be approximated by means of several geometrical shapes, e.g., polytopes [Bro12, WLSL15], ellipsoids [ZLX14, TSOMPE12, YL12, Com05] and zonotopes [XPOM$^+$15, LAC$^+$11, LSA$^+$13c, Com03].

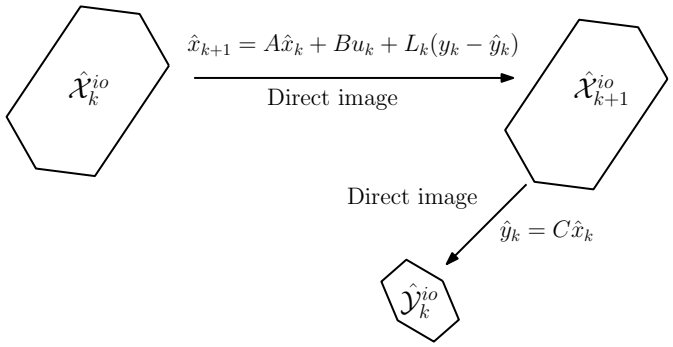

(a) State estimation using IOA.

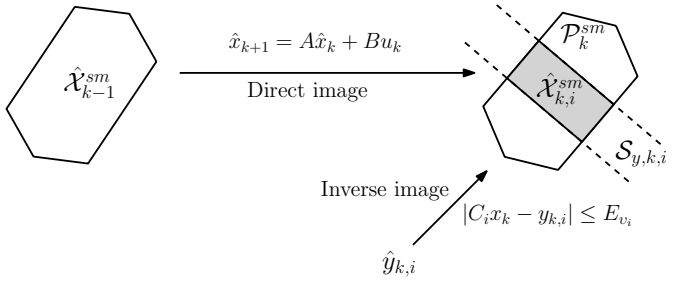

(b) State estimation using SMA.

Figure 3.1: Graphical interpretation of state estimation algorithms using IOA and SMA.

3.2 Comparison of IOA and SMA from the state estimation point of view

The state estimation using SMA and IOA is introduced in Chapter 2 based on [ABC05] and [Com15b], respectively. The main goal of this section is to compare both approaches from the state estimation point of view. Just for sake of clarity, the analytical comparison will be focused on the single-output case in this section as in [ABC05]. But, according to [LSA+13a], the generalization of the comparison can be easily extended to the multi-output case considering Remark 2.2. It is worth mentioning that there are other manners to formulate the state estimation for the multi-output case using SMA approach based on [LSA+13a].

Moreover, Proposition 3.1 can be used in order to obtain the comparable structure of the state estimation using IOA and SMA.

Proposition 3.1. *Considering the dynamical model (2.4) and the Luenberger observer structure in (2.5), the center and the shape matrix of the state-bounding observer, i.e., $\hat{\mathcal{X}}^{io} = \langle c_x^{io},\ R_x^{io} \rangle$ can be computed using*

$$c_x^{io} = c_p^{io} + L^{io}(y_- - C c_p^{io}), \tag{3.1a}$$

$$R_x^{io} = \begin{bmatrix} (I - L^{io}C)\bar{R}_p^{io} & -L^{io}E_v \end{bmatrix}, \tag{3.1b}$$

where

$$c_p^{io} = A c_{x,-}^{io} + B u_-, \tag{3.2a}$$

$$R_p^{io} = \begin{bmatrix} A\bar{R}_{x,-}^{io} & E_\omega \end{bmatrix}. \tag{3.2b}$$

Proof. According [LSA+13a], computation of the state-bounding observer using the Luenberger observer structure in (2.5) for the dynamical model (2.4) can be divided into two *prediction* and *update* steps. In the prediction step the estimated set at time instant $k-1$ is used to compute the priori estate estimation. Then, this prior state estimation is updated with the information from the measurement (the obtained estimated set in update step is called posteriori estimated set). Therefore, the prior state estimation set $\mathcal{P}^{io} = \langle c_p^{io},\ R_p^{io} \rangle$ can be computed using the system matrices A and B, and the input at the previous time step, i.e., u_- (using the knowledge of the system) as in (3.2). Then, the obtained set can be updated using the observer gain L^{io} as (3.1). □

So far, from the comparison of (2.19) with (3.1), it is still not evident how to relate both state estimation approaches because of the different temporal information of the measured output used for each approach. More precisely, the state estimation using the IOA considers information of the output measurements at the previous time instant while state estimation using SMA is obtained by using the information of the measurements at the current time instant. But, in the case that the parameter λ in SMA and the observer gain in IOA are identical, the same width of the state bounding zonotopes will be obtained. However, the center of the state bounding zonotopes are still different due to use of different temporal information of the measured output. Therefore, both state estimation approaches should be synchronized such that both use the measured output y given at the same time instant.

Thus, following [Oga95], the IOA proposed by [Com15b] can be modified leading to

a current IOA (CIOA) given by

$$\hat{\mathcal{X}}^{cio} = \langle c_x^{cio},\ R_x^{cio} \rangle, \tag{3.3}$$

where c_x^{cio} and R_x^{cio} denote the center and the segments of the zonotope (3.3) bounding the set of estimated states. Following the same idea as Proposition 3.1, by introducing the prior estimated set in prediction step as $\mathcal{P}_k^{cio} = \langle c_p^{cio},\ R_p^{cio} \rangle$, both center and segments of $\hat{\mathcal{X}}^{cio}$ can be propagated at the discrete-time instant k as

$$c_x^{cio} = c_p^{cio} + L^{cio}(y - Cc_p^{cio}), \tag{3.4a}$$

$$R_x^{cio} = \begin{bmatrix} (I - L^{cio}C)\bar{R}_p^{cio} & -L^{cio}E_v \end{bmatrix}, \tag{3.4b}$$

with

$$c_p^{cio} = Ac_{x,-}^{cio} + Bu_-, \tag{3.5a}$$

$$R_p^{cio} = \begin{bmatrix} A\bar{R}_{x,-}^{cio} & E_\omega \end{bmatrix}. \tag{3.5b}$$

As it can be seen from (3.4), the state estimation set $\hat{\mathcal{X}}^{cio}$ can be obtained based on the information of the measurement given at the current time instant. When using the CIOA, the similarity of the c_p^{cio} with the c_p^{sm} and also R_p^{cio} with R_p^{sm} can be observed by comparing (3.4) with (2.19). It can also be noted that, using the same initial condition for both approaches, i.e., x_0 belongs to the both initial zonotope $\hat{\mathcal{X}}_0^{cio} = \langle c_{x,0}^{cio},\ R_{x,0}^{cio} \rangle$ and $\hat{\mathcal{X}}_0^{sm} = \langle c_{x,0}^{sm},\ R_{x,0}^{sm} \rangle$, and taking into account the formulation of CIOA, the only difference between the approaches is related to the different manners of selecting the observer gain L^{cio} and the parameter λ.

According to [ABC05], state estimation using SMA is parametrized by means of a vector λ at each time instant k in (2.18) and the proposed method to minimize the size of the zonotope (2.18) is designed based on the minimization of its segments as it is introduced in Theorem 2.2. In addition, the optimal value of λ is obtained as in (2.23) according to [ABC05]. Therefore, if the observer gain is designed following Theorem 3.1, the state bounding zonotopes provided by CIOA and SMA are identical.

Theorem 3.1. *Considering the dynamical model (2.4) and $x \in \hat{\mathcal{X}}^{cio}$ at time k, the optimal observer gain $L^{cio,*}$ that minimizes the F-radius of the state-bounding zonotope in (3.3) at time instant $k+1$ is computed as*

$$L^{cio,*} = \left(R_x^{cio} R_x^{cio\top} C^\top\right) \left(C R_x^{cio} R_x^{cio\top} C^\top + E_v E_v^\top\right)^{-1}. \tag{3.6}$$

Proof. Taking into account the segments of the zonotope $\hat{\mathcal{X}}^{cio}$ are obtained as the columns of the matrix in (3.4b), the size of the estimated state at each time instant depends on the Frobenius norm of this matrix. Therefore, the optimal observer gain L^{cio} given by (3.6) is computed by minimizing the Frobenius norm of R_x^{cio} in (3.4). Furthermore, taking into account the fact that minimizing F-radius of a zonotope (which plays the same role as P-radius in LMI-based robust stability analysis) is equivalent to minimize the trace of its covariance and considering Definition B.7, it can be written that

$$\begin{aligned}
\left\|R_x^{cio}\right\|_{\mathrm{F}}^2 &= tr(R_x^{cio} R_x^{cio\top}) = tr\left(\begin{bmatrix}(I - L^{cio})CR_p^{cio} \\ -L^{cio}E_v\end{bmatrix}\begin{bmatrix}(I - L^{cio})CR_p^{cio} & -L^{cio}E_v\end{bmatrix}\right) \\
&= tr\left(\begin{bmatrix}\left((I - L^{cio})CR_p^{cio}\right)\left((I - L^{cio})CR_p^{cio}\right)^\top & \left((I - L^{cio})CR_p^{cio}\right)\left(-L^{cio}E_v\right)^\top \\ \left(-L^{cio}E_v\right)\left((I - L^{cio})CR_p^{cio}\right)^\top & \left(-L^{cio}E_v\right)\left(-L^{cio}E_v\right)^\top\end{bmatrix}\right) \\
&= \left((I - L^{cio})CR_p^{cio}\right)\left((I - L^{cio})CR_p^{cio}\right)^\top + \left(-L^{cio}E_v\right)\left(-L^{cio}E_v\right)^\top.
\end{aligned} \tag{3.7}$$

Therefore, the optimal value of the observer gain L^{cio} is determined such that $\dfrac{\partial \left\|R_x^{cio}\right\|_{\mathrm{F}}^2}{\partial L^{cio}} = 0$. Thus, by considering (3.7), it can be written that

$$-2R_p^{cio} R_p^{cio\top} + 2L^{cio,*} C R_p^{cio} R_p^{cio\top} C^\top + 2L^{cio,*} E_v E_v^\top = 0. \tag{3.8}$$

Finally, after the proper manipulation of (3.8), the optimal observer gain can be expressed as in (3.6). □

In the IOA case, the effect of measurements is considered through the selection of the observer gain. Thus, if the observer gain L^{io} is selected as proposed in (2.9) according to the standard IOA, the value of the observer gain will depend on the relative values of the measurement noise and input disturbances as in the SMA. It means, the gain in the IOA and λ in SMA plays the same role for state estimation.

Moreover, by designing the gain of the IOA as proposed by [Com15b], the formulation of the observer gain and the optimal parameter λ^* proposed by [ABC05] for the SMA, are identical because these parameters are independent with respect to the information of the output measurements. Thus, the temporal synchronization of both approaches

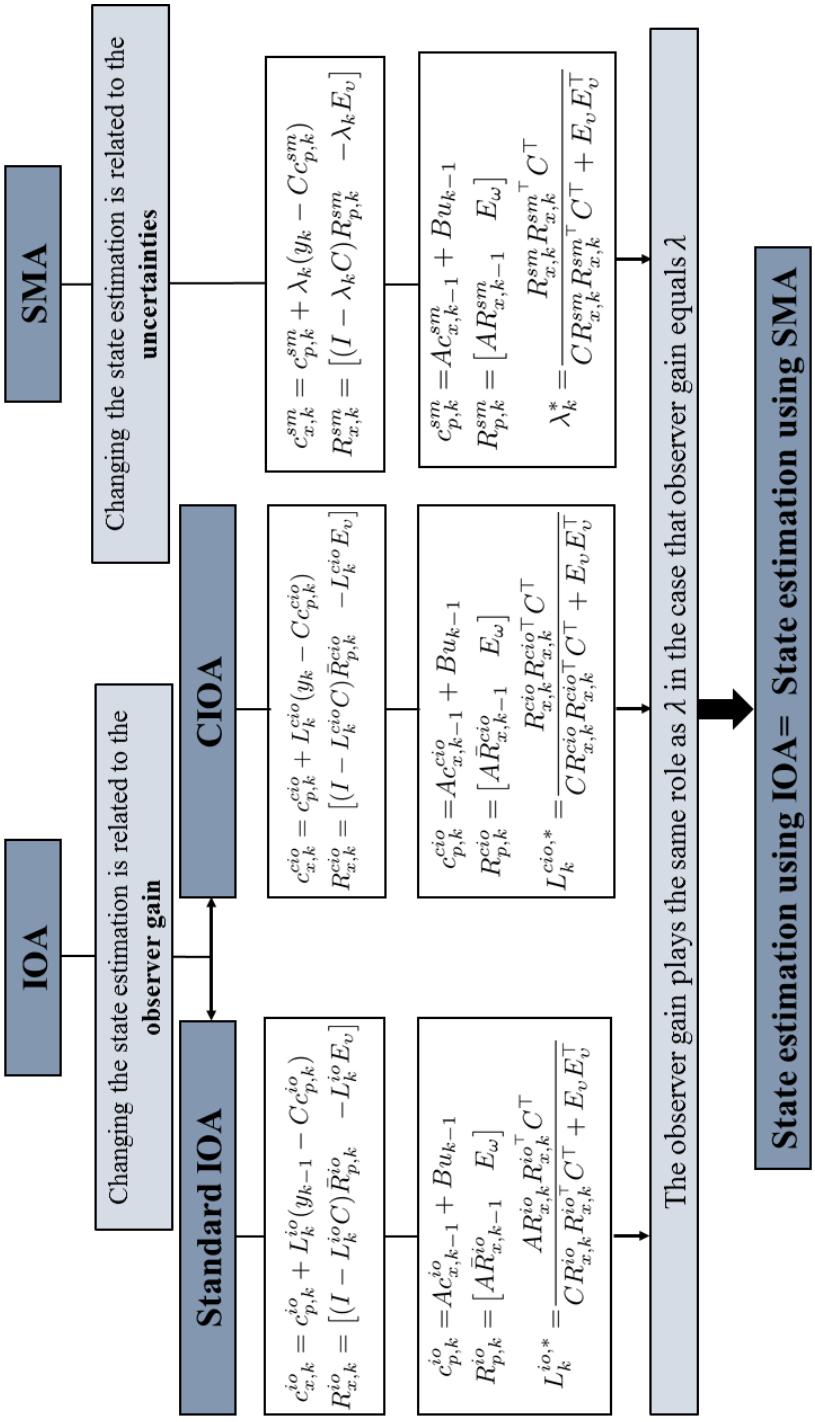

Figure 3.2: IOA and SMA in state estimation framework.

can be done if instead of the standard structure of the IOA, the CIOA is used. Later on, CIOA is proposed based on using the zonotopic definition of the set for modeling the bounded uncertainties. Consequently, the optimal gain of CIOA is obtained based on minimizing the size of the obtained zonotope in (3.3) whose center and shape matrix can be computed using (3.4). Therefore, the similarity of the SMA and the IOA is proved by introducing the CIOA. Figure 3.2 summarizes the comparison of the IOA and SMA.

3.3 Comparison of IOA and SMA from the FD point of view

Model-based FD is based on comparing the measured outputs from the system with their estimation using the model of the healthy system. If an inconsistency is detected, the existence of a fault will be proved. So far, in this chapter, IOA and SMA are both described and compared in the state estimation context. In this section, the comparison of both methods will be performed when applied to FD framework. In addition, the considered faults can be classified into different categories depending on their locations as

- actuator faults, which affects the system inputs,
- sensor faults that affect the measurements of the inputs and outputs of the system.

In this thesis, different actuator and sensor faults will be considered. Including their effect, the dynamical model (2.4) can be rewritten as

$$x_+ = Ax + Bu + E_\omega \omega + F_a f_a, \tag{3.9a}$$

$$y = Cx + E_\upsilon \upsilon + F_y f_y, \tag{3.9b}$$

where vectors $f_a \in \mathbb{R}^{n_u}$ and $f_y \in \mathbb{R}^{n_y}$ denote the actuator and output sensor faults with their associated matrices $F_a \in \mathbb{R}^{n_x \times n_u}$ and $F_y \in \mathbb{R}^{n_y \times n_y}$, respectively. Furthermore, the other type of fault that is considered in this thesis is known as input sensor fault which its effect is considered on the input of the observer (2.5) as

$$\hat{x}_+ = A\hat{x} + B\left(u + F_u f_u\right) + L(y - \hat{y}), \tag{3.10}$$

where $f_u \in \mathbb{R}^{n_u}$ represents the input sensor fault with its associated matrix $F_u \in \mathbb{R}^{n_u \times n_u}$.

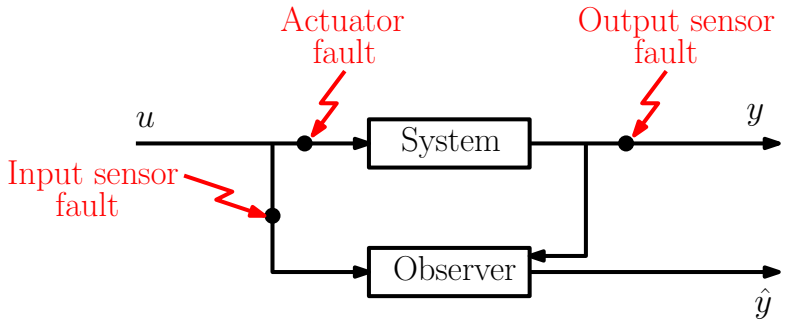

Figure 3.3: Graphical interpretation of the different actuator and sensors faults.

Figure 3.3 shows the schematic graphical interpretation of the different actuator and sensors faults.

Assumption 3.1. *The additive fault represented in* (3.9) *and* (3.10) *are assumed to be bounded by a unit hypercube expressed as centered zonotopes, i.e., for all* $k \geq 0$, $f_\bullet \in \langle 0,\ I_{n_{f_\bullet}} \rangle$, *where the subscript* $\bullet$ *can be respectively assigned to* y, u *or* a *associated with the considered output sensor, input sensor and actuator faults, respectively.*

□

The sensitivity of the residual to a fault characterizes how the different considered actuator and sensor faults affect the residual. Mathematically speaking, it can be obtained as the difference between the residuals that are obtained from healthy and faulty operations of the system presented in (2.4) and (3.9), respectively, normalized by the fault size [Ger98].

3.3.1 FD analysis using SMA

As it is mentioned in Appendix B, the FD test based on SMA can be done by using Algorithm 2.2. The graphical interpretation of the proposed FD test in healthy and faulty cases is shown in Figure 3.4. As it can be seen from Figure 3.4, $\mathcal{P}^{sm}$ and $\mathcal{S}$ are affected by the fault. Then, their intersection is empty. Consequently, the fault can be detected using Algorithm 2.2.

As shown in Appendix B, $\mathcal{P}^{sm}$ in the first step of Algorithm 2.2 can be computed as in (2.21) using (2.20). Then, given the zonotope $\mathcal{P}^{sm}$ in (2.21) and considering the

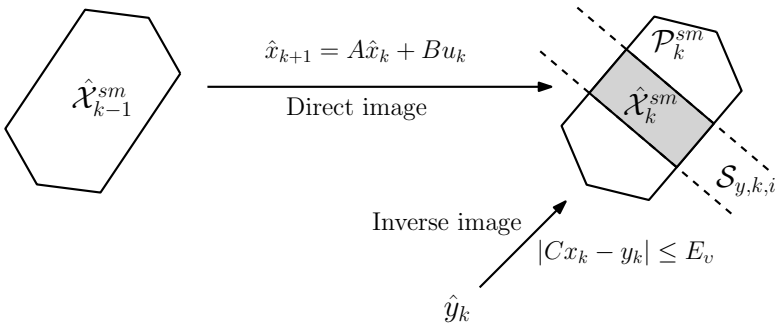

(a) Healthy operation of the system.

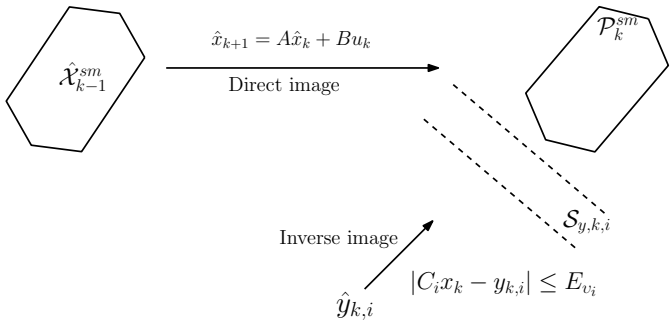

(b) Faulty operation of the system.

Figure 3.4: Graphical interpretation of FD test using the SMA.

vector C_i from each measurement (where index i indicates the i^{th} row), the zonotope support strip $\mathcal{S}_p^{sm}$ can be introduced at time instant k as

$$\mathcal{S}_p^{sm} = \left\{ x \in \mathbb{R}^{n_x} : \underline{s_{p,i}^{sm}} \leq C_i x \leq \overline{s_{p,i}^{sm}} \right\}, \tag{3.11}$$

where $\underline{s_{p,i}^{sm}}$ and $\overline{s_{p,i}^{sm}}$ are the minimum and the maximum values of the zonotope support strip, respectively, which can be computed as

$$\overline{s_{p,i}^{sm}} = C_i c_p^{sm} + \left\| R_p^{sm^\top} C_i^\top \right\|_1, \tag{3.12a}$$

$$\underline{s_{p,i}^{sm}} = C_i c_p^{sm} - \left\| R_p^{sm^\top} C_i^\top \right\|_1. \tag{3.12b}$$

As can be seen in (3.12), the effect of state disturbance is embedded in matrix R_p^{sm} that can be computed using (2.20b). Similarly, in order to consider the effect of measurement noise from the second step of the Algorithm 2.2, the strip $\mathcal{S}_y$ in (2.22) can

be rewritten for each output as

$$\mathcal{S}_{y_i} = \{x \in \mathbb{R}^{n_x} : |y_i - C_i x| \leq E_{v,i}\}, \tag{3.13}$$

where y_i indicates each output measurement. The normalized form of the strip $\mathcal{S}_y$ can be derived as

$$\mathcal{S}_{y_i} = \left\{x \in \mathbb{R}^{n_x} : -1 \leq \frac{y_i}{E_{v,i}} - \frac{C_i}{E_{v,i}} x \leq +1\right\}. \tag{3.14}$$

In general, each measurement allows to determine a set of consistent states as it is defined in (3.13), where $\mathcal{S}_y$ is the region between two hyperplanes that is normalized in (3.14). Then, based on [LSA+13b], the computation of measurement strip can be done using (3.14) that is considered component-wise. Thus, $\overline{s_{y,i}}$ and $\underline{s_{y,i}}$ values of the strip $\mathcal{S}_y$ can be calculated at each time instant k by using the measurement data in (3.14) as

$$\overline{s_{y,i}} = \frac{y_i}{E_{v,i}} + 1, \tag{3.15a}$$

$$\underline{s_{y,i}} = \frac{y_i}{E_{v,i}} - 1. \tag{3.15b}$$

Then, the intersection between the zonotope support strip in (3.11) and the measurement strip in (3.14) is empty if

$$\underline{s^{sm}_{p,i}} > \overline{s_{y,i}}, \tag{3.16a}$$

$$\overline{s^{sm}_{p,i}} < \underline{s_{y,i}}. \tag{3.16b}$$

Consequently, the fault will be detected if one of the conditions in (3.16) is satisfied. Based on conditions (3.16), the minimum detectable abrupt fault will be characterized for the considered type of faults assuming that are introduced as in (3.9) and (3.10).

Case I: Minimum detectable output sensor fault

The dynamical model (3.9) in the case of output sensor fault can be rewritten as follows:

$$x_+ = Ax + Bu + E_\omega \omega, \tag{3.17a}$$

$$y = Cx + E_v v + F_y f_y. \tag{3.17b}$$

Therefore, the minimum magnitude of output sensor fault that can be detected is obtained by considering conditions (3.16) and following Theorem 3.2.

Theorem 3.2. *(Minimum detectable output sensor fault) Considering the faulty dynamical model (3.17) and the conditions (3.16), the minimum detectable abrupt output sensor fault can be characterized as*

$$\mathfrak{F}_{y,i}\, f_{y,i} > 2 \left\| R_p^{sm^\top} C_i^\top \right\|_1 + 2, \tag{3.18}$$

where the term $\mathfrak{F}_y = \dfrac{F_y}{E_\upsilon}$ *represents the sensitivity with respect to the considered output sensor fault while the obtained expression for the output sensor fault is normalized using* E_υ*. Moreover, the value* 2 *refers to the consideration of the worst-case scenario, i.e., the prediction is considered with the extreme value (it is located at either the lower or the upper bound of the considered threshold).*

Proof. Following Algorithm 2.2, it can be written that

$$C_i c_p^{sm} + \left\| R_p^{sm^\top} C_i^\top \right\|_1 < \frac{y_i}{E_{\upsilon,i}} - 1. \tag{3.19}$$

Then, considering the dynamical model (3.17), (3.19) becomes

$$C_i c_p^{sm} + \left\| R_p^{sm^\top} C_i^\top \right\|_1 < C_i x + \frac{\upsilon_i}{E_{\upsilon_i}} + \mathfrak{F}_{y,i}\, f_{y,i} - 1. \tag{3.20}$$

Moreover, by considering the worst-case scenario, where the disturbances have a maximal influence in the opposite direction compared to that of the occurring fault, (3.20) can be written in faultless scenario, i.e., $f_y = 0$, as

$$C_i c_p^{sm} + \left\| R_p^{sm^\top} C_i^\top \right\|_1 = C_i x + \frac{\upsilon_i}{E_{\upsilon_i}} - 1. \tag{3.21}$$

Then, considering the worst-case scenario, (3.19) can be written as $C_i c_p^{sm} + \left\| R_p^{sm^\top} C_i^\top \right\|_1 = 2 \left\| R_p^{sm^\top} C_i^\top \right\|_1$. It means, x is placed in the border of the zonotope support strip (the measurement strip is placed in the farthest possible location). Furthermore, minimizing $C_i x + \dfrac{\upsilon_i}{E_{\upsilon_i}}$, the minimum detectable abrupt output sensor fault can be expressed as in (3.18). □

Case II: Minimum detectable input sensor fault

The minimum detectable input sensor fault can be computed considering the faulty input that is injected to the model as in (3.10). Therefore, in this case, the model/observer is affected by the faulty input. In this regard, (2.20) is expressed as

$$c_p^{sm} = Ac_{x,-}^{sm} + B(u_- + F_u f_{u,-}), \tag{3.22a}$$

$$R_p^{sm} = \begin{bmatrix} AR_{x,-}^{sm} & E_\omega \end{bmatrix}. \tag{3.22b}$$

Now, the FD test is based on Algorithm 2.2. Moreover, the computation of the minimum magnitude of the abrupt input sensor fault that can be detected can be determined by means of Theorem 3.3.

Theorem 3.3. *(Minimum detectable input sensor fault) Considering* (3.22) *and the conditions* (3.16)*, the minimum detectable abrupt input sensor fault can be expressed as*

$$\mathfrak{F}_{u,i}\, f_{u,i} > 2 \left\| R_p^{sm^\top} C_i^\top \right\|_1 + 2, \tag{3.23}$$

where the term $\mathfrak{F}_u = -CBF_u$ *is the sensitivity with respect to the considered input sensor fault.*

Proof. Considering that Algorithm 2.2 can be used for detecting the fault based on SMA, the FD test is performed by checking the intersection between the zonotope support strip and the measurement strip that can be computed in the same way as in (3.12) and (3.15), respectively. Thus, in the case of input sensor fault, the conditions (3.16) can be rewritten as

$$C_i c_p^{sm} + \mathfrak{F}_{u,i}\, f_{u,i} + \left\| R_p^{sm^\top} C_i^\top \right\|_1 < \frac{y_i}{E_{v,i}} - 1. \tag{3.24}$$

Hence, by assuming the worst-case scenario, the expression (3.23) can be obtained by the suitable manipulation of (3.24). □

It is worth mentioning that the detection of the input sensor fault depends on the direction of vector C and the input of the system. Thus, the input should be designed to guarantee that the input sensor fault is not in the orthogonal direction of vector C. Otherwise, the fault can not be detected.

Case III: Minimum detectable actuator fault

The faulty dynamical model (3.9) in the case of actuator fault is rewritten as

$$x_+ = Ax + Bu + E_\omega \omega_k + F_a f_a, \tag{3.25a}$$

$$y = Cx + E_\upsilon \upsilon. \tag{3.25b}$$

The minimum magnitude of abrupt actuator fault that can be detected is obtained by considering (3.16) and following Theorem 3.4.

Theorem 3.4. *(Minimum detectable actuator fault) Considering the dynamical model (3.25) and the conditions (3.16), the minimum detectable abrupt actuator fault can be computed as*

$$\mathfrak{F}_{a,i}\ f_{a,i} > 2 \left\| R_p^{sm^\top} C_i^\top \right\|_1 + 2, \tag{3.26}$$

where $\mathfrak{F}_a = CF_a$ is the sensitivity with respect to the given actuator fault.

Proof. Considering the faulty dynamical model (3.25) and conditions (3.16) to guarantee the detection of the fault, it can be written as

$$C_i c_p^{sm} + \left\| R_p^{sm^\top} C_i^\top \right\|_1 < C_i x + \frac{\upsilon_i}{E_{\upsilon,i}} + \mathfrak{F}_{a,i}\ f_{a,i} - 1. \tag{3.27}$$

Therefore, the expression of the minimum detectable actuator fault can be obtained as it is written in (3.26) by considering the worst-case scenario and adequate manipulation of (3.27). □

Similarly to the case of input sensor fault, the minimum magnitude of the actuator fault that can be detected is related to the direction of the vector C and the input. Therefore, the input should be designed to avoid the problem of having the actuator fault and vector C in the same orthogonal direction.

Remark 3.1. *It can be noted that the interpretation of the term $2 \left\| R_p^{sm^\top} \right\|_1$ in the case of SMA stands for the width of the zonotopes $\mathcal{P}^{sm}$ in (2.21), where the effect of state disturbance is taken into account. On the other hand, the effect of measurement noise is considered through $\mathcal{S}_y$ in (3.14). Then, based on the consideration of the two mentioned uncertainties, it can be guaranteed that a fault to be detectable should have a higher effect in comparison with the effect of uncertainties. Therefore, the characterized MDF*

Algorithm 3.1 Strip-based FD test using IOA

$k \longleftarrow 0$
$\mathcal{X}_0^{io} = \langle c_{x,0}^{io},\ R_{x,0}^{io} \rangle$
while 1 **do**
  Obtain and store input-output data $\{u_k, y_k\}$
  Compute the state estimation $\hat{\mathcal{X}}_k^{io}$ using (3.1)
  Compute the strip from the measured output $\mathcal{S}_{y,k}$ using (2.22)
  if $\hat{\mathcal{X}}_k^{io} \cap \mathcal{S}_{y,k} = \emptyset$ **then**
    $Fault \leftarrow true$
  else
    $Fault \leftarrow false$
  end if
  $k \longleftarrow k + 1$
end while

is known as the smallest magnitude of the considered fault whose effect is higher than the effect of the uncertainties. □

3.3.2 FD analysis using IOA

Now, the IOA is applied to FD in order to characterize the MDF for the same type of considered faults than in the case of SMA. The standard procedure of the FD test based on IOA relies on checking the inconsistency of the measurements with their provided estimations by the observer model. In other words, any inconsistency between the measured outputs using sensors and the estimated behavior that is computed by using the system model, called residual, is known as a fault occurrence[2].

However, considering the standard method of residual generation in order to characterize the MDF, it is not possible to determine a clear relationship of IOA and SMA in FD framework since a common FD test that allows relating both approaches is required. A possible solution in order to homogenize the approaches is to use the zonotope support strip in the case of IOA for formulating the FD conditions. In this context, the generated residual is formulated in terms of strip mathematical expression that can be compared with the SMA. Moreover, the strip $\mathcal{S}_y$ can be obtained using (3.14) at each time instant k, where the effect of the measurement noise is taken into account (same as the second step in the case of SMA mentioned in Section 2.3). On the other hand, considering the vector C, the zonotope support strip S_x^{io} can be defined for $\hat{\mathcal{X}}^{io}$ based

[2]See [Ger98] for further details.

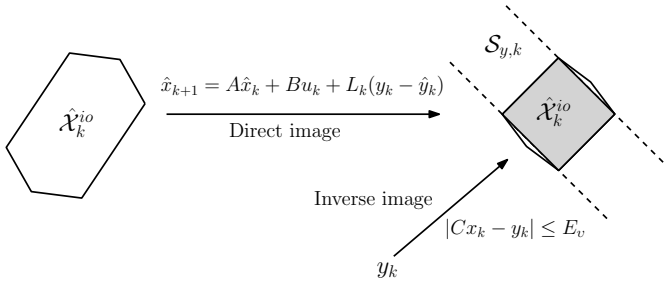

(a) Healthy operation of the system.

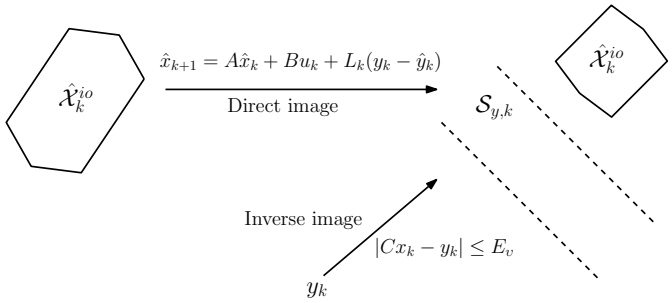

(b) Faulty operation of the system.

Figure 3.5: Graphical interpretation of the strip-based FD test using IOA.

on using the state estimation of the IOA in (3.1) at each time instant k as

$$S_x^{io} = \left\{ x \in \mathbb{R}^{n_x} : \underline{s_{x,i}^{io}} \leq C_i x \leq \overline{s_{x,i}^{io}} \right\}, \tag{3.28}$$

where $\underline{s_{x,i}^{io}}$ and $\overline{s_{x,i}^{io}}$ are the minimum and the maximum values of the zonotope support strip, respectively. Furthermore, $\overline{s_{x,i}^{io}}$ and $\underline{s_{x,i}^{io}}$ are determined at each time instant k as

$$\overline{s_{x,i}^{io}} = C_i c_x^{io} + \left\| R_x^{io^\top} C_i^\top \right\|_1, \tag{3.29a}$$

$$\underline{s_{x,i}^{io}} = C_i c_x^{io} - \left\| R_x^{io^\top} C_i^\top \right\|_1. \tag{3.29b}$$

Remark 3.2. *The effect of the state disturbance is embedded into matrix R_x^{io}, which can be computed using (3.1b).* □

Therefore, the existence of the fault will be proved by checking

$$\hat{\mathcal{X}}^{io} \cap \mathcal{S}_y = \emptyset, \tag{3.30}$$

such that in the case of empty intersection, the fault will be detected. Otherwise, FD cannot be guaranteed. Thus, one of the following conditions should be satisfied in the case of faulty operation of the system:

$$\underline{s^{io}_{x,i}} > \overline{s_{y,i}}, \tag{3.31a}$$

$$\overline{s^{io}_{x,i}} < \underline{s_{y,i}}. \tag{3.31b}$$

Algorithm 3.1 summarizes the strip-based FD test using IOA. Moreover, the graphical interpretation of Algorithm 3.1 is shown in Figure 3.5.

Next, the FD performance for different type of abrupt faults will be characterized when the FD test in (3.30) is considered.

Case I: Minimum detectable output sensor fault

The system to be monitored in the case of output sensor fault can be described as (3.17). Considering the zonotope support strip in (3.29) and the normalized form of the measurements strip in (3.15), the minimum detectable abrupt output sensor fault based on the IOA can be computed by using Theorem 3.5.

Theorem 3.5. *(Minimum detectable output sensor fault) Considering the faulty dynamical model* (3.17) *and the conditions* (3.31)*, the minimum magnitude of the abrupt output sensor fault that is detectable in one step can be computed as*

$$\mathfrak{F}_{y,i}\, f_{y,i} > 2 \left\| R_x^{io^\top} C_i^\top \right\|_1 + 2, \tag{3.32}$$

Proof. Considering the dynamical model (3.17), by substituting the zonotope support strip in (3.29) and the normalized form of the measurements strip in (3.15) into one of the faulty conditions (3.31) yields

$$C_i c_x^{io} + \left\| R_x^{io^\top} C_i^\top \right\|_1 < C_i x + \frac{\upsilon_i}{E_{\upsilon_i}} + \mathfrak{F}_{y,i}\, f_{y,i} - 1. \tag{3.33}$$

Moreover, considering the worst-case value of x and minimizing $C_i x + \frac{\upsilon_i}{E_{\upsilon_i}}$, the minimum detectable output sensor fault can be characterized as in (3.32) after the algebraic manipulation of (3.33). □

Case II: Minimum detectable input sensor fault

Considering the faulty input for the observer model (3.10), (3.1) can be rewritten as

$$c_x^{io} = (Ac_{x,-}^{io} + B(u_- + F_u f_{u,-})) + L^{io}(y_- - C(Ac_{x,-}^{io} + B(u_- + F_u f_{u,-}))), \quad (3.34a)$$

$$R_x^{io} = \begin{bmatrix} (I - L^{io}C)\bar{R}_p^{io} & -L^{io}E_v \end{bmatrix}, \quad (3.34b)$$

Now, by considering (3.34), the minimum detectable abrupt input sensor fault can be calculated by the following Theorem 3.6.

Theorem 3.6. *(Minimum detectable input sensor fault) Considering the faulty model (3.34) and the conditions (3.31), the minimum detectable abrupt input sensor fault can be characterized as*

$$\mathfrak{F}_{u,i}\ f_{u,i} > 2 \left\| R_x^{io^\top} C_i^\top \right\|_1 + 2, \quad (3.35)$$

Proof. Considering the faulty model (3.34), the faulty conditions (3.31) can be rewritten by using (3.29) and (3.15) as

$$C_i c_x^{io} + \mathfrak{F}_{u,i}\ f_{u,i} + \left\| R_x^{io^\top} C_i^\top \right\|_1 < \frac{y_i}{E_{v,i}} - 1. \quad (3.36)$$

Then, the minimum detectable input sensor fault can be characterized as (3.35) by assuming the worst-case scenario and the corresponding manipulation of (3.36). □

Note from (3.35) that the magnitude of the minimum detectable input sensor fault depends on the input and the direction of the vector C. Therefore, the input u should be designed in the way that the orthogonal direction of the vector C and the direction of the given fault will be different. Otherwise, the input sensor fault will never be detected.

Case III: Minimum detectable actuator fault

Considering the faulty dynamical model (3.25), the minimum detectable abrupt actuator fault can be computed following the Theorem 3.7.

Theorem 3.7. *(Minimum detectable actuator fault) Considering the faulty dynamical model (3.25) and the conditions (3.31), the minimum detectable abrupt actuator fault*

can be calculated as

$$\mathfrak{F}_{a,i}\ f_{a,i} > 2\left\|R_x^{io^\top} C_i^\top\right\|_1 + 2. \tag{3.37}$$

Proof. Considering the dynamical model (3.25) and inserting the strips (3.29) and (3.15) into one of the faulty conditions (3.31) yields

$$C_i c_x^{io} + \left\|R_x^{io^\top} C_i^\top\right\|_1 < C_i x + \frac{\upsilon_i}{E_{\upsilon,i}} + \mathfrak{F}_{a,i}\ f_{a,i} - 1. \tag{3.38}$$

Consequently, the minimum magnitude of the actuator fault that can be detected is derived based on (3.38) by assuming the worst-case value of x and υ as it is expressed in (3.37). □

Additionally, the detection of the actuator fault is related to the orthogonal direction of the vector C. Thus, in order to guarantee the FD, the input u should be designed in such a way that the orthogonal direction of the vector C and the direction of the given fault will be different.

3.3.3 Comparative assessment

Algorithm 3.1 leads to obtain the comparable structure of the IOA and the SMA in FD framework. Consequently, the minimum detectable abrupt fault that is derived by the presented approaches can be compared with each other under this circumstance. Therefore, the key point of FD test is to check the intersection between the measurement strip and the state estimation support strip comparing Algorithm 2.2 with Algorithm 3.1.

Actually, the formulation of the MDF is characterized based on the conditions (3.16) and (3.31) considering Algorithms 2.2 and 3.1 for both the SMA and IOA, respectively. As it can be observed from Algorithms 2.2 and 3.1, the effect of the measurement noise is considered when determining the measurement strip (3.13) in both approaches. Furthermore, in the case of SMA, the effect of state disturbance is considered through the computation of zonotope support strip in (3.11), where the state disturbance effect is embedded in the matrix R_p^{sm} that can be obtained using (2.20b). Moreover, in the case of IOA, the effect of the state disturbance is taken into account similarly as the IOA through the zonotope support strip (3.28), where the state disturbance effect is embedded in the matrix R_x^{io} that can be obtained using (3.1b). In both IOA and SMA, the strip from the

measurement data can be obtained considering the unknown but bounded uncertainties as in (3.14), where the normalized form of the maximum and the minimum values of the output prediction can be defined as upper and lower bounds of the strip that is formulated in (3.15). On the other hand, the supporting hyperplanes are characterized using the obtained sets from state estimation. Then, according to Algorithm 2.2, the approximated set of the estimated states $\mathcal{P}^{sm}$ can be used for computing the zonotope support strip in (3.12). Meanwhile, according to Algorithm 3.1, the zonotope support strip that is computed in (3.29) is generated using the state-bounding zonotope $\hat{\mathcal{X}}^{io}$.

Furthermore, the minimum detectable sensor and actuator faults are characterized based on the SMA in (3.18), (3.23) and (3.26), respectively. Besides, the minimum magnitude of same kind of faults that can be detected are derived in (3.32), (3.35) and (3.37) based on IOA.

From the mathematical comparison of both approaches, it can be noted that in the SMA, the MDF magnitude depends on the width of the zonotope $\mathcal{P}^{sm}$, which is obtained from the first step of its state estimation algorithm. On the other hand, the characterization of the MDF in the IOA depends on the width of the zonotope $\hat{\mathcal{X}}^{io}$, which is obtained from its state estimation. Indeed, the magnitude of the MDF in SMA is related to the R_p^{sm} that is obtained based on (2.20b) as $R_p^{sm} = \begin{bmatrix} AR_{x,-}^{sm} & E_\omega \end{bmatrix}$. Besides, the minimum magnitude of the fault that can be detected based on IOA depends on R_x^{io} that, according to (3.1), it can be written as $R_x^{io} = \begin{bmatrix} (I - L^{io}C)\bar{R}_p^{io} & -L^{io}E_\upsilon \end{bmatrix}$.

Furthermore, the influence of the observer gain should be considered in computing the MDF. It means, in the IOA, the observer gain L^{io} is not only designed to guarantee the convergence of the observer, but also it can be used to guarantee the desired FD performance. From the mathematical point of view, when the observer gain is considered null ($L^{io} = 0$), the same formulation of the MDF is obtained in both approaches since $R_x^{io} = R_p^{sm}$. But, it should be considered that in the case that $L^{\text{io}} = 0$, the observer becomes a simulator and it can only be used in ideal conditions and with perfect knowledge of the initial states. Thus, in the case of $L^{io} = 0$, the MDF determined by the SMA and IOA are identical. Otherwise, the FD test using IOA is more conservative in general than the SMA one.

Moreover, as it was explained before, the difference between the IOA and SMA in the state-estimation framework is related to the use of different temporal information from the given measurement y. Therefore, by considering the same initial conditions,

the same values of λ^* and $L^{io,*}$ can be obtained in steady state when using (2.23) and (2.9), respectively. Furthermore, if $\lambda^* = L^{io,*}$ and when k tends to infinity, it will be obtained that $R^{io}_{x,\infty} = R^{sm}_{p,\infty}$. Then, the only difference is related to the center of the state bounding zonotope. Therefore, the identical MDF can be computed based on both IOA and SMA since the mathematical expression of the minimum magnitude of the fault that can be detected is independent of the center of the state-bounding zonotope.

Furthermore, the advantage of IOA is related to the observer gain that can be tuned to obtain better FD performance. Moreover, another advantage of IOA in comparison with SMA is related to fact that after occurrence the fault, it is not possible to monitor the system behaviour with the SMA. But, IOA can monitor the system even after the fault occurrence. This issue is a major limitation in the use of SMA in FD applications.

In Section 3.3, the approaches are synchronized by modifying IOA to the form of CIOA from state estimation point of view. Using the information of the measurements at current time instant based on the CIOA leads to obtain the same state estimation using IOA and SMA[3]. So far, according to Algorithm 3.1, the strip can be obtained using (2.22) and the state estimation is obtained using (3.4). When the current information of the output for state estimation is used, both (2.22) and (3.4) are influenced by the fault, simultaneously. Therefore, the empty intersection cannot be obtained since (2.22) and (3.4) are moved together by the influence of the fault. Therefore, the intersection will never be empty. Consequently, the fault will never be detected. Hence, the CIOA can not be used for FD. Figure 3.6 summarizes the comparison of the IOA and SMA when applied to FD.

[3]See the formulation of the state estimation in (3.4).

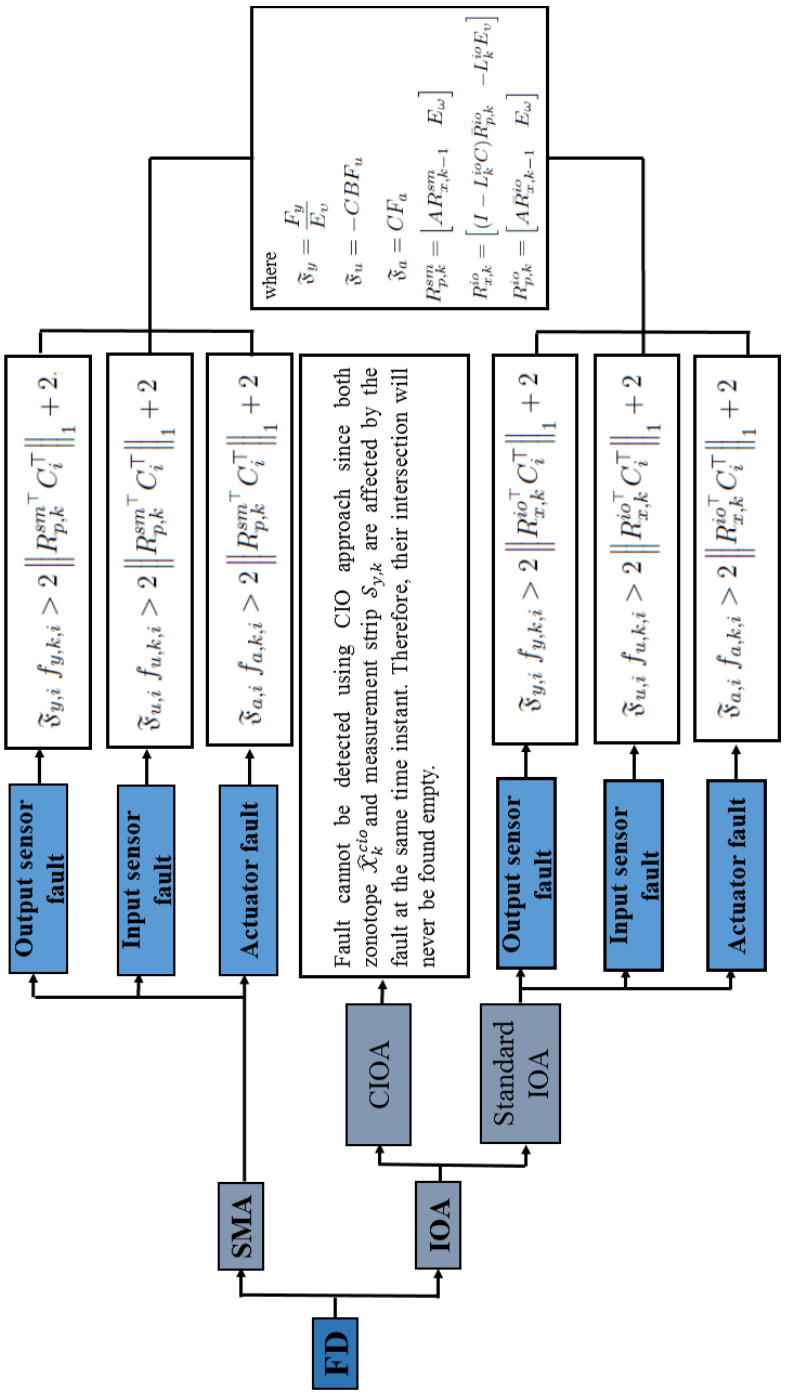

Figure 3.6: IOA and SMA applied to FD.

3.4 Case study

3.4.1 Plant description

The illustration of comparative analysis of IOA and SMA will be performed by using the two-tanks system, which is based on [Joh00]. For a description of this application example see Section A.2 in Appendix A.

Moreover, bounded disturbances influencing all the state-space directions and the measurement noise are modeled respectively with E_ω and E_υ as

$$E_\omega = \begin{bmatrix} 0.08 & 0 \\ 0 & 0.08 \end{bmatrix}, \quad E_\upsilon = \begin{bmatrix} 0.01 \end{bmatrix}. \tag{3.39}$$

3.4.2 State estimation

In this section, the state estimation using IOA, CIOA and SMA is compared in order to validate the obtained mathematical analyses presented in Section 3.2.

As it is derived in Section 2.3.2, the state estimation using SMA in (2.18) at time instant k can be obtained by using Proposition 2.4. On the other hand, the state estimation based on IOA at time instant k can be computed using the following information of the output measurement:

- the information of the measured output at the previous time instant y_{k-1} using Proposition 3.1,
- the information of the measured output at the current time instant y_k using (3.3), (3.4) and (3.5).

The state estimation using IOA, CIOA and SMA approaches at time instant $k = 100$ are shown in Figure 3.7. As can be observed from Figure 3.7, the state estimation using the IOA and CIOA are different because of the different temporal information of the measured output. But, when the CIOA is used instead of IOA, the identical state estimation as SMA will be obtained. Notice that the same initial conditions are considered for obtaining the results in Figure 3.7. During the simulation, the optimal value of the parameter λ is determined by (2.23) when using the SMA.

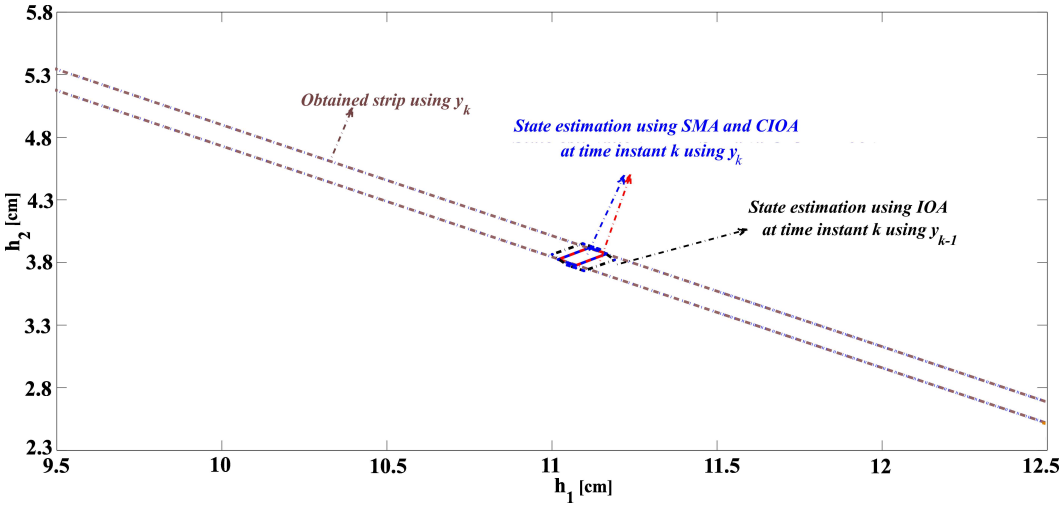

Figure 3.7: State estimation in the state space.

Table 3.1: The constants $L^{io,*}$, $L^{cio,*}$ and λ^* in steady state.

SMA	**Standard IOA**	**CIOA**
$\lambda^*_\infty = \begin{bmatrix} 0.6980 \\ 0.6221 \end{bmatrix}$	$L^{io,*}_\infty = \begin{bmatrix} 0.6980 \\ 0.6221 \end{bmatrix}$	$L^{cio,*}_\infty = \begin{bmatrix} 0.6980 \\ 0.6221 \end{bmatrix}$

In addition, the observer gain in the case of IOA and the observer gain in the case of CIOA are computed using (2.9) and (3.6), respectively. Further analysis is done during steady-state operation of the system in order to compare the distinct gains using observer-based approaches (i.e., IOA and CIOA) and parameter λ in the SMA since the computed $L^{io,*}$, $L^{cio,*}$ and λ^* are constant when k tends to infinity. Looking at (2.23), (2.9) and (3.6), it can be noted that the values of λ^*, $L^{io,*}$ and $L^{cio,*}$ are independent parameters with respect to the information of the measured output, i.e., these parameters are designed to minimize the size of the state bounding zonotope. Therefore, by using the same initial conditions, the same values of λ^*, $L^{io,*}$ and $L^{cio,*}$ can be obtained in steady state when using (2.23), (2.9) and (3.6). In this regard, Table 3.1 shows the obtained results during steady-state operation of the system from the simulation of the approaches.

Moreover, the time evaluation of the state estimation can be computed at each time

Table 3.2: MDF during steady state.

	Actuator fault		**Input sensor fault**		**Output sensor fault**
	f^{a_1}	f^{a_2}	f^{u_1}	f^{u_2}	f^{y_1}
SMA	±0.285	±0.66	±0.2 V	±0.04 V	±0.7 V
IOA	±0.285	±0.66	±0.2 V	±0.04 V	±0.7 V

instant. The interval hull of the state estimation is projected into the output space by using the system matrix C. Figure 3.8 is obtained from the simulation as a result of the projection of the state estimation into the output space. Note from Figure 3.8 that the maximum and the minimum bounds of the obtained zonotopic state estimations using both CIOA and SMA are the same. But, there is one-time-instant delay between the results obtained using the standard IOA and the other approaches since the information of the output measurement at $k-1$ given k is used in IOA.

In order to emphasize the difference between the IOA and the other approaches, the center of the zonotopic state estimations are projected into the output space and shown in Figure 3.8. It can be observed from Figure 3.8, the center of the zonotopic state estimations are determined using CIOA and SMA approaches are the same.

3.4.3 Application to FD

In this section, the extension of the comparison of both IOA and SMA approaches is performed when applied to FD. Although, as shown in the previous section, both CIOA and SMA approaches are equivalent when applied to state estimation CIOA cannot be used for FD tasks as discussed in Section 3.3. Thus, instead of using CIOA this section considers IOA for comparison purposes. The comparison is based on the minimum fault magnitude that can detect the considered approaches. In this regard, the same actuator and sensor fault scenarios as Section 3.3 are considered in this case study.

The minimum detectable output sensor, input sensor and actuator faults can be computed using Theorems 3.2, 3.3 and 3.4 for the IOA and Theorems 3.2, 3.3 and 3.4 for SMA, respectively. The obtained results are reported in Table 3.2, all of them evaluated in steady-state regime.

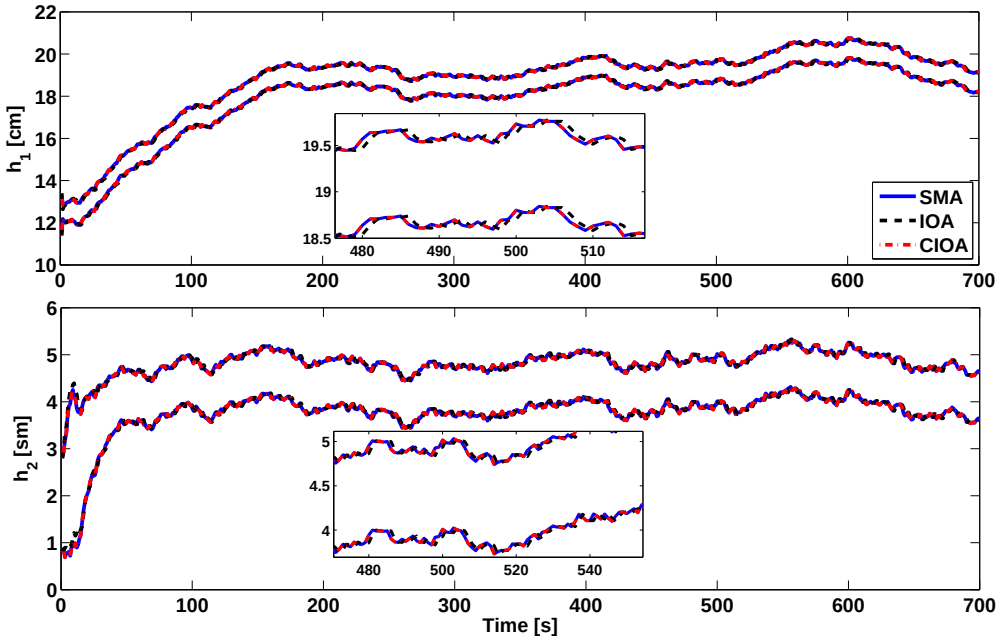

(a) Projection of the state estimation into the output space.

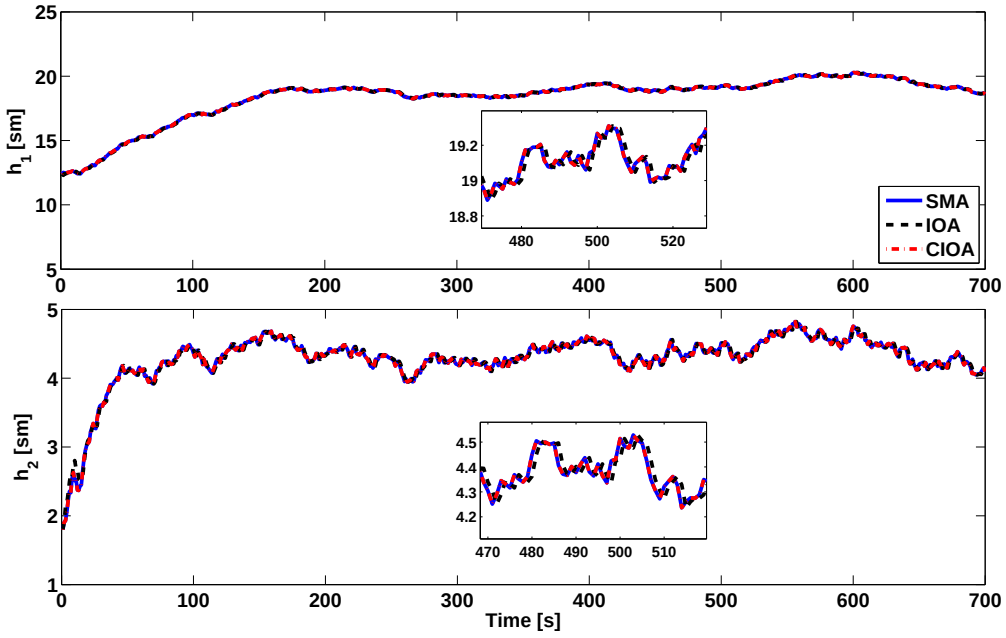

(b) The centers of the projection of the state estimation into the output space.

Figure 3.8: State estimation into the output space.

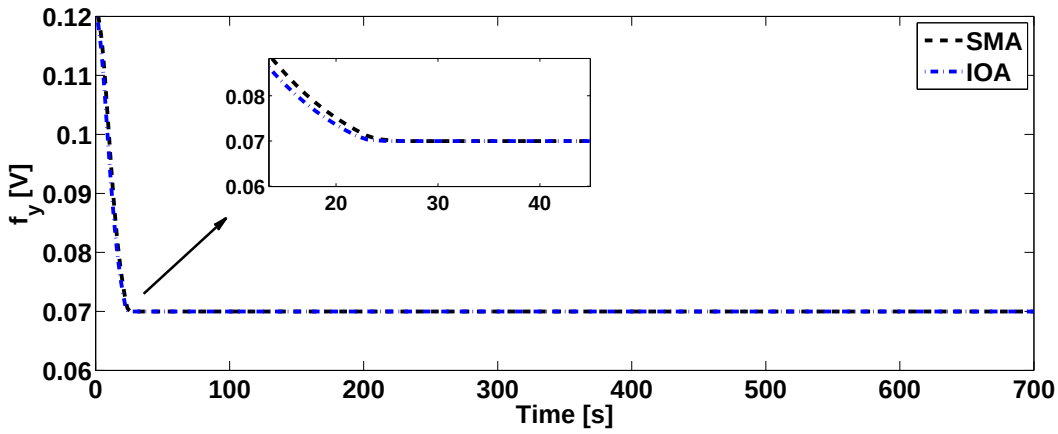

Figure 3.9: Minimum detectable output sensor fault.

According to Table 3.2, the minimum magnitude of the sensor and actuator faults able to be detected through the use of both SMA and IOA are identical since the zonotope-shape matrices of the state estimations are also identical when using both approaches in steady state, i.e., $R^{io}_{x,\infty} = R^{sm}_{p,\infty}$. Therefore, as discussed in Section 3.3, the use of both SMA and IOA results in the same MDF magnitudes in steady state.

For the purpose of further analysis, a sensor fault scenario, affecting the output sensor, is considered in whole time range (no only in steady state). Figure 3.9 shows the minimum magnitude of the output sensor fault that can be detected using both SMA and IOA. Based on the results shown in Figure 3.9, IOA conservativeness is slightly greater with respect to SMA during the transient regime. However, as already presented in Table 3.2 and shown in Figure 3.9, the same MDF magnitude is obtained during steady state since $R^{io}_{x,\infty} = R^{sm}_{p,\infty}$. Moreover, Table 3.2 shows that if the magnitude of the considered fault satisfies $f_y > 0.7$ V, it will be detectable for both SMA and IOA. Otherwise, it will be not detectable by any of both approaches. In the following, this result will be verified in simulation considering two scenarios where the fault appears at time instant $k = 200$ and its magnitude changes as follows:

- Scenario 1: Output sensor fault $f_y = 0.8$, i.e., slightly bigger than 0.7,
- Scenario 2: Output sensor fault $f_y = 0.6$, i.e., slightly smaller than 0.7.

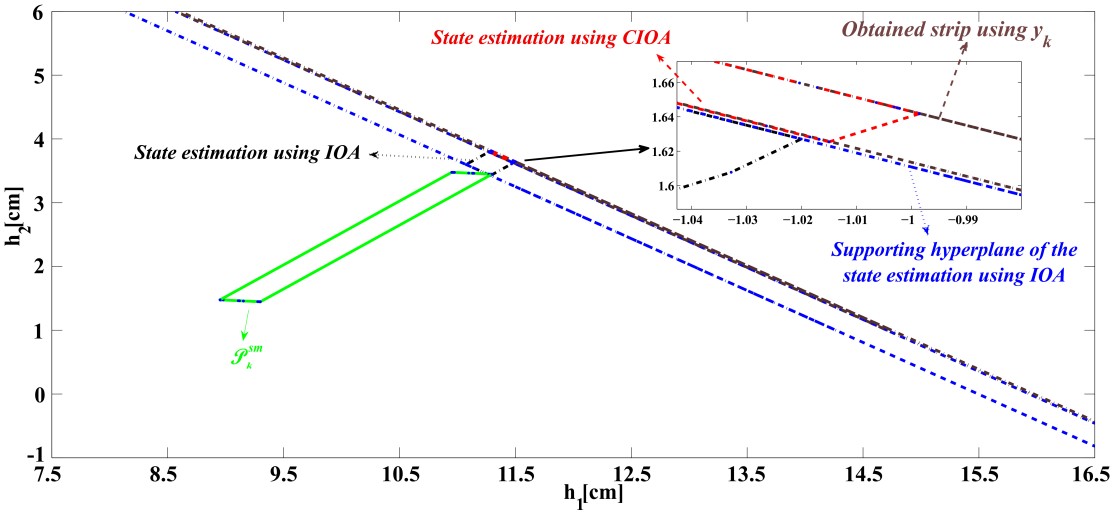

Figure 3.10: Scenario 1: FD results using SMA and IOA in the case $f_y = 0.8$V.

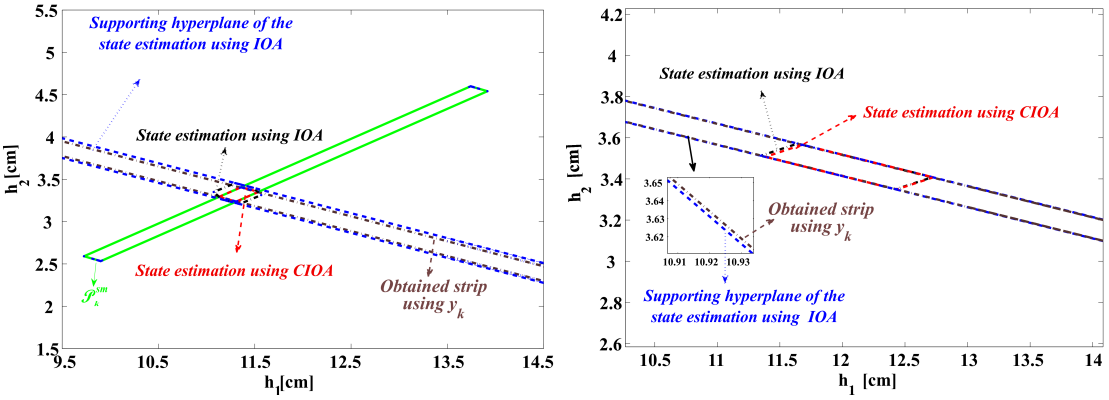

(a) Before occurrence of the fault.

(b) After occurrence of the fault.

Figure 3.11: The FD test using SMA and strip-based IOA in the case $f_y = 0.8$ V before and after occurrence of the fault.

Figure 3.10 shows the FD results using both SMA and IOA for Scenario 1 (i.e., when $f_y = 0.8$ V). From this figure, it can be observed that both SMA and IOA can detect the fault as it was anticipated in the minimun fault detectability analysis. By comparing Algorithm 2.2, which introduces the FD test based on SMA, and Algorithm 3.1, which

introduces the FD using the strip-based IOA, it can be seen that both approaches use the same information of the measured output for generating the strip. Therefore, the same strips are computed when applied to FD by both approaches as shown in Figure 3.10. The only difference between IOA and SMA is the use of different state bounding zonotopes for checking the intersection with the strip obtained by using the measurement. More precisely, in the case of SMA, the state bounding zonotope is computed using (2.20) and, in the case of IOA, the state bounding zonotope is computed using (3.1) for consistency test.

Figure 3.10 is obtained at time instant $k = 201$ (one time instant after the fault occurrence). That figure shows that the existence of the fault is detected by both SMA and IOA since the empty intersection is obtained between the measurement strip and the zonotopes computed by (2.20) and (3.1) for SMA and IOA, respectively. In addition, the state estimation determined by CIOA is also shown in Figure 3.10. It can be observed that the state estimation using CIOA is affected by the fault based on using the measurement information from the same time instant of the fault occurrence. Thus, the state estimation set is moved together with the measurement strip. Consequently, the empty intersection that indicates the existence of a fault will never occur using CIOA. For this reason, this approach is not used for FD purposes.

Figure 3.11 shows the FD results using SMA and IOA before and after the fault occurrence. The existence of the intersection between the strip $\mathcal{S}_y$ and the zonotopes $\mathcal{P}^{sm}$ and $\hat{\mathcal{X}}^{\text{io}}$ can be seen in Figure 3.11. Then, after detecting the fault with both approaches, monitoring the system with SMA should be stopped but the system could still be monitored using IOA as shown in Figure 3.11. Thus, the ability of monitoring the system after the fault occurrence can be considered as an advantage of IOA with respect to using SMA.

Now, the FD test results will be presented in the case of Scenario 2, which considers the fault magnitude as $f_y = 0.6$ V, i.e., satisfying $f_y < 0.7$ V. As shown in Figure 3.12, the fault cannot be detected by any of the approaches. This figure shows the strip $\mathcal{S}_y$ and the zonotopes $\mathcal{P}^{sm}$ and $\mathcal{X}^{\text{io}}$ at time instant $k = 201$. Note that $\mathcal{S}_y \cap \hat{\mathcal{X}}^{\text{io}} \neq \emptyset$ in this case. Then, when using Algorithm 3.1, the fault cannot be detected by using IOA. Similarly, using Algorithm 2.2, since $\mathcal{S}_y \cap \mathcal{P}^{sm} \neq \emptyset$, SMA will neither be able to detect the fault. Finally, Figure 3.13 shows the FD test before and after the occurrence of the fault. This figure shows that both IOA and SMA are not able to determine the existence of the fault in accordance with the results presented in Table 3.2.

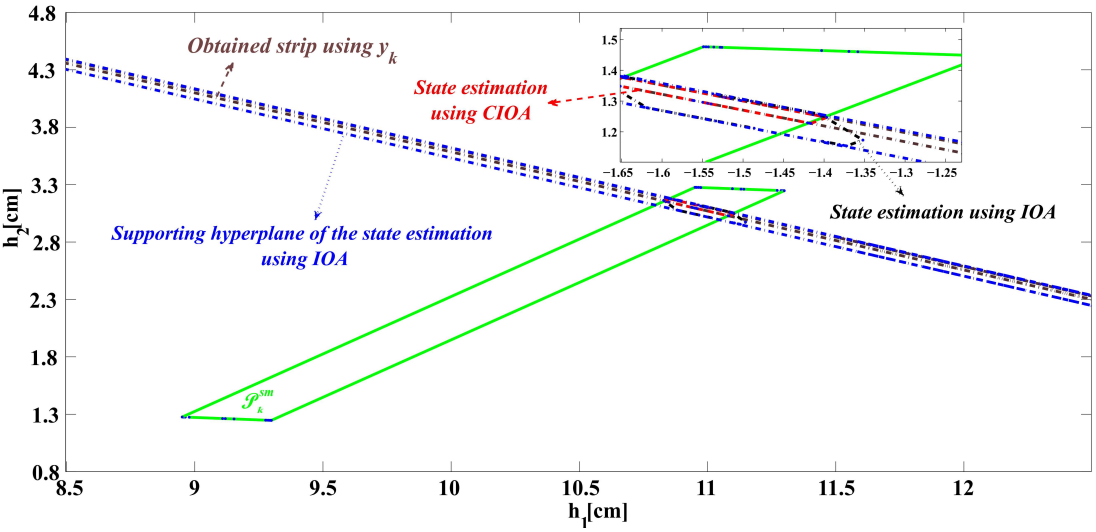

Figure 3.12: Scenario 2: FD results using SMA and IOA in the case $f_y = 0.6$ V.

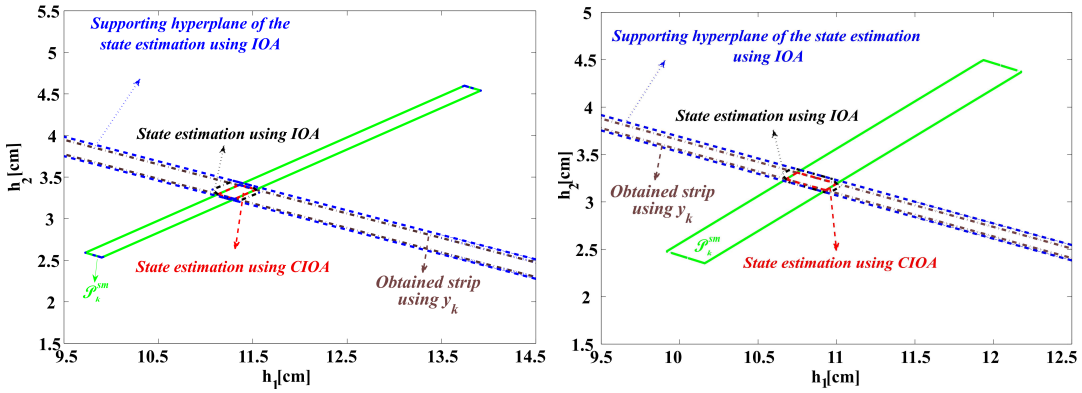

(a) Before occurrence of the fault.

(b) After occurrence of the fault.

Figure 3.13: FD test using SMA and strip-based IOA in the case $f_y = 0.6$ V before and after occurrence of the fault.

3.5 Summary

In this chapter, both IOA and SMA are considered for both state estimation and FD tasks in uncertain linear systems. Both approaches are analyzed and compared from

the mathematical point of view using a zonotopic representation of the involved sets. Mathematical and algorithmic formulations of both approaches are introduced to facilitate a fair comparison. As a result, it has been proved that, in the case that the observer gain in IOA is designed based on a current IOA, the state estimation bounding zonotopes are the same as those obtained using SMA. Furthermore, the application of both IOA and SMA is analyzed when applied to FD tasks for different type of faults. The performance of both approaches are characterized in terms of a MDF, allowing also the quantitative comparison. The obtained results show that the use of the strip-based FD test for IOA leads to demonstrate that both IOA and SMA presents comparable performance in state-steady regime. Finally, a two-tanks system is considered as a case study for illustrating the effectiveness of both approaches in state estimation and FD purposes. So far, this chapter has not only concentrated on the state estimation but also on FD performance by computing the minimum magnitude of the fault that can be detected. In this regard, different observer-based approaches will be further investigated in the next chapter. Furthermore, the relation between the classical IOA and the set invariance approach (SIA) will be discussed dealing with the computation of MDF.

Chapter 4

Mixed SIA and sensitivity analysis using IOA

This chapter addresses the characterization of the MDF by means of residual sensitivity integrated with the SIA when using an IOA as a FD scheme. Uncertainties (disturbances and noise) are considered as of unknown but bounded nature. A zonotopic-set representation towards reducing set operations to simple matrix calculations is utilized to bound the state/output estimations provided by the IOA. In order to show the connection between sensitivity and set-invariance analyses, mathematical expressions of the MDF are derived when considering different types of faults. Finally, a simulation case study based on a quadruple-tank system is employed to both illustrate and discuss the effectiveness of the proposed approach. IOA FD scheme is used to test the MDF obtained from the integration of both residual sensitivity analysis and SIA in the considered case study.

4.1 Introduction

The research of FD approaches able to improve performance of the system considering both the fault and uncertainty/disturbance effect still is an active area of research [PY17] even though already exist important contributions in the last years [CP12, Din08, ZDLW03]. In this regard, there are several approaches associated with generating the residual [Ger98, CP99]. So far, one of the most used approach for generating the residual is IOA [PQES03]. IOA is mainly used to estimate the states from the

measurements using either stochastic (e.g., KF) or deterministic approaches (e.g., Luenberger observers) for modeling the uncertainties. Then, the FD test is based on generating the residual using the output estimation error [CP99, PQES03, ABC05, Com15b].

Recent developments in the field of model-based FD have led to a renewed interest in using set-theoretical approaches in FD framework. SIA is one of the techniques where the invariant sets for the residual can be computed in each healthy or faulty operation of the system [Kof05, KHS07, SZDDM08, OMDDS10]. Consequently, when the system reaches the steady state, the corresponding residual trajectory ultimately converges to one of these invariant sets. As long as both healthy and faulty sets are separated, the FD can be performed [SZDDM08, OMDDS10].

A Robust Positively Invariant (RPI) set is a bounded region in the state-space that the system state can be confined in spite of the effect of the bounded system uncertainties [SDD10, XSP+13]. Furthermore, a minimal Robust Positively Invariant (mRPI) set is a unique and compact RPI set that is contained in any closed RPI set [SZDDM08, RKKM05]. One major drawback of the SIA is related to the limitation of computing the finite description of the RPI set. In recent years, researchers have investigated a variety of approaches. So far, the proposed approaches can be classified into two main categories: (i) explicit approaches, where the RPI set is computed using the explicit formulation of the set boundary [KHS07], (ii) iterative approaches, where the recursive iteration of the approximation of the system dynamics can be used to reach the RPI set [AR08, SHO13]. Moreover, the SIA can be used for checking the separation of healthy and faulty residual sets in steady state.

The MDF is a typical performance index used to characterize the performance of the FD scheme. The way of computing the MDF depends on the particular model-based approach and the way that faults and uncertainty are modeled. As it was mentioned in Section 3.1, one possible way to model the fault is based on considering it either as a state or as an unknown input of a dynamic system and the estimation of the fault is done by means of an observer. Alternatively, the fault can be modeled as a uncertain parameter that should be estimated by means of parameter estimation schemes [TB14, TTQ13, SDW13]. Moreover, the MDF is highly affected by the gain of the observer due to its influence in the FD performance. The effect of the observer gain in FD has already been explored in [MPES10].

In [XSP+13], the relation between the classical IOA and the SIA is discussed. Then,

in [PPOM16b, KPP+17], the characterization of the minimum magnitude of the fault that can be detected is proposed using both the IOA and SIA. However, there has been little discussion about the combination of the mentioned approaches. Then, IOA and the SIA are still known as two different techniques in FD framework. In this regard, this chapter is devoted to develop a passive robust FD approach using IOA in combination with SIA. Moreover, another contribution of the chapter is to determine the MDF using the proposed approach. System uncertainty is assumed to be unknown but bounded. This fact implies that the IOA can deliver no just a single punctual estimation for the output/state but a set that, in this chapter, is bounded using zonotopes. On the one hand, the characterization of the MDF is done by using the classical sensitivity analysis. On the other hand, this characterization is carried out by using SIA. Mathematical expressions of the MDF for different type of sensor and actuator faults are obtained with the goal of connecting both sensitivity and set-based approaches. Contrary to most existing FD design techniques, the sensitivity to both faults and disturbances is evaluated using a set-based approach enclosing all the possible temporal scenarios of faults and disturbances within specified ranges. The combination of these features makes the approach original compared to the existing available FD techniques. Finally, the effectiveness of the proposed approach is illustrated using a case study based on a quadruple-tank system.

The structure of the chapter is the following: The integrated observer structure is introduced in Section 4.2. Then, the MDF is characterized in Section 4.3 dealing with different type of sensor and actuator faults. The case study description and discussion of the obtained results are presented in Section 4.4. Finally, the general conclusions are drawn in Section 4.5.

4.2 Integrated FD test

Both mentioned IOA and SIA in Sections 2.3.1 and 2.3.3 are considered as reliable set-theoretical FD tests that can be used depending on the purpose of the investigation. In general, the FD test is provided based on checking the consistency of the residual r in real time, which is computed on-line, with the healthy residual zonotope that can be computed based on either IOA or SIA. Then, any inconsistencies can be understood as the occurrence of the fault.

So far, the thesis has mainly focused on using the zonotopic representation of sets. But, the obtained set in (2.31) is a polyhedral RPI set of the state estimation error. In this regard, since the set in (2.31) is symmetric around the origin and considering the zonotopic representation of sets, Proposition 4.1 implies that $\tilde{\mathcal{X}}$ can also be represented using a zonotope.

Proposition 4.1. *(Zonotopic representation of the RPI set for $\tilde{x}$) Consider a state estimation error dynamics in (2.29), the zonotopic RPI set of the state estimation error can be computed as*

$$c_{\tilde{x}_{j+1}} = (A - LC)\, c_{\tilde{x}_j}, \tag{4.1a}$$

$$R_{\tilde{x}_{j+1}} = \begin{bmatrix} (A - LC)R_{\tilde{x}_j} & E_d \end{bmatrix}, \tag{4.1b}$$

where $j \in \mathbb{N}$ denotes the j^{th} element of the set. Then, in the steady state, i.e., when $j \to \infty$, it can be written that

$$c_{\tilde{x}_\infty} = 0, \tag{4.2a}$$

$$\left\| R_{\tilde{x}_{\infty_i}} \right\|_1 = \left\| R_{\infty_i} \right\|_1, \tag{4.2b}$$

where i denotes the i^{th} row of the matrices.

Proof. Consider the dynamical model of the state estimation error in (2.29) and assume that the initial state estimation error $\tilde{x}_0$ belongs to the zonotopic set $\tilde{\mathcal{X}}_0 = \langle c_{\tilde{x}_0},\ R_{\tilde{x}_0} \rangle$ that is defined as an RPI set, since $\tilde{x} \in \langle c_{\tilde{x}},\ R_{\tilde{x}} \rangle$, $\omega \in \langle 0,\ I_{n_\omega} \rangle$ and $v \in \langle 0,\ I_{n_v} \rangle$ for all $k \geq 0$, it can be written that

$$\tilde{x}_{j+1} \in \left\langle c_{\tilde{x}_{j+1}},\ R_{\tilde{x}_{j+1}} \right\rangle = \left\langle (A - LC)c_{\tilde{x}_j},\ (A - LC)R_{\tilde{x}_j} \right\rangle \oplus \langle 0,\ E_\omega \rangle \oplus \langle 0,\ -LE_v \rangle, \tag{4.3}$$

is another RPI set with arbitrarily expected precision enclosing the mRPI set of the state estimation error in (2.29). Thus, the center and the shape matrix of the set in (4.3) can be unfolded as in (4.1). Furthermore, the state estimation error will converge to the RPI set in steady state. Thus, the RPI set of $\tilde{x}$ can be computed by recursive propagation of the zonotopic set (4.1) starting from the initial set $\tilde{\mathcal{X}}_0 = \langle c_{\tilde{x}_0},\ R_{\tilde{x}_0} \rangle$ that belongs to the RPI set which can be computed using the any available method such as Ultimate Bound (UB) method recalled in Section 2.3.3. Furthermore, it can be stated

that if $j \to \infty$ (i.e., in steady state), the following conditions will be satisfied:

$$c_{\tilde{x}_{j+1}} = c_{\tilde{x}_j}, \tag{4.4a}$$

$$\left\|R_{\tilde{x}_{j+1}}\right\|_1 = \left\|R_{\tilde{x}_j}\right\|_1. \tag{4.4b}$$

Therefore, the same formulations as (4.2) for the center and the shape matrix of $\tilde{\mathcal{X}}$ can be obtained by substitution of conditions (4.4) in (4.1). □

Now, considering Proposition 4.1, the zonotopic representation of the residual set in steady state can be computed by computing the projection of $\tilde{x}$ into the residual space as

$$c^{si}_{r,\infty} = C c_{\tilde{x},\infty}, \tag{4.5a}$$

$$R^{si}_{r,\infty} = \begin{bmatrix} C R_{\tilde{x},\infty_i} & E_v \end{bmatrix}, \tag{4.5b}$$

where superscript *si* denotes the SIA.

Finally, considering the residual that is obtained in (4.5) as a healthy residual set that is generated based on the nominal model, i.e., considering only the effect of the uncertainties (noises and disturbances), the FD test with the SIA is done by comparing the residual that is computed on-line at each time instant, denoted by r, with the RPI residual set that is computed off-line in steady state. The fault is detected if

$$r \notin \left\langle c^{si}_{r_\infty},\ R^{si}_{r_{\infty_i}} \right\rangle. \tag{4.6}$$

Otherwise, the system remains healthy.

Remark 4.1. *From the mathematical point of view, in order to check whether* (4.6) *is satisfied or not, the Gilbert-Johnson-Keerthi (GJK) algorithm as proposed in [LC06b] can be used.* □

Moreover, Proposition 4.2 can be used in order to combine the FD principles mentioned in Sections 2.3.1 and 2.3.3 based on both IOA and SIA.

Proposition 4.2. *Considering the steady state and the general Luenberger observer structure in* (2.5)*, in healthy operation of the system*

$$\left\langle c^{io}_{r,\infty},\ R^{io}_{r,\infty} \right\rangle = \left\langle c^{si}_{r,\infty},\ R^{si}_{r,\infty} \right\rangle. \tag{4.7}$$

Then, the FD test is the same using both IOA and SIA. Thus, it can be done by checking whether

$$r \in \langle c_{r^h,\infty},\ R_{r^h,\infty} \rangle, \tag{4.8}$$

where c_{r^h} and R_{r^h} are the center and the shape (generator) matrix of the healthy residual zonotope denoted by r^h, respectively (i.e., $r^h = \langle c_{r^h},\ R_{r^h} \rangle$). Moreover, c_{r^h} and R_{r^h} can be computed using either SIA or IOA when k tends to infinity.

Proof. The residual in the case of IOA can be written using the state estimation error as in (2.28). Moreover, the dynamics of the state estimation error using IOA can be written using (2.5) as (2.29).

But, based on [XSP+13], considering the steady-state operation of the system, the size of the residual zonotope in (2.14) during the steady-state operation of the system, i.e., $\langle c^{io}_{r,\infty},\ R^{io}_{r,\infty} \rangle$, obtained using the IOA converges towards the smallest residual set (healthy set) computed by the SIA, i.e., $\langle c^{is}_{r,\infty},\ R^{is}_{r,\infty} \rangle$. Therefore, the same residual zonotopes can be predicted based on both the IOA and SIA, if k tends to infinity (steady state). Then, since having the same set that introduces the healthy residual, the same FD principle can be obtained using both approaches. □

Then, considering Proposition 4.2, residual (2.28) can be used to compute the healthy residual zonotope in steady state.

Remark 4.2. *Note that for the sake of simplified notation, r^h is used instead of r^{io} or r^{is} for denoting the healthy residual since they are equal in steady state dealing with the faultless scenario.* □

In this regard, the input-output form of the output y in (2.4) can be written using the shift operator q^{-1} as

$$y = \mathscr{H}_u(q^{-1})u + \mathscr{H}_\omega(q^{-1})\omega + \mathscr{H}_\upsilon(q^{-1})\upsilon, \tag{4.9}$$

with

$$\mathscr{H}_u(q^{-1}) = C\xi_1(q^{-1})B, \tag{4.10a}$$
$$\mathscr{H}_\omega(q^{-1}) = C\xi_1(q^{-1})E_\omega, \tag{4.10b}$$
$$\mathscr{H}_\upsilon(q^{-1}) = E_\upsilon, \tag{4.10c}$$

where $\xi_1(q^{-1}) = (qI - A)^{-1}$.

On the other hand, the input-output form of the output prediction $\hat{y}$ can be expressed using observer (2.5) as

$$\hat{y} = \mathscr{T}_u(q^{-1})u + \mathscr{T}_y(q^{-1})y, \tag{4.11}$$

with

$$\mathscr{T}_u(q^{-1}) = C\xi_2(q^{-1})B, \tag{4.12a}$$
$$\mathscr{T}_y(q^{-1}) = C\xi_2(q^{-1})L, \tag{4.12b}$$

where $\xi_2(q^{-1}) = (qI - (A - LC))^{-1}$.

Now, using (4.9) and (4.11), the input-output form of the healthy residual can be expressed using the shift operator q^{-1} as

$$r^h = \mathscr{G}_u(q^{-1})\, u + \mathscr{G}_\omega(q^{-1})\, \omega + \mathscr{G}_\upsilon(q^{-1})\, \upsilon, \tag{4.13}$$

with

$$\mathscr{G}_u(q^{-1}) = \big(I - \mathscr{T}_y(q^{-1})\big)\, \mathscr{H}_u(q^{-1}) - \mathscr{T}_u(q^{-1}), \tag{4.14a}$$
$$\mathscr{G}_\omega(q^{-1}) = \big(I - \mathscr{T}_y(q^{-1})\big)\, \mathscr{H}_\omega(q^{-1}), \tag{4.14b}$$
$$\mathscr{G}_\upsilon(q^{-1}) = \big(I - \mathscr{T}_y(q^{-1})\big)\, \mathscr{H}_\upsilon(q^{-1}). \tag{4.14c}$$

As it can be seen from (4.13), the obtained residual is only affected by the additive uncertainties (disturbance and noise). Furthermore, $\mathscr{G}_\omega$ and $\mathscr{G}_\upsilon$ indicate the sensitivity of the residual with respect to the disturbance and noise, respectively.

Thus, the obtained healthy residual in (4.13) can be used for the FD test in (4.8) following Proposition 4.3.

Proposition 4.3. *Considering the input-output form of the residual in (4.13), the FD test in (4.8) can be also done by checking the satisfaction of*

$$r_\infty \in \mathscr{G}_{u_i}(1)u_\infty \pm \left\|\mathscr{G}_{\omega_i}(1) + \mathscr{G}_{\upsilon_i}(1)\right\|_1, \tag{4.15}$$

where the index i indicates the i^{th} row of the transfer function $\mathscr{G}$. In case that (4.15) is not satisfied a fault is detected.

Proof. Since $u \in \langle u,\ 0\rangle$, $\omega \in \langle 0,\ I_{n_\omega}\rangle$ and $\upsilon \in \langle 0,\ I_{n_\upsilon}\rangle$ for all $k \geq 0$, the healthy residual set in steady state can be written as

$$r_\infty^h \in \left\langle c_{r_\infty^h},\ R_{r_\infty^h} \right\rangle = \langle \mathscr{G}_u(1)u_\infty,\ 0\rangle \oplus \langle 0,\ \mathscr{G}_\omega(1)\rangle \oplus \langle 0,\ \mathscr{G}_\upsilon(1)\rangle\,. \tag{4.16}$$

Note that the steady state expression of (4.13) can be obtained by setting $q = 1$. Then, (4.16) can also be expressed as a zonotopic representation as

$$c_{r_\infty^h} = \mathscr{G}_u(1)u_\infty, \tag{4.17a}$$

$$R_{r_\infty^h} = \begin{bmatrix} \mathscr{G}_\omega(1) & \mathscr{G}_\upsilon(1) \end{bmatrix}. \tag{4.17b}$$

Now, by considering both Definition B.23 and (4.17), upper and lower bounds of the residual zonotope, which are respectively denoted by $\overline{r^h}$ and $\underline{r^h}$, can be computed as

$$\overline{r_\infty^h} = \mathscr{G}_{u_i}(1)u_\infty + \|\mathscr{G}_{\omega_i}(1) + \mathscr{G}_{\upsilon_i}(1)\|_1\,, \tag{4.18a}$$

$$\underline{r_\infty^h} = \mathscr{G}_{u_i}(1)u_\infty - \|\mathscr{G}_{\omega_i}(1) + \mathscr{G}_{\upsilon_i}(1)\|_1\,. \tag{4.18b}$$

Thus, considering (4.18) as upper and lower bounds, the fault can be detected if $r_\infty \notin [\underline{r_\infty^h},\ \overline{r_\infty^h}]$. □

Hence, the fault can be detected by generating the residual in real time and comparing it with the residual set that was computed off-line using Proposition 4.3. A deeper discussion about the computation of the minimum magnitude of the fault that can be detected using the approach presented in this section will be provided in Section 4.3.

4.3 Characterization of the MDF using sensitivity analysis integrated with a SIA

The characterization of the MDF is presented in this section. In this thesis, MDF is defined as the minimum magnitude of the fault that can be detected. Furthermore, the same mentioned sensor and actuator faults introduced in Chapter 3 are also considered in this chapter.

Moreover, the combination of classical sensitivity analysis and the SIA (called integrated approach in Section 4.2) is employed to deal with the computation of the MDF.

4.3.1 Minimum detectable output sensor fault

The dynamical model (3.17) is considered to deal with the output sensor fault. Therefore, the faulty dynamical model (3.17) can be written in input-output form using the shift operator q^{-1} as

$$y = \mathscr{H}_u(q^{-1})u + \mathscr{H}_\omega(q^{-1})\omega + \mathscr{H}_\upsilon(q^{-1})\upsilon + \mathscr{H}_{f_y}(q^{-1})f_y, \tag{4.19}$$

where

$$\mathscr{H}_{f_y}(q^{-1}) = F_y. \tag{4.20}$$

Furthermore, using the Luenberger observer (2.5), the output prediction can be expressed in input-output form as in (4.11). Then, the input-output form of the residual in the case of output sensor fault can be expressed as

$$r = \mathscr{G}_u(q^{-1})\ u + \mathscr{G}_\omega(q^{-1})\ \omega + \mathscr{G}_\upsilon(q^{-1})\ \upsilon + \mathscr{G}_{f_y}(q^{-1})f_y, \tag{4.21}$$

with

$$\mathscr{G}_{f_y}(q^{-1}) = \left(I - \mathscr{T}_y(q^{-1})\right)\mathscr{H}_{f_y}(q^{-1}). \tag{4.22}$$

Therefore, (4.21) encompasses the effect of uncertainties (disturbance and noise) and also the effect of the fault. Furthermore, $\mathscr{G}_\omega(q^{-1})$, $\mathscr{G}_\upsilon(q^{-1})$ and $\mathscr{G}_{f_y}(q^{-1})$ denote the sensitivity of the residual with respect to the disturbance, noise and output sensor fault, respectively.

Now, the minimum detectable output sensor fault can be computed following Theorem 4.1.

Theorem 4.1. *(Minimum detectable output sensor fault) Considering the faulty dynamical model (3.17) and the observer structure (2.5), the minimum magnitude of the*

output sensor fault can be characterized as

$$\overline{f_{y_j,\infty}} = \max \overline{f_{y_{ji},\infty}}, \qquad \overline{f_{y_{ji},\infty}} = +2\frac{\|(I - C_i\xi_{2_i}(1)L_i)\,(C_i\xi_1(1)E_{\omega_i} + E_{v_i})\|_1}{\left\|\left(I - C_{ij}\xi_{2_{ij}}(1)L_{ij}\right)F_{y_{ij}}\right\|_1}, \quad (4.23a)$$

$$\underline{f_{y_j,\infty}} = \min \underline{f_{y_{ji},\infty}}, \qquad \underline{f_{y_{ji},\infty}} = -2\frac{\|(I - C_i\xi_{2_i}(1)L_i)\,(C_i\xi_1(1)E_{\omega_i} + E_{v_i})\|_1}{\left\|\left(I - C_{ij}\xi_{2_{ij}}(1)L_{ij}\right)F_{y_{ij}}\right\|_1}, \quad (4.23b)$$

where $\overline{f_{y_j,\infty}}$ *and* $\underline{f_{y_j,\infty}}$ *are upper and lower bounds of the MDF in the case of output sensor fault, respectively. Additionally, the indices* i *and* j *indicate the* i^{th} *row and* j^{th} *column of the transfer functions, respectively. Moreover, the value* 2 *is included to consider the worst-case scenario, i.e., the residual is considered to be in the extreme value (it is located at either the lower or the upper bound of the considered threshold).*

Proof. Given the residual in (4.21), considering the faulty residual in the case of an output sensor fault, and following the FD test presented in Proposition 4.2, the following condition should be satisfied in steady state in faulty scenario (i.e., $f_y(q^{-1}) \neq 0 \Rightarrow f_{y_\infty} \neq 0$):

$$r_\infty \notin \mathscr{G}_{u_i}(1)u_\infty \pm \|\mathscr{G}_{\omega_i}(1) + \mathscr{G}_{v_i}(1)\|_1\,, \quad (4.24)$$

where r_∞ corresponds to the residual that is obtained at $k \to \infty$ using (4.21). Moreover, since $u \in \langle u,\ 0\rangle$, $\omega \in \langle 0,\ I_{n_\omega}\rangle$, $v \in \langle 0,\ I_{n_v}\rangle$ and considering Assumption 3.1 in steady state $\forall\, i, j$, the following condition follows

$$\mathscr{G}_{f_{y_{ij}}}(1)f_{y_{j,\infty}} \notin 0 \pm 2\,\|\mathscr{G}_{\omega_i}(1) + \mathscr{G}_{v_i}(1)\|_1\,. \quad (4.25)$$

Therefore, the MDF in the case of an output sensor fault can be calculated by simplifying (4.25) as

$$f_{y_j,\infty} \notin 0 \pm 2\frac{\|\mathscr{G}_{\omega_i}(1) + \mathscr{G}_{v_i}(1)\|_1}{\left\|\mathscr{G}_{f_{y_{ij}}}(1)\right\|_1}. \quad (4.26)$$

Finally, the MDF can be characterized as it is formulated in (4.23) by the substitution of (4.14b), (4.14c) and (4.22) into (4.26) to obtain the sensitivity with respect to ω, v and f_y, respectively. □

4.3.2 Minimum detectable input sensor fault

In this section, the effect of input sensor fault is considered as in Section 3.3.2. It means, the observer model is influenced by the fault as (3.10).

Thus, the input-output form of the dynamical model (2.4) can be written using the shift operator q^{-1} as

$$y = \mathscr{H}_u(q^{-1})u + \mathscr{H}_\omega(q^{-1})\omega + \mathscr{H}_\upsilon(q^{-1})\upsilon. \tag{4.27}$$

Moreover, the observer (3.10) affected by the input sensor fault can be expressed in the input-output form when using the shift operator q^{-1} as

$$\hat{y} = \mathscr{T}_u(q^{-1})u + \mathscr{T}_y(q^{-1})y + \mathscr{T}_{f_u}(q^{-1})f_u, \tag{4.28}$$

where

$$\mathscr{T}_{f_u}(q^{-1}) = C\xi_2(q^{-1})BF_u. \tag{4.29}$$

Therefore, using (4.27) and (4.28), the input-output form of the residual in the case of an input sensor fault is expressed as

$$r = \mathscr{G}_u(q^{-1})\ u + \mathscr{G}_\omega(q^{-1})\ \omega_k + \mathscr{G}_\upsilon(q^{-1})\ \upsilon + \mathscr{G}_{f_u}(q^{-1})f_u, \tag{4.30}$$

with

$$\mathscr{G}_{f_u}(q^{-1}) = -\mathscr{T}_{f_u}(q^{-1}). \tag{4.31}$$

Furthermore, (4.30) allows to express the residual in terms of the effect of the uncertainties (additive disturbance and noise) and the considered type of fault. In (4.30), $\mathscr{G}_\omega(q^{-1})$ and $\mathscr{G}_\upsilon(q^{-1})$ indicate the sensitivity of the residual with respect to the disturbance ω and the measurement noise υ, respectively. Moreover, the sensitivity of the obtained residual with respect to the input sensor fault is indicated by $\mathscr{G}_{f_u}(q^{-1})$.

Theorem 4.2 can be used to compute the minimum detectable input sensor fault.

Theorem 4.2. *(Minimum detectable input sensor fault) Given a dynamical model (2.4) and monitoring the system using the observer (3.10), the minimum detectable input*

sensor fault can be computed as

$$\overline{f_{u_j,\infty}} = \max \overline{f_{u_{ji},\infty}}, \qquad \overline{f_{u_{ji},\infty}} = +2\frac{\|(I - C_i\xi_{2_i}(1)L_i)\,(C_i\xi_1(1)E_{\omega_i} + E_{v_i})\|_1}{\left\|-C_{ij}\xi_{2_{ij}}(1)B_{ij}F_{u_{ij}}\right\|_1}, \quad (4.32a)$$

$$\underline{f_{u_j,\infty}} = \min \underline{f_{u_{ji},\infty}}, \qquad \underline{f_{u_{ji},\infty}} = -2\frac{\|(I - C_i\xi_{2_i}(1)L_i)\,(C_i\xi_1(1)E_{\omega_i} + E_{v_i})\|_1}{\left\|-C_{ij}\xi_{2_{ij}}(1)B_{ij}F_{u_{ij}}\right\|_1}, \quad (4.32b)$$

where $\overline{f_{u_j,\infty}}$ *and* $\underline{f_{u_j,\infty}}$ *are upper and lower bounds of the minimum detectable input sensor fault, respectively.*

Proof. As mentioned in the proof of Theorem 4.1, in the faulty scenario, i.e., $f_u(q^{-1}) \neq 0 \Rightarrow f_{u,\infty} \neq 0$, the condition (4.24) can be written considering (4.30) and based on Proposition 4.2. Thus, in the faulty condition (input sensor fault) the satisfaction of the following condition should be proved $\forall i, j$:

$$\mathscr{G}_{f_{u_{ij}}}(1) f_{u_j,\infty} \notin 0 \pm 2\left\|\mathscr{G}_{\omega_i}(1) + \mathscr{G}_{v_i}(1)\right\|_1. \quad (4.33)$$

Then, the MDF can be computed using (4.33) as

$$f_{u_j,\infty} \notin 0 \pm 2\frac{\|\mathscr{G}_{\omega_i}(1) + \mathscr{G}_{v_i}(1)\|_1}{\left\|\mathscr{G}_{f_{u_{ij}}}(1)\right\|_1}. \quad (4.34)$$

Hence, the same formulation as (4.32) is obtained by substituting (4.14b), (4.14c) and (4.31) in (4.34) for the sensitivity with respect to ω, v and f_u, respectively. □

4.3.3 Minimum detectable actuator fault

The dynamical model including an actuator fault can be written as (3.25). Furthermore, the measurement equation in (3.25) can be expressed in input-output form using the shift operator q^{-1} as

$$y = \mathscr{H}_u(q^{-1})u + \mathscr{H}_\omega(q^{-1})\omega + \mathscr{H}_v(q^{-1})v + \mathscr{H}_{f_a}(q^{-1})f_a, \quad (4.35)$$

where

$$\mathscr{H}_{f_a}(q^{-1}) = C\xi_1(q^{-1})F_a. \quad (4.36)$$

On the other hand, the observer (2.5) can be used for monitoring the dynamical model (3.25), which can be expressed in input-output form as (4.11). Then, the residual in the case of the actuator fault in input-output form can be written as

$$r = \mathscr{G}_u(q^{-1})\, u + \mathscr{G}_\omega(q^{-1})\, \omega + \mathscr{G}_\upsilon(q^{-1})\, \upsilon + \mathscr{G}_{f_a}(q^{-1}) f_a, \tag{4.37}$$

with

$$\mathscr{G}_{f_a}(q^{-1}) = \left(I - \mathscr{T}_y(q^{-1})\right) \mathscr{H}_{f_a}(q^{-1}), \tag{4.38}$$

where $\mathscr{G}_{f_a}$ denotes the sensitivity of the residual with respect to the actuator fault. Moreover, $\mathscr{G}_\omega$ and $\mathscr{G}_\upsilon$ indicate the sensitivity of the residual with respect to the disturbance ω and the measurement noise υ, respectively.

Theorem 4.3 can be used to compute the minimum detectable actuator fault.

Theorem 4.3. *(Minimum detectable actuator fault) Considering a dynamical model (2.4) and the observer in (2.5), the minimum detectable actuator fault can be computed as*

$$\overline{f_{a_j,\infty}} = \max \overline{f_{a_{ji},\infty}}, \qquad \overline{f_{a_{ji},\infty}} = +2\frac{\left\|\left(I - C_i\xi_{2_i}(1)L_i\right)\left(C_i\xi_1(1)E_{\omega_i} + E_{\upsilon_i}\right)\right\|_1}{\left\|\left(I - C_{ij}\xi_{2_{ij}}(1)L_{ij}\right) C_{ij}\xi_{1_{ij}}(1)F_{a_{ij}}\right\|_1}, \tag{4.39a}$$

$$\underline{f_{a_j,\infty}} = \min \underline{f_{a_{ji},\infty}}, \qquad \underline{f_{a_{ji},\infty}} = -2\frac{\left\|\left(I - C_i\xi_{2_i}(1)L_i\right)\left(C_i\xi_1(1)E_{\omega_i} + E_{\upsilon_i}\right)\right\|_1}{\left\|\left(I - C_{ij}\xi_{2_{ij}}(1)L_{ij}\right) C_{ij}\xi_{1_{ij}}(1)F_{a_{ij}}\right\|_1}, \tag{4.39b}$$

where $\overline{f_{a_j,\infty}}$ and $\underline{f_{a_j,\infty}}$ are upper and lower bounds of the minimum detectable actuator fault, respectively.

Proof. The way of obtaining the proof is similar to those used for Theorems (4.1) and (4.2). When considering faulty scenario, i.e., $f_a(q^{-1}) \neq 0 \Rightarrow f_{a,\infty} \neq 0$, using the residual (4.37) and based on Proposition 4.2, the condition (4.24) should be satisfied and written $\forall i, j$ as

$$\mathscr{G}_{f_{a_{ij}}}(1) f_{a_j,\infty} \notin 0 \pm 2\left\|\mathscr{G}_{\omega_i}(1) + \mathscr{G}_{\upsilon_i}(1)\right\|_1. \tag{4.40}$$

Now, simplifying (4.40) yields

$$f_{a_j,\infty} \notin 0 \pm 2\frac{\left\|\mathscr{G}_{\omega_i}(1) + \mathscr{G}_{\upsilon_i}(1)\right\|_1}{\left\|\mathscr{G}_{f_{a_{ij}}}(1)\right\|_1}. \tag{4.41}$$

Therefore, the minimum detectable actuator fault can be formulated as (4.39) by substituting (4.14b), (4.14c) and (4.38) in (4.41). □

Table 4.1: Residual sensitivity with respect to different type of actuator and sensor faults.

	Residual sensitivity
Output sensor fault	$\mathscr{G}_{f_y}(q^{-1}) = \left(I - C\xi_2(q^{-1})L\right) F_y$
Input sensor fault	$\mathscr{G}_{f_u}(q^{-1}) = -C\xi_2(q^{-1})BF_u$
Actuator fault	$\mathscr{G}_{f_a}(q^{-1}) = \left(I - C\xi_2(q^{-1})L\right) C\xi_1(q^{-1})F_a$

4.3.4 Comparative assessment

This section attempts to find the bridge between the approaches characterizing the MDF obtained using the classical sensitivity framework when IOA and SIA are used. As a result of considering different mentioned actuator and sensors faults, the sensitivity of the residual with respect to the fault is computed differently. Table 4.1 summarizes the derived formulation for different sensitivity in previous sections. Consequently, the characterized formulation for computing the minimum magnitude of the given fault is different. Table 4.2 summarizes the characterization of the MDF for different type of considered faults.

Further analysis on the physical meaning of the different type of the considered faults will be discussed in Section 4.4 based on a case study.

4.4 Case study

4.4.1 General description

A quadruple-tank system used to illustrate the approach proposed in the previous sections. The quadruple tank is a multi input/multi output process proposed by [Joh00] and is described in Section A.1 of Appendix A.

Moreover, bounded disturbances influencing all the state-space directions and the

Table 4.2: Different minimum detectable actuator and sensor faults.

	MDF
Output sensor fault	$\overline{f_{y_j,\infty}} = \max \overline{f_{y_{ji},\infty}}, \quad \overline{f_{y_{ji},\infty}} = +2\frac{\|(I - C_i\xi_{2_i}(1)L_i)\,(C_i\xi_1(1)E_{\omega_i} + E_{v_i})\|_1}{\left\|\left(I - C_{ij}\xi_{2_{ij}}(1)L_{ij}\right)F_{y_{ij}}\right\|_1}$ $\underline{f_{y_j,\infty}} = \min \underline{f_{y_{ji},\infty}}, \quad \underline{f_{y_{ji},\infty}} = -2\frac{\|(I - C_i\xi_{2_i}(1)L_i)\,(C_i\xi_1(1)E_{\omega_i} + E_{v_i})\|_1}{\left\|\left(I - C_{ij}\xi_{2_{ij}}(1)L_{ij}\right)F_{y_{ij}}\right\|_1}$
Input sensor fault	$\overline{f_{u_j,\infty}} = \max \overline{f_{u_{ji},\infty}}, \quad \overline{f_{u_{ji},\infty}} = +2\frac{\|(I - C_i\xi_{2_i}(1)L_i)\,(C_i\xi_1(1)E_{\omega_i} + E_{v_i})\|_1}{\left\|-C_{ij}\xi_{2_{ij}}(1)B_{ij}F_{u_{ij}}\right\|_1}$ $\underline{f_{u_j,\infty}} = \min \underline{f_{u_{ji},\infty}}, \quad \underline{f}_{u_{ji,\infty}} = -2\frac{\|(I - C_i\xi_{2_i}(1)L_i)\,(C_i\xi_1(1)E_{\omega_i} + E_{v_i})\|_1}{\left\|-C_{ij}\xi_{2_{ij}}(1)B_{ij}F_{u_{ij}}\right\|_1}$
Actuator fault	$\overline{f_{a_j,\infty}} = \max \overline{f_{a_{ji},\infty}}, \quad \overline{f_{a_{ji},\infty}} = +2\frac{\|(I - C_i\xi_{2_i}(1)L_i)\,(C_i\xi_1(1)E_{\omega_i} + E_{v_i})\|_1}{\left\|\left(I - C_{ij}\xi_{2_{ij}}(1)L_{ij}\right)C_{ij}\xi_{1_{ij}}(1)F_{a_{ij}}\right\|_1}$ $\underline{f_{a_j,\infty}} = \min \underline{f_{a_{ji},\infty}}, \quad \underline{f_{a_{ji},\infty}} = -2\frac{\|(I - C_i\xi_{2_i}(1)L_i)\,(C_i\xi_1(1)E_{\omega_i} + E_{v_i})\|_1}{\left\|\left(I - C_{ij}\xi_{2_{ij}}(1)L_{ij}\right)C_{ij}\xi_{1_{ij}}(1)F_{a_{ij}}\right\|_1}$

measurement noise are modeled respectively with E_ω and E_υ in (A.3) as

$$E_\omega = \begin{bmatrix} 0.05 & 0.01 & 0 & 0 & 0 & 0 & 0 \\ 0.05 & 0 & 0.01 & 0 & 0 & 0 & 0 \\ 0.05 & 0 & 0 & 0.01 & 0 & 0 & 0 \\ 0.05 & 0 & 0 & 0 & 0.01 & 0 & 0 \end{bmatrix}, \quad E_\upsilon = \begin{bmatrix} 0_{2x5} & 0.1\ I_2 \end{bmatrix}. \tag{4.42}$$

Then, the effect of the fault is modeled through the selection of matrix $F_\bullet$ where the subscript $\bullet$ can be assigned by y, u and a depending on the kind of fault considered (see (3.17), (3.10) and (3.25)).

Furthermore, both state and measurement uncertainty vectors, i.e., ω and υ, and all the considered fault vectors, i.e., f_a, f_y and f_u, are assumed to be normalized in $[-1,\ 1]$. Accordingly, the matrices E_ω, E_υ, F_a, F_y and F_u are defined. Furthermore, the observer gain is computed based on the proposed method in [Com15b].

In this regard, further investigation will be done for the case study by considering the single additive actuator and sensors faults to compute the minimum magnitude of them that can be detected in the next section.

4.4.2 MDF analysis

In this section, the actuator and the sensor faults are considered for the case study as single additive fault not appearing at the same time. First, the magnitude of MDF is computed based on the theoretical formulation that are derived in Section 4.3. Then, the simulation is employed in order to validate the obtained results.

Minimum detectable actuator fault

The actuator is electrically driven allowing to manipulate the valve. Moreover, the valve actuator can be either open/closed or in intermediate positions. As it is mentioned in the description of the case study, the range of flow parameter is considered between 0 and 1. This parameter is related to the position of the valve during the experiment and the flow to the lower and upper tanks are affected by the position of the valve through $\gamma_j K_{p_j} v_j$ and $(I - \gamma_j) K_{p_j} v_j$ with $j = 1, 2$, respectively.

Furthermore, the effect of actuator fault can be simulated based on (faulty) dynamical model (3.25) through matrix F_a and the vector f_a. In this case, single actuator fault is considered based on the elements of the vector f_a , i.e.,

$$f_a = \begin{bmatrix} f_{a_1} \\ f_{a_2} \end{bmatrix}, \tag{4.43}$$

where f_{a_1} and f_{a_2} indicate the fault affecting each actuator. Furthermore, the following matrix F_a is selected to simulate the actuator fault:

$$F_a = 5B. \tag{4.44}$$

All the previously mentioned points are considered to simulate the actuator fault for the case study. Then, considering Theorem 4.3, the minimum magnitude of the actuator fault that can be detected is obtained in steady state as

$$f_{a_1} = \pm 0.0879, \tag{4.45a}$$

$$f_{a_2} = \pm 0.4095. \tag{4.45b}$$

In this case study, the flow parameters are considered as $\gamma_1 = 0.7$ and $\gamma_2 = 0.6$.

As it can be seen in (4.45), the magnitude of the minimum actuator fault that can be detected is ± 0.0879 for f_1 and ± 0.4095 for f_2. It means that when the magnitude of the actuator fault is higher than the magnitudes obtained in (4.45) can be detected. Otherwise, fault of smaller magnitude are not detectable. Considering $\gamma_1 > 0.7 \pm 0.0879$ or $\gamma_2 > 0.6 \pm 0.4095$, the fault is detected.

Furthermore, the size of the MDF is obtained based on the simulation by increasing the magnitude of the actuator fault from 0 until the magnitude that can be detected at the end of the simulation, i.e., steady state. The following magnitude are obtained form the simulation:

$$f_{a_1}^{\circ} = \pm 0.0650, \tag{4.46a}$$

$$f_{a_2}^{\circ} = \pm 0.3800, \tag{4.46b}$$

where the superscript $\circ$ shows the magnitude is obtained from the simulation.

Now by comparing (4.45) with (4.46), there is no significant difference between the obtained MDF using the theoretical approach and the simulation is found. Thus, (4.46) confirms the obtained magnitude in (4.45) using Theorem 4.3.

For the goal of further analysis, the magnitude of fault f_2 in the pump valve is considered as a single step additive fault considering the following scenarios to assess the FD performance:

- slightly bigger than 0.4095,
- slightly smaller than 0.4095.

In Figure 4.1, the obtained residuals from the simulation are shown in the case that the position of the γ_2 is considered as a faulty parameter with $\gamma_2 > 0.6 \pm 0.4095$ and γ_1 is considered healthy in steady state. Precisely, the fault is added to the valve actuator through the dynamical model (3.25) at $k = 200$ with the magnitude bigger than 0.4095 for the case of actuator fault. In addition, the projection of the invariant residual sets that are generated based on the healthy mode of the system (considering both outputs) is shown in Figure 4.1.

As seen in Figure 4.1, from time step $k = 0$ until $k = 200$, both actuators are healthy and working with $\gamma_1 = 0.7$ and $\gamma_2 = 0.6$. Thus, the generated residuals are inside the healthy invariant sets. On the other hand, the residual sets change at $k = 200$ due to

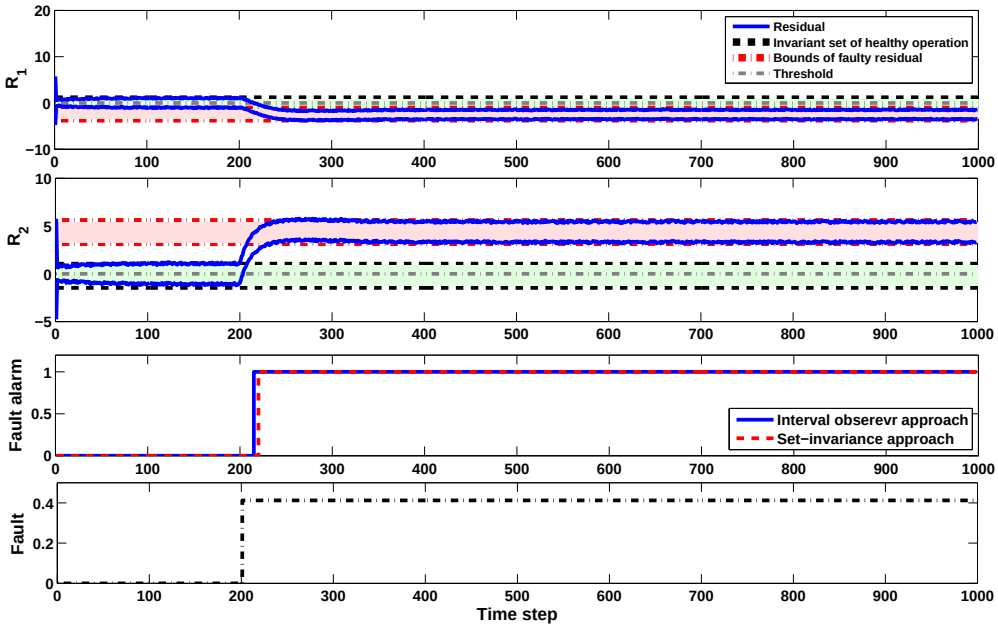

Figure 4.1: FD test in the case of actuator fault with the magnitude bigger than 0.4095.

the occurrence of the fault and go outside of their obtained invariant sets.

Now, the IOA and SIA can be compared in the proposed FD framework. As it can be seen in Figure 4.1, using the IOA, the fault can be detected sooner since, according to Algorithm 2.1, FD test considering the IOA is done only by cheeking if $0 \notin \langle c_r^{io},\ b(R_r^{io})\rangle$. But, based on the SIA, the existence of the fault is proved when the residual (that is determined iteratively at each time instant) satisfies $r_k \notin \left\langle c_{r_\infty}^{is},\ R_{r_{\infty_i}^{is}} \right\rangle$. Thus, moving the residual from the healthy set to the faulty residual set can take more time in comparison with only cheeking if $0 \notin \langle c_r^{io},\ b(R_r^{io})\rangle$. Therefore, the existence of the fault is proved later. What is interesting from Figure 4.1 is that, by considering the proposed FD approach, both IOA and SIA are able to detect the fault with the magnitude slightly bigger than 0.4095 (bottom plot in Figure 4.1 shows the applied fault magnitude). The FD decision is indicated by 1 in case the fault is detected and 0 otherwise.

Considering Remark 4.1, the computational burden of the IOA comes from the type of the considered sets (here zonotopes) in order to bound the effect of uncertainties. As it was mentioned before, the computationally efficient way to implement the FD test without increasing the false alarm rate is to check whether or not 0 belongs to an

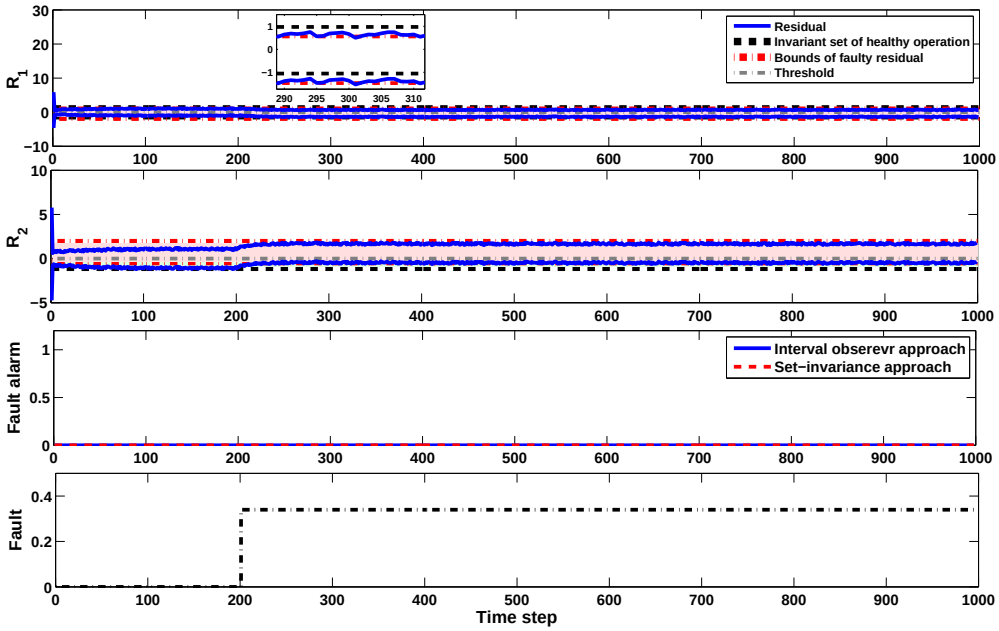

Figure 4.2: FD test in the case of actuator fault with the magnitude smaller than 0.4095.

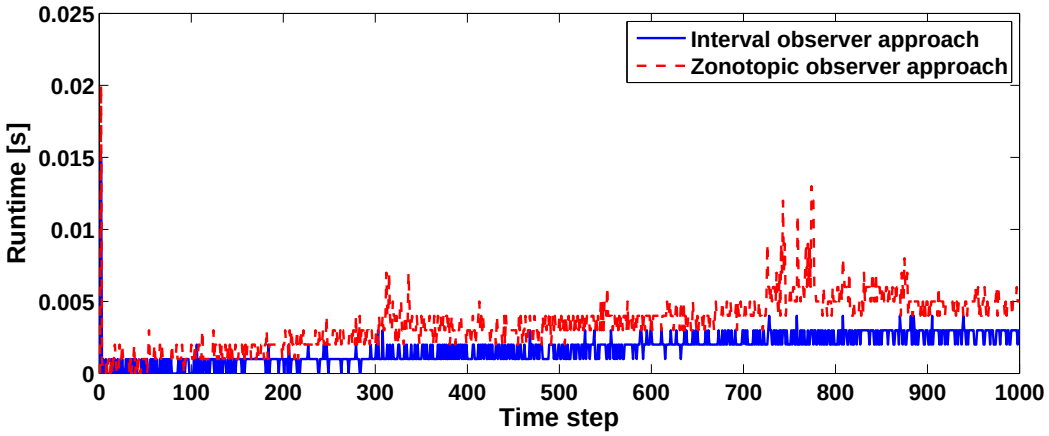

Figure 4.3: Runtime comparison using interval and zonotopic observer-based approaches at each time step.

aligned box enclosing the zonotope $\langle c_{rio},\ R_{rio}\rangle$. In this regard, Figure 4.3 compares the runtime of the FD test considering $0 \notin \langle c_{rio},\ b(R_{rio})\rangle$ (known as IOA) versus the FD test using the exact zonotope (known as zonotopic IOA) at each time instant. Furthermore,

Table 4.3: Runtime comparison using interval and zonotopic observer-based approaches considering the whole time range of the simulation.

	Runtime [s]
IOA	1.6240
Zonotopic IOA	3.0430

Table 4.3 compares the runtime for considering the whole time range of the simulation. It can be observed from both Figure 4.3 and Table 4.3 that the computational burden when using the aligned box enclosing the zonotope $\langle c_{r^{io}},\ R_{r^{io}} \rangle$ for detecting the fault is less than the case of using the exact zonotope.

Likewise, the FD test is applied to the case that the magnitude of the actuator fault is slightly smaller than 0.4095, as shown in the bottom plot of Figure 4.2. It can be observed from Figure 4.2 that the fault is not detectable for both SIA and IOA since neither Algorithm 2.1 nor (4.6) are satisfied. Therefore, the fault with the magnitude smaller than 0.4095 cannot be detected.

Minimum detectable output sensor fault

The MDF analysis in the case of output sensor fault is based on Theorem 4.1. As it is mentioned, the outputs of the quadruple-tank system are the water levels in Tanks 1 and 2 that are obtained as voltages from the measurement devices. In this case study, the height of each tank is 20 cm. Then, each output of the system is between $0 - 10$ V since $K_c = 0.50$ V/cm.

In this case, the simulation of the fault is carried out based on the dynamical model (3.17) and the element of vector f_y, i.e.,

$$f_y = \begin{bmatrix} f_{y_1} \\ f_{y_2} \end{bmatrix}, \tag{4.47}$$

where f_{y_1} and f_{y_2} show the effect of the fault influencing each output. On the other

hand, matrix F_y is defined with the whole range of the measurement as

$$F_y = \begin{bmatrix} 10 & 0 \\ 0 & 10 \end{bmatrix}. \tag{4.48}$$

Turning now to the main goal of this section, the minimum detectable output sensor fault can be determined in steady state using (4.23) based on Theorem 4.1 as

$$f_{y_1} = \pm 0.2808 \text{ V}, \tag{4.49a}$$
$$f_{y_2} = \pm 0.5710 \text{ V}. \tag{4.49b}$$

Thus, note that output sensor faults with a magnitude bigger than 0.2808 V for f_{y_1} and 0.5710 V for f_{y_2} are detectable in steady state. In this case, the operating points that are considered for the water levels of the Tanks 1 and 2 are around 12.4 cm (or 6.2 V) and 12.7 (or 6.35 V), respectively. Thus, the existence of the fault can be detected on each sensor, in the case that the corresponding magnitude is bigger magnitude than the obtained results in (4.49).

Moreover, the following magnitude of MDF is obtained based on the simulation by increasing the size of the output sensor fault until the magnitude that can be detected in steady state, i.e., at the end of simulation:

$$f_{y_1}^{\circ} = \pm 0.2750 \text{ V}, \tag{4.50a}$$
$$f_{y_2}^{\circ} = \pm 0.5650 \text{ V}. \tag{4.50b}$$

The similarity of results is apparent from the comparison of the two magnitudes presented in (4.49) and (4.50) using theoretical approach and simulation to compute MDF. Therefore, (4.50) can be considered as a validation of (4.49) which is obtained based on Theorem 4.1. Regarding the FD performance, the following scenarios are considered when one of the output measured voltages from the level measurement devices (e.g., f_{y_1}) is influenced by a single additive step fault:

- slightly bigger than 0.2808 V,
- slightly smaller than 0.2808 V.

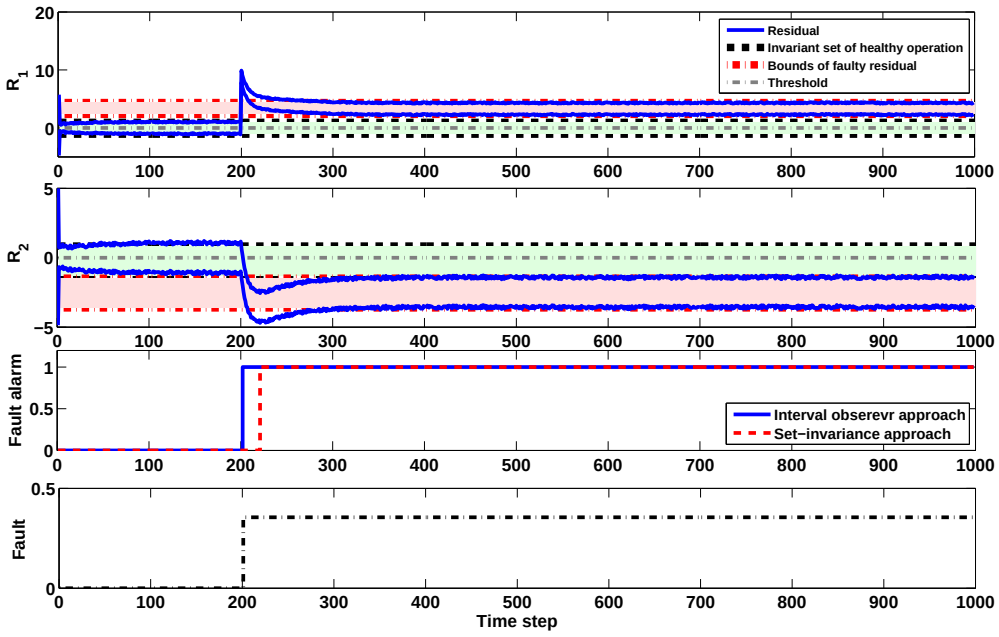

Figure 4.4: FD test in the case of output sensor fault with the magnitude bigger than 0.2808 V.

The output sensor fault is simulated for the case study from $k = 200$ until the end of the simulation and the FD test presented in Algorithm 2.1 is used in order to show the FD performance. In the first scenario, the FD test is applied when the magnitude of te fault is slightly bigger than 0.2808 V. Figure 4.4 shows the obtained results from the simulation of the first scenario. As can be seen from Figure 4.4, the system is working properly until $k = 200$ since the residual is inside of the healthy invariant set. But, after the occurrence of the fault at $k = 200$, the residuals are effected by the given fault and the empty intersection can be found between the residual sets and the healthy invariant sets. Thus, the fault alarm is activated (equal to one) indicating the detection of the fault (see the bottom plot in Figure 4.4). The other point that is worth mentioning regarding Figure 4.4 is related to the comparison of IOA and SIA from the detection time point of view. It can be seen in Figure 4.4 that the decision of the fault occurrence is faster using the IOA in comparison with the SIA. As it is mentioned, the satisfaction of FD test in (4.6) based on SIA required more time than the use of Algorithm 2.1. This faster FD decision shows the advantage of IOA in comparison with the SIA. But, the point regarding the Figure 4.4 is that the fault with the obtained magnitude based on the theoretical formulation is detectable for both mentioned approaches.

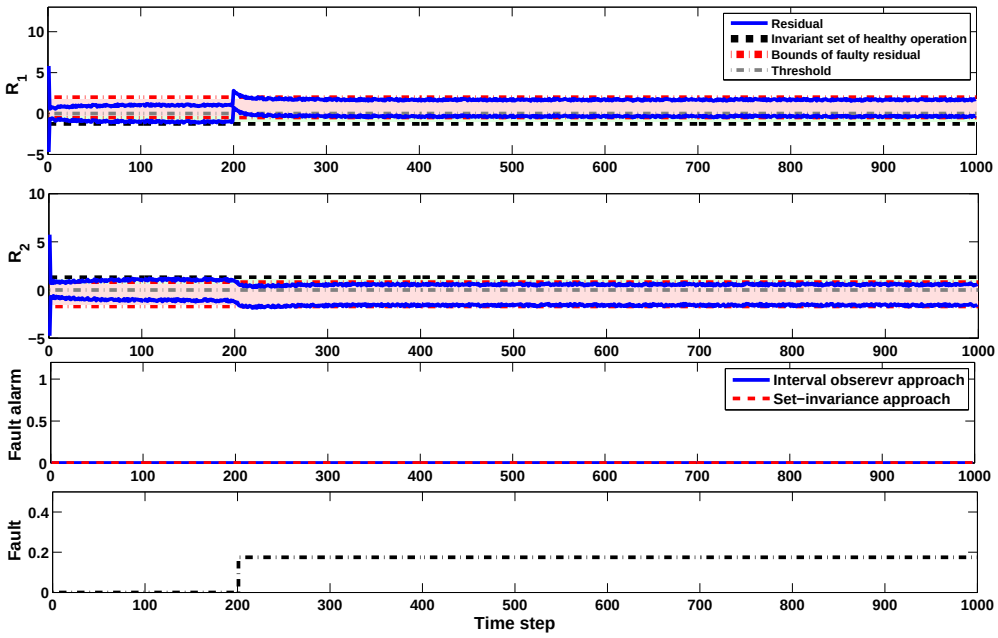

Figure 4.5: FD test in the case of output sensor fault with the magnitude smaller than 0.2808 V.

Furthermore, the FD test is applied to the case that a fault occurs with a magnitude slightly smaller than 0.2808 V. Figure 4.5 shows the simulation of this scenario. The overlap between the residual set and the invariant set can be observed from Figure 4.5. Therefore, the effect of the fault is not detectable since this overlap exists. Thus, if the output sensor fault occurs with the magnitude smaller than 0.2808 V, the fault cannot be detected. In other words, a difference grater than 0.2808 V between the output measurement and its actual value can be associated with the occurrence of the fault. Therefore, the fault with the magnitude shown in bottom plot of Figure 4.5 is not detectable for both SIA and IOA since neither Algorithm 2.1 nor (4.6) are satisfied.

Minimum detectable input sensor fault

As mentioned in Section 4.3.2, this type of fault affects the output estimation provided by the observer. The fault effect is simulated through the observer (3.10) for monitoring the dynamical model (2.4). Simulation of the fault is carried out through the elements

of vector f_u, i.e.,

$$f_u = \begin{bmatrix} f_{u_1} \\ f_{u_2} \end{bmatrix}, \tag{4.51}$$

where f_{u_1} and f_{u_2} denote the effect of the fault influencing each observer input. Furthermore, matrix F_u is defined with the whole range of the input as

$$F_u = \begin{bmatrix} 5 & 0 \\ 0 & 5 \end{bmatrix}. \tag{4.52}$$

Now, using all the points that are mentioned above, the minimum detectable input sensor fault can be theoretically obtained using (4.32) based on Theorem 4.2 as

$$f_{u_1} = \pm 0.0878 \text{ V}, \tag{4.53a}$$
$$f_{u_2} = \pm 0.6416 \text{ V}. \tag{4.53b}$$

As mentioned before, the system input is the voltage increment around 3 V (the linearization point) for both pumps. Thus, considering the values presented in (4.53), the fault with bigger magnitude than 0.0878 V influencing f_{u_1} and 0.6416 V influencing f_{u_2} is detectable. To ensure the obtained results in (4.53), the MDF is determined based on the simulation by increasing the magnitude of the fault from 0 V until the magnitude that is detectable. The following magnitude of the fault is obtained at the end of the simulation (steady state):

$$f_{u_1}^{\circ} = \pm 0.0850 \text{ V}, \tag{4.54a}$$
$$f_{u_2}^{\circ} = \pm 0.6200 \text{ V}. \tag{4.54b}$$

Similar to previous cases (actuator and output sensor faults), no significant difference is obtained by comparing (4.53), obtained from Theorem 4.2, and (4.54), with the value obtained from the simulation. Hence, (4.54) confirms the magnitude of the fault in (4.53).

Finally, the FD performance is assessed considering the following scenarios:

- slightly bigger than 0.0878 V,
- slightly smaller than 0.0878 V.

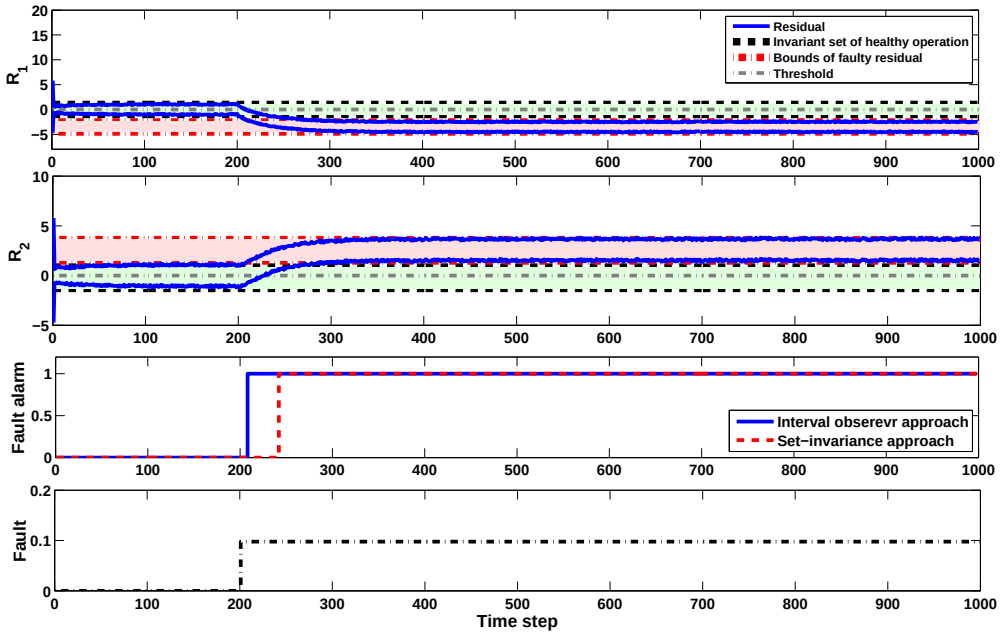

Figure 4.6: FD test in the case of input sensor fault with the magnitude bigger than 0.0878 V.

Figure 4.6 shows the FD test in the case that the fault is considered in the input of the observer model as a single additive step fault with the magnitude slightly bigger than 0.0878 V. Moreover, the occurrence of the fault is simulated from time instant $k = 200$ and it remains until the end of the simulation.

As it can be seen from Figure 4.6, from time instant $k = 0$ until$k = 200$ both residual sets are inside of the healthy invariant sets. It means, the system inputs are not affected by the fault. Therefore, the system is working properly. But, after $k = 200$ the residual sets moves toward the outside of the healthy invariant sets due to the fault effect. Hence, the existence of the fault is proved after $k = 200$ since the intersection between the invariant sets that show the healthy operation of the system and the residual sets that are generated iteratively during the simulation can be found empty. Furthermore, the fault with this magnitude can be detected since $0 \notin \langle c_r^{io},\ b(R_r^{io})\rangle$. Thus, Figure 4.6 shows the activation of the fault alarm proving the existence of the fault. But, as it is explained previously, it can be observed that the FD decision is faster using IOA in comparison with the SIA.

Now, the FD test is applied when the fault occurs in the input of the observer with

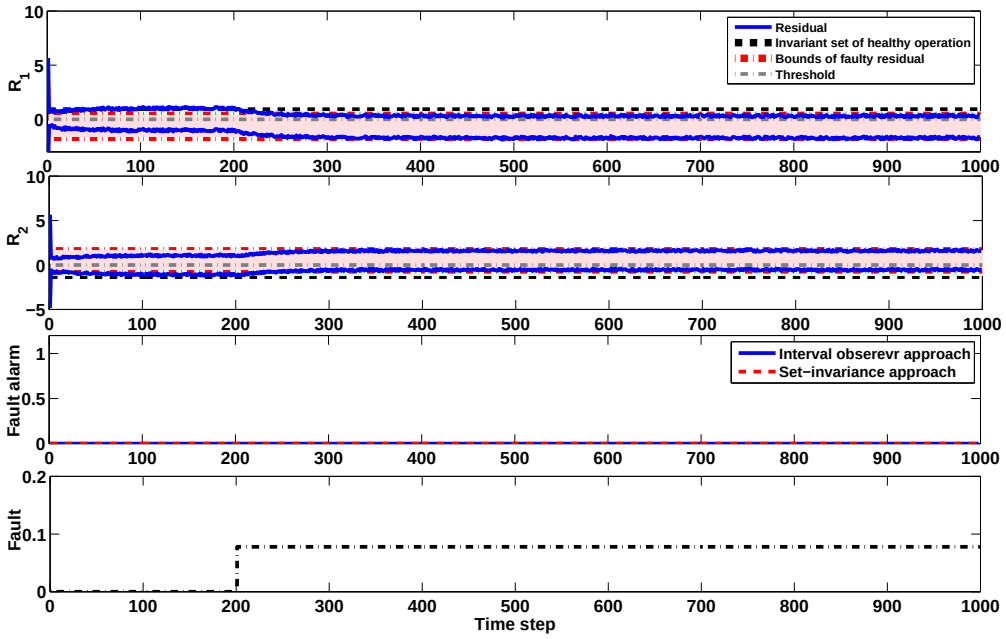

Figure 4.7: FD test in the case of input sensor fault with the magnitude smaller than 0.0878 V.

the magnitude slightly smaller than 0.0878 V and the result from the simulation is shown in Figure 4.7. This figure also shows that the residual sets are inside of the invariant sets in all the considered time range. Therefore, fault magnitude that is shown in the bottom plot of Figure 4.7 is not detectable since neither Algorithm 2.1 nor (4.6) are satisfied. The overlap between the invariant sets and the residual sets proves that the fault can not be detected with the magnitude smaller than 0.0878 V. The fault can never be detected if the overlap between the invariant set and the residual exists.

4.4.3 Discussion

This section discusses the computation of the MDF using IOA and SIA considering the classical sensitivity analysis. In order to detect the fault using both IOA and SIA, first the residual set in healthy operation of the system is obtained. Then, the residual (obtained in real-time) is compared with the healthy one. Furthermore, the FD test using both approaches is almost similar. In the IOA, the residual zonotope is calculated on-line and the fault detection test is based on checking if zero is inside. On the other hand, in the SIA, the healthy residual set (RPI set), which is computed off-line, defines

the non-faulty behaviour.

Since the FD principles can be integrated as it is introduced in Section 4.2. It particular, the healthy zonotopic residual set using an IOA in steady state, i.e., when $k \to \infty$, converges toward the healthy residual set computed using SIA. Then, assuming the initial state estimation error $\tilde{x}_0$ belongs to the zonotopic set $\tilde{\mathcal{X}}_0 = \langle c_{\tilde{x},0},\ R_{\tilde{x},0} \rangle$ that is defined as an RPI set, the corresponding residual set is computed as a zonotopic set using Proposition 4.1.

By understanding the possible way to ingrate the FD test using IOA and SIA as in Proposition 4.2, minimum detectable sensors and actuator faults are characterized in (4.23), (4.32) and (4.39) using the integrated FD principle, respectively. Using the classical sensitivity analysis, the MDF formulations in Section 4.3 is obtained considering the steady state operation of the system that lead to establish a bridge between SIA and IOA in FD framework. Further research is carried out in this section based on using the considered case study to assess the effectiveness of the obtained expressions for computing minimum magnitude of the fault that can be detected.

Three different mentioned fault scenarios in Section 4.3 are considered for the case study in order to test the obtained MDF formulations for the case of actuator and sensor faults. First, the magnitude of each type of fault that can be detected is computed theoretically based on Section 4.3. Then, the MDF magnitudes are compared with the one that are obtained form the simulation where the size of the fault is increased until the detectable magnitude for each case. Then, for completeness of the analysis, the FD test using the IOA and SIA are simulated based on Algorithm 2.1 and (4.6) for both slightly bigger and slightly smaller magnitudes of the fault that are obtained theoretically in order to show the effectiveness and advantage of the IOA in comparison with the SIA. As it can be observed from Figures 4.1, 4.4 and 4.6, both IOA and SIA are able to detect the fault whose the magnitudes are simulated bigger that the obtained MDF. But, the IOA is faster in detecting the fault in comparison with SIA since the corresponding FD test is based on cheeking if $0 \notin \langle c_r^{io},\ b(R_r)^{io} \rangle$. On the other hand, FD decision with SIA is based on checking $r_k \notin \langle c_{r,\infty}^{is},\ R_{r,\infty_i}^{is} \rangle$ that requires more time than IOA FD test. Faster decision about the existence of the fault can be undrestood as an advantage of IOA in comparison with SIA. Furthermore, the FD test based on both approaches is also applied considering the slightly smaller magnitudes that the obtained MDF. Figures 4.2, 4.5 and 4.7 show that the faults whose magnitudes are not detectable for the both IOA and SIA. Therefore, using sensitivity analysis with the integrated IOA

and SIA allows to determine the minimum magnitude of the fault that can be detected for both IOA and SIA.

4.5 Summary

This chapter has developed a study to characterize the MDF for linear uncertain systems when the IOA is used. Moreover, sensitivity analysis and SIA have been integrated for the FD purposes. Accordingly, the MDF has been characterized based on the sensitivity analysis integrated with SIA considering all the possible uncertainties in state and output measurement. Comparing both approaches yields to the same value of the MDF. Finally, a case study based on quadruple-tanks system is used to illustrate the obtained results. So far, this method has only been applied to compute the MDF and less attention has been paid to compute the MIF. In this regard, a robust FDI approach that combines both a zonotopic IOA and a SIA will be provided in the next chapter dealing with not only the computation of MDF, but the computation of the MIF. Moreover, the computation of the MDF is done only during the steady state operation of the system. This limitation will be more relaxed in the next chapter and the MDF and MIF will be characterized in both transient and steady states.

Chapter 5

Integrated IOA and SIA ensuring FDI properties

The aim of this chapter is to provide a robust FDI approach that combines both zonotopic IOA and SIA approaches. The effect of the uncertainty is taken into account considering zonotopic-set representations in both the transient and steady states. The SIA is used to characterize the fault detectability and isolability conditions in the steady-state operation of the system. The MDF and the MIF are characterized for several type of faults in separate formulations utilizing the integration of classical sensitivity analysis and SIA. Finally, a simulation example based on a two-tanks system is employed to both illustrate and discuss the effectiveness of the proposed approach.

5.1 Introduction

So far, one of the most widely used paradigms for generating the residual is the observer-based approach [PQES03]. Observer-based approaches provide state and output estimations from the measurements and the model either stochastic (e.g., Kalman filters) or deterministic approaches (e.g., Luenberger observers) uncertainties. Then, the FD test is based on generating the residual using the output estimation error [CP99, PQES03, ABC05, Com15b].

Recently, there has been an increasing interest in using set-theoretical approaches in FDI framework. Among them, SIA is one of the most used FDI techniques. There is a large number of published studies describing the SIA [Kof05, KHS07, SZDDM08,

OMDDS10, SDD10, XSP+13, RKKM05]. One major drawback of the set-invariance approach is related to the limitation of computing the finite description of its boundary in all cases. There is a large number of published studies describing the computation of invariant sets[1].

Recently, researchers have highlighted the interest of using the capability of the SIA in FDI framework during the transient operation of the system using the set-theoretical approaches [XSP+13, PPOM16b, KPP+17]. In this regard, the main contribution of this chapter is to integrate the observer-based and SIA to develop a FDI scheme that can be used in both transient and steady-state operations of a system. Furthermore, the MDF and the MIF are characterized based on the combination of the classical sensitivity analysis and the SIA. Finally, a well-known benchmark based on the two-tank system is used as a case study to illustrate the results obtained in the chapter and show the effectiveness of the proposed approach.

The structure of the chapter is the following: on-line propagation of the residual set and the FDI design integrating the observer-based and set-invariance approaches are proposed in Section 5.2. In Section 5.3, the application of the proposed approach to a two-tank system is used in order to illustrate its effectiveness. Finally, the conclusions are drawn in Section 5.4.

5.2 Zonotopic FDI observer design

The main objective of this section is to design a zonotopic FDI observer that can benefit from IOA and SIA approaches in order to combine the benefits of them and overcome their drawbacks.

5.2.1 On-line propagation of the residual set

Given the observer (2.5) and considering unknown but bounded uncertainties, two main approaches that are presented in Chapter 4 to detect faults, i.e., i) IOA and ii) SIA, are also considered in this chapter. As it is mentioned in Section 5.1, each of them has its own advantages and drawbacks. In the former approach, the FD principle leads to detect the fault in both transient and steady-state operations of the system since its

[1] More information was reported in Section 4.1.

residual generation is performed on-line. The latter approach only works in steady state since its residual generation is performed off-line.

Therefore, the most serious weakness of the SIA in comparison with the IOA is related to its limited use in transient state. On the other hand, one important feature of SIA is the ability of providing both detectability and isolability properties in comparison with IOA. Therefore, the purpose of this chapter is to propose an FDI approach based on IOA that integrates IOA and SIA that can

- be used during the whole time range (both transient and steady states), and
- guarantee both detectability and isolability properties.

According to [AR08] and [SHO13], the RPI set in SIA (see Section 2.3.3), can be alternatively computed by recursive iteration of $\hat{x}$. Thus, the dynamical model (2.4) and the zonotopic state bounding observer in Proposition 2.1 can be used to obtain the zonotopic representation of the state estimation error and consequently the RPI set. Coming back to the main issue discussed at the beginning of this section, it is now time to compute the RPI set of the state estimation error. In this regard, Proposition 4.1 implies that $\Phi^{\tilde{x}}$ can also be represented as a zonotope. Moreover, Proposition 4.1 can be used to project the state estimation error $\tilde{x}$ into the residual space as (4.5). Therefore, considering Proposition 4.1, the residual set in steady state is invariant and can be considered as a set that combines the polytopic UB method with the zonotopic iterative approximation. Then, when the system is working in either healthy or faulty modes, the residual set characterizing these modes can be computed. The benefit of generating the residual in this way is to track the residual trajectories not only in steady state but also in transient state. Furthermore, in the case of having several types of faults, as long as the faulty and the healthy sets are separated, the proposed FDI approach will be able to work correctly.

In the case of IOA, the fault is detected by testing the consistency of the obtained residual based on the current behavior of the system and a fixed threshold (ideally 0). On the other hand, in the case of SIA, the residual invariant set in the healthy operation of the system is fixed and determined off-line. Then, the fault is detected by means of checking the inconsistency of the obtained residual of the current behaviour and the healthy residual set. Now, considering the zonotopic representation of an RPI set using Proposition 4.1 and through its iterative capability to generate the residual set, both FD

principles can be combined. That is by using the same concept of SIA for FD test, that is based on checking if the obtained residual set belongs to healthy residual set of the system, instead of zero in the case of IOA. The healthy residual set can be generated at each time instant and compared with the current residual set. In this regard, not only the fault can be detected in both steady and transient states but also the fault can be isolated since the separated invariant sets representing different behaviors of the system can be obtained.

5.2.2 FDI design

As mentioned before, the IOA can detect the fault in both transient and steady-state mode of a system. On the other hand, the FD test using the SIA can be applied only in steady state. But, in SIA, the invariant residual set that introduces the healthy mode of the system is computed off-line. In this regard, both healthy and faulty residual sets can be separated and considering this separation, the fault can be both detected and isolated. Furthermore, both on-line and off-line analysis can be used to generate the invariant set characterizing the residual, i.e.,

$$r = \underbrace{y - \hat{y}}_{\text{on-line}} = \underbrace{C(x - \hat{x}) + E_v v}_{\text{off-line}}. \tag{5.1}$$

The proposed method suggested in Proposition 4.1 leads to compute the residual in an on-line way. Therefore, after reaching the state state, the computed residual set can be considered as an invariant set that combines the polytopic UB expression with the zonotopic iterative approximation. Then, if the system is working in healthy operation, this set introduces the healthy operation (that can be computed in both transient state and steady-state). Alternatively, in the case of occurrence of the fault, the residual trajectories can be bounded by another set that characterizes the faulty operation of the system. Then, the separation of the healthy and fault sets is due to a fault occurrence. Moreover, in the case of having several families of the fault, such an observer is also be able to ensure the isolability property. Given the classical Luenberger observer (2.5), it is possible to design one or several observers using Proposition 4.1 to satisfy the separation of the healthy and faulty sets to guarantee both detectability and isolability properties. Similar to the Chapter 3, different actuator and sensor faults will be considered in this chapter. Furthermore, the dynamics of state estimation error in

(2.29) can be rewritten in faulty operation of the system as

$$\tilde{x}_+ = (A - LC)\tilde{x} + E_d d + F f, \tag{5.2}$$

where

$$F = \begin{bmatrix} F_a & -LF_y & -BF_u \end{bmatrix}, \tag{5.3a}$$

$$f = \begin{bmatrix} f_a & f_y & f_u \end{bmatrix}^\top. \tag{5.3b}$$

It is worth mentioning that, based on Assumption 3.1, only one fault can be considered at the same time in the observer structure. Therefore, those elements of F and f that are related to the given fault are retained and the remainder elements are eliminated, e.g., in the case of an actuator fault, $F = \begin{bmatrix} F_a \end{bmatrix}$ and $f = \begin{bmatrix} f_a \end{bmatrix}$. Considering $f \neq 0$, the effect of the uncertainty and fault should be considered when computing the zonotopic set bounding state estimation error that is defined in Proposition 5.1.

Proposition 5.1. *Consider the dynamical model (3.9) and the observer (3.10), the decomposition of the center $c_{\tilde{x}}$ and the shape matrix $R_{\tilde{x}}$ of the zonotopic set bounding the state estimation error in (5.2) into the effects of the disturbance and fault can be recursively defined as*

$$\tilde{x}_+ \in \left\langle c_{\tilde{x}_{d_+}},\ R_{\tilde{x}_{d_+}} \right\rangle \oplus \left\langle c_{\tilde{x}_{f_+}},\ R_{\tilde{x}_{f_+}} \right\rangle, \tag{5.4}$$

with

$$c_{\tilde{x}_{d_+}} = (A - LC)\, c_{\tilde{x}_d}, \tag{5.5a}$$

$$R_{\tilde{x}_{d_+}} = \begin{bmatrix} (A - LC)\bar{R}_{\tilde{x}_d} & E_d \end{bmatrix}, \tag{5.5b}$$

$$c_{\tilde{x}_{f_+}} = (A - LC)\, c_{\tilde{x}_f}, \tag{5.5c}$$

$$R_{\tilde{x}_{f_+}} = \begin{bmatrix} (A - LC)\bar{R}_{\tilde{x}_f} & F \end{bmatrix}. \tag{5.5d}$$

where the subscripts d and f denote the effects of uncertainties (i.e., state disturbance and measurement noise) and the fault, receptively.

Proof. Assume $\tilde{x} \in \langle c_{\tilde{x}_d},\ R_{\tilde{x}_d} \rangle \oplus \langle c_{\tilde{x}_f},\ R_{\tilde{x}_f} \rangle$ and consider Assumptions 2.2 and 3.1, the

zonotopic form of the state estimation error in (4.1) can be expressed as

$$x_+ \in \langle (A-LC)c_{\tilde{x}_d},\ (A-LC)R_{\tilde{x}_d} \rangle \oplus \left\langle (A-LC)c_{\tilde{x}_f},\ (A-LC)R_{\tilde{x}_f} \right\rangle \oplus \langle 0,\ E_d \rangle \oplus \langle 0,\ F \rangle\,. \quad (5.6)$$

Furthermore, consider that the superposition principle can be explicitly invoked in the linear setting. Therefore, using Definition B.22, the center and the generator matrices in (5.6) can be reorganized as in (5.5). Thus, $\tilde{x}_+ \in \left\langle c_{\tilde{x}_{d_+}},\ R_{\tilde{x}_{d_+}} \right\rangle \oplus \left\langle c_{\tilde{x}_{f_+}},\ R_{\tilde{x}_{f_+}} \right\rangle$. □

Consequently, the state estimation error can be projected into the residual space using (5.1). Thus, Proposition 5.1 allows to derive the residual set decomposing the effects of the disturbance and fault as

$$c_{r_{d_+}} = C c_{\tilde{x}_{d_+}}\,, \quad (5.7a)$$

$$R_{r_{d_+}} = \begin{bmatrix} C R_{\tilde{x}_{d_+}} & E_v \end{bmatrix}, \quad (5.7b)$$

$$c_{r_{f_+}} = C c_{\tilde{x}_{f_+}}\,, \quad (5.7c)$$

$$R_{r_{f_+}} = \begin{bmatrix} C R_{\tilde{x}_{f_+}} \end{bmatrix}. \quad (5.7d)$$

Furthermore, the effects of the uncertainty and fault on the residual set can be known as the residual sensitivity with respect to the uncertainty and fault. Therefore, this type of on-line observer can be used in both transient and steady state to guarantee detectability and isolability in the case of satisfaction of conditions in Theorems 5.1 and 5.2.

Theorem 5.1. *(Detectability condition) Consider Definition B.25 and the decomposed form of the residual set in (5.7), the fault will be detected if*

$$s_{f_{\bullet,l}} > s_{d_u}, \quad (5.8a)$$

$$s_{f_{\bullet,u}} < s_{d_l}, \quad (5.8b)$$

with

$$s_{f_{\bullet,l}} = \left(C_i c_{r_{f_\bullet}} - \left\| C_i R_{r_{f_\bullet}} \right\|_1 \right) + \left(C_i c_{r_d} - \left\| C_i R_{r_d} \right\|_1 \right), \quad (5.9a)$$

$$s_{f_{\bullet,u}} = \left(C_i c_{r_{f_\bullet}} + \left\| C_i R_{r_{f_\bullet}} \right\|_1 \right) + \left(C_i c_{r_d} + \left\| C_i R_{r_d} \right\|_1 \right), \quad (5.9b)$$

$$s_{d_l} = C_i c_{r_d} - \left\| C_i R_{r_d} \right\|_1, \quad (5.9c)$$

$$s_{d_u} = C_i c_{r_d} + \left\| C_i R_{r_d} \right\|_1, \quad (5.9d)$$

where i corresponds to the i^{th} row of the vector C. Moreover, s_{f_l} and s_{f_u} are the minimum and the maximum values of the zonotope support strip in the faulty case, respectively. Furthermore, s_{d_l} and s_{d_u} are the minimum and the maximum values of the zonotope support strip in the healthy case, respectively.

Proof. Consider (5.7) in faultless scenario, i.e., $f_\bullet = 0$, $r \in \langle c_{r_d},\ R_{r_d} \rangle$. But, in the case of faulty operation of the system $r \notin \langle c_{r_d},\ R_{r_d} \rangle$. Therefore, it can be written that

$$\langle c_{r_d},\ R_{r_d} \rangle \oplus \left\langle c_{r_{f_\bullet}},\ R_{r_{f_\bullet}} \right\rangle \notin \langle c_{r_d},\ R_{r_d} \rangle . \tag{5.10}$$

Then, by computing the zonotope support strip using Definition B.25 for the residual sets in both healthy and faulty operations of the system, (5.10) will be obtained if the inequality in (5.8) is satisfied. □

Theorem 5.2. *(Isolability condition) Consider the decomposed form of the residual set in (5.7) and Definition B.25 to compute the zonotope support strip, a necessary condition that should be added to detectability condition in Theorem 5.1 in order to ensure the isolation of a fault $f_{\bullet_p}$ from a fault $f_{\bullet_q}$ is*

$$s_{f_{\bullet,l_p}} > s_{f_{\bullet,u_q}}, \tag{5.11a}$$

$$s_{f_{\bullet,u_p}} < s_{f_{\bullet,l_q}}, \tag{5.11b}$$

with

$$s_{f_{\bullet,l_p}} = C_i c_{r_{f_{\bullet_p}}} - \left\| C_i R_{r_{f_{\bullet_p}}} \right\|_1, \tag{5.12}$$

$$s_{f_{\bullet,u_p}} = C_i c_{r_{f_{\bullet_p}}} + \left\| C_i R_{r_{f_{\bullet_p}}} \right\|_1, \tag{5.13}$$

$$s_{f_{\bullet,l_q}} = C_i c_{r_{f_{\bullet_q}}} - \left\| C_i R_{r_{f_{\bullet_q}}} \right\|_1, \tag{5.14}$$

$$s_{f_{\bullet,u_q}} = C_i c_{r_{f_{\bullet_q}}} + \left\| C_i R_{r_{f_{\bullet_q}}} \right\|_1, \tag{5.15}$$

where $s_{f_{\bullet,l_p}}$ and $s_{f_{\bullet,u_p}}$ are the minimum and the maximum values of the zonotope support strip in the case of occurrence of $f_{\bullet_p}$, respectively. Furthermore, $s_{f_{\bullet,l_q}}$ and $s_{f_{\bullet,u_q}}$ are the minimum and the maximum values of the zonotope support strip in the case of occurrence of $f_{\bullet_q}$, respectively.

Proof. The proof follows in the same way than Theorem 5.1. Then, consider (5.7) and

(5.8), it can be written that $f_{\bullet_p}$ is isolable from $f_{\bullet_q}$ if

$$\left\langle c_{r_{f_{\bullet_p}}},\ R_{r_{f_{\bullet_p}}} \right\rangle \notin \left\langle c_{r_{f_{\bullet_q}}},\ R_{r_{f_{\bullet_q}}} \right\rangle. \tag{5.16}$$

Thus, (5.16) can be written using Definition B.25 as (5.11) for the purpose of isolation of $f_{\bullet_p}$ from $f_{\bullet_q}$ □

5.2.3 Characterization of MDF and MIF

Up to now, the chapter has focused on detectability and isolability properties of the proposed approach during both transient and steady-state operations of the system. It is mentioned that the detectability and isolability can be achieved in the case of satisfaction of the Theorems 5.1 and 5.2. Then, MDF and MIF can be characterized using the input-output forms of the measurement y, output prediction $\hat{y}$ and the residual r derived in Section 4.3. Then, considering all the mentioned points and the detectability conditions in Theorem 5.1, the minimum magnitude of the fault that can be detected can be characterized following Theorem 5.3.

Theorem 5.3. *(MDF) The MDF is characterized using conditions in (5.8), Proposition 5.1 and the decomposed form of the residual set in (5.7) as*

$$\begin{aligned} \overline{f^{\text{Det}}_{\text{min}_{\bullet_{j,\infty}}}} &= \max \overline{f^{\text{Det}}_{\text{min}_{\bullet_{ji,\infty}}}}, \\ \overline{f^{\text{Det}}_{\text{min}_{\bullet_{ji,\infty}}}} &= +2\, \frac{\|\mathscr{G}_{d_i}(1)\|_1}{\left\|\mathscr{G}_{f_{\bullet_{ij}}}(1)\right\|_1}, \end{aligned} \tag{5.17a}$$

$$\begin{aligned} \underline{f^{\text{Det}}_{\text{min}_{\bullet_{j,\infty}}}} &= \min \underline{f^{\text{Det}}_{\text{min}_{\bullet_{ji,\infty}}}}, \\ \underline{f^{\text{Det}}_{\text{min}_{\bullet_{ji,\infty}}}} &= -2\, \frac{\|\mathscr{G}_{d_i}(1)\|_1}{\left\|\mathscr{G}_{f_{\bullet_{ij}}}(1)\right\|_1}, \end{aligned} \tag{5.17b}$$

where the superscript Det *refers to the detectable fault and the factor* 2 *appears because the worst-case scenario is considered, where the uncertainties have a maximum influence in the opposite direction compared to that of the fault occurrence. The indices i and j refer to the i^{th} row and j^{th} column of the transfers $\mathscr{G}_d$ and $\mathscr{G}_f$ (residual sensitivity with respect to the uncertainty and fault), respectively.*

Proof. Based on (5.7), in the time domain and in steady state (limit as $k \to \infty$), $r_\infty \in \left\langle c_{r_{d_\infty}},\ R_{r_{d_\infty}} \right\rangle \oplus \left\langle c_{r_{f_\infty}},\ R_{r_{f_\infty}} \right\rangle$. On the other hand, considering $f^{\text{Det}}_{\text{min}_\bullet} \in [\underline{f^{\text{Det}}_{\text{min}_\bullet}},\ \overline{f^{\text{Det}}_{\text{min}_\bullet}}]$, it

can be written that

$$f^{\text{Det}}_{\min_\bullet} \in \left\langle c_{f^{\text{Det}}_{\min_\bullet}},\ R_{f^{\text{Det}}_{\min_\bullet}} \right\rangle, \tag{5.18}$$

where $c_{f^{\text{Det}}_{\min_\bullet}}$ and $R_{f^{\text{Det}}_{\min_\bullet}}$ show the center and the shape matrix of the MDF zonotope, respectively. Considering the worst-case scenario, the limit of the MDF can be understood as a maximum and minimum value of its zonotope support strip that can be computed using (5.18) and Definition B.25. Therefore, the MDF is known as

$$\overline{f^{\text{Det}}_{\min_{\bullet_j}}} = \max \overline{f^{\text{Det}}_{\min_{\bullet_j}}} = C_i c_{f^{\text{Det}}_{\min_\bullet}} + \left\| C_i R_{f^{\text{Det}}_{\min_\bullet}} \right\|_1, \tag{5.19a}$$

$$\underline{f^{\text{Det}}_{\min_{\bullet_j}}} = \min \underline{f^{\text{Det}}_{\min_{\bullet_j}}} = C_i c_{f^{\text{Det}}_{\min_\bullet}} - \left\| C_i R_{f^{\text{Det}}_{\min_\bullet}} \right\|_1. \tag{5.19b}$$

Then, consider $\omega \in \langle 0,\ I_{n_\omega} \rangle$ and $\upsilon \in \langle 0,\ I_{n_\upsilon} \rangle$, in the steady state for the faulty case, i.e., $f_\bullet \neq 0$, it is satisfied

$$r_\infty \in \langle \mathscr{G}_u(1) u_\infty,\ 0 \rangle \oplus \langle 0,\ \mathscr{G}_d(1) \rangle \oplus \left\langle \mathscr{G}_{f_\bullet}(1) c_{f^{\text{Det}}_{\min_\bullet}},\ \mathscr{G}_{f_\bullet}(1) R_{f^{\text{Det}}_{\min_\bullet}} \right\rangle. \tag{5.20}$$

Moreover, the decomposed form of the center and the shape matrix of residual zonotope in steady state can be computed using (5.20) as

$$c_{r_{d_\infty}} = \mathscr{G}_u(1) u_\infty, \tag{5.21a}$$

$$R_{r_{d_\infty}} = \left[\mathscr{G}_d(1) \right], \tag{5.21b}$$

$$c_{r_{f_{\bullet,\infty}}} = \mathscr{G}_{f_\bullet}(1) c_{f^{\text{Det}}_{\min_\bullet}}, \tag{5.21c}$$

$$R_{r_{f_{\bullet,\infty}}} = \left[\mathscr{G}_{f_\bullet}(1) R_{f^{\text{Det}}_{\min_\bullet}} \right], \tag{5.21d}$$

where the subindex r_{d_∞} and r_{f_∞} show the residual sensitivity with respect to the effect of uncertainty and fault in steady state, respectively.

Now, consider Theorem 5.1 in the faulty mode of the system, i.e., satisfaction of the detectability conditions in (5.8), it can be stated that in steady state, the fault will be detected if

$$s_{f_{\bullet,l,\infty}} > s_{d_{u,\infty}}, \tag{5.22a}$$

$$s_{f_{\bullet,u,\infty}} < s_{d_{l,\infty}}. \tag{5.22b}$$

Then, consider (5.21) and Definition B.25, it follows that

$$s_{f_{\bullet,l,\infty}} = \left(C_i c_{r_{f_{\bullet,\infty}}} - \left\|C_i R_{r_{f_{\bullet,\infty}}}\right\|_1\right) + \left(C_i c_{r_{d_\infty}} - \left\|C_i R_{r_{d_\infty}}\right\|_1\right), \tag{5.23a}$$

$$s_{f_{\bullet,u,\infty}} = \left(C_i c_{r_{f_{\bullet,\infty}}} + \left\|C_i R_{r_{f_{\bullet,\infty}}}\right\|_1\right) + \left(C_i c_{r_{d_\infty}} + \left\|C_i R_{r_{d_\infty}}\right\|_1\right), \tag{5.23b}$$

$$s_{d_{l,\infty}} = C_i c_{r_{d_\infty}} - \left\|C_i R_{r_{d_\infty}}\right\|_1, \tag{5.23c}$$

$$s_{d_{u,\infty}} = C_i c_{r_{d_\infty}} + \left\|C_i R_{r_{d_\infty}}\right\|_1, \tag{5.23d}$$

Next, by considering the worst-case scenario, i.e., the residual is considered with the extreme value (it is located at either the lower or the upper bound of the zonotope support strip of the considered threshold), it can be written that the fault can be detected if

$$\left(C_i c_{r_{f_{\bullet,\infty}}} - \left\|C_i R_{r_{f_{\bullet,\infty}}}\right\|_1\right) > +2\left\|C_i R_{r_{d_\infty}}\right\|_1 \tag{5.24a}$$

$$\left(C_i c_{r_{f_{\bullet,\infty}}} + \left\|C_i R_{r_{f_{\bullet,\infty}}}\right\|_1\right) < -2\left\|C_i R_{r_{d_\infty}}\right\|_1 \tag{5.24b}$$

Finally, the MDF can be characterized considering (5.19) and by substitution of residual sensitivity (5.21) and (5.23) in (5.24), which in (5.17). □

The condition in Theorem 5.1 is sufficient only for detecting the fault and the MDF, which is characterized in Theorem 5.3. Moreover, the fault can be isolated if the intersection between the residual sets (computed based on different type of faults) is empty. Therefore, the condition in Theorem 5.2 should also be satisfied together with condition (5.8) in order to guarantee both detection and isolation of the fault.

Furthermore, using residual in (5.7) and condition in Theorem 5.2, the minimum magnitude of the fault that can ensure both detection and isolation is characterized following Theorem 5.4.

Theorem 5.4. *(MIF) The MIF of a fault $f_{\bullet_p}$ from a fault $f_{\bullet_q}$ is characterized using the conditions in Theorems 5.1 and 5.2, and also, considering the decomposed form of the residual set in (5.7) as*

$$\overline{f^{\text{Iso}}_{\min_{\bullet_{p_j,\infty}}}} = \max \overline{f^{\text{Iso}}_{\min_{\bullet_{p_{ji},\infty}}}},$$

$$\overline{f^{\text{Iso}}_{\min_{\bullet_{p_{ji},\infty}}}} = +2\,\frac{\|\mathscr{G}_{d_i}(1)\|_1}{\left\|\mathscr{G}_{f_{\bullet_{p_{ij}}}}(1)\right\|_1} + \frac{\left\|\mathscr{G}_{f_{\bullet_{q_i}}}(1)\right\|_1}{\left\|\mathscr{G}_{f_{\bullet_{p_{ij}}}}(1)\right\|_1}, \tag{5.25a}$$

$$\underline{f^{\text{Iso}}_{\min_{\bullet_{p_j,\infty}}}} = \min \underline{f^{\text{Iso}}_{\min_{\bullet_{p_{ji},\infty}}}},$$

$$\underline{f^{\text{Iso}}_{\min_{\bullet_{p_{ji},\infty}}}} = -2\,\frac{\|\mathscr{G}_{d_i}(1)\|_1}{\left\|\mathscr{G}_{f_{\bullet_{p_{ij}}}}(1)\right\|_1} + \frac{\left\|\mathscr{G}_{f_{\bullet_{q_i}}}(1)\right\|_1}{\left\|\mathscr{G}_{f_{\bullet_{p_{ij}}}}(1)\right\|_1}, \tag{5.25b}$$

where the superscript Iso *refers to the isolable fault and the factor* 2 *appears because the worst-case scenario is considered considering the effect of uncertainties* d *and fault* $f_{\bullet_q}$ *that have a maximum influence in the opposite direction compared to that of the fault occurrence* $f_{\bullet_p}$.

Proof. The proof follows a similar procedure than the one used in Theorem 5.3. In this regard, based on (5.7), it can be written in the time domain and in steady state (limit as $k \to \infty$) that $r_\infty \in \langle c_{r_{d_\infty}},\ R_{r_{d_\infty}} \rangle \oplus \left\langle c_{r_{f_{\bullet_{p,\infty}}}},\ R_{r_{f_{\bullet_{p,\infty}}}} \right\rangle$ in the case of occurrence of $f_{\bullet_p}$. Moreover, $r_\infty \in \langle c_{r_{d_\infty}},\ R_{r_{d_\infty}} \rangle \oplus \left\langle c_{r_{f_{\bullet_{q,\infty}}}},\ R_{r_{f_{\bullet_{q,\infty}}}} \right\rangle$ in the case of occurrence of $f_{\bullet_q}$. On the other hand, considering $f^{\text{Iso}}_{\min_{\bullet_p}} \in [\underline{f^{\text{Iso}}_{\min_{\bullet_p}}},\ \overline{f^{\text{Iso}}_{\min_{\bullet_p}}}]$, it can be written that

$$f^{\text{Iso}}_{\min_{\bullet_p}} \in \left\langle c_{f^{\text{Iso}}_{\min_{\bullet_p}}},\ R_{f^{\text{Iso}}_{\min_{\bullet_p}}} \right\rangle, \tag{5.26a}$$

$$f^{\text{Iso}}_{\min_{\bullet_q}} \in \left\langle c_{f^{\text{Iso}}_{\min_{\bullet_q}}},\ R_{f^{\text{Iso}}_{\min_{\bullet_q}}} \right\rangle, \tag{5.26b}$$

where $c_{f^{\text{Iso}}_{\min_{\bullet_p}}}$, $R_{f^{\text{Iso}}_{\min_{\bullet_p}}}$ and $c_{f^{\text{Iso}}_{\min_{\bullet_q}}}$, $R_{f^{\text{Iso}}_{\min_{\bullet_q}}}$ show the center and the shape matrix of the MIF zonotope in the case of occurrence of the $f_{\bullet_p}$ and $f_{\bullet_q}$, respectively. Furthermore, considering the isolability condition in Theorem 5.2, in the case of occurrence of $f_{\bullet_p}$, i.e., $f_{\bullet_p} \neq 0$, and when $k \to \infty$, it can be derived that

$$r_\infty \in \langle \mathscr{G}_u(1)u_\infty,\ 0 \rangle \oplus \langle 0,\ \mathscr{G}_d(1) \rangle \oplus \left\langle \mathscr{G}_{f_{\bullet_p}}(1) c_{f^{\text{Iso}}_{\min_{\bullet_p}}},\ \mathscr{G}_{f_{\bullet_p}}(1) R_{f^{\text{Iso}}_{\min_{\bullet_p}}} \right\rangle. \tag{5.27}$$

On the other hand, for the case of occurrence of $f_{\bullet_q}$, it is satisfied

$$r_\infty \in \langle \mathscr{G}_u(1)u_\infty,\ 0 \rangle \oplus \langle 0,\ \mathscr{G}_d(1) \rangle \oplus \left\langle \mathscr{G}_{f_{\bullet_q}}(1) c_{f^{\text{Iso}}_{\min_{\bullet_q}}},\ \mathscr{G}_{f_{\bullet_q}}(1) R_{f^{\text{Iso}}_{\min_{\bullet_q}}} \right\rangle. \tag{5.28}$$

Now, the residual sensitivity with respect to the effect of uncertainties in steady state can be obtained as in (5.21a) and (5.21b). Furthermore, the residual sensitivity with respect to the effect of faults $f_{\bullet_p}$ and $f_{\bullet_q}$ in steady state can be computed as

$$c_{r_{f_{\bullet_p},\infty}} = \mathscr{G}_{f_{\bullet_p}}(1) c_{f^{\text{Iso}}_{\min_{\bullet_p}}}, \tag{5.29a}$$

$$R_{r_{f_{\bullet_p},\infty}} = \left[\mathscr{G}_{f_{\bullet_p}}(1) R_{f^{\text{Iso}}_{\min_{\bullet_p}}}\right], \tag{5.29b}$$

$$c_{r_{f_{\bullet_p},\infty}} = \mathscr{G}_{f_{\bullet_q}}(1) c_{f^{\text{Iso}}_{\min_{\bullet_q}}}, \tag{5.29c}$$

$$R_{r_{f_{\bullet_q},\infty}} = \left[\mathscr{G}_{f_{\bullet_q}}(1) R_{f^{\text{Iso}}_{\min_{\bullet_q}}}\right]. \tag{5.29d}$$

Besides, the isolability condition in (5.11) can be rewritten during steady state as

$$s_{f_{\bullet,l_p,\infty}} > s_{f_{\bullet,u_q,\infty}}, \tag{5.30a}$$

$$s_{f_{\bullet,u_p,\infty}} < s_{f_{\bullet,l_q,\infty}}, \tag{5.30b}$$

where

$$s_{f_{\bullet,l_p,\infty}} = \left(C_i c_{r_{f_{\bullet_p},\infty}} - \left\|C_i R_{r_{f_{\bullet_p},\infty}}\right\|_1\right) + \left(C_i c_{r_{d_\infty}} - \left\|C_i R_{r_{d_\infty}}\right\|_1\right), \tag{5.31a}$$

$$s_{f_{\bullet,u_p,\infty}} = \left(C_i c_{r_{f_{\bullet_p},\infty}} + \left\|C_i R_{r_{f_{\bullet_p},\infty}}\right\|_1\right) + \left(C_i c_{r_{d_\infty}} - \left\|C_i R_{r_{d_\infty}}\right\|_1\right), \tag{5.31b}$$

$$s_{f_{\bullet,l_q,\infty}} = \left(C_i c_{r_{f_{\bullet_q},\infty}} - \left\|C_i R_{r_{f_{\bullet_q},\infty}}\right\|_1\right) + \left(C_i c_{r_{d_\infty}} - \left\|C_i R_{r_{d_\infty}}\right\|_1\right), \tag{5.31c}$$

$$s_{f_{\bullet,u_q,\infty}} = \left(C_i c_{r_{f_{\bullet_q},\infty}} + \left\|C_i R_{r_{f_{\bullet_q},\infty}}\right\|_1\right) + \left(C_i c_{r_{d_\infty}} - \left\|C_i R_{r_{d_\infty}}\right\|_1\right). \tag{5.31d}$$

Then, by considering the worst-case scenario for both uncertainties and the considered fault (here $f_{\bullet_q}$) with respect to the other faults (here $f_{\bullet_p}$), the isolability condition can be rewritten as

$$\left(C_i c_{r_{f_{\bullet_p},\infty}} - \left\|C_i R_{r_{f_{\bullet_p},\infty}}\right\|_1\right) > \left(C_i c_{r_{f_{\bullet_q},\infty}} + \left\|C_i R_{r_{f_{\bullet_q},\infty}}\right\|_1\right), \tag{5.32a}$$

$$\left(C_i c_{r_{f_{\bullet},\infty}} + \left\|C_i R_{r_{f_{\bullet},\infty}}\right\|_1\right) < \left(C_i c_{r_{f_{\bullet_q},\infty}} - \left\|C_i R_{r_{f_{\bullet_q},\infty}}\right\|_1\right). \tag{5.32b}$$

Finally, the MIF can be characterized considering (5.26) and by substitution of the residual sensitivity with respect to disturbances (5.21a), (5.21b) and the residual sensitivity with respect to faults (5.29) in (5.32) results in (5.25). □

The minimum magnitude of the fault that establishes if a fault is detectable and

isolable according to Theorems 5.3 and 5.4. Therefore, it can be written that in the case of satisfaction of both conditions in (5.8) and (5.11), the fault can be detected and isolated. Furthermore, another possible manner to guarantee both detection and isolation at the same time can be achieved by considering (5.32). This condition shows that the isolation of the fault depends on the direction of vector C. Thus, in the case of having the occurrence of the faults in different directions, the fault can be isolated with the same magnitude of the MDF. In this regard, further analysis of the approaches will be discussed in Section 5.3 based on a case study.

5.3 Case study

5.3.1 Plant description

The proposed FDI scheme will be tested using a two-tank system based on the well-known benchmark proposed in [Joh00] as in Appendix A.

As it is explained in Section A.2, the input of the two-tank system is the pump flow rate that is determined when applying voltage v of the pump. Therefore, the action of the pump is to pour the tanks by extracting the water from the basin. Moreover, Tank 1 is placed below Tank 2. But, in this chapter, the outputs of the process are the water levels in both upper and lower tanks that are obtained as voltages from the measurement devices. Therefore, in this chapter, matrices A and B are considered the same as system matrices in Section 3.4.1. So far, since the purpose is to measure the water levels in both upper and lower tanks, matrix C in (A.7) is considered as

$$C = \begin{bmatrix} 0.5 & 0 \\ 0 & 0.5 \end{bmatrix}. \tag{5.33}$$

Furthermore, taking into account the state disturbance and the measurement noise, E_ω and E_υ are simulated in (A.3) with

$$E_\omega = \begin{bmatrix} 0.05 & 0 \\ 0 & 0.05 \end{bmatrix}, \qquad E_\upsilon = \begin{bmatrix} 0.01 & 0 \\ 0 & 0.01 \end{bmatrix}. \tag{5.34}$$

As it can observed in (5.34), E_ω is used to define a disturbance influencing all the

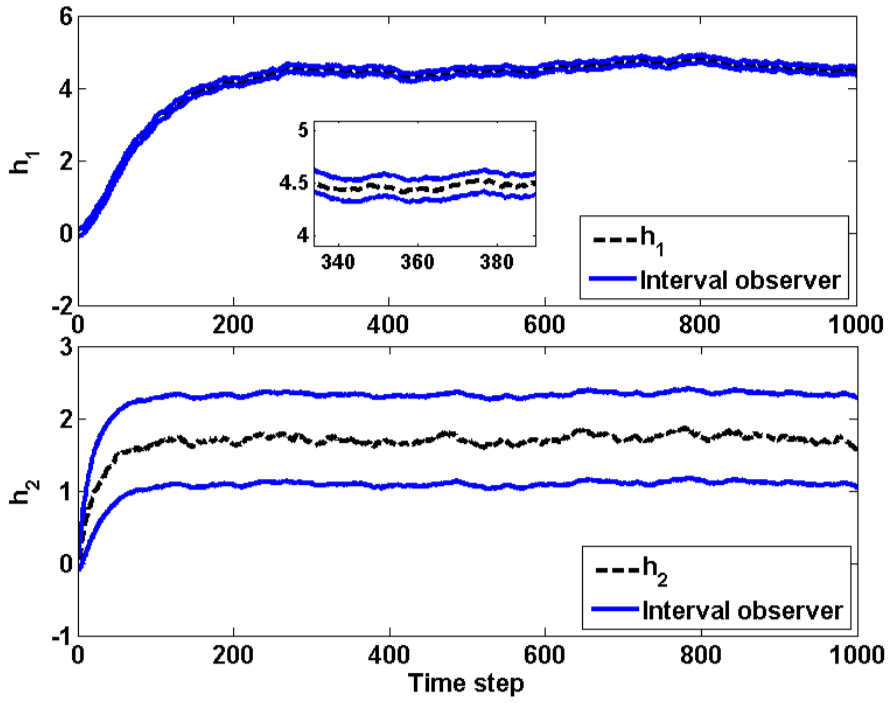

Figure 5.1: State estimation in healthy operation of the system.

states and the measurement noise affecting both outputs is modeled through E_v.

5.3.2 Performing FDI

Healthy operation of the system

The first step in the FPI process is to obtain the state estimation. In this regard, the additive uncertainties (ω and v) are assumed unknown but bounded based on the zonotopic definition of a set during the simulations as in (2.3). Figure 5.1 shows the projection of the computed state-bounding zonotope into the state-space when the system is working in its healthy mode.

As discussed in Sections 2.3.1 and 2.3.3, there are two different approaches for bounding the effect of uncertainty in the residual. On the one hand, the on-line IOA that is able to generate the residual set in both transient state and steady state. On the other hand, the SIA that is an off-line procedure to compute the residual set in steady state

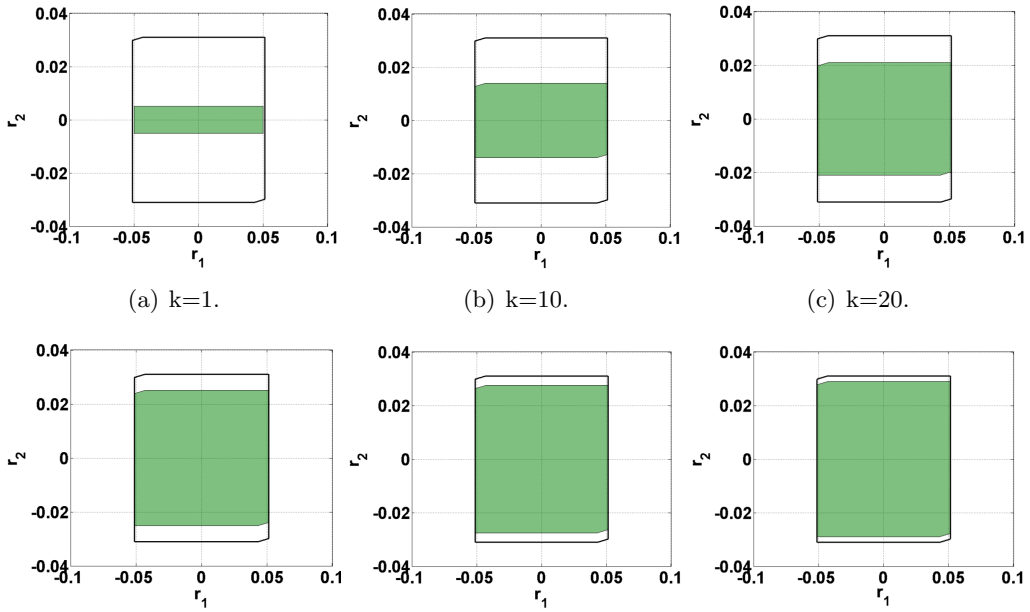

(a) k=1. (b) k=10. (c) k=20.

(d) k=30. (e) k=40. (f) k=50.

Figure 5.2: On-line propagation of residual set using zonotopic IOA during transient state and healthy operation of the system.

(see (5.1)). Figure 5.2 presents the residual set based on on-line IOA that is obtained from the transient operation of the healthy system. The obtained residual zonotopes at time instants $k = 1$, $k = 10$, $k = 20$, $k = 30$, $k = 40$ and $k = 50$ are shown in Figure 5.2 for the healthy functioning of the system in (A.3). From the results in Figure 5.2, it can be seen that the residual generated using the proposed on-line zonotopic observer (the green zonotopes) ultimately converges to the one that is represented by the black solid line. Based on the system description, outputs of the considered two-tank system are the water level in both upper and lower tanks. Therefore, the residual zonotopic set can be generated as a plane zonotope (2D zonotope) at each time step, where r_1 and r_2 denote the difference between the predicted values of the h_1 and h_2 with their real measured values given by the sensor, respectively.

From the results in Figure 5.2, it can be observed that the residual generated by an on-line zonotopic observer is also converging to the one that is shown in Figure 5.3, which can be considered as an RPI set for the residual. Furthermore, Figure 5.3 shows the obtained residual set from the SIA based on (2.31).

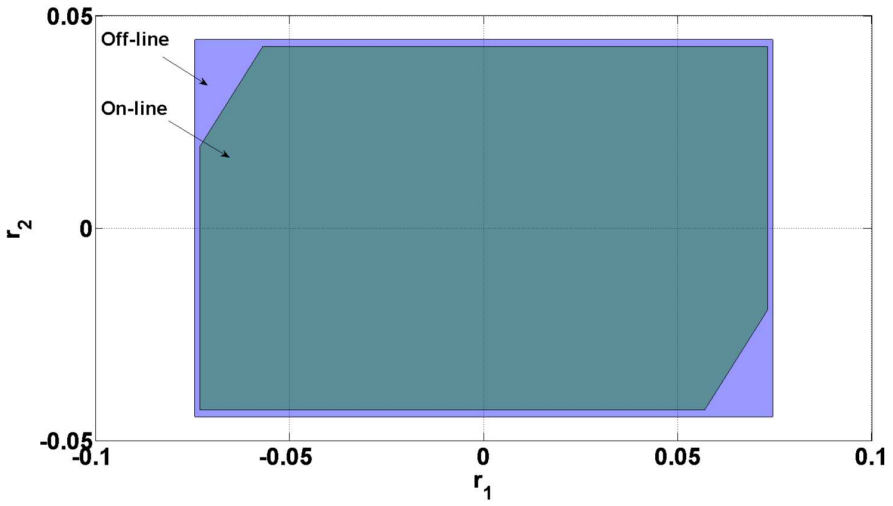

Figure 5.3: Comparison of the residual set using on-line and off-line approaches in steady state.

What is interesting in Figure 5.3 is related to the comparison of the residual zonotopes obtained based the off-line and on-line approaches. A comparison of the two results reveals that no significant differences were found between the size of the residual zonotopes in steady state. Therefore, the obtained RPI set for the residual based the proposed on-line zonotopic IOA is confirmed by the use of SIA. Furthermore, it is true that the difference between the computed RPI set is not significant but the size of the RPI set that is computed on-line is a bit tighter than the one computed off-line. Thus, it can be considered that the off-line SIA is more conservative than the on-line IOA since the RPI set is computed off-line. This result may be explained by the fact that the iterative propagation of the uncertainties in zonotopic IOA is more accurate than the off-line computation procedure. Furthermore, the mathematical burden is increased using the on-line approach but it allows obtaining a more accurate result.

This section presents the analysis of the system in healthy operation. The next step is to test the proposed so-called on-line IOA during the faulty case.

Faulty operation of the system

Following Section 5.2, the MDF can be computed using Theorem 5.3 for different types of actuator and sensor faults. The effect of faults on the state and the measurements

are modeled through the components of matrix F in (5.3). Furthermore, in order to analyze the effect of different type of faults on the system, actuator and sensor faults are simulated, separately.

In the first simulation, the actuator fault is considered. In this regard, the position of the valve is controlled by using the electrical actuator. As it is explained in the description of the case study, the position of the valve during the experiment is related to the flow parameter γ in the range between $[0,\ 1]$. Thus, the flow to the lower and upper tanks is influenced by the valve position through $\gamma K_p\omega$ and $(1-\gamma)K_pv$, respectively. To simulate the single actuator fault, faulty dynamical model (3.9) is considered as (3.25).

From (3.25), it can be observed that system is affected by the actuator fault through matrix F_a and the vector f_a, i.e.,

$$F_a = 10B, \qquad f_a = \begin{bmatrix} f_a \end{bmatrix}, \tag{5.35}$$

where matrix F_a is selected to simulate the actuator fault. Moreover, f_a denotes the direction of the fault effect on the actuator. Then, considering all the details mentioned regarding to the system simulation and simulation of the actuator fault, Theorem 5.3 can be used in order to compute the MDF. Therefore, the minimum magnitude of the actuator fault that can be detected is obtained using (5.17). Thus, the MDF in the case of actuator fault is computed during steady-state operation of the system as

$$f_{\min_a}^{\text{Det}} = \pm 0.3310. \tag{5.36}$$

To test the obtained magnitudes, the occurrence of the fault is simulated at $k = 500$, which simulates the fault in steady state. Furthermore, based on the description of the case study, the flow parameter is considered as $\gamma = 0.6$. In this regard, the two following scenarios for a single step additive actuator fault are considered in steady state:

- scenario (i): $f_a = 0.3330$, i.e, slightly bigger than the magnitude $f_{\min_a}^{\text{Det}} = \pm 0.3310$,
- scenario (ii): $f_a = 0.3280$, i.e, slightly smaller than the magnitude $f_{\min_a}^{\text{Det}} = \pm 0.3310$.

Figure 5.4 shows the FD test results for both scenarios. As it can be seen in Figure 5.4, the residual sets obtained in healthy and faulty operation are separated in the case of fault occurrence considering the first scenario. Therefore, the fault can be detected. But, considering the second scenario, the overlap between the healthy and faulty

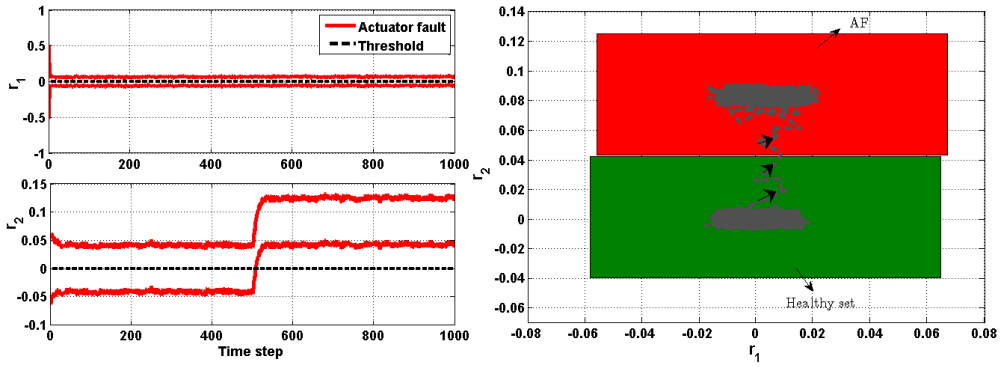

(a) $f_a = 0.3330$ at $k = 500$.

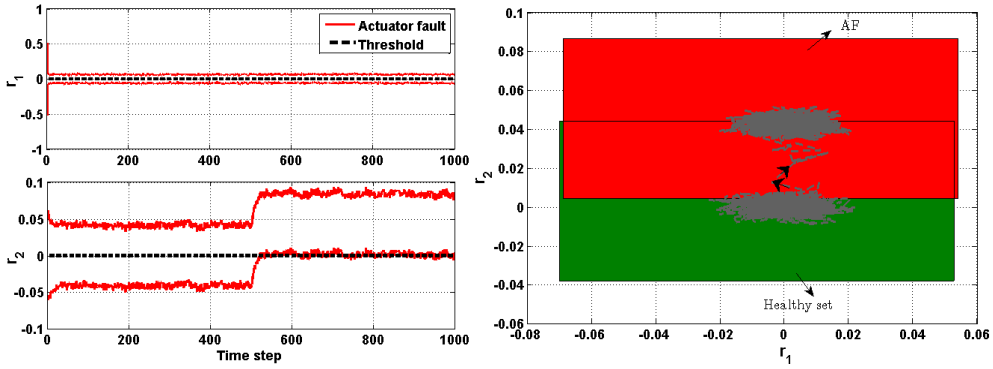

(b) $f_a = 0.3280$ at $k = 500$.

Figure 5.4: FD results in the case of occurrence of the actuator fault during steady state, i.e., $k = 500$.

residual sets means the fault with the considered magnitudes is not detectable.

Further analysis is carried out for the case of actuator fault at $k = 500$ by projecting the faulty residual set into each residual space as can be seen on the left side of the Figure 5.4. It can be observed that the threshold, i.e., ideally in classical IOA is considered zero, is out of the area between the upper and lower bounds of the residual set in Figure 5.3.2. Then, the existence of the fault will be proved. On the other hand, the threshold is between the area of the maximum and minimum bounds of the residual set in Figure 5.3.2, where the second scenario is considered for the fault magnitude. Therefore, the fault with the magnitude $f_a < 0.3310$ is not detectable. Hence, Figure 5.4 confirms through simulations the obtained results in (5.36). This illustrates that proposed on-line zonotopic IOA is well suited to the fault detectability of the classical

IOA.

Remark 5.1. *The healthy zonotopic set that is shown in Figures 5.2 and 5.3 is obtained without considering the reduction operator $\downarrow_q$ since the computational burden is not to much for this case study. But, in the faulty operation of the system since the computational burden is increased, the reduction operator $\downarrow_q$ is used to fix the dimension of the generator matrices with the maximum value. Due to this reason, the healthy residual set that is shown in Figure 5.3 and Figure 5.4 are not exactly the same.* □

Moreover, the MDF analysis is done considering the output sensor fault. In this regard, the faulty dynamical model (3.17) is considered.

As mentioned in the description of the case study, the outputs of the system are the water levels in Tanks 1 and 2 that can be measured using the measurement devices as voltages. Based on the physical features, the height of each tank is 20 cm. Then, each output of the system is between $[0 \;\; 10]$ V since $K_c = 0.50$ V/cm. To simulate the output sensor fault, the terms F_y and f_y in (3.17) is considered in the simulation as

$$F_y = \begin{bmatrix} 10 & 0 \\ 0 & 10 \end{bmatrix}, \qquad f_y = \begin{bmatrix} f_{y_1} \\ f_{y_2} \end{bmatrix}, \tag{5.37}$$

where the matrix F_y is defined with the whole range of the measurement. Moreover, f_{y_1} and f_{y_2} present the influence of the fault on each output. Then, the minimum magnitude of the sensor fault that can be detected can be computed based on Theorem 5.3. Using (5.17), the minimum magnitude of the output sensor fault that can be detected is computed during steady-state operation of the system as

$$f^{\text{Det}}_{\min_y} = \begin{bmatrix} \pm 0.2575 \text{ V} \\ \pm 0.0082 \text{ V} \end{bmatrix}. \tag{5.38}$$

As further analysis, the occurrence of the output sensor fault is separately simulated at $k = 500$, in order to test the obtained magnitude during steady state. Furthermore, based on the description of the case study, the operating points that are considered for the water levels of the Tanks 1 and 2 are around 12.4 cm (or 6.2 V) and 1.8 (or 0.9 V), respectively. Then, the FD test is done considering the following scenarios for a single step additive output sensor fault are considered during steady state:

- slightly bigger than the magnitude $f^{\text{Det}}_{\min_y} = \begin{bmatrix} \pm 0.2575 \text{ V} \\ \pm 0.0082 \text{ V} \end{bmatrix}$,
- slightly smaller than the magnitude $f^{\text{Det}}_{\min_y} = \begin{bmatrix} \pm 0.2575 \text{ V} \\ \pm 0.0082 \text{ V} \end{bmatrix}$.

Following the explained scenarios, there are four different magnitudes to be tested on each sensor as

- scenario (i): $f_{y_1} = 0.2580$ V, i.e, slightly bigger than the magnitude $f^{\text{Det}}_{\min_{y_1}} = \pm 0.2575$ V,
- scenario (ii): $f_{y_1} = 0.2570$ V, i.e, slightly smaller than the magnitude $f^{\text{Det}}_{\min_{y_1}} = \pm 0.2575$ V,
- scenario (iii): $f_{y_2} = 0.0084$ V, slightly bigger than the magnitude $f^{\text{Det}}_{\min_{y_2}} = \pm 0.0082$ V,
- scenario (iv): $f_{y_2} = 0.0080$ V, slightly smaller than the magnitude $f^{\text{Det}}_{\min_{y_2}} = \pm 0.0082$ V.

It is worth mentioning that subscripts 1 and 2 denote the effect of the fault on the sensor that is measuring the water level of Tanks 1 and 2, respectively. The results from the implementation of the scenarios are reported in Figures 5.5 and 5.6.

Looking at Figures 5.5 and 5.6, it can be observed that separation of the healthy and faulty residual sets is obtained when slightly bigger faults than the magnitudes obtained in (5.38) are considered and the existence of the fault can be detected by means of the obtained separations. Considering the second scenario, which corresponds to a fault slightly smaller than the obtained magnitudes in (5.38) is considered, the fault can not be detected since the healthy and faulty residual sets overlap. Furthermore, it can be seen that the threshold, i.e., zero, is out of the area between the upper and lower bounds of the residual set when implementing the first scenario of the two cases. Then, this is an indication of the occurrence of the fault. Moreover, threshold is inside of the area between the upper and lower bounds of the faulty residual set when implementing the second scenario of the two cases and it can be considered that the fault with this magnitude is not detectable. Thus, Figures 5.5 and 5.6 confirm through the simulation the obtained results previously presented in (5.38).

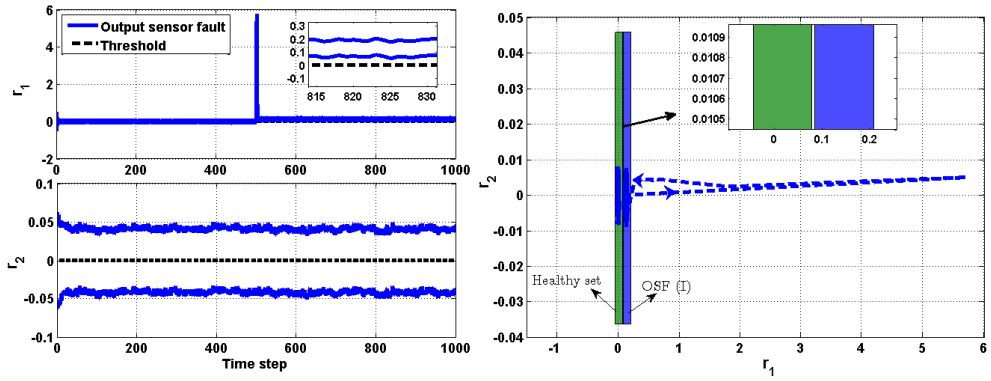

(a) $f_{y_1} = 0.2580$ V at $k = 500$.

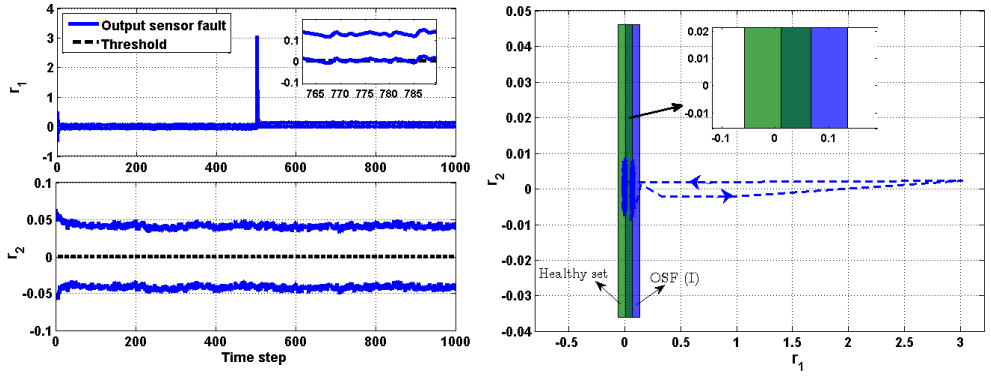

(b) $f_{y_1} = 0.2570$ V at $k = 500$.

Figure 5.5: FD results in the case of occurrence of the sensor fault (f_{y_1}) during steady state, i.e., $k = 500$.

The last simulation that is considered for the case study is related to the case of input sensor fault. As mentioned before, the input sensor fault is a type of the fault that the input of the observer is influenced by the fault (see (3.10)). The simulation of the input sensor fault is carried out through the matrix F_u and the vector f_u, i,e.,

$$F_u = 5, \qquad f_u = f_u, \tag{5.39}$$

where matrix F_u is defined with the whole range of the input which is between [0, 5] V. Furthermore, f_u denotes the effect of the fault influencing observer input. Then, the minimum magnitude of the input sensor fault is computed using Theorem 5.3 as

$$f^{\text{Det}}_{\min_u} = \pm 0.6620 \text{ V}. \tag{5.40}$$

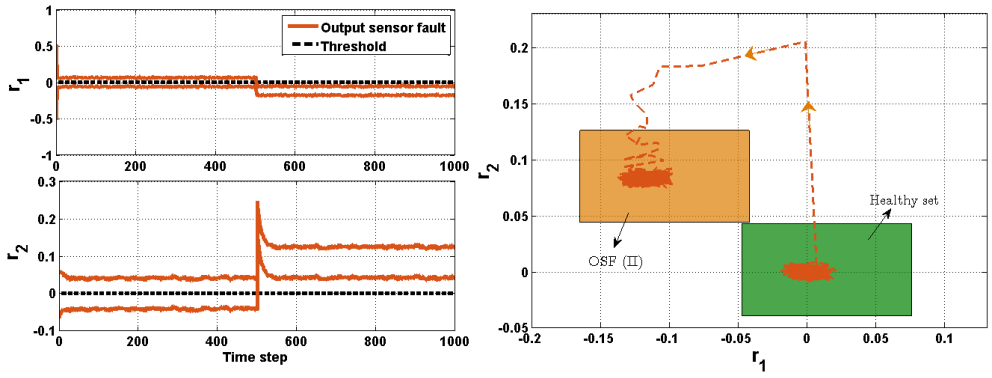

(a) $f_{y_2} = 0.0084$ V at $k = 500$.

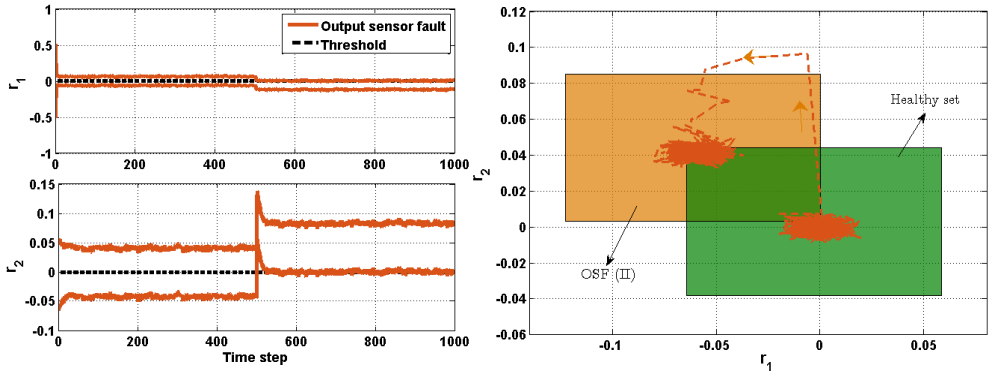

(b) $f_{y_2} = 0.0080$ V at $k = 500$.

Figure 5.6: FD results in the case of occurrence of the sensor fault (f_{y_2}) during steady state, i.e., $k = 500$.

Similar to the actuator and output sensor faults, the MDF in the case of input sensor fault is obtained during steady-state operation of the system. Then, regarding the FD performance in this case, the fault is simulated at $k = 500$ to illustrate the steady state. Furthermore, the following scenarios are considered for the implementation of the FD test:

- scenario (i): $f_u = 0.6640$ V, slightly bigger than the magnitude $f^{\text{Det}}_{\min_u} = \pm 0.6620$ V,
- scenario (ii): $f_u = 0.6600$ V, slightly smaller than the magnitude $f^{\text{Det}}_{\min_u} = \pm 0.6620$ V.

Figure 5.7 shows the FD test considering the mentioned scenarios during steady state for the case of input sensor fault. As can be seen in Figure 5.7, considering the input

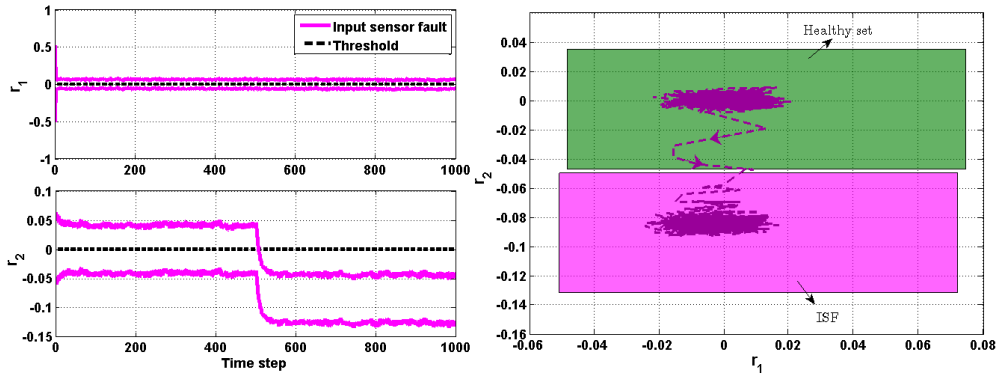

(a) $f_u = 0.6640$ V at $k = 500$.

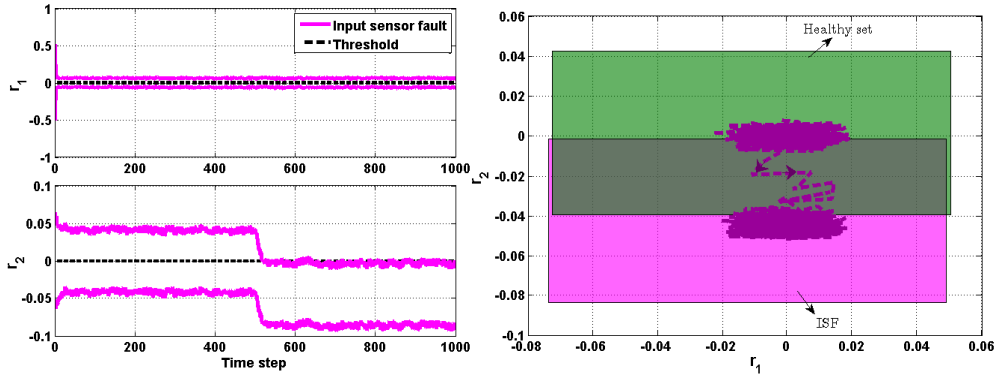

(b) $f_u = 0.6600$ V at $k = 500$.

Figure 5.7: FD results in the case of occurrence of the input sensor fault during steady state, i.e., $k = 500$.

sensor fault with bigger magnitude reported in (5.40), the separation of the healthy and faulty residual sets is obtained. Thus, the existence of the fault is proved. Also, the obtained overlap between the healthy and faulty residual sets when considering output sensor fault with smaller magnitude is presented in Figure 5.7 corresponding to the magnitude that cannot be detected in steady state.

Further analysis is done by projecting the residual set into each residual space. It can be seen from the left side of the Figure 5.7, when the first scenario is simulated, zero is out of the area between the upper and lower bounds of the residual set. Then, the fault will be detected. On the other hand, when the second scenario is simulated, zero is inside of the area between the upper and lower bounds of the residual set. Then, the fault cannot be detected.

Table 5.1: MDF during steady-state operation of the system.

	Actuator fault $f^{\mathbf{Det}}_{\mathbf{min}_a}$	**Output sensor fault** $f^{\mathbf{Det}}_{\mathbf{min}_{y_1}}$ [V]	$f^{\mathbf{Det}}_{\mathbf{min}_{y_2}}$ [V]	**Input sensor fault** $f^{\mathbf{Det}}_{\mathbf{min}_u}$ [V]
Theoretical	± 0.3310	± 0.2575	± 0.0082	± 0.6620
Simulation	± 0.3200	± 0.2900	± 0.0078	± 0.6900

Furthermore, Table 5.1 summarizes the obtained MDF in all the cases (actuator and sensor faults) using Theorem 5.3. Furthermore, those magnitudes of the fault that can be still detected at the end of the simulation, i.e., in steady state is obtained using the simulation and reported in Table 5.1.

From Table 5.1, the magnitude of the fault that can be detected considering the whole time range of the simulation is almost the same as the one obtained based on the theoretical approach. However, in the case of sensor fault and due to the re-injection of the fault involved by the observer structure leading to some transient behavior (see the overshoot in Figures 5.5 and 5.6), the magnitude of the detectable fault is improved on the whole time range of the simulation compared to steady state only.

As it is mentioned before, the fault with the magnitude obtained using Theorem 5.3 is only related to the detectability analysis and this magnitude of the fault is not valid in the case of isolability analysis. After detecting the fault by means of obtaining the separated sets in healthy and fault operation of the system, the isolation of the fault depends on satisfaction of the conditions in Theorem 5.2. In this regard, the magnitude of the different faults that are obtained using MIF analysis in Theorem 5.4 for the case study are reported on Table 5.2.

It can be seen from the results that are presented in Table 5.2, there are some cases that do not exist in the considered case study. These cases are denoted by $-$ in Table 5.2. Furthermore, there are some other cases that the faults always can be isolable if they are larger than the MDF magnitude. These cases are shown by # in Table 5.2. A possible explanation for having # might be related to the direction of the fault in the case study that always there are some faults with the different directions, e.g., minimum isolable input sensor fault with respect to the output sensor fault. In these cases, after obtaining the separation between the healthy and faulty sets, the faulty sets are also separated. Figure 5.8 illustrate one of the cases that always can be isolable with MDF magnitude

Table 5.2: MIF during steady-state operation of the system.

	f_a	f_{y_1} [V]	f_{y_2} [V]	f_u [V]
$f^{\text{Iso}}_{\text{min}_a}$	–	#	#	± 0.3460
$f^{\text{Iso}}_{\text{min}_{y_1}}$	± 0.2808	–	#	± 0.2691
$f^{\text{Iso}}_{\text{min}_{y_2}}$	± 0.0089403	± 0.008571	–	± 0.0085701
$f^{\text{Iso}}_{\text{min}_u}$	± 0.7219	#	#	–

since the direction of the faults are always different for the considered case study.

The implementation of the fault is done using the magnitudes that are obtained based on Theorem 5.3 and reported in Table 5.1 as $f_u = 0.6640$ V that is slightly bigger than the magnitude $f^{\text{Det}}_{\text{min}_u} = \pm 0.6620$ V for the case of occurrence of f_u and $f_{y_2} = 0.0084$ V that is slightly bigger than the magnitude $f^{\text{Det}}_{\text{min}_{y_2}} = \pm 0.0082$ V for the case of occurrence of f_{y_2}. As can be seen in Figure 5.8, the occurrence of the input sensor fault f_u and output sensor fault f_{y_2} are always separable by the magnitude that is obtained based on Theorem 5.3.

However, the overlap can be obtained between the faulty residual sets in some cases implementing the fault with the obtained magnitude in Table 5.1. Figure 5.9 illustrates one of the cases, e.g., the case of occurrence f_{y_2} and f_a at the same time.

In this case, the fault magnitudes are considered $f_a = 0.3330$ that is slightly bigger than $f^{\text{Det}}_{\text{min}_a} = \pm 0.3310$ and $f_{y_2} = 0.0.0084$ V that is slightly bigger than $f^{\text{Det}}_{\text{min}_{y_2}} = \pm 0.0082$ V for the case of occurrence of f_a and f_{y_2}, respectively. Figure 5.9 shows that the separation between the faulty sets cannot be obtained when the occurrence of the faults are simulated with the magnitudes reported in Table 5.1.

Then, the magnitudes that are obtained in Table 5.2 are implemented in the simulation for the considered cases: $f_{y_2} = 0.009$V and $f_a = 0.35$. Therefore, as can be seen in Figure 5.10, the fault with the magnitude using Table 5.2 can be not only detectable, but also, can be isolable since the intersection between the faulty residual sets are obtained empty and the faulty sets are separated from each other and the healthy residual set.

Further analysis is done based on the simulation of the case of occurrence of all type of possible faults for the case study by considering slightly bigger magnitudes than the

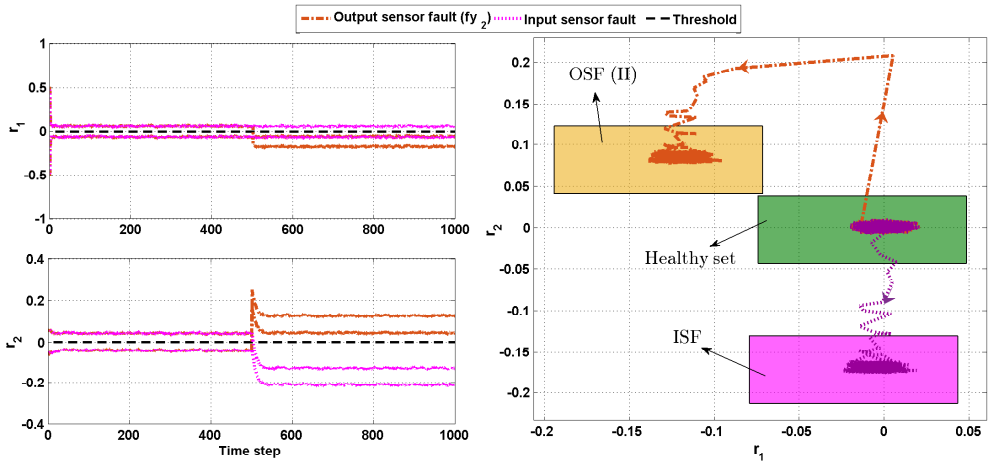

Figure 5.8: Always separable (ISF and OSF (II) denote the residual set when simulation input sensor fault f_u and output sensor fault f_{y_2}, respectively).

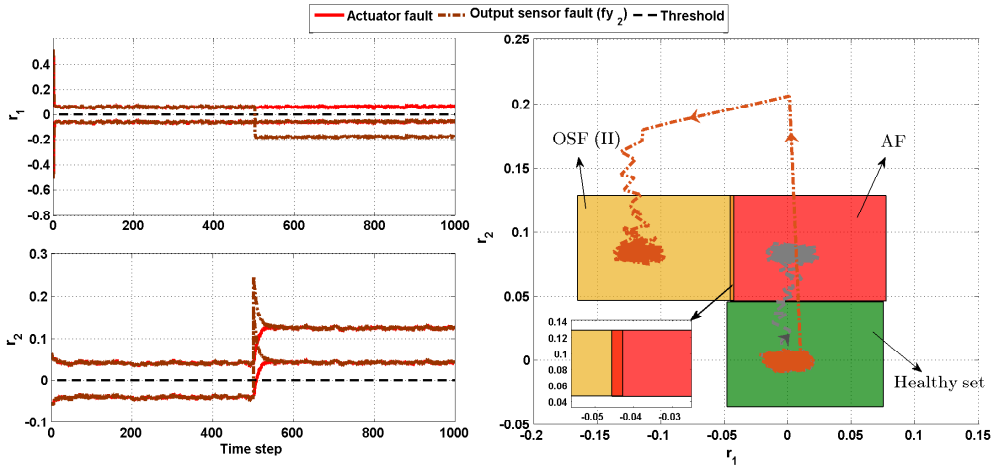

Figure 5.9: FD results when the obtained magnitude using MDF is considered for the case of occurrence of f_{y_2} and f_a at the same time (AF denotes the residual set when simulation actuator fault f_a).

maximum MIF for the faults obtained in Table 5.2 as

$$f_a = 0.35,$$
$$f_{y_1} = 0.29 \text{ V},$$
$$f_{y_2} = 0.0095 \text{ V},$$
$$f_u = 0.73 \text{ V}.$$

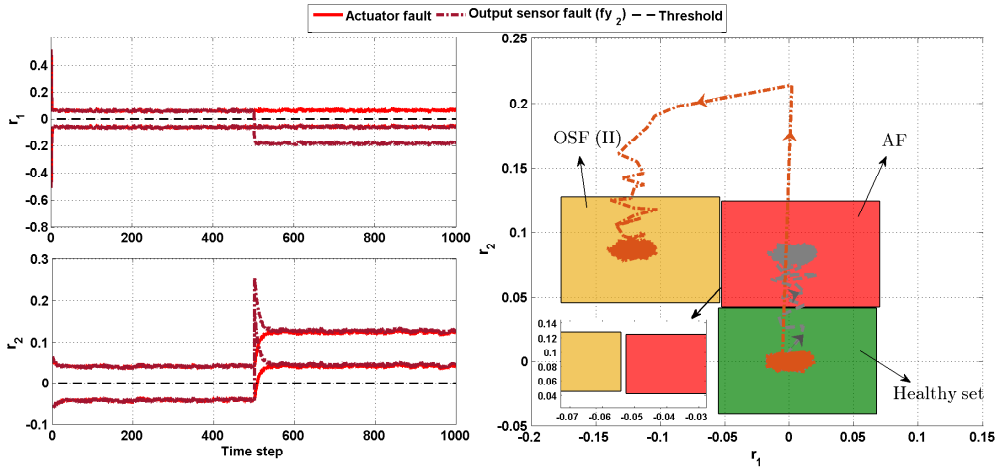

Figure 5.10: FD results when the obtained magnitude using MIF is considered.

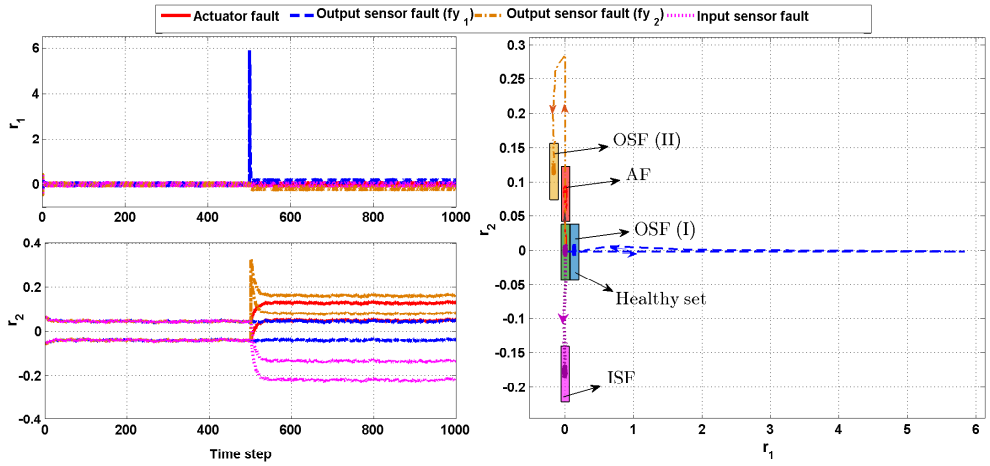

Figure 5.11: FD results when the maximum magnitude that obtained using MIF analysis in Table 5.2 for each type of faults is simulated.

Figure 5.11 presents the case of occurrence of the fault with the maximum value obtained in Table 5.2, all type of faults are perfectly separated. This case correspond to a fault magnitudes that properly detectable and isolable.

5.4 Summary

This chapter has proposed a zonotopic interval observer-based FDI algorithm integrated with the SIA. As a novelty, in the proposed FDI design, fault detectability and fault isolability can be guaranteed in both transient and steady states. The influences of all possible state disturbance and measurement noise are addressed using the zonotopic-set representation of a set. Furthermore, MDF and MIF have been characterized based on the sensitivity analysis integrated with SIA. Finally, a case study based on two-tank system is used to illustrate the obtained results. In model-based approaches, the observer gain plays an important role since it determines the MDF for a given type of fault and allows enhancing the observer FD properties. There has been little discussion about the effect of the observer gain in the previous chapters. Therefore, the effect of the observer gain over the state-bounding observer will be further analyzed in order to improve the algorithm for enhancing the sensitivity to the fault with respect to the influence of disturbance with the goal of improving the FDI performance in the next chapter.

Chapter 6

Interval observer FD rather than state estimation

Enhancing the sensitivity to faults with respect to disturbances, rather than optimizing the precision of the state estimation using KF is the subject of this chapter. The stochastic paradigm (KF) is based on minimizing the trace of the state estimation error covariance. In the context of the bounded-error paradigm using Zonotopic Kalman Filters (ZKF), this is analog to minimize the covariation trace. From this analogy and keeping a similar observer-based structure as in ZKF, a criterion jointly inspired by set-membership approaches and approximate decoupling techniques coming from parity-space residual generation is proposed. Its on-line maximization provides an optimal time-varying observer gain leading to the so-called FD-ZKF filter that allows enhancing the FD properties. The characterization of MDF magnitude is done based on a sensitivity analysis. The effect of the uncertainty is addressed using a set-membership approach and a zonotopic representation reducing set operations to simple matrix calculations. A case study based on a quadruple-tank system is used both to illustrate and compare the effectiveness of the results obtained from the FD-ZKF approach compared to a pure ZKF approach.

6.1 Introduction

Within the context of model-based FDI approaches, a large and growing amount of literature has reported several approaches to improve the FD methods such that the

residual is obtained to be insensitive to the uncertainty, while at the same time sensitive to the faults [CP12, Din08, ZDLW03]. This is the case of FD filters that are designed by considering the robustness against disturbance, noise or any uncertainties using, e.g., H_∞ optimization, LMIs or μ design techniques [ZDLW03, SCP96]. But, recent results show that the filter design technique considering only the rejection of the effect of uncertainties has not been successful since the sensitivity to the fault needs to be considered in FD filter design [LZ07]. This is the case of [HP96] where the multi-objective FD design based on H_-/H_∞ techniques is considered. Indeed, the worst case of the fault sensitivity is taken into account by the smallest not null singular value of the transfer function matrix from fault to residual at either $\omega = 0$ or over a given frequency range [LWY05, Hen10]. Then, a significant amount of literature has been published discussing this multi-objective design task formulated as an optimization problem, e.g., H_∞/H_∞, H_2/H_∞ or H_2/H_2 problems [LZ07, JLP06, WYL07, DJFD00].

On the other hand, a considerable amount of literature has been reported on different state-bounding algorithms based on stochastic and deterministic approaches. A recent study, proposed by [Com15b], deals with the standard Kalman filtering together with the zonotopic state estimation. This work establishes an explicit bridge between stochastic/Gaussian and set-based/zonotopic frameworks relying on the analogy between covariances and covariation. Then, in [Com15a] and [Com16], both deterministic (bounded) and stochastic (Gaussian) disturbances have been taken into account in order to propose the extended version of Zonotopic and Gaussian Kalman Filter with the aim of merging Gaussian Kalman filtering and zonotopic state bounding to achieve robust FD. Furthermore, there is a large volume of reported studies about fault detectability, in particular [MPES10], where the main objective is to compute the minimum magnitude of the fault that can be detected when an IOA is used.

The main contribution of this chapter is to make use of a similar observer-based structure as in ZKF in order to propose an approach enhancing the sensitivity to faults with respect to disturbances, rather than only optimizing the precision of the state estimation as is usually considered in KF. As for ZKF, a generic discrete-time linear time-varying (LTV) dynamic model of the system is considered. Contrary to most existing multi-objective FD design techniques, the sensitivity to both faults and disturbances is evaluated using a set-based approach enclosing all the possible temporal scenarios of faults and disturbances within specified ranges. Moreover, the proposed criterion combining the sensitivity to both faults and disturbances makes it possible to efficiently

obtain on-line time-varying optimal FD observer gains, without any requirement on the considered frequency ranges. The combination of these features makes the approach original compared to most multi-objective optimization-based FD techniques. Finally, the effectiveness of the proposed approach is illustrated using a case study based on quadruple-tank system.

Regarding the structure of the chapter, the problem formulation is addressed in Section 6.2. The observer structure and the FD algorithm are discussed in Section 6.3. The computation of a time-varying observer gain optimizing a set-based criterion modeling the trade-off between the sensitivity to faults and the robustness to disturbances is proposed in Section 6.4. The discussion of the comparative assessment and the characterization of the MDF for the FD-ZKF and ZKF approaches are presented in Section 6.5. The application to a quadruple-tank system is used in order to illustrate the effectiveness of the proposed approach in Section 6.6. Finally, conclusions are drawn in Section 6.7.

6.2 Problem formulation

This chapter addresses the problem of FD in dynamical systems modeled as an uncertain time-varying state-space representation in discrete-time as

$$x_{k+1} = A_k x_k + B_{u,k} u_k + E_k \upsilon_k, \tag{6.1a}$$

$$y_k = C_k x_k + D_{u,k} u_k + F_k \upsilon_k, \tag{6.1b}$$

where $k \in \mathbb{N}$ indicates the discrete time. Furthermore, $x \in \mathbb{R}^{n_x}$ is the state vector, $u \in \mathbb{R}^{n_u}$ and $y \in \mathbb{R}^{n_y}$ denote the known input and the known output (measurement) vectors, respectively. The system matrices of appropriate dimensions are $A \in \mathbb{R}^{n_x \times n_x}$, $B_u \in \mathbb{R}^{n_x \times n_u}$, $C \in \mathbb{R}^{n_y \times n_x}$ and $D_u \in \mathbb{R}^{n_x \times n_u}$. Moreover, the random vector $\upsilon \in \mathbb{R}^{n_\upsilon}$ denotes an additive uncertainty that is bounded by a unit hypercube expressed as a centered zonotope, i.e., $\forall k \geq 0, \upsilon_k \in \left[-1, \quad 1\right]^{n_\upsilon} = \left\langle 0, \ I_{n_\upsilon} \right\rangle$, where $I_{n_\upsilon} \in \mathbb{R}^{n_\upsilon \times n_\upsilon}$ denotes the identity matrix. Furthermore, E and F are non-empty matrices with appropriate dimensions. Moreover, the bounded uncertainty vector υ_k is considered as the combination of the disturbance and the fault. Therefore, the decomposed form of υ_k is written as

$$\upsilon_k = \begin{bmatrix} d_k \\ f_k \end{bmatrix},$$

where $d \in [-1,\ 1]^{n_d} = \langle 0,\ I_{n_d} \rangle$ and $f \in [-1,\ 1]^{n_f} = \langle 0,\ I_{n_f} \rangle$, respectively, modeling the disturbances and faults that possibly influence the system. Consequently, E_k and F_k can be decomposed as

$$E_k = \begin{bmatrix} B_{d,k} & B_{f,k} \end{bmatrix},$$
$$F_k = \begin{bmatrix} D_{d,k} & D_{f,k} \end{bmatrix},$$

where B_d, B_f, D_d and D_f denote non-empty matrices with suitable dimensions.

Henceforth, the index $k+1$ will be replaced by $+$ and k will be omitted for the sake of simplified notations. Then, the dynamical model (6.1) is simply rewritten while remaining fully LTV as

$$x_+ = Ax + B_u u + E\upsilon, \tag{6.2a}$$
$$y = Cx + D_u u + F\upsilon. \tag{6.2b}$$

The initial state x_0 belongs to the zonotopic set $\mathcal{X}_0 = \langle c_0,\ R_0 \rangle$, where $c_0 \in \mathbb{R}^{n_x}$ denotes the center and $R_0 \in \mathbb{R}^{n_x \times r_{R_0}}$ is a non-empty matrix containing the generators matrix R_0 of the initial zonotope $\mathcal{X}_0$. The pair (A, C) is assumed to be detectable. Moreover, monitoring the system with the dynamical model (6.2) considering the influence of disturbances and the possible effect of the fault (when it exists) can be done deriving a set-membership observer from the expression

$$x_+ = Ax + B_u u + E\upsilon + G(y - Cx - D_u u - F\upsilon), \tag{6.3}$$

where G is the observer gain that provides degrees of freedom to tune the system monitoring with respect to its aim, i.e., with the goal of optimizing the detection of faults according to some given criterion. In order to highlight the link with an observer that will be formalized in Section 6.3.1, it can be noticed that replacing the variables in the right-hand side of (6.3) by the zonotope they belong to, the terms corresponding to centers will result in a classical Luenberger observer with observer gain G (6.4a), while the generator/shape matrix terms will provide an explicit way to parameterize with G the zonotopic enclosures of the classical observation error (6.4b). An optimal tuning of the time-varying observer gain matrix G based on a set-based optimization criterion expressing the desired FD performance (rather than the only state estimation) is addressed in the following of the chapter.

6.3 Structure of the observer-based FD tests

6.3.1 General observer structure

In this chapter, the observer-based FD is performed by means of a KF using zonotopic sets instead of Gaussian probability density functions (PDF), known as ZKF. Considering the one-step ahead predictor form, also called delayed form of the KF, the underlying observer structure is determined using the ZKF approach proposed in [Com15b] and following the same idea as Proposition 2.1, which can be further tuned with respect to the FD purpose to increase the FD performance. Therefore, the following Proposition 6.1 is obtained based on (6.3).

Proposition 6.1. *(Observer structure) Considering the dynamical model (6.2), the center c and the shape matrix R of the zonotopic observer can be recursively defined as*

$$c_+ = (A - GC)c + (B_u - GD_u)u + Gy, \tag{6.4a}$$

$$R_+ = \begin{bmatrix} (A - GC)\bar{R}, & (E - GF) \end{bmatrix}, \tag{6.4b}$$

where $\bar{R} = \downarrow_q \{R\}$. Furthermore, the state inclusion property $x \in \langle c, R \rangle$ holds for all $k \geq 0$.

Proof. Assuming $x \in \langle c,\ R \rangle$ and $v \in \langle 0,\ I_{n_v} \rangle$ for all $k \geq 0$ where the inclusion property is preserved, (6.3) can be written using the reduction operator as

$$x_+ \in \langle c_+,\ R_+ \rangle = \langle (A{-}GC)c,\ (A{-}GC)\bar{R} \rangle \oplus \langle (B_u{-}GD_u)u,\ 0 \rangle \oplus \langle 0,\ (E{-}GF) \rangle \oplus \langle Gy,\ 0 \rangle. \tag{6.5}$$

Thus, based on Definitions B.22 and B.24, the center c_+ and the shape matrix R_+ in (6.5) can be expressed as in (6.4), where the center c can be interpreted as a classical punctual state estimate of the unknown state x and the shape matrix R characterizes a zonotopic enclosure of the classical observation error $e = x - c$. □

6.3.2 FD based on the innovation term

The standard form of FD test is based on checking the consistency of the measurements with a fault-free model. In this work, the fault-free model is obtained by setting $f = 0$

in (6.1). Then, $\upsilon = \begin{bmatrix} d \\ 0 \end{bmatrix}$.

The innovation is usually defined as the difference between the measured value of a variable at time k and the optimal forecast of that value based on the information available prior to time k. In this work, the measured value of the output is y, and c, which will result from iterations based on (6.4a) with some optimal G, stands for the above mentioned optimal forecast in the considered one-step ahead predictor form (or delayed form) of KF. The reader interested in additional material about formal/detailed links between the set-membership and stochastic paradigms and their joint use for the design of some innovation-based FD tests is referred to [Com15b] and [Com15a, Com16], respectively. In particular, explicit links with the computation and evaluation forms of prediction error/residuals are formalized in [Com15a, Com16].

Proposition 6.2. *(FD test design) Considering a faultless scenario ($f = 0$), the center c_ε and the shape matrix R_ε of a zonotope containing the origin 0, i.e., satisfying $0 \in \langle c_\epsilon, R_\epsilon \rangle$ at time k is*

$$c_\varepsilon = y - (Cc + D_u u)\,, \tag{6.6a}$$

$$R_\varepsilon = \begin{bmatrix} -CR, & -F \end{bmatrix}. \tag{6.6b}$$

Proof. The output equation (6.2b) can be rewritten as follows:

$$0 = y - Cx - D_u u - F\upsilon. \tag{6.7}$$

Substituting $x \in \langle c,\ R \rangle$ for x in (6.7) and $\upsilon \in \langle 0,\ I_{n_\upsilon} \rangle$ yields

$$0 \in \langle y,\ 0 \rangle \oplus \langle\, -Cc, -CR\, \rangle \oplus \langle\, -D_u u,\ 0 \rangle \oplus \langle 0,\ -F \rangle, \tag{6.8}$$

which completes the proof by applying Definition B.22 and Property B.24. □

It is worth noting that the time-varying center c_ε can be equivalently identified/interpreted at time k as:

i) a prediction error which is homogeneous to the system output in terms of physical units,

ii) a residual r whose computation form corresponds to the right term of (6.6a), and

Algorithm 6.1 FD test based on the innovation term

1: $k \longleftarrow 0$
2: $\langle c, R \rangle = \langle c_0, R_0 \rangle$
3: **for** $k = 0 : (k_{\max} - 1)$ **do**
4: $(y, u) =$ `GetMeasurementAndControlInput`
5: $G =$ `OptObsGain`(c, R)
6: $\langle c_+,\ R_+ \rangle$ using (6.4)
7: $\langle c_\varepsilon,\ R_\varepsilon \rangle$ using (6.6)
8: **if** $0 \notin \langle c_\varepsilon,\ b(R_\varepsilon) \rangle$ **then**
9: $Fault \leftarrow true$
10: **else**
11: $Fault \leftarrow false$
12: **end if**
13: **end for**

iii) an innovation term ε, as explained in the text introducing the Proposition 6.2.

Since $\langle 0, R_\varepsilon \rangle = \langle R_\varepsilon \rangle$ is a centered zonotope and, as such, a centrally symmetric domain, and since $\varepsilon = r = c_\varepsilon$, it can be noticed that $0 \in \langle c_\varepsilon, R_\varepsilon \rangle$ as stated in Proposition 6.2 equivalently can be rewritten as $\varepsilon \in \langle R_\varepsilon \rangle$ and/or $r \in \langle R_\varepsilon \rangle$. As a result, the zonotope shape matrix R_ε (6.6b) gives explicit information for the evaluation of the residual r.

Therefore, the FD test is based on computing (6.6) and the fault is detected when $0 \notin \langle c_\varepsilon,\ R_\varepsilon \rangle$. A computationally efficient way to implement the detection test without increasing the false alarm rate consists in testing whether 0 belongs or not to an aligned box enclosing the zonotope $\langle c_\varepsilon, R_\varepsilon \rangle$

$$0 \notin \langle c_\varepsilon, b(R_\varepsilon) \rangle, \tag{6.9}$$

where $\langle c_\varepsilon, b(R_\varepsilon) \rangle$ is enclosed by an aligned box characterized by $b(R_\varepsilon) = diag(|R_\varepsilon|\,\mathbf{1})$, considering that $|.|$ is the element-by-element absolute value operator, $\mathbf{1}$ is a column vector of ones and $diag(.)$ returns a diagonal matrix from a vector of diagonal elements.

Algorithm 6.1 summarizes the FD test in Proposition 6.2. Note that the first step of Algorithm 2.1 is related to initialization. Then, the explicit value of the optimal observer gain should be computed using either an observation-based or an FD-based criterion. Moreover, a function $G =$ `OptObsGain`(c, R) implementing such computations will be presented later in the chapter. Then, the one-step ahead state prediction $\langle c_+, R_+ \rangle$ as well as the value of the residual vector $r = c_\varepsilon$ and its adaptive threshold $b(R_\varepsilon)$ can be computed based on u, y and G. So, the FD test is based on computing the next-step

bounding set with the computed optimal gain and Proposition 6.1. Finally, the residual is generated using Proposition 6.2 and the fault is detected when $0 \notin \langle c_\varepsilon,\ b(R_\varepsilon)\rangle$.

6.4 Optimal zonotopic observer gain

6.4.1 Observer structure

The observer gain has important implications in the behavior of the state bounding observer resulting from Proposition 6.1. Contrary to a first intuition, it is not clear that those computed observer gains that are *suitable* for the observation purpose are also *suitable* for the purpose of FD. In this regard, using the same observer structure, the focus of this section will be placed on first giving a brief overview of computing the observer gain with only state observation purposes. Then, computing the optimal observer gain regarding FD will be considered by using a disturbance/fault reach set-based criterion.

In order to characterize them as functions of the tuning matrix G, the reach sets describing the influence of the disturbances and the effect of a fault on the estimated state sets, the observer structure in Proposition 6.1 can be decomposed and rewritten as shown in Proposition 6.3.

Proposition 6.3. *(Superposed form of the observer structure) Considering the dynamical model (6.2), the decomposition of the center c and the shape matrix R of the state bounding observer into the effects of the disturbance and fault can be recursively defined as*

$$x_+ \in \langle c_{d_+},\ R_{d_+}\rangle \oplus \langle c_{f_+},\ R_{f_+}\rangle, \tag{6.10}$$

with

$$c_{d_+} = (A - GC)c_d + (B_u - GD_u)u + Gy, \tag{6.11a}$$

$$R_{d_+} = \left[(A - GC)\bar{R}_d,\quad (B_d - GD_d)\right], \tag{6.11b}$$

$$c_{f_+} = (A - GC)c_f, \tag{6.11c}$$

$$R_{f_+} = \left[(A - GC)\bar{R}_f,\quad (B_f - GD_f)\right], \tag{6.11d}$$

where $\bar{R}_d = \downarrow_q \{R_d\}$ and $\bar{R}_f = \downarrow_q \{R_f\}$. Additionally, the inclusion property is preserved for all $k \geq 0$, i.e., $x \in \langle c_d,\ R_d\rangle \oplus \langle c_f,\ R_f\rangle$.

Proof. Assuming $x \in \langle c_d,\ R_d\rangle \oplus \langle c_f,\ R_f\rangle$ at time instant k, $d \in \langle 0, I_{n_d}\rangle$ and $f \in \langle 0, I_{n_f}\rangle$, it is possible to write the zonotopic form of the observer in (6.3) as

$$\begin{aligned} x_+ \in & \langle (A-GC)c_d, (A-GC)R_d\rangle \oplus \langle (A-GC)c_f, (A-GC)R_f\rangle \oplus \langle (B_u - GD_u)u, 0\rangle \\ & \oplus \langle Gy, 0\rangle \oplus \langle 0, (B_d - GD_d)\rangle \oplus \langle 0, (B_f - GD_f)\rangle. \end{aligned} \tag{6.12}$$

Furthermore, consider that the superposition principle can be explicitly invoked in the linear setting. Therefore, using Definition B.22, the center and the generator matrix in (6.12) can be reorganized as in (6.11). Thus, $x_+ \in \langle c_{d+},\ R_{d+}\rangle \oplus \langle c_{f+},\ R_{f+}\rangle$. This gives the proof by induction. □

Since $x \in \langle c_d,\ R_d\rangle \oplus \langle c_f,\ R_f\rangle$ is independent from the observer gain at time instant k, the effect of the disturbance and the fault at time instant k can be reformulated as a one-step prediction from time instant $k-1$ in order to parameterize the effect of the observer gain. Thus, the effect of the disturbance and fault at time instant k in Proposition 6.3 can be formulated as

$$c_d = (A_- - G_-C_-)c_{d_-} + (B_{u_-} - G_-D_{u_-})u_- + G_-y_-, \tag{6.13a}$$

$$R_d = \left[(A_- - G_-C_-)R_{d_-},\quad (B_{d_-} - G_-D_{d_-})\right], \tag{6.13b}$$

$$c_f = (A_- - G_-C_-)c_{f_-}, \tag{6.13c}$$

$$R_f = \left[(A_- - G_-C_-)R_{f_-},\quad (B_{f_-} - G_-D_{f_-})\right], \tag{6.13d}$$

where the subscript $-$ is a short notation of $k-1$. Therefore, the state-bounding zonotope becomes an affine function of the (previous) observer gain $x \in \langle c_d(G_-),\ R_d(G_-)\rangle \oplus \langle c_f(G_-),\ R_f(G_-)\rangle$.

The use of Proposition 6.3 instead of Proposition 6.1 allows the separation of the effects of the disturbances and the faults. Therefore, computing the observer gain for observation purposes is done considering (6.11a) and (6.11b) while tuning the observer gain for FD purposes is done considering (6.11a) to (6.11d). Then, the expected strength of the proposed FD scheme lies in the fact that not only the influence of disturbances is used, but also the *relative* influence of disturbances and faults can be used to set up an optimization criterion quantifying the satisfaction level of an FD goal.

6.4.2 Optimal observer gain for observation purposes

When designing the gain for state-observation purposes, the main goal will be only reducing the effect of state estimation uncertainty. The computation of the optimal

observer gain for an observation purpose is investigated in [Com15b] which shows that there is a strong analogy between the KF and ZKF where the usually Gaussian probability density functions (PDF) are replaced by zonotopic sets. Therefore, the optimal observer gain G^* can be obtained by minimizing the F-radius[1] of the zonotope $\langle c_+,\ R_+ \rangle$ in (6.4). According to [Com15b], minimizing the F-radius of a zonotope is equivalent to minimizing the trace of its covariation. Therefore, considering Definition B.26, an accuracy criterion related to the size of the next state-bounding zonotope can be written as

$$J = tr(R_+ R_+^T) = \|R_+\|_F^2 . \tag{6.14}$$

Then, considering the fault-free model ($f = 0$) which is the standard approach for a general purpose state observation, J may be expressed as

$$J = tr(R_{d_+} R_{d_+}^T) = \left\|R_{d_+}\right\|_F^2 . \tag{6.15}$$

Moreover, given the state-bounding zonotope at time instant k as $x \in \langle c,\ R \rangle$, G^* can be computed explicitly using Theorem 6.1 in order to minimize the effect of uncertainty over the next state-bounding zonotope $x_+ \in \langle c_+,\ R_+ \rangle$.

Theorem 6.1. *Considering $x \in \langle c,\ R \rangle$ at time k, the optimal observer gain G^* minimizing the F-radius of the state-bounding zonotope at time instant $k+1$, or precisely, minimizing the criterion $J = tr(R_+ R_+^T)$ obtained in (6.15), is computed as*

$$G^* = AK^*, \tag{6.16}$$

with

$$\begin{aligned} K^* &= LS^{-1}, \\ L &= \bar{P}C^T, \\ S &= C\bar{P}C^T + Q_\omega, \end{aligned}$$

where the covariation matrices are introduced as $Q_\omega = D_d D_d^T$, $Q_\upsilon = B_d B_d^T$ and $\bar{P} = \bar{R}_d \bar{R}_d^T$.

Proof. The proof follows from the results presented in [Com15b]. □

[1] Further information about Frobenius norm can be found in [Com15b].

6.4.3 Optimal observer gain for FD purposes

Now, this section will concentrate on the design of the observer gain for FD purposes. Such a gain is computed to maximize the effect of faults with respect to disturbances. In this regard, an optimal tuning based on an FD criterion (FD-ZKF) rather than an observation criterion (ZKF) is used in order to enhance the FD properties of the observer. By analogy with the KF, minimizing the F-radius of a zonotope is equivalent to minimizing the trace of its covariation. Therefore, the following accuracy criterion can be written to maximize the influence of faults while minimizing that of disturbances:

$$J\left(G_{-}\right)=\frac{tr\left(cov\left(R_{f}(G_{-})\right)\right)}{tr\left(cov\left(R_{d}(G_{-})\right)\right)}. \tag{6.17}$$

Remark 6.1. *The criterion proposed in (6.17) follows a general idea that was inspired by optimal approximate decoupling techniques coming from parity-space residual generation as presented in [Din08]. Note that the notion of worst-case highly depends on a related evaluation criterion. An intuitive interpretation motivating the use of the original optimization criterion (6.17) is that it makes it possible to obtain an optimal time-varying observer gain maximizing the size (covariation) of a reachable set describing the influence of all the specified faults while minimizing the size (covariation) of a reachable set describing the influence of all the specified disturbances. This is in contrast with methods maximizing the influence of extreme faults (e.g. those involving the lowest sensitivity in terms of H_{-}) while minimizing the influence to extreme disturbances (e.g. those involving the maximal sensitivity expressed in terms of H_{∞}). Moreover, the proposed time-varying optimal observer gain can be expressed in a mathematically tractable way and the complexity of its computation remains compatible with on-line implementations.*

Once the optimization criterion based on a matrix parameter is chosen as (6.17), Proposition 6.4 can be used in order to parameterize the optimization criterion based on a vector ω rather than a matrix parameter like G_{-}.

Proposition 6.4. *Considering the definition of matrix trace and introducing $\omega = col\left(G_{-}\right)$, where $col(.)$ denotes the vertical concatenation of the matrix columns, the FD optimization criterion (6.17) can be parameterized with a parameter vector as*

$$J\left(G_{-}\right)=\frac{\omega^{T}\left(M_{f}^{T}M_{f}\right)\omega+2N_{f}^{T}M_{f}\omega+\left(N_{f}^{T}N_{f}\right)}{\omega^{T}\left(M_{d}^{T}M_{d}\right)\omega+2N_{d}^{T}M_{d}\omega+\left(N_{d}^{T}N_{d}\right)}, \tag{6.18}$$

with

$$M_f = \begin{bmatrix} -\left(\left(C_- R_{f_-}\right)^T \otimes I\right) \\ -\left(D_f^T\right) \otimes I \end{bmatrix}, \quad N_f = \begin{bmatrix} col\left(A_- R_{f_-}\right) \\ col\left(B_{f_-}\right) \end{bmatrix}, \tag{6.19a}$$

$$M_d = \begin{bmatrix} -\left(\left(C_- R_{d_-}\right)^T \otimes I\right) \\ -\left(D_d^T\right) \otimes I \end{bmatrix}, \quad N_d = \begin{bmatrix} col\left(A_- R_{d_-}\right) \\ col\left(B_{d_-}\right) \end{bmatrix}. \tag{6.19b}$$

Proof. Taking into account the Definition B.26, the covariation of the matrices R_f and R_d can be written as

$$cov\left(R_f(G_-)\right) = \left(R_f(G_-)\right)\left(R_f(G_-)\right)^T, \tag{6.20a}$$

$$cov\left(R_d(G_-)\right) = \left(R_d(G_-)\right)\left(R_d(G_-)\right)^T, \tag{6.20b}$$

where both are quadratic functions of the elements of G_-. Then, considering the definition of the matrix trace, the trace of both $cov\left(R_f(G_-)\right)$ and $cov\left(R_d(G_-)\right)$ can be expressed based on column vectors as

$$tr\left(cov\left(R_f(G_-)\right)\right) = col\left(R_f(G_-)\right)^T col\left(R_f(G_-)\right), \tag{6.21a}$$

$$tr\left(cov\left(R_d(G_-)\right)\right) = col\left(R_d(G_-)\right)^T col\left(R_d(G_-)\right). \tag{6.21b}$$

Additionally, using Kronecker product to introduce matrices M and N in (6.19), which are independent matrices with respect to G_- (for both disturbance and fault cases), the column form of R_d and R_f can be written as

$$col\left(R_f(G_-)\right) = M_f\,\omega + N_f, \tag{6.22a}$$

$$col\left(R_d(G_-)\right) = M_d\,\omega + N_d, \tag{6.22b}$$

where the column vector $\omega = col\left(G_-\right)$ is obtained by reshaping the observer gain matrix G_- through a vertical concatenation of its column vectors. Then, the substitution of (6.22) into (6.21) yields

$$\begin{aligned} tr\left(cov\left(R_f(G_-)\right)\right) &= \left(\omega^T M_f^T + N_f^T\right)\left(M_f\omega + N_f\right) \\ &= \omega^T\left(M_f^T M_f\right)\omega + 2N_f^T M_f\omega + \left(N_f^T N_f\right), \end{aligned} \tag{6.23a}$$

$$\begin{aligned} tr\left(cov\left(R_d(G_-)\right)\right) &= \left(\omega^T M_d^T + N_d^T\right)\left(M_d\omega + N_d\right) \\ &= \omega^T\left(M_d^T M_d\right)\omega + 2N_d^T M_d\omega + \left(N_d^T N_d\right). \end{aligned} \tag{6.23b}$$

Therefore, after the substitution of (6.23) in (6.17), the parameterized optimization criterion with FD purposes can be obtained as (6.18). □

Before continuing the analysis, some covariation matrices are first introduced

$$\tilde{Q}_f = \begin{bmatrix} Q_f & L_f^T \\ L_f & 0 \end{bmatrix}, \quad \tilde{Q}_d = \begin{bmatrix} Q_d & L_d^T \\ L_d & 0 \end{bmatrix}, \tag{6.24a}$$

$$Q_f = M_f^T M_f, \qquad Q_d = M_d^T M_d, \tag{6.24b}$$

$$L_f = N_f^T M_f, \qquad L_d = N_d^T M_d, \tag{6.24c}$$

$$\tilde{c}_f = N_f^T N_f, \qquad \tilde{c}_d = N_d^T N_d. \tag{6.24d}$$

It can be seen from (6.24) that those matrices with subscript f are related to the effect of the fault while those matrices with subscript d are related to the influence of the disturbance. Then, the FD optimization criterion (6.18) given in Proposition 6.4, which is obtained to describe the maximization of the effect of the faults (numerator) with respect to the effect of the disturbances (denominator), can be rewritten (simplified) using (6.24) as

$$J(\tilde{\omega}) = \frac{\tilde{\omega}^T \tilde{Q}_f \tilde{\omega} + \tilde{c}_f}{\tilde{\omega}^T \tilde{Q}_d \tilde{\omega} + \tilde{c}_d}, \tag{6.25}$$

where $\tilde{\omega} = \begin{bmatrix} \omega \\ 1 \end{bmatrix}$. The criterion (6.25) is a ratio of two quadratic functions. Apart from the constant terms in (6.25), the strong formal analogy with the design of parity space residuals using approximate decoupling techniques [PC91] can be observed. Though similar mathematical techniques can be used to solve the related optimization as detailed hereafter in Theorem 6.2, the purpose followed in this work is significantly different since it consists in obtaining a time-varying update of the gain of a state-bounding observer with a Kalman-like structure.

Theorem 6.2. *(Optimal observer gain with FD purposes) Maximizing the criterion (6.17) and, equivalently, (6.25) means finding $\tilde{\omega}^*$ such that $J(\tilde{\omega}^*) = \max_{\tilde{\omega}} J(\tilde{\omega})$. The solution satisfies $\tilde{\omega}^* \in \ker\left(\tilde{Q}_f - J^*\tilde{Q}_d\right)$ and the optimal observer gain G^* is determined by reshaping the solution of the generalized eigenvectors related to the greatest generalized eigenvalue of the pair $\left(\tilde{Q}_f,\ \tilde{Q}_d\right)$.*

Proof. Consider Proposition 6.4 and select $\tilde{\omega}^*$ to be the optimal value of $\tilde{\omega} = \dfrac{\partial J(\tilde{\omega})}{\partial \tilde{\omega}} = 0$.

Algorithm 6.2 Steps to compute the optimal observer gain based on the FD-ZKF approach

function $G = \texttt{OptObsGain}(\tilde{Q}_f, \tilde{Q}_d)$,
$[V, D] = \texttt{eig}(\tilde{Q}_f, \tilde{Q}_d)$ (to compute the generalized eigenvalue/vector decomposition),
$D = \texttt{diag}(D)$,
$I = \texttt{find}(D == \max(D))$,
$J = D(I(1))$,
$\omega = V(:, I(1))$,
$\omega = \frac{\omega}{\omega(end)}$,
$\texttt{col}(G) = \omega(1, (end-1))$,
$G = \texttt{reshape}(\texttt{col}(G), [n_x,\ n_y])$.
end

Hence, taking the derivative of (6.25) with respect to $\tilde{\omega}$ and setting it to zero successively yields

$$\begin{aligned} \tilde{\omega}^T \tilde{Q}_f \tilde{\omega} + \tilde{c}_f - J\tilde{\omega}^T \tilde{Q}_d \tilde{\omega} - J\tilde{c}_d = 0, \\ 2\tilde{\omega}^T \tilde{Q}_f - J2\tilde{\omega}^T \tilde{Q}_d = 0, \\ \left(\tilde{Q}_f - J^* \tilde{Q}_d\right) \tilde{\omega}^* = 0, \end{aligned} \tag{6.26}$$

where the symmetric nature of $\tilde{Q}_f$ and $\tilde{Q}_d$ is taken into account. Therefore, a non-null solution satisfies

$$\tilde{\omega}^* \in ker\left(\tilde{Q}_f - J^* \tilde{Q}_d\right). \tag{6.27}$$

Thus, finding $\tilde{\omega}^*$ that maximizes J can be achieved by computing the generalized eigenvalues and the related eigenvectors of the pair $\left(\tilde{Q}_f,\ \tilde{Q}_d\right)$. More precisely, the maximal value J^* of J for which a non-null solution exists is the greatest generalized eigenvalue of $(\tilde{Q}_f, \tilde{Q}_d)$ since the solutions J to $det(\tilde{Q}_f - J\tilde{Q}_d) = 0$ ensure a non-zero kernel $ker(\tilde{Q}_f - J\tilde{Q}_d)$. Then, the generalized eigenvector related to J^* gives $\tilde{\omega}^*$. Finally, the optimal observer gain matrix is calculated by reshaping ω^* into a matrix as $G^* = col^{-1}(\omega^*)$. □

The statement and proof of Theorem 6.2 provide the core results of this chapter leading to Algorithm 6.2 which implements the computation of the optimal observer gain for the proposed FD-ZKF FD filter.

A graphical representation of the proposed methodology using an observer gain G (based on the ZKF approach) and the optimal observer gain G^* (using the proposed

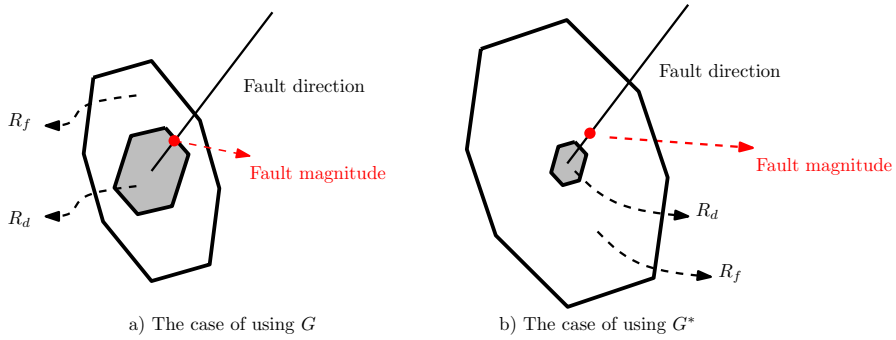

Figure 6.1: Intuitive graphical representation of the proposed method by means of plane zonotopes.

FD-ZKF approach) for designing the state-bounding observer is presented in Figure 6.1: The image of unit hypercubes modeling the range of the possible disturbances and faults are illustrated by gray and empty zonotopes, respectively. Then, considering the same magnitude and direction of the fault f in both cases, the detection of the fault cannot be guaranteed with the gain G (see Figure 6.1a). Indeed, Figure 6.1a illustrates a limit case between detection and non-detection: the influence of the fault exactly compensates that of the worst case disturbance, i.e., the red point is on the border of R_d. However, in Figure 6.1b, the influence of the fault is far outside from the influence of disturbances. Therefore, the detection of the fault with the same fault magnitude (and even smaller ones) can be guaranteed only with G^*, i.e., when the observer gain results from the optimization of an FD criterion. The richer underlying set-based representation compared to a basic vector-norm approach provides additional degrees of freedom to deal with relative directions and bounds in the space characterizing the influence of the possible disturbance and fault signals.

6.5 Comparative assessment

In this section, a comparative assessment of ZKF which optimizes the state observation criterion (6.15) and FD-ZKF which optimizes the FD criterion (6.17) is presented. To that purpose, the MDF will be characterized based on a classical sensitivity analysis in order to show the effect of the observer gain over the MDF. Then, it is possible to compare the approaches using the mathematical expression of the MDF based on the model of a numerical example (which will be discussed in Section 6.6).

Directly evaluating the MDF through simulations is an alternative way to show the improvement given by FD-ZKF compared to ZKF. A model-based analysis/characterization of the sensitivity to the faults is proposed in the following of this section. Here, the MDF is the minimum abrupt (step) fault that can be surely detected in steady state. For the sake of comparison only, it is assumed that the system is Linear Time-Invariant (LTI), whereas the general problem formulation of ZKF and FD-ZKF is still valid for LTV systems.

In order to characterize the minimum magnitude of the fault that can be detected, the input-output form of the discrete-time dynamical model (6.2) is expressed as

$$y(z) = \mathscr{T}_u(z)u(z) + \mathscr{T}_d(z)\ d(z) + \mathscr{T}_f(z)\ f(z), \tag{6.28}$$

where the transfer function $\mathscr{T}(z)$ can be computed as

$$\mathscr{T}(z) = C(zI - A)^{-1}B + D. \tag{6.29}$$

Notice that the related input, disturbance and fault are denoted by the subscripts of $\mathscr{T}(z)$, B and D as u, d and f, respectively. The subscripts u, d and f are eliminated in (6.29) for the sake of simplified notations. Alternatively, considering (6.3) rather than (6.2), the measurement equation can also be expressed as

$$y(z) = \mathscr{H}_u(z)u(z) + \mathscr{H}_d(z)d(z) + \mathscr{H}_f(z)f(z) + \mathscr{H}_y(z)y(z), \tag{6.30}$$

with

$$\mathscr{H}_\bullet(z) = C\ \big(zI - (A - GC)\big)^{-1}\ (B_\bullet - GD_\bullet) + D_\bullet, \tag{6.31a}$$
$$\mathscr{H}_y(z) = C\ \big(zI - (A - GC)\big)^{-1}G, \tag{6.31b}$$

where subscript $\bullet$ can be assigned by u, d and f depending on the kind of input considered. Furthermore, (6.30) can be written as

$$(I - \mathscr{H}_y(z))y(z) = \mathscr{H}_u(z)u(z) + \mathscr{H}_d(z)d(z) + \mathscr{H}_f(z)f(z). \tag{6.32}$$

Therefore, the input-output form of the residual/innovation term can be written

using (6.32) as

$$\begin{aligned}\varepsilon(z) = r(z) =& (I - \mathscr{H}_y(z))y(z) - \mathscr{H}_u(z)u(z) \\ =& \underbrace{\mathscr{H}_d(z)d(z)}_{\varepsilon_d(z)} + \underbrace{\mathscr{H}_f(z)f(z)}_{\varepsilon_f(z)},\end{aligned} \tag{6.33}$$

where $\varepsilon_d(z)$ and $\varepsilon_f(z)$ refer to the (observer gain dependent) effect of the disturbance and the fault on the residual term. Thus, $\mathscr{H}_d(z)$ and $\mathscr{H}_f(z)$ can be interpreted as the sensitivity of the residual with respect to disturbances and faults, respectively.

Theorem 6.3. *Given an observer as (6.4) and the input-output form of its measurement equation as (6.30), the MDF in steady state is given under the single-fault assumption as*

$$\underline{f}_j^{\infty} = \min_i \underline{f}_{ji}^{\infty}, \qquad \underline{f}_{ji}^{\infty} = 2\,\frac{\|\mathscr{H}_{d,i}(1)\|_1}{\|\mathscr{H}_{f,ij}(1)\|_1}, \tag{6.34}$$

where the magnitude f_j of the single step faults that are necessarily detected satisfy $f_j > \underline{f}_j^{\infty}$ or $f_j < -\underline{f}_j^{\infty}$, with $j = 1, ..., n_f$. A fault is said to be necessarily detected if $\exists k,\ 0 \notin \langle c_\varepsilon,\ b(R_\varepsilon)\rangle$ is satisfied. Whereas j is an index for single faults, i refers to the rows of $\mathscr{H}_d(z)$ and $\mathscr{H}_f(z)$. More precisely, $\mathscr{H}_{d,i}(1)$ is the i^{th} row of $\mathscr{H}_d(1)$ and $\mathscr{H}_{f,ij}(1)$ is the element at the i^{th} row and j^{th} column of $\mathscr{H}_f(1)$.

Proof. Since $\varepsilon(z) = \varepsilon_d(z) + \varepsilon_f(z)$ in z-domain, the residual can be expressed in the time domain and in steady state (limit as $k \to \infty$) as

$$\varepsilon^{\infty} = \varepsilon_d^{\infty} + \varepsilon_f^{\infty} = \mathscr{H}_d(1)d^{\infty} + \mathscr{H}_f(1)f^{\infty}. \tag{6.35}$$

Considering $d \in [-1,\ 1]^{n_d} = \langle 0,\ I_{n_d}\rangle$ and a faultless scenario (it means $f(z) = 0 \Rightarrow f^{\infty} = 0$), the residual in steady state can be expressed according to (6.35) as

$$\varepsilon^{\infty} \in 0 \pm |\mathscr{H}_d(1)|\mathbf{1}, \tag{6.36}$$

where $|\cdot|$ is the element-by-element absolute value operator and $\mathbf{1}$ is a column vector of ones of appropriate dimension. Hence, $|\mathscr{H}_d(1)|\mathbf{1}$ is a vector whose i^{th} element is the 1-norm (scalar) of the i^{th} row $\mathscr{H}_{d,i}(1)$ of the matrix $\mathscr{H}_d(1)$. Thus, the i^{th} element ε_i^{∞} of the residual ε^{∞} allows the detection of a fault if $\varepsilon_i^{\infty} \notin 0 \pm \|\mathscr{H}_{d,i}(1)\|_1$. Furthermore, (6.35) can be rewritten $\forall i$ as $\varepsilon_i^{\infty} = \varepsilon_{d,i}^{\infty} + \varepsilon_{f,i}^{\infty}$.

Therefore, in steady state, the condition ensuring the detection of the j^{th} fault from

the i^{th} component of the residual is:

$$\mathscr{H}_{f,ij}(1)\ f_j^{\infty} \notin 0 \pm 2\left\|\mathscr{H}_{d,i}(1)\right\|_1 . \tag{6.37}$$

The factor 2 comes from the worst-case scenario where the disturbances have a maximal influence in the opposite direction compared to that of the occurring fault. Thus, it can be written that

$$f_j^{\infty} \notin 0 \pm 2\ \frac{\left\|\mathscr{H}_{d,i}(1)\right\|_1}{\left\|\mathscr{H}_{f,ij}(1)\right\|_1}. \tag{6.38}$$

Equation (6.37) can be rewritten as (6.38) so that $\underline{f}_{ji}^{\infty}$ in (6.34) interprets as the minimum magnitude f_j such that the j^{th} fault is necessarily detected by the i^{th} scalar residual ε_i^{∞} taken alone. This results in (6.34) when considering all the scalar components of the innovation term. □

Finally, the comparison of the ZKF and FD-ZKF approaches can be done in the FD framework using Theorem 6.3. As it can be seen from (6.31), the transfer functions $\mathscr{H}_d$ and $\mathscr{H}_f$ in (6.34) depend on the observer gain. In the ZKF approach, the observer gain can be computed explicitly based on Section 6.4.2 using Theorem 6.1. In the FD-ZKF approach, the observer gain can be computed based on Section 6.4.3 using Algorithm 6.2. Because of their distinct observer gains, the FD performance is expected to be different between the ZKF and FD-ZKF approaches. In this regard, further quantitative comparison of the approaches will be discussed in Section 6.6 based on a case study.

6.6 Case study

6.6.1 Plant description

In this section, the same quadruple-tank system as explained in Section A.1 of Appendix A is considered to illustrate the approach proposed in this chapter. Therefore, considering the non-linear model (A.1) and its linearized form (A.2) around the same working points reported in Section A.1, a discrete-time linear model using the Euler

discretization with a sampling time of 1s can be written as

$$\tilde{h}_+ = A\tilde{h} + B_u\tilde{v} + B_d d + B_f f, \tag{6.39a}$$

$$y = C\tilde{h} + D_u\tilde{v} + D_d d + D_f f, \tag{6.39b}$$

with the same system matrices as (A.4) [2]. Moreover, taking into account the state disturbance and measurement noise, $B_d d$ and $D_d d$ are used in (6.39) with

$$B_d = \begin{bmatrix} 0.05 & 0.01 & 0 & 0 & 0 & 0 & 0 \\ 0.05 & 0 & 0.01 & 0 & 0 & 0 & 0 \\ 0.05 & 0 & 0 & 0.01 & 0 & 0 & 0 \\ 0.05 & 0 & 0 & 0 & 0.01 & 0 & 0 \end{bmatrix}, \tag{6.40a}$$

$$D_d = \begin{bmatrix} 0_{2x5} & 0.1\ I_2 \end{bmatrix}. \tag{6.40b}$$

As it can be seen in (6.40a), the first column of B_d is used to define a disturbance influencing all the states, e.g., rain simultaneously getting into all the tanks. The idea of considering the rain that can have large influence on the direction defined by the first column of matrix B_d in (6.40a) is to model a kind of flow (disturbance) affecting all tanks at the same time. In addition, disturbances aiming at enclosing modeling errors like, e.g., linearization and discretization errors, are introduced through the next diagonal block in B_d. Therefore, bounded disturbances acting in all the state-space directions and the measurement noise are modeled with B_d and D_d, respectively.

Furthermore, the effect of faults on the state and the measurements is modeled through the terms $B_f f$ and $D_f f$, respectively. The possible faults that are considered are actuator faults, sensor faults and leakages. Hence, the following matrices are chosen in the simulation in order to simulate all these faults:

$$B_f = \begin{bmatrix} 10B_u & 0.3\ I_4 & 0_{4x2} \end{bmatrix}, \tag{6.41a}$$

$$D_f = \begin{bmatrix} 0_{2x6} & 10\ I_2 \end{bmatrix}. \tag{6.41b}$$

Consistently with the problem formulation in Section 6.2, the uncertain input vectors d and f are assumed to be normalized in [-1,+1]. The values of B_d, D_d, B_f and D_f are defined accordingly. Then, a 10% step fault f_i is simulated with $f_i = 0.1$ after the fault

[2] It is worth mentioning that B_u and D_u in (6.39) is equal to B and D in (A.3), respectively.

occurrence.

6.6.2 FD-ZKF filter implementation

The observer gain can be iteratively computed for the quadruple-tank system presented in (6.39) using Theorem 6.1 in the case of ZKF, and Algorithm 6.2 in the case of FD-ZKF. In both cases, the FD test is implemented based on Algorithm 6.1.

6.6.3 Performing FD

Two FD tests are considered in this section. Both are implemented using the Algorithm 6.1. They only differ from the observer gain used: it is determined using the ZKF or FD-ZKF approach as explained in the Section 6.4.

Regarding the disturbance scenario, (6.40) is used to simulate all the possible disturbances acting in all the directions. Furthermore, regarding the fault simulation, the following fault scenario is set in all the simulations: from time instants $k = 0$ to $k = 200$, the system is healthy. Then, an additive step (abrupt) fault occurs at time instant $k = 200$ and it remains in the system until $k = 1000$. Moreover, single faults are considered based on the elements of the vector f, i.e.,

$$f = \begin{bmatrix} f_1 & f_2 & f_3 & f_4 & f_5 & f_6 & f_7 & f_8 \end{bmatrix}^T, \tag{6.42}$$

where f_1 and f_2 indicate the actuator faults, f_3, f_4, f_5 and f_6 are the leakage faults and the sensor faults are denoted by f_7 and f_8.

In the first simulation, the FD test is done when considering the actuator fault f_1, i.e, the faultless scenario is considered from the beginning of the simulation until time instant $k = 200$. Then, the occurrence of the actuator fault f_1 is simulated at $k = 200$ and it remains until the end of the simulation. Figure 6.2 shows the projection of the computed state-bounding zonotope into the state space when the actuator fault occurs at time instant $k = 200$. The state estimation in this figure is carried out by considering Proposition 6.1 using ZKF and FD-ZKF approaches to compute the observer gain. As it was mentioned before, the fault is simulated after time instant $k = 200$. Thus, before this time instant, the system is only affected by the effect of disturbances and noises. Consequently, the bounds that are obtained at the first 200 time instants show the effect

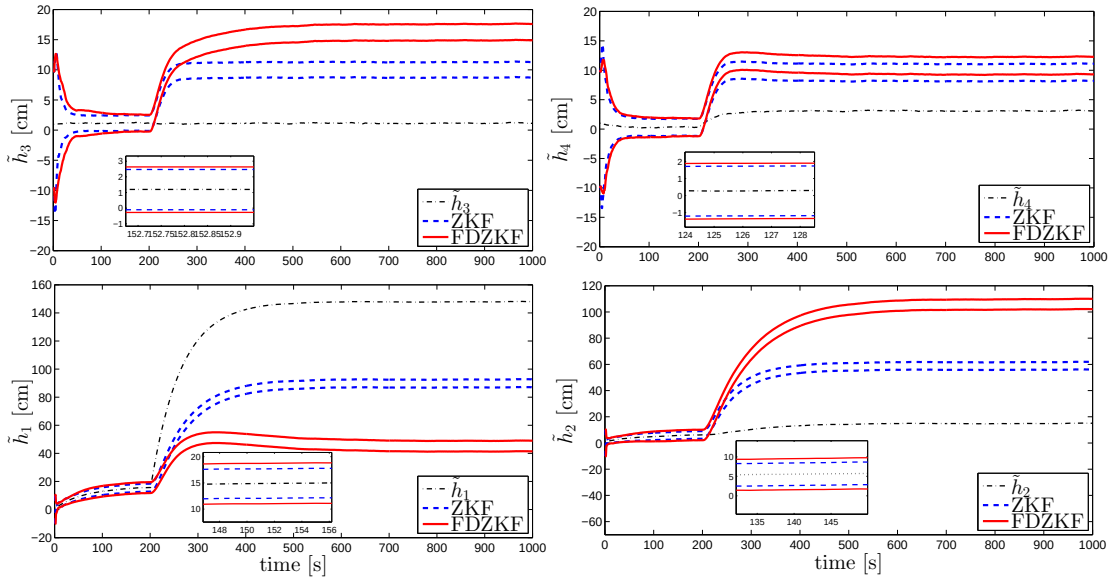

Figure 6.2: State estimation in the case of an actuator fault f_1

of both disturbances and noises. As it can be seen from the time instant $k = 0$ until $k = 200$ where the system is only affected by the disturbance, the observer can properly follow the system using both observer gains.

Furthermore, Figure 6.2 shows that the state estimation bounds are a bit more conservative with FD-ZKF compared to ZKF for $0 \leq k < 200$. A possible explanation is related to the criteria used by both approaches. The ZKF optimization criterion is defined considering only the observation purposes whereas the FD-ZKF criterion is defined considering FD performance. Thus, it is normal to obtain a better state estimation with ZKF. What is interesting in Figure 6.2 is that even by considering FD purpose with the FD-ZKF approach, no significant differences are obtained from the perspective of state estimation in comparison with ZKF.

After time instant $k = 200$, the effect of the actuator fault can be seen on the state estimation in Figure 6.2. The inconsistency of the observation by the model using both ZKF and FD-ZKF approaches and the nominal behaviour of the system allows to detect the fault. Furthermore, comparing the approaches after the fault occurrence reveals the improvement provided by the FD-ZKF approach since its estimation envelope has more changes with respect to the behaviour of the true system, so showing an increased

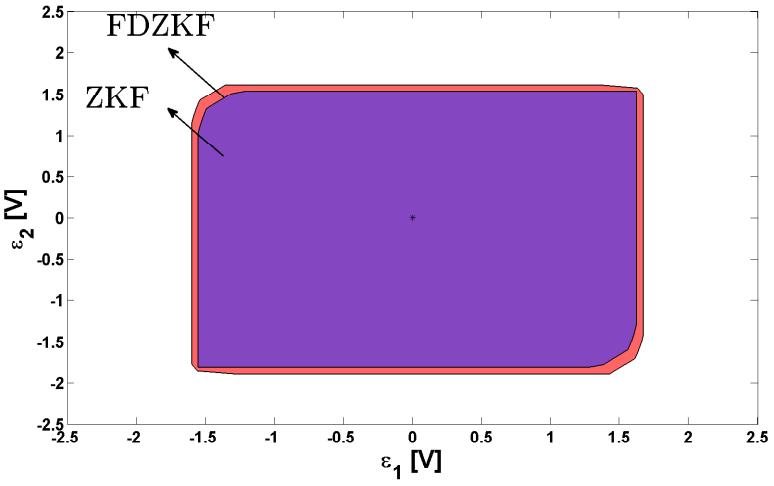

Figure 6.3: Zonotopes bounding the innovation/residual before the occurrence of the fault at $k = 100$

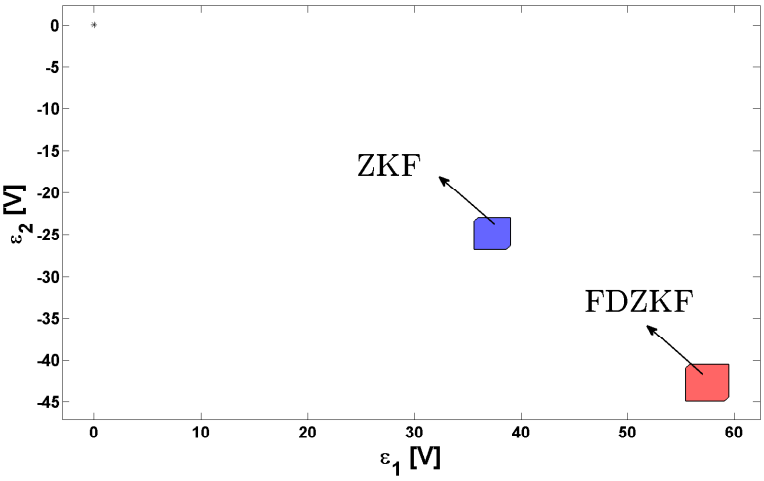

Figure 6.4: Zonotopes bounding the innovation/residual after the occurrence of the fault at $k = 600$

sensitivity to the considered fault. Additionally, it can be observed that the improved sensitivity of the FD-ZKF approach is persistent, even after reaching the steady state.

For further illustration, the FD test is done based on Algorithm 6.1 considering the innovation term. As it is shown in Figure 6.3, a threshold (here zero) is included by both innovation zonotopes generated by ZKF and FD-ZKF approaches, respectively, before

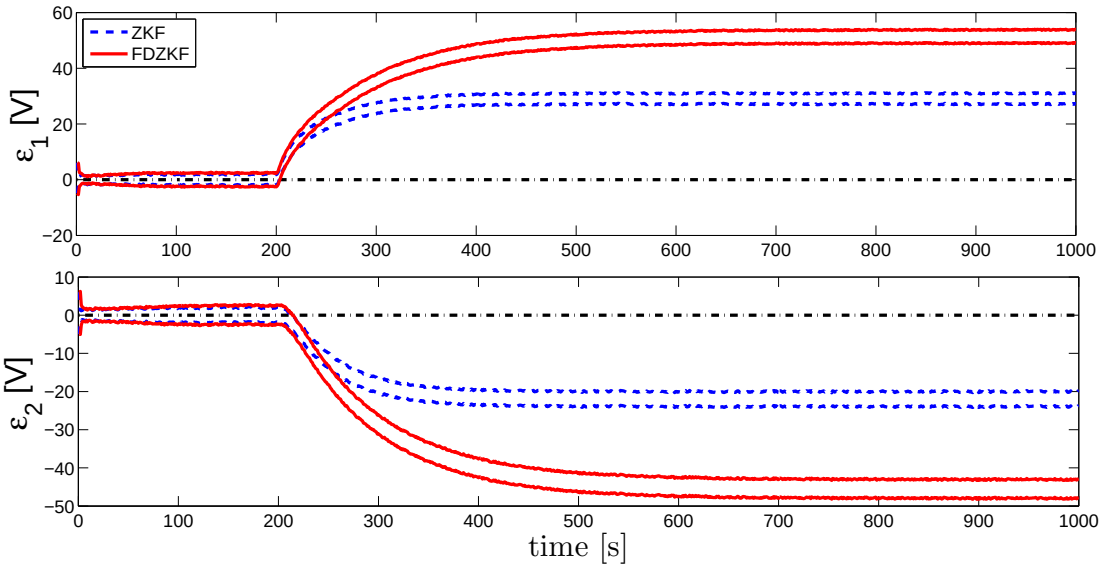

Figure 6.5: Envelopes of the scalar innovation terms

the occurrence of the fault. But, after the fault occurrence, both zonotopes move and the fault can be detected since zero is outside of the zonotopes bounding the innovation. The higher sensitivity of the FD-ZKF approach in comparison with ZKF approach can be seen in Figure 6.4 since its generated zonotope moves further from the non-faulty region. Therefore, it can be obsrved that FD-ZKF is more sensitive with respect to the effect of the fault.

Moreover, for the completion of the analysis, it is also interesting to combine the innovation terms and see the effect of the fault over both innovation terms together. In this regard, the ratio between the Euclidean norm of the center and the generator matrix of the innovation term is computed for both ZKF and FD-ZKF approaches. In particular, the ratio $\frac{\|c_\varepsilon\|_2}{\|R_\varepsilon\|_2}$ is compared when the state-bounding observer is designed using both approaches. Figure 6.6 shows the results obtained in this context.

As expected from the previous results in Figure 6.5, the most sensitive performance is obtained with FD-ZKF. But, now Figure 6.6 presents a single scalar criterion aggregating all the scalar components of the innovation that provides a well-defined basis for the comparison of the approaches. Indeed, directly comparing the values of the optimization criteria (6.15) and (6.17) is not relevant since they consider different goals. Moreover,

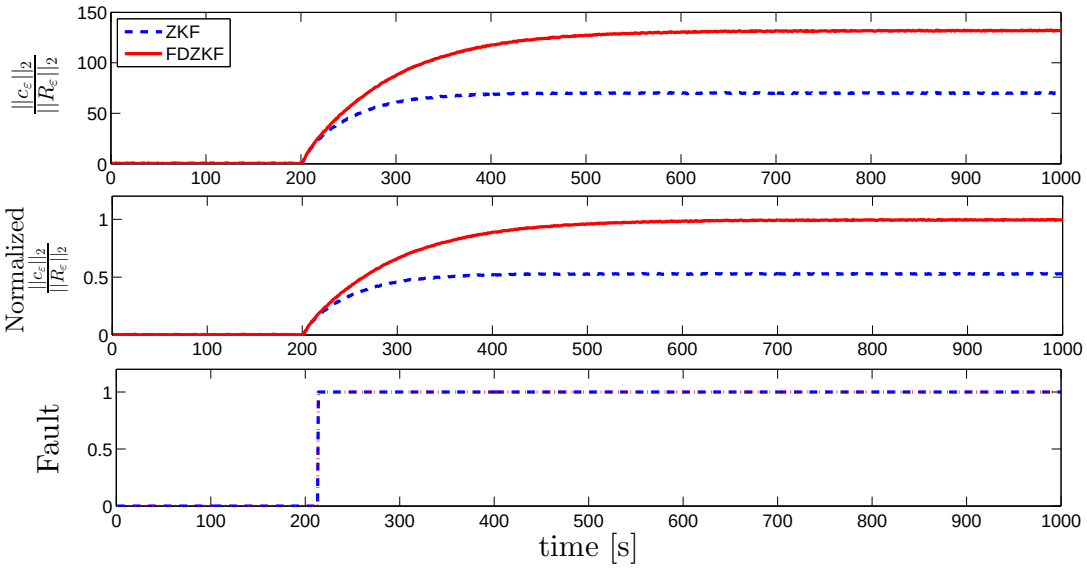

Figure 6.6: Ratio $\dfrac{\|c_\varepsilon\|_2}{\|R_\varepsilon\|_2}$ and the FD test in the case of an actuator fault f_1.

considering independently each scalar term of the innovation as in Figure 6.5 may significantly complicate the sensitivity analysis when the number of sensors is greater than 2 or 3. Moreover, the bottom plot in Figure 6.6 shows the FD test decision resulting from both approaches: 0 means no-fault affecting the system and 1 means the fault is detected.

The second considered scenario corresponds to a sensor fault. The output of the system is measured from the level measurement device. Since the height of each tank is 20 cm, the output of the system from the level measurement device is between $0-10$ V. The matrix D_f in (6.41b) is defined with the whole range of the measurement. Then, the simulation of a step sensor fault with a magnitude of 10% of the whole range is simulated after the fault occurrence with

$$f = \begin{bmatrix} 0 & 0 & 0 & 0 & 0 & 0 & 0 & 0.1 \end{bmatrix}^T. \tag{6.43}$$

As in the case of the actuator fault, the ratio between the Euclidean norm of the center and the generator matrix of the innovation term is computed and reported in Figure 6.7. Once again, the sensitivity to the fault with FD-ZKF is improved compared

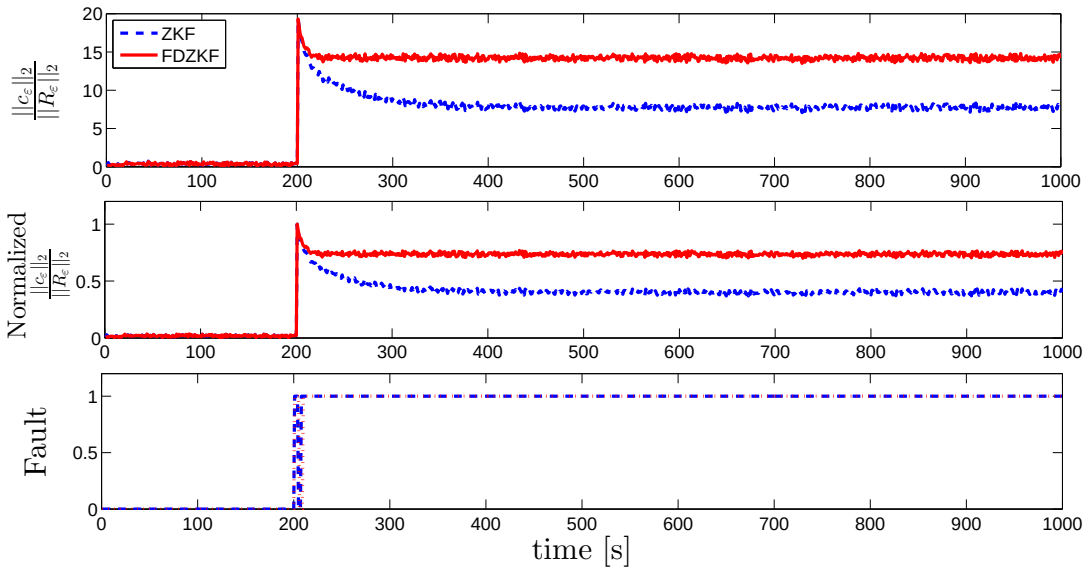

Figure 6.7: Ratio $\frac{\|c_\varepsilon\|_2}{\|R_\varepsilon\|_2}$ and the FD test in the case of a sensor fault f_8

to ZKF.

The last scenario considered to test the proposed FD-ZKF approach corresponds to a leakage fault f_3 simulated using B_f as in (6.41a). Figure 6.8 shows a similar improvement of the sensitivity with FD-ZKF and an analog detection ability compared to the other fault scenarios (sensor and actuator faults).

6.6.4 MDF analysis

Based on Theorem 6.3, the computation of the MDF is influenced by the observer gain. In order to compute the MDF for the case study, (6.34) is used. Therefore, based on the different observer gains G_∞^* obtained with ZKF and FD-ZKF, magnitudes of the the MDF can be determined. Moreover, the constant observer gain that is obtained in steady state can be used to compute the MDF that can be detected in order to compare the performance of the observer when using FD-ZKF and ZKF approaches. In this regard, the following observer gains are obtained in steady state from the simulation of

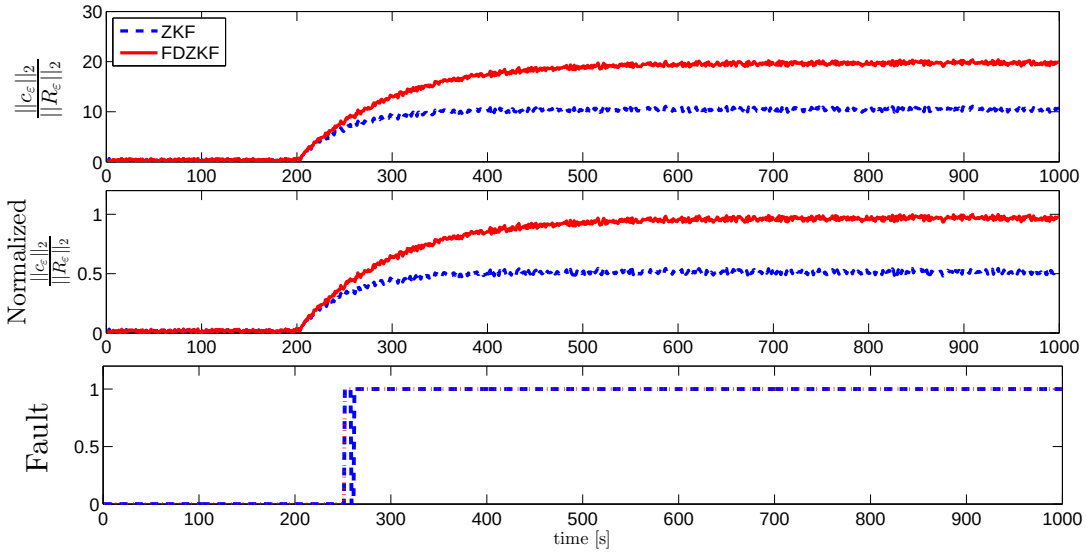

Figure 6.8: Ratio $\dfrac{\|c_\varepsilon\|_2}{\|R_\varepsilon\|_2}$ and the FD test in the case of a leakage fault f_3

the two approaches:

$$\text{FD-ZKF approach:} \qquad G_\infty^* = \begin{bmatrix} 0.0679 & 0.0804 \\ 0.0807 & 0.0746 \\ 0.0469 & 0.0391 \\ 0.0484 & 0.0469 \end{bmatrix}, \tag{6.44a}$$

$$\text{ZKF approach:} \qquad G_\infty^* = \begin{bmatrix} 0.0828 & 0.0730 \\ 0.0731 & 0.0845 \\ 0.0446 & 0.0421 \\ 0.0466 & 0.0475 \end{bmatrix}, \tag{6.44b}$$

where G_∞^* is the obtained optimal gain in steady state.

Then, the obtained results based on Theorem 6.3 are reported in Table 6.1. This means that the detection of the fault with the magnitude either bigger than the obtained magnitude in Table 6.1 or smaller than the obtained magnitude in Table 6.1 with negative sign can be guaranteed. Furthermore, from Table 6.1 and for the considered faults, the size of the MDF is systematically smaller in case of the FD-ZKF. This illustrates

Table 6.1: MDF (theoretical sensitivity analysis under a steady-state operation)

	Actuator fault			**Leakage fault**			**Sensor fault**	
	f_1	f_2	f_3	f_4	f_5	f_6	f_7	f_8
ZKF approach	0.0641	0.5291	0.4340	0.4300	0.4340	0.4300	0.4082	0.5826
FD-ZKF approach	0.0578	0.4812	0.3898	0.3641	0.3898	0.3641	0.3667	0.4934
Improvement	9.8284%	9.0531%	10.1843%	15.3256%	10.1843%	15.3256%	10.1666%	15.3107%

the sensitivity improvement obtained by the proposed optimal tuning of the observer gain in a FD framework.

Further simulations are carried out for the case study by changing the fault magnitudes. It is interesting to see the magnitude of the faults that can be detected considering not only the steady state (Table 6.2), but also the whole time range of the simulation as reported in Table 6.3. By increasing the magnitude of the fault, the FD-ZKF detection test (Algorithm 6.1) is used to see whether the fault with this magnitude can be detected or not. The results of this analysis are collected in Tables 6.2 and 6.3.

Table 6.2 shows those magnitudes of the fault that can be still detected at the end of the simulation, i.e., in steady state. Therefore, data from this table can be compared with the data in Table 6.1, which shows the theoretical MDF magnitudes obtained from Theorem 6.3. In this regard, by comparing Tables 6.1 and 6.2, no significant differences are found between the size of the MDF in all the cases. Hence, Table 6.2 confirms through numerical simulations the theoretical values previously reported in Table 6.1 and the improvement achieved by FD-ZKF. Further analysis is done in Table 6.3 to obtain the magnitude that can be detectable in whole the time range of the simulation.

Moreover, it can be observed from the comparison of Tables 6.2 and 6.3, that the magnitude of the fault that can be detected considering the whole time range of the simulation is almost the same in the case of actuator and leakage fault. However, in the case of sensor faults and because of the fault reinjection involved by the observer structure leading to some transient behavior (see the overshoot in Figure 6.7), the magnitude of the detectable fault is improved on the whole time range of the simulation compared to steady state only. This illustrates that FD-ZKF is well suited to also address time-varying and transient behaviors to enhance the FD ability.

Table 6.2: MDF at the end of the simulation

	Actuator fault			**Leakage fault**			**Sensor fault**	
	f_1	f_2	f_3	f_4	f_5	f_6	f_7	f_8
ZKF approach	0.0472	0.5012	0.4132	0.4121	0.4122	0.4313	0.3990	0.5912
FD-ZKF approach	0.0421	0.4620	0.3621	0.3412	0.3592	0.3552	0.3492	0.4897
Improvement	10.8051%	7.8212%	12.3669%	17.2046%	12.8578%	17.6443%	12.4812%	17.1685%

Table 6.3: MDF by considering the whole time range of the simulation

	Actuator fault			**Leakage fault**			**Sensor fault**	
	f_1	f_2	f_3	f_4	f_5	f_6	f_7	f_8
ZKF approach	0.04901	0.4997	0.4139	0.4098	0.4134	0.4231	0.3582	0.5718
FD-ZKF approach	0.0431	0.4631	0.3597	0.3396	0.3517	0.3497	0.3013	0.4698
Improvement	12.0588%	7.3244%	13.0950%	17.1303%	14.9250%	17.3481%	15.8850%	17.8384%

6.7 Summary

This chapter has proposed a new FD observer based on a ZKF, called FD-ZKF, that enhances the sensitivity to faults while increasing the robustness to disturbances. As a novelty, in the proposed FD-ZKF approach, the time-varying observer gain is optimized by considering the FD purposes and it can be perceived as an extended version to FD of the ZKF approach where the observer gain is only computed for state observation purposes. In the proposed algorithm, the influences of all possible disturbances and faults within the specified ranges have been considered to compute the observer gain with the aim of increasing the sensitivity to faults with respect to disturbances. This is achieved through the optimization of a set-based criterion explicitly taking the relative influence of faults with respect to disturbances into account. Furthermore, the MDF is characterized using a classical sensitivity analysis in order to show the effectiveness of the proposed time-varying observer gain on FD performance. The comparison of FD-ZKF and ZKF approaches has been conducted on a case study based on a quadruple-tank system. The obtained results show a significant improvement of the FD-ZKF approach in comparison with the ZKF approach in FD performance. Furthermore, a quite small difference is obtained between the approaches when computing the state-bounding sets. Thus, a small relaxation of the state observation ability has given sufficient freedom

degrees to significantly enhance the efficiency of FD. As can be seen from the beginning of the thesis, almost all the proposed approaches in state estimation and FD frameworks have only been applied when the system is affected by the time-varying uncertainties and no research has been done for the case that time-invariant uncertainties influence the system. Therefore, the main focus of the next chapter will be on the design of an IOA for linear dynamic systems affected by both time-invariant and time-varying uncertainties.

Chapter 7

Interval observer design for a system subject to both TIU and TVU

This chapter proposes the design of an IOA for linear dynamic systems affected by both TIU and TVU. First, set-based and trajectory-based IOA schemes are compared and analyzed dealing with the different type of uncertainties. Then, an integrated set-based and trajectory-based observer is proposed in order to overcome the drawbacks of using the set-based approach, i.e., the non-preservation of the parameter uncertainty time dependency and the wrapping effect. Furthermore, H_∞ performance is considered in order to compute the observer gain by using an LMI technique. Finally, a numerical example and a real case study based on a two-tank system are employed for both illustrating and analyzing the effectiveness of the proposed approach.

7.1 Introduction

In order to bound the uncertainty effect in the system using interval observers considering an unknown-but-bounded deterministic framework, there exist two main approaches: the *set-based IOA* [Com15b] and the *trajectory-based IOA* [PSQ05a]. In the set-based IOA, the set that bounds the outputs/states is determined using the observer equations based on previous approximated sets and using a one-step

ahead prediction. On the other hand, for the trajectory-based IOA, a set of pointwise trajectories generated by selecting particular values of the uncertainty is used [REZ12, PSQ05a, Com15b, PPOMZ17]. Based on the literature, each approach has its own advantages and disadvantages. The set-based IOA is affected by some problems, e.g., wrapping effect, range evaluation of an interval function (in this case, the state-space function) and the uncertain parameter time dependency [PSQ05a]. However, in the second case, the interval hull of the state estimation is built following real trajectories generated by selecting particular values of the interval parameter vector. Consequently, this approach overcomes the wrapping effect and preserves the uncertain parameter time dependency, but in the case of the trajectory function, the problem of the interval function range evaluation still remains. On the other hand, set-based IOA present a lower computationally complexity than trajectory-based IOA and, consequently, they seem to be more suitable for real-time applications [KP05, LAC+12].

According to [PSQ03], it is possible to classify the approaches dealing with the time variance of the uncertain parameters into the *time-varying approach* and the *time-invariant approach*. The former class assumes that unknown but bounded uncertain parameters can vary at each time instant since one-step ahead recursion algorithms are used. However, in the latter class, it is guaranteed that the unknown but bounded uncertain parameters cannot vary at each time instant [PSQ05a]. Concerning the preservation of time dependency of uncertainty in the reported approaches in the literature, one possibility is to evolve the observer dynamics from the initial state to the present state by driving a functional relationship between states and parameters at every time instant [PSQ03] but with a high computational cost. To avoid such a complexity, the observer is usually designed to satisfy the monotonicity condition [ERZ13, KPPOM17] such that only propagating some trajectories is enough to bound the effect of the uncertainty in the estimation provided by the observer.

When applying interval observers to FD, additionally to the problem of generating the detection thresholds by uncertainty propagation, another important problem is how to design the observer gain to be as robust as possible against the unavoidable effect of uncertainties. In this regard, there has been an increasing interest in computing the observer gain in several manners to minimize the effect of uncertainties. Thus, the observers can be designed by considering the robustness against disturbances, noise or any other uncertainties using, as e.g., H_∞ optimization, LMIs, among other strategies [SCP96, ZDLW03]. The topic has grown in importance and becomes more challenging

if the system is affected by both TIU and TVU [REZ12, PPOMZ17].

The main contribution of this chapter is to design a robust IOA whose observer gain is computed by using LMI techniques to achieve H_∞ performance, i.e., to be as robust as possible against the effect of uncertainty. Furthermore, the relationship between the set-based IOA and trajectory-based IOA is investigated in order to connect them under some conditions taking into account both TIU and TVU. The proposed approach is illustrated through a numerical example and a two-tank real system.

Regarding the structure of this chapter, the problem formulation is addressed in Section 7.2. The set-based IOA and trajectory-based IOA structures and their robust design are discussed in Sections 7.3 and 7.4, respectively. The discussion and the comparative assessment are presented in Section 7.5. Applications based on both a numerical example and a real two-tank system are used in order to illustrate the effectiveness of the proposed approach in Section 7.6. Finally, conclusions are drawn in Section 7.7.

7.2 Problem formulation

7.2.1 Problem set-up

This chapter considers that the uncertain system is represented by a discrete-time LTI model in state-space form as follows:

$$x_{k+1} = [A_0 + \Delta A(\theta)]\, x_k + B u_k + E_\omega \omega_k, \tag{7.1a}$$

$$y = C x_k + E_\upsilon \upsilon_k, \tag{7.1b}$$

where $u \in \mathbb{R}^{n_u}$, $y \in \mathbb{R}^{n_y}$ and $x \in \mathbb{R}^{n_x}$ are the input, the output and the state vectors, respectively. Moreover, $A_0 \in \mathbb{R}^{n_x \times n_x}$, $B \in \mathbb{R}^{n_x \times n_u}$ and $C \in \mathbb{R}^{n_y \times n_x}$ are the state-space matrices. Both state disturbance and process noise vectors are considered as TVU and defined by $\omega \in \mathbb{R}^{n_x}$ and $\upsilon \in \mathbb{R}^{n_y}$, respectively. Moreover, E_ω and E_υ are the associated distribution matrices with appropriate dimensions while $k \in \mathbb{N}$ indicates the discrete time. Furthermore, it is assumed that the vector of time-invariant uncertain parameter θ belongs to an admissible set Θ, i.e.,

$$\Theta = \left\{ \theta \in \mathbb{R}^{n_\theta} : \ \underline{\theta}_i \leq \theta_i \leq \overline{\theta}_i \ \ \forall i = 1, \ldots, n_\theta \right\}, \tag{7.2}$$

where n_θ denotes the number of uncertain parameters. Moreover, the matrix A_0 contains the nominal values of the parameters while $\Delta A(\theta)$ represents the uncertainty associated with.

Assumption 7.1. *It is assumed that, for all* $\theta \in \Theta$,

$$\underline{\Delta A} < \Delta A(\theta) < \overline{\Delta A}, \tag{7.3}$$

where $\underline{\Delta A} \in \mathbb{R}^{n_x \times n_x}$ *and* $\overline{\Delta A} \in \mathbb{R}^{n_x \times n_x}$ *are constant and known matrices that contain the minimum and maximum values of* $\Delta A(\theta)$*, respectively.* □

Additionally, the additive uncertainties, i.e., time-varying measurement disturbance ω and process noise v, are assumed unknown but bounded as it is reported in (2.2).

7.2.2 General observer structure

Monitoring the system behavior with the dynamical model (7.1) can be done by designing a Luenberger observer of the form in (2.5) [1].

To take into account the effects of TVU, i.e., ω and v, and TIU, i.e., $\Delta A(\theta)$, over the output/state estimation provided by (2.5), two different strategies are described next: one based on bounding the uncertainty effect in the observer estimation and the other based on designing the observer gain L to minimize such effect.

7.3 Set-based interval observation

7.3.1 Set-based interval observer structure

In set-based IOA, the underlying observer structure is determined using the algorithm proposed by [MdOPB12]. Generally speaking, in this approach, the set of states at time instant $k+1$ is approximated by using propagation algorithms from the set of states at time k (for more information see [PSQ05b] and [Com15b]). Moreover, the gain matrix L can be further tuned with respect to the state estimation purpose, i.e., to increase the robustness of the state estimation.

[1] The system matrix A in (2.5) must be replaces by A_0 in this chapter based on the dynamical model (7.1).

The main idea of the set-based IOA resides in using a structure such as the interval model to estimate the interval $[\hat{x}_{k+1}]$ from the previous interval $[\hat{x}_k]$. One of the basic algorithms in this case, which is introduced in [Moo66] and called the Moore's algorithm, estimates the states based on the Taylor Series decomposition. Furthermore, different types of algorithms that are evaluated to estimate the states in the set-based IOA are described in the survey paper [PSQ05a].

As mentioned before, the effect of uncertainty can be expressed using a zonotopic-set representation, i.e., a particular type of polytope, reducing the set operations to simple matrix calculations. In this regard, the zonotopic representation of ω and υ in (2.2) can be written as (2.3). Moreover, disturbance and noise bounds represented in (2.3) are assumed to be bounded by a unitary hypercube zonotopes centered at the origin as it is considered in Assumption 2.2. Now, assuming the initial state x_0 belongs to the zonotopic set $\mathcal{X}_0 = \langle c_0,\ R_0 \rangle$, where $c_0 \in \mathbb{R}^{n_x}$ denotes the center and $R_0 \in \mathbb{R}^{n_x \times r_{R_0}}$ is non-empty matrix containing the generators matrix of the initial zonotope $\mathcal{X}_0$, the zonotopic observer structure can be defined by following Proposition 7.1.

Proposition 7.1. *(Zonotopic-observer structure) Considering the observer scheme* (2.5) *and the uncertainties modelled as in Assumptions 7.1, 2.2 and 2.3, the center* c *and the segment matrix* R *of the zonotope that bounds the state estimation provided by the observer* (2.5) *can be recursively defined as*

$$c_{k+1} = \text{mid}(A^{obs}(\theta))c_k + Bu_k + Ly_k, \tag{7.4a}$$

$$R_{k+1} = \left[\diamond(A^{obs}(\theta)\bar{R}_k) \quad \frac{\text{diam}(A^{obs}(\theta))}{2} c_k \quad E_\omega \quad -LE_\upsilon \right], \tag{7.4b}$$

where $A^{obs}(\theta) = [A_0 + \Delta A(\theta)] - LC$, $\bar{R}_k = \downarrow_q \{R_k\}$ *(see Property B.1),* mid *denotes the center and* diam *is the diameter of the interval. Moreover, the state inclusion property* $x_k \in \langle c_k,\ R_k \rangle$ *holds for all* $k \geq 0$ *(see Properties B.2 and B.3) making use of a zonotope inclusion* $\diamond(\mathcal{Z})$ *operator.*

Proof. Assume $x_k \in \langle c_k,\ R_k \rangle$, $\omega_k \in \langle 0,\ I_{n_\omega} \rangle$ and $\upsilon_k \in \langle 0,\ I_{n_\upsilon} \rangle$, where the inclusion property is preserved by using the reduction operator, which means $x_k \in \langle c_k,\ \bar{R}_k \rangle$. Thus, the zonotopic representation of the IOA can be written using (2.5) as follow:

$$\begin{aligned} x_{k+1} \in \langle c_{k+1},\ R_{k+1} \rangle = &\left\langle (A^{obs}(\theta))c_k,\ (A^{obs}(\theta))\bar{R}_k \right\rangle \oplus \langle Bu_k,\ 0 \rangle \\ &\oplus \langle 0,\ E_\omega \rangle \oplus \langle Ly_k,\ 0 \rangle \oplus \langle 0,\ -LE_\upsilon \rangle . \end{aligned} \tag{7.5}$$

Thus, based on Definitions B.22 and B.24 and Property B.3, c_{k+1} and R_{k+1} in (7.5) can be derived as in (7.4). □

Both TIU and TVU are considered unknown but bounded in their uncertainty intervals and can vary arbitrarily at each time instant within the interval obtained using the zonotopic observer approach and Definition B.23.

7.3.2 Robust set-based interval observer design

In order to reduce the effect of uncertainties on the state estimation and achieving the accurate estimation, the well-known H_∞ technique is used in this chapter [Din08].

In this regard, considering Lemma B.2, and according to [CP12], the uncertain parameter in (7.1a) can be approximated only based on uncertain term. Then, (7.1a) can be written as

$$x_{k+1} = A_0 x_k + B u_k + E_\omega \omega_k + E_\theta \theta, \tag{7.6}$$

with

$$\Delta A(\theta) \approx E_\theta \theta, \tag{7.7}$$

where E_θ is the associated non-empty distribution matrix of suitable dimensions that shows the direction of the TIU.

Keeping in mind that the zonotopic observer structure in Proposition 7.1 can be rewritten using Assumption 7.2 and Proposition 7.2.

Assumption 7.2. *The additive TIU represented in (7.7) are assumed to be bounded by a unit hypercube expressed as the centered zonotopes, i.e.,* $\forall\ k \geq 0,\ \theta \in [-1,\ 1]^{n_\theta} = \langle 0,\ I_{n_\theta} \rangle$*, where* I_{n_θ} *denotes the identity matrix.* □

Proposition 7.2. *Considering the observer (2.5) and Assumptions 7.1, 2.2 and 2.3, the center c and the shape matrix R of the zonotope bounding the observer estimation can be recursively defined as*

$$c_{k+1} = (A_0 - LC)c_k + Bu_k + Ly_k, \tag{7.8a}$$

$$R_{k+1} = \begin{bmatrix} (A_0 - LC)\bar{R}_k & E_\omega & -L_k E_\upsilon & E_\theta \end{bmatrix}. \tag{7.8b}$$

Proof. Assume $x_k \in \langle c_k,\ R_k \rangle$, $\omega_k \in \langle 0,\ I_{n_\omega} \rangle$, $\upsilon_k \in \langle 0,\ I_{n_\upsilon} \rangle$ and $\theta \in \langle 0,\ I_{n_\theta} \rangle$ for all

$k \geq 0$, where the inclusion property is preserved and (2.5) can be written using the reduction operator as

$$\begin{aligned} x_{k+1} \in \langle c_{k+1},\ R_{k+1} \rangle = & \langle (A_0 - LC)c_k,\ (A_0 - LC)\bar{R}_k \rangle \oplus \langle Bu_k,\ 0 \rangle \\ & \oplus \langle Ly_k,\ 0 \rangle \oplus \langle 0,\ E_w \rangle \oplus \langle 0,\ -LE_v \rangle \oplus \langle 0,\ E_\theta \rangle. \end{aligned} \tag{7.9}$$

Thus, based on Definitions B.22 and B.24, the center c_{k+1} and the shape matrix R_{k+1} in (7.9) can be expressed as in (7.8). □

Now, the dynamics of the state estimation error considering the model (7.6) and using the observer (2.5) are introduced in Proposition 7.3.

Proposition 7.3. *Given that the state estimation error in the set-based IOA is defined as*

$$e_k = x_k - \hat{x}_k, \tag{7.10}$$

then, considering the dynamical model (2.4) *and the observer structure* (2.5)*, the dynamics of the state estimation error can be obtained as*

$$e_{k+1} = (A_0 - LC)e_k + E_d d_k, \tag{7.11}$$

where

$$E_d = \begin{bmatrix} E_\theta & E_\omega & -LE_v \end{bmatrix}, \tag{7.12}$$

$$d_k = \begin{bmatrix} \theta & \omega_k & v_k \end{bmatrix}^\top. \tag{7.13}$$

Proof. Based on Lemma B.2, (7.1a) can be rewritten as in (7.6). Therefore, considering the state estimation error as in (7.10), the dynamics of the state estimation error can be obtained using (7.1), (7.6), (2.5) and (7.10), yielding (7.11). □

Considering the transfer function $\mathscr{G}_{ed}(z)$ from uncertainties to the state estimation error, where z denotes the z-transform, the H_∞ norm of $\mathscr{G}_{ed}(z)$ is known as the maximum singular value of $\mathscr{G}_{ed}(z)$. Then, according to [Din08], Theorem 7.1 can be used to compute the observer gain minimizing the effect of the uncertainty and leading to a robust observer.

Theorem 7.1. *Given a scalar $\gamma > 0$, the state estimation error dynamics in (7.11) are stable and satisfy the following H_∞ performance index:*

$$\|\mathscr{G}_{ed}(z)\|_\infty < \gamma, \tag{7.14}$$

if there exists a symmetric positive definite matrix $P \in \mathbb{R}^{n_x \times n_x}$, i.e., $P > 0$, and a matrix $M \in \mathbb{R}^{n_x \times n_y}$ such that

$$\begin{bmatrix} -P & PA_0 - MC & PE_\theta & PE_\omega & -ME_v & 0 \\ * & -P & 0 & 0 & 0 & I \\ * & * & \gamma I & 0 & 0 & 0 \\ * & * & * & \gamma I & 0 & 0 \\ * & * & * & * & \gamma I & 0 \\ * & * & * & * & * & \gamma I \end{bmatrix} < 0. \tag{7.15}$$

In the case that the LMI (7.15) can be solved, the gain of the observer can be computed as

$$L = P^{-1}M. \tag{7.16}$$

Proof. Considering the Proposition 7.3, the transfer function $\mathscr{G}_{ed}(z)$ can be obtained as

$$\mathscr{G}_{ed}(z) = (zI - (A_0 - LC))^{-1}E_d. \tag{7.17}$$

Then, according to [Din08], it can be written that $(A_0 - LC)$ is a stable matrix and $\left\|(zI - (A_0 - LC))^{-1}E_d\right\| < \gamma$. Furthermore, there exists a symmetric positive definite P such that

$$\begin{bmatrix} -P & P(A_0 - LC) & PE_d & 0 \\ (A_0 - LC)^\top P & -P & 0 & I \\ {E_d}^\top P & 0 & \gamma I & 0 \\ 0 & I & 0 & \gamma I \end{bmatrix} < 0. \tag{7.18}$$

Now, by substituting (7.12) into (7.18) and using the Schur complement, (7.18) can be rewritten as

$$\begin{bmatrix} -P & P(A_0 - LC) & PE_\theta & PE_\omega & -PLE_\upsilon & 0 \\ * & -P & 0 & 0 & 0 & I \\ * & * & \gamma I & 0 & 0 & 0 \\ * & * & * & \gamma I & 0 & 0 \\ * & * & * & * & \gamma I & 0 \\ * & * & * & * & * & \gamma I \end{bmatrix} < 0. \tag{7.19}$$

Now, by introducing the new variable $M = PL$, the LMI in (7.15) can be obtained. □

7.3.3 Guaranteed state estimation using an optimization-based method

Considering Definition B.29, the size of the zonotope in (7.8) can be measured by W-radius of a zonotope, e.g., $\mathcal{H} = \langle c, R \rangle$ with $R \in \mathbf{B}^{n_H}$, where $\mathbf{B} = [-1,\ 1]$ is a hypercube with proper dimension, is defined as ι_w, and it is computed using

$$\begin{aligned} \iota_{w,k+1} &= \max_{\varrho_{k+1} \in \mathbf{B}^{(n_\varrho + n_x + 2n_y)}} \|R_{k+1}\varrho_{k+1}\|_{2,W}^2 \\ &= \max_{\varrho_{k+1} \in \mathbf{B}^{(n_\varrho + n_x + 2n_y)}} \varrho_{k+1}^\top R_{k+1}^\top W R_{k+1}\varrho_{k+1}, \end{aligned} \tag{7.20}$$

where $\varrho \in \mathbb{R}^{n_\varrho}$ is unitary box and W is weighting matrix. Then, the gain of the observer can be obtained from minimizing the size of the state-bounding zonotope as in Theorem 7.2.

Theorem 7.2. *Consider that the state-bounding zonotope $\hat{\mathcal{X}}$ in Proposition 7.2 is parametrized by means of the observer gain, i.e., $\hat{\mathcal{X}}_{k+1}(L) = \langle c_{k+1}(L),\ R_{k+1}(L) \rangle$. Then, considering $\rho \in (0,\ 1)$ and $\epsilon > 0$, the minimization criterion of the size of the zonotope $\hat{\mathcal{X}}$*

$$\iota_{w,k+1} \leq \rho \iota_{w,k} + \epsilon \tag{7.21}$$

holds if there exist matrices $W \in \mathbb{R}^{n_x}$, $W = W^\top > 0$, $Y \in \mathbb{R}^{n_x \times n_y}$, diagonal matrices $\Gamma \in \mathbb{R}^{n_x \times n_x}$, $\Upsilon \in \mathbb{R}^{n_y \times n_y}$, and $\Omega \in \mathbb{R}^{n_x \times n_x}$ such that

$$\begin{bmatrix} \rho W & * & * & * & * \\ 0 & \Gamma & * & * & * \\ 0 & 0 & \Upsilon & * & * \\ 0 & 0 & 0 & \Omega & * \\ WA_0 - YC & WE_\omega & -YE_\upsilon & WE_\theta & W \end{bmatrix} > 0, \tag{7.22a}$$

$$\Gamma > 0, \ \ \Upsilon > 0, \ \ \Omega > 0, \tag{7.22b}$$

$$tr(\Gamma) + tr(\Upsilon) + tr(\Omega) < \epsilon, \tag{7.22c}$$

are satisfied.

Proof. Considering (7.20) and (7.21), it follows that

$$\max_{\varrho_{k+1} \in \mathbf{B}^{(n_\varrho + n_x + 2n_y)}} \|R_{k+1}\varrho_{k+1}\|_{2,W}^2 - \max_{\mathring{\varrho}_k \in \mathbf{B}^{n_{\mathring{\varrho}}}} \rho \left\|\bar{R}_k \mathring{\varrho}_k\right\|_{2,W}^2 - \epsilon \leq 0. \tag{7.23}$$

Then, for any $\bar{R}$ and $\mathring{\varrho} \in \mathbf{B}^{n_{\mathring{\varrho}}}$,

$$\max_{\mathring{\varrho}_k \in \mathbf{B}^{n_{\mathring{\varrho}}}} \left\|\bar{R}_k \mathring{\varrho}_k\right\|_{2,W}^2 \geq \left\|\bar{R}_k \mathring{\varrho}_k\right\|_{2,W}^2. \tag{7.24}$$

Now, by defining $\varrho_k = \begin{bmatrix} \mathring{\varrho}_k^\top & \alpha_1^\top & \alpha_2^\top & \alpha_3^\top \end{bmatrix}^\top$, where $\mathring{\varrho}_k \subset \mathbf{B}^{n_{\mathring{\varrho}}}$, $\alpha_1 \subset \mathbf{B}^{n_\omega}$, $\alpha_2 \subset \mathbf{B}^{n_\upsilon}$ and $\alpha_3 \subset \mathbf{B}^{n_\upsilon}$, then, a sufficient condition for any $\varrho \in \mathbf{B}^{n_\varrho + n_\omega + 2n_\upsilon}$ and $\mathring{\varrho} \in \mathbf{B}^{n_{\mathring{\varrho}}}$ can be obtained as

$$\|R_{k+1}\varrho_{k+1}\|_{2,W}^2 - \rho \left\|\bar{R}_k \mathring{\varrho}_k\right\|_{2,W}^2 - \epsilon < 0. \tag{7.25}$$

Furthermore, considering the shape matrix of the state-bounding zonotope in (7.8) and defining $Y = WL$, it can be derived that

$$\tilde{R}_{k+1} = \begin{bmatrix} WA_0 - YC & WE_\omega & -YE_\upsilon & WE_\theta \end{bmatrix}. \tag{7.26}$$

Then, (7.25) can be rewritten as

$$\Pi^\top \tilde{R}_{k+1}^\top W^{-1} \tilde{R}_{k+1} \Pi - \rho \mathring{\varrho}_k^\top \bar{R}_k^\top W \bar{R}_k \mathring{\varrho}_k - \epsilon < 0, \tag{7.27}$$

where $\Pi = \begin{bmatrix} \bar{R}_k \mathring{\varrho}_k \\ \alpha_1 \\ \alpha_2 \\ \alpha_3 \end{bmatrix}$. Thus, if there exist diagonal positive semi-definite matrices Γ, Υ and Ω, then it can be written for any $\alpha_1 \in \mathbb{R}^{n_x}$, $\alpha_2 \in \mathbb{R}^{n_y}$ and $\alpha_3 \in \mathbb{R}^{n_\theta}$ that

$$\alpha_1^\top \Gamma \alpha_1 = \sum_{i=1}^{n_x} \alpha_1^2 \Gamma_i \leq tr(\Gamma), \tag{7.28a}$$

$$\alpha_2^\top \Upsilon \alpha_2 = \sum_{i=1}^{n_y} \alpha_2^2 \Upsilon_i \leq tr(\Upsilon), \tag{7.28b}$$

$$\alpha_3^\top \Omega \alpha_3 = \sum_{i=1}^{n_\theta} \alpha_3^2 \Omega_i \leq tr(\Omega), \tag{7.28c}$$

where Γ_i, Υ_i and Ω_i are the diagonal elements of Γ, Υ and Ω, respectively. Therefore, using (7.28), it can be obtained that

$$tr(\Gamma) - \alpha_1^\top \Gamma \alpha_1 \geq 0, \quad \forall \alpha_1 \in \mathbf{B}^{n_x}, \tag{7.29a}$$

$$tr(\Upsilon) - \alpha_2^\top \Upsilon \alpha_2 \geq 0, \quad \forall \alpha_2 \in \mathbf{B}^{n_y}, \tag{7.29b}$$

$$tr(\Omega) - \alpha_3^\top \Omega \alpha_3 \geq 0, \quad \forall \alpha_3 \in \mathbf{B}^{n_\theta}. \tag{7.29c}$$

Furthermore, adding (7.29) to (7.27), a sufficient condition of (7.27) can be obtained as

$$\begin{aligned} &\Pi^\top \tilde{R}_{k+1}^\top W^{-1} \tilde{R}_{k+1} \Pi - \rho \mathring{\varrho}_k^\top \bar{R}_k^\top W \bar{R}_k \mathring{\varrho}_k + tr(\Gamma) - \alpha_1^\top \Gamma \alpha_1 + tr(\Upsilon) \\ &\quad - \alpha_2^\top \Upsilon \alpha_2 + tr(\Omega) - \alpha_3^\top \Omega \alpha_3 - \epsilon < 0. \end{aligned} \tag{7.30}$$

It means, (7.29) is positive by satisfying the sufficient condition in (7.30) and knowing that (7.29) is positive. Thus, (7.27) is satisfied. Then, if $tr(\Gamma) + tr(\Upsilon) + tr(\Omega) < \epsilon$ in (7.22b) holds, it can be obtained that

$$\Pi^\top \left(\tilde{R}_k^\top W^{-1} \tilde{R}_k - \begin{bmatrix} \rho W & 0 & 0 & 0 \\ 0 & \Gamma & 0 & 0 \\ 0 & 0 & \Upsilon & 0 \\ 0 & 0 & 0 & \Omega \end{bmatrix} \right) \Pi < 0. \tag{7.31}$$

Moreover, from (7.31), it can be derived that

$$\begin{bmatrix} \rho W & 0 & 0 & 0 \\ 0 & \Gamma & 0 & 0 \\ 0 & 0 & \Upsilon & 0 \\ 0 & 0 & 0 & \Omega \end{bmatrix} - \tilde{R}_k^\top W^{-1} \tilde{R}_k > 0 \tag{7.32}$$

Now, using the Schur complement and considering (7.26), the LMI in (7.22) can be obtained. □

In order to overcome the problems associated to the set-based IOA, e.g., wrapping effect and range evaluation of an interval function, already discussed in Section 7.1, the state estimation can be computed using the trajectory-based IOA that relies on the computation of the approximated state set using point-wise trajectories. A discussion of such approach will be the main topic of the next section.

7.4 Trajectory-based interval observation

7.4.1 Trajectory-based interval observer structure

In the trajectory-based IOA, the value of the parameter uncertainty is unknown but bounded within an interval and its invariance can be guaranteed at each time instant. In this approach, the interval of the states can be estimated at each iteration by using specific state trajectories corresponding to particular values of uncertainties $\Delta A(\theta)$.

According to [PSQ03], the loss of the time dependency of the parametric uncertainty in the set-based IOA and the problem of wrapping effect can be avoided by deriving a function based on the relationship between the states and parameters from the initial state to the current state by considering the observer dynamics (2.5) as

$$\hat{x}(k) = (A^{obs}(\theta))^k x_0 + \sum_{j=0}^{k-1} (A^{obs}(\theta))^{k-1-j} \; B^{obs} \; u_k^{obs}(j), \tag{7.33}$$

where

$$B^{obs} = \begin{bmatrix} B & L & E_\omega & -LE_\upsilon \end{bmatrix}, \qquad u_k^{obs} = \begin{bmatrix} u_k & y_k & \omega_k & \upsilon_k \end{bmatrix}^\top.$$

Then, considering $\theta \in \Theta$, both upper and lower bounds of the state estimation of the dynamical model (7.1), i.e., $\hat{\mathcal{X}}(k) = [\underline{\hat{x}}(k),\ \overline{\hat{x}}(k)]$, can be obtained by solving the following optimization problems:

$$\overline{\hat{x}}_k = \max_{\theta\in\Theta} \Big[(A^{obs}(\theta))^k \hat{x}(0) + \sum_{j=0}^{k-1} (A^{obs}(\theta))^{k-1-j}\ B^{obs}\ u_k^{obs}(j)\Big], \tag{7.34a}$$

$$\underline{\hat{x}}_k = \min_{\theta\in\Theta} \Big[(A^{obs}(\theta))^k \hat{x}(0) + \sum_{j=0}^{k-1} (A^{obs}(\theta))^{k-1-j}\ B^{obs}\ u_k^{obs}(j)\Big], \tag{7.34b}$$

subject to

$$x_0 \in \square\mathcal{X}_0, \tag{7.34c}$$

where $\underline{\hat{x}}(k)$ and $\overline{\hat{x}}(k)$ denote the lower and upper bounds of the interval approximation, respectively.

Remark 7.1. *It is worth mentioning that both upper and lower bounds of the interval approximation should be solved separately for each component.* □

Numerical methods can be used to solve the optimization problems in (7.34) for computing $\overline{\hat{x}}$ and $\underline{\hat{x}}$ [2]. However, the computational burden is high. Alternatively, when designing the observer to result in a monotonic system as in [ERP13], the solution of (7.34) is achieved using the extreme values of $\theta \in \Theta$. This means that just considering two different observers, one per each extreme value, for estimating the upper and lower bounds, is enough for reducing the computational load.

Proposition 7.4. *Considering the monotonic system, the time-invariant uncertainty $\theta \in \Theta$, Lemma B.1 and Assumption 7.1, the numerical solution of (7.34) is achieved using the structure of the trajectory-based interval observer approach with the purpose of estimating the state as*

$$\overline{x_{k+1}} = (A_0 - \overline{L}C)\overline{x_k} + Bu_k + \overline{L}y_k + \overline{E_d}\ \overline{d_k} + \overline{\xi_k}, \tag{7.35a}$$

$$\underline{x_{k+1}} = (A_0 - \underline{L}C)\underline{x_k} + Bu_k + \underline{L}y_k + \underline{E_d}\ \underline{d_k} + \underline{\xi_k}, \tag{7.35b}$$

[2] This approach is deeply investigated in [PSQ03].

with

$$\overline{E_d} = \begin{bmatrix} E_\omega & -\overline{L}E_\upsilon \end{bmatrix}, \qquad \overline{d_k} = \begin{bmatrix} \overline{\omega_k} & \overline{\upsilon_k} \end{bmatrix}^\top, \tag{7.36a}$$

$$\underline{E_d} = \begin{bmatrix} E_\omega & -\underline{L}E_\upsilon \end{bmatrix}, \qquad \underline{d_k} = \begin{bmatrix} \underline{\omega_k} & \underline{\upsilon_k} \end{bmatrix}^\top, \tag{7.36b}$$

$$\overline{\xi_k} = \overline{\Delta A^+}\ \overline{x_k^+} - \underline{\Delta A^+}\overline{x_k^-} - \overline{\Delta A^-}\underline{x_k^+} + \underline{\Delta A^-}\ \underline{x_k^-}, \tag{7.36c}$$

$$\underline{\xi_k} = \underline{\Delta A^+}\ \underline{x_k^+} - \overline{\Delta A^+}\underline{x_k^-} - \underline{\Delta A^-}\overline{x_k^+} + \overline{\Delta A^-}\ \overline{x_k^-}, \tag{7.36d}$$

$$\overline{\Delta A^+} = \max\left\{0,\ \overline{\Delta A}\right\}, \qquad \overline{\Delta A^-} = \overline{\Delta A^+} - \overline{\Delta A}, \tag{7.36e}$$

$$\underline{\Delta A^+} = \max\left\{0,\ \underline{\Delta A}\right\}, \qquad \underline{\Delta A^-} = \underline{\Delta A^+} - \underline{\Delta A}, \tag{7.36f}$$

$$\overline{x^+} = \max\left\{0,\ \overline{x}\right\}, \qquad \overline{x^-} = \overline{x^+} - \overline{x}, \tag{7.36g}$$

$$\underline{x^+} = \max\left\{0,\ \underline{x}\right\}, \qquad \underline{x^-} = \underline{x^+} - \underline{x}. \tag{7.36h}$$

where $\overline{L} \in \mathbb{R}^{n_x \times n_y}$ *and* $\underline{L} \in \mathbb{R}^{n_x \times n_y}$ *are the gains of upper and lower observers, respectively.*

Proof. Considering the monotonic system, the function in (7.33) can be unfolded as

$$\hat{x}(k) = (A^*(\theta))^k x_0 + \sum_{j=0}^{k-1} (A^*(\theta))^{k-1-j} \left(Bu_k(j) + Ly_k(j) + E_\omega \omega_k(j) - LE_\upsilon \upsilon_k(j) \right). \tag{7.37}$$

It can be seen from (7.37) that the estimation is not only depends on θ but also depends on ω and υ. Consequently, the optimization problem in (7.34) can be rewritten as

$$\overline{\hat{x}}_k = \max_{\theta \in \Theta} \left[(A^*(\theta))^k x_0 + \sum_{j=0}^{k-1} (A^*(\theta))^{k-1-j} \left(Bu_k(j) + Ly_k(j) + E_\omega \omega_k(j) - LE_\upsilon \upsilon_k(j) \right) \right], \tag{7.38a}$$

$$\underline{\hat{x}}_k = \min_{\theta \in \Theta} \left[(A^*(\theta))^k x_0 + \sum_{j=0}^{k-1} (A^*(\theta))^{k-1-j} \left(Bu_k(j) + Ly_k(j) + E_\omega \omega_k(j) - LE_\upsilon \upsilon_k(j) \right) \right], \tag{7.38b}$$

subject to

$$x_0 \in \square \mathcal{X}_0. \tag{7.38c}$$

Now, considering the time-invariant uncertainty $\theta \in \Theta$ and using Lemma B.1 and Assumption 7.1, the following inequality is stated:

$$\underline{\xi_k} \leq \Delta A(\theta) x_k \leq \overline{\xi_k}. \tag{7.39}$$

Then, iteratively solving the optimization problem in (7.38) can be generated by using (7.35). In this regard, the loss of the time dependency of the parametric uncertainty in the set-based interval observer approach and the problem of wrapping effect can also be avoided. □

Remark 7.2. *In fact, $\overline{E_d}$ and $\underline{E_d}$ are the constant matrices computed considering the gains of upper and lower observers, respectively. Moreover, $\overline{d_k}$ and $\underline{d_k}$ introduce the extreme value of the time-varying uncertainties since considering the unknown but bounded assumption. Therefore, it is guaranteed that $\overline{E_d}\ \overline{d_k} < E_d d_k < \underline{E_d}\ \underline{d_k}$.* □

Consequently, the estimation of the lower and upper bounds of the output measurement y can be computed as

$$\overline{y_k} = C^+ \overline{x_k} - C^- \underline{x_k}, \tag{7.40a}$$

$$\underline{y_k} = C^+ \underline{x_k} - C^- \overline{x_k}, \tag{7.40b}$$

where $C^+ = \max\{0,\ C\}$ and $C^- = C^+ - C$.

7.4.2 Robust trajectory-based interval observer design

There are two issues that should be taken into account when designing the robust observer in the case of the trajectory-based IOA. First, the convergence of the observer point should be guaranteed, which will be done based on the H_∞ technique. Second, the monotonicity of the observer in spite of non-monotonicity of the system state matrix should also be satisfied (see the following Property 7.1 for the monotonicity property).

Property 7.1. *(Monotonicity property) If the variation of the state function regarding to all the states and parameters is positive, the discrete time system will satisfy the monotonicity property. Moreover, those systems that are satisfied this property are the monotonic systems.*

Therefore, the following condition should be fulfilled together with the Lyapunov

stability condition:

$$(A_0 - \overline{L}C),\ (A_0 - \underline{L}C) > 0,\ \text{or},\ (A_0 - \overline{L}C),\ (A_0 - \underline{L}C) \in \mathbb{R}_+^{n_x \times n_x}. \tag{7.41}$$

The dynamics of state estimation error can be obtained by following Proposition 7.5, which are required for using the H_∞ technique.

Proposition 7.5. *Given that the upper and lower bounds of the state estimation error for trajectory-based IOA are respectively defined as*

$$\overline{e_{k+1}} = \overline{x_{k+1}} - x_{k+1}, \tag{7.42a}$$

$$\underline{e_{k+1}} = x_{k+1} - \underline{x_{k+1}}, \tag{7.42b}$$

then, based on (2.4) and (7.35), and also considering Lemma B.2, the upper and lower bounds dynamics of the state estimation error can be obtained as

$$\overline{e_{k+1}} = (A_0 - \overline{L}C)\ \overline{e_k} + \overline{E_{e_d}}\,\overline{e_{d_k}}, \tag{7.43a}$$

$$\underline{e_{k+1}} = (A_0 - \underline{L}C)\ \underline{e_k} + \underline{E_{e_d}}\ \underline{e_{d_k}}, \tag{7.43b}$$

with

$$\overline{E_{e_d}} = \begin{bmatrix} \overline{E_d} & E_\theta \end{bmatrix}, \qquad \overline{e_{d_k}} = \begin{bmatrix} \overline{d_k} & \overline{e_\theta} \end{bmatrix}^\top, \tag{7.44a}$$

$$\underline{E_{e_d}} = \begin{bmatrix} \underline{E_d} & E_\theta \end{bmatrix}, \qquad \underline{e_{d_k}} = \begin{bmatrix} \underline{d_k} & \underline{e_\theta} \end{bmatrix}^\top, \tag{7.44b}$$

where $\overline{e_\theta}$ and $\underline{e_\theta}$ show the effect of the time invariant uncertain parameter θ on the upper and lower bounds dynamics of the state estimation error, respectively.

Proof. By substituting (7.1) and (7.35) in (7.42a), it can be written that

$$\begin{aligned} \overline{e_{k+1}} =& (A_0 - \overline{L}C)\overline{x_k} - (A_0 x_k - \overline{L}C)x_k + \overline{L}E_\upsilon \upsilon_k + E_\omega \overline{\omega_k} \\ & - \overline{L}E_\upsilon \overline{\upsilon_k} + \overline{\xi_k} - \Delta A(\theta)x_k - E_\omega \omega_k. \end{aligned} \tag{7.45}$$

Then, (7.45) can be rearranged as

$$\overline{e_{k+1}} = \Big((A_0 - \overline{L}C)\,(\overline{x_k} - x_k)\Big) + \Big(E_\omega\,(\overline{\omega_k} - \omega_k)\Big) - \Big(\overline{L}E_\upsilon\,(\overline{\upsilon_k} - \upsilon_k)\Big) + \Big(\overline{\xi_k} - \Delta A(\theta_k)x_k\Big). \tag{7.46}$$

Based on (7.39) and introducing the following parameters:

$$\overline{e_{\omega_k}} = \overline{\omega_k} - \omega_k, \quad \overline{e_{\upsilon_k}} = \overline{\upsilon_k} - \upsilon_k, \quad \overline{e_{\xi_k}} = \overline{\xi_k} - \Delta A(\theta_k)x_k,$$

(7.46) can be rewritten as

$$\overline{e_{k+1}} = \left((A_0 - \overline{L}C)\,\overline{e_k}\right) + \left(E_\omega \overline{e_{\omega_k}}\right) - \left(\overline{L}E_\upsilon \overline{e_{\upsilon_k}}\right) + \left(\overline{e_{\xi_k}}\right).$$

Moreover, considering Lemma B.2, the term $\overline{e_{\xi_k}}$ can be approximately computed as

$$\overline{e_{\xi_k}} \approx E_\theta \overline{e_\theta}. \tag{7.47}$$

Hence, considering (7.47), the upper bound dynamics of the state estimation error can be derived as

$$\overline{e_{k+1}} = \left((A_0 - \overline{L}C)\,\overline{e_k}\right) + \left(E_\omega \overline{e_{\omega_k}}\right) - \left(\overline{L}E_\upsilon \overline{e_{\upsilon_k}}\right) + \left(E_\theta \overline{e_\theta}\right). \tag{7.48}$$

Therefore, the upper bound dynamics of the state estimation error in (7.43a) can be obtained by substitution of the terms in (7.44a) and (7.36a) into (7.48). Following the same procedure, (7.43b) can be obtained for the lower bound dynamics of the state estimation error. □

Now, by defining the transfer function $\mathcal{G}_{ed}(z)$ for the upper and lower state estimation error dynamics as $\overline{\mathcal{G}_{ed}(z)}$ and $\underline{\mathcal{G}_{ed}(z)}$, the maximum singular value (H_∞ norm) of transfer functions $\overline{\mathcal{G}_{ed}(z)}$ and $\underline{\mathcal{G}_{ed}(z)}$ are denoted by $\left\|\overline{\mathcal{G}_{ed}(z)}\right\|_\infty$ and $\left\|\underline{\mathcal{G}_{ed}(z)}\right\|_\infty$, respectively. Then, Theorem 7.3 can be used design two robust observers for the estimation of the upper and lower bounds of state-bounding observer considering the effect of uncertainties. Thus, both convergence and monotonicity properties of the observer are considered to design such observers.

Theorem 7.3. *Taken into account the satisfaction of the monotonicity property and given a scalar $\gamma > 0$, upper and lower state estimation error dynamics in (7.43) are stable and satisfy the following H_∞ performance indices:*

$$\left\|\overline{\mathcal{G}_{ed}(z)}\right\|_\infty < \gamma, \qquad \left\|\underline{\mathcal{G}_{ed}(z)}\right\|_\infty < \gamma, \tag{7.49}$$

and, taking into account the satisfaction of the monotonicity property, there exists a symmetric positive definite matrix $\overline{P} \in \mathbb{R}^{n_x \times n_x}$ *and a matrix* $\overline{M} \in \mathbb{R}^{n_x \times n_y}$ *such that*

$$\begin{bmatrix} -\overline{P} & \overline{P}A_0 - \overline{M}C & \overline{P}E_\theta & \overline{P}E_\omega & -\overline{M}E_\upsilon & 0 \\ * & -\overline{P} & 0 & 0 & 0 & I \\ * & * & \gamma I & 0 & 0 & 0 \\ * & * & * & \gamma I & 0 & 0 \\ * & * & * & * & \gamma I & 0 \\ * & * & * & * & * & \gamma I \end{bmatrix} < 0, \tag{7.50a}$$

$$\overline{P}A_0 - \overline{M}C \geq 0. \tag{7.50b}$$

Analogously, for the lower observer, there exists a symmetric positive definite matrix $\underline{P} \in \mathbb{R}^{n_x \times n_x}$ *and a matrix* $\underline{M} \in \mathbb{R}^{n_x \times n_y}$ *such that*

$$\begin{bmatrix} -\underline{P} & \underline{P}A_0 - \underline{M}C & \underline{P}E_\theta & \underline{P}E_\omega & -\underline{M}E_\upsilon & 0 \\ * & -\underline{P} & 0 & 0 & 0 & I \\ * & * & \gamma I & 0 & 0 & 0 \\ * & * & * & \gamma I & 0 & 0 \\ * & * & * & * & \gamma I & 0 \\ * & * & * & * & * & \gamma I \end{bmatrix} < 0, \tag{7.51a}$$

$$\underline{P}A_0 - \underline{M}C \geq 0. \tag{7.51b}$$

Thus, solving the LMIs in (7.50) *and* (7.51)*, the gain of the upper and lower observers, i.e.,* $\overline{L}$ *and* $\underline{L}$*, can be respectively obtained as*

$$\overline{L} = \overline{P}^{-1}\overline{M}, \tag{7.52a}$$

$$\underline{L} = \underline{P}^{-1}\underline{M}. \tag{7.52b}$$

Proof. The proof follows considering the same procedure as in the one used into the proof of the Theorem 7.1. The only deference is related to the second LMI for upper and lower observers to satisfy the monotonicity property, i.e., $A_0 - LC > 0$. □

7.5 Integrated set/trajectory approach

7.5.1 Comparative assessment

Using the results presented in Sections 7.3 and 7.4, the state-bounding observer can be designed by using both (7.8) and (7.35), which corresponds, respectively, to the set-based IOA and trajectory-based IOA. According to Section 7.3.2, in the set-based IOA, the satisfaction of the LMI in Theorem 7.1 is required in order to guarantee the robustness of the interval observation. Moreover, the size of the obtained state-bounding zonotope can be minimized using the LMI (7.15) in Theorem 7.2. On the other hand, according to Section 7.4.2, both robustness and monotonicity property of the trajectory-based IOA can be guaranteed through the satisfaction of the LMIs (7.50) and (7.51) in Theorem 7.3 for computing the gains of the upper and lower observers.

In an attempt to make both approaches comparable, the interval hull [3] introduced in Definition B.23 is used for the case of set-based IOA. In this regard, the interval hull of the state-bounding zonotopic set in (7.8) can be written as

$$x_{k,\mathrm{sup},i} = c_{k,i} + \|R_{k,i}\|_1 \,, \tag{7.53a}$$

$$x_{k,\mathrm{inf},i} = c_{k,i} - \|R_{k,i}\|_1 \,, \tag{7.53b}$$

where $x_{k,\mathrm{sup}} \in \mathbb{R}^{n_x}$ and $x_{k,\mathrm{inf}} \in \mathbb{R}^{n_x}$ are the maximum and the minimum values of the $\mathcal{X}$, respectively. Moreover, Moreover, $\|R_{k,i}\|_1$ stands for row sum where $R_{k,i}$ is the i-th row of R_k. In Figure 7.1, there is a schematic diagram of the interval hull for a two-dimensional zonotope.

Therefore, considering (7.53) instead of (7.8) leads to compute the extreme values of the trajectories of the state-bounding set in the set-based IOA. Since the main structure of the trajectory-based IOA relies on computing the extreme values of the state estimation, using the concept of interval hull for the set-based IOA allows to compare the results of the set-based IOA and trajectory-based IOA.

By looking at both approaches with the purpose of further analysis, Proposition 7.6 can be used in order to compare the nominal values of the state estimation that can be obtained using each approach.

[3] An interval hull of a set is defined as the smallest centered interval vector that contains the set.

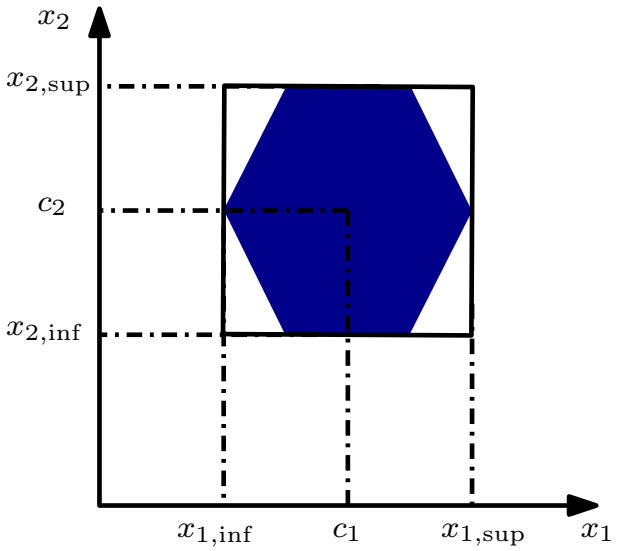

Figure 7.1: Schematic diagram of the interval hull of the two-dimensional zonotope.

Proposition 7.6. *Considering the monotonic system with the symmetric parameter uncertainty, the mean values of computed upper and lower bounds of the state estimation using* (7.35) *in the case of trajectory-based IOA play the same role as the center of the zonotope in set-based IOA, i.e.,*

$$\frac{\overline{x_k} + \underline{x_k}}{2} = c_k. \tag{7.54}$$

Proof. Considering the monotonic system and assuming that $\overline{L} = \underline{L} = L$, $\overline{d_k} = \underline{d_k}$ and $\overline{\xi_k} = \underline{\xi_k}$, the mean value of $\overline{x_{k+1}}$ and $\underline{x_{k+1}}$ can be obtained using (7.35) as

$$\left(\frac{\overline{x_{k+1}} + \underline{x_{k+1}}}{2}\right) = (A_0 - LC)\left(\frac{\overline{x_k} + \underline{x_k}}{2}\right) + Bu_k + Ly_k + E_d\left(\frac{\overline{d_k} + \underline{d_k}}{2}\right) + \left(\frac{\overline{\xi_k} + \underline{\xi_k}}{2}\right). \tag{7.55}$$

Therefore, by substitution of (7.54) into (7.55), it can be written that

$$\left(\frac{\overline{x_{k+1}} + \underline{x_{k+1}}}{2}\right) = (A_0 - LC)c_k + Bu_k + Ly_k + E_d\left(\frac{\overline{d_k} + \underline{d_k}}{2}\right) + \left(\frac{\overline{\xi_k} + \underline{\xi_k}}{2}\right). \tag{7.56}$$

Now, by considering Assumption 2.2, (7.56) can be rewritten as

$$\left(\frac{\overline{x_{k+1}} + \underline{x_{k+1}}}{2}\right) = (A_0 - LC)c_k + Bu_k + Ly_k. \tag{7.57}$$

Then, comparing the right-hand side of (7.57) and (7.8a), it can be seen that the center of the state-bounding observer using the set-based IOA and the mean values of both $\overline{x_k}$ and $\underline{x_k}$ can be related. □

Remark 7.3. *It is worth mentioning that the equality in* (7.54) *exists when the system is monotonic with the symmetric uncertainty. Otherwise, there exists over approximation and the condition in* (7.54) *is not longer satisfied.*

On the other hand, the size of the interval bounding the set of states [4] (upper and lower bounds) that are computed using both approaches for the state estimation is related in Proposition 7.7.

Proposition 7.7. *Given the interval hull in Definition B.23, the relationship between the shape matrix considering the set-based IOA and the extreme values of the interval observation provided by the trajectory-based IOA can be written as*

$$x_{k,\mathrm{sup},i} = c_{k,i} + \|R_{k,i}\|_1 = \frac{\overline{x_{k,i}} - \underline{x_{k,i}}}{2}, \tag{7.58a}$$

$$x_{k,\mathrm{inf},i} = c_{k,i} - \|R_{k,i}\|_1 = \frac{\underline{x_{k,i}} - \overline{x_{k,i}}}{2}. \tag{7.58b}$$

Proof. Based on the structure of the trajectory-based IOA, it can be observed that the interval computed from the upper and lower observers plays the same role as the interval hull computed using the set-based IOA. Thus, by considering Proposition 7.6, it follows that

$$\overline{x_{k,i}} - \frac{\overline{x_{k,i}} + \underline{x_{k,i}}}{2} = c_{k,i} + \|R_{k,i}\|_1, \tag{7.59a}$$

$$\frac{\overline{x_{k,i}} + \underline{x_{k,i}}}{2} - \underline{x_{k,i}} = c_{k,i} - \|R_{k,i}\|_1. \tag{7.59b}$$

Then, (7.58) can be obtained after some algebraic manipulations of (7.59). □

[4] This part shows the effect of the uncertainties since the deterministic approach is used.

7.5.2 Integrated scheme

By considering the relationship between both interval observer approaches, an integrated scheme combining them is proposed for interval observation. This integrated approach can be obtained using Propositions 7.6 and 7.7 as it is proposed in Theorem 7.4.

Theorem 7.4. *Given Propositions 7.6 and 7.7, the nominal value of the state-bounding observer x_{nom} can be computed as*

$$x_{k+1,\text{nom}} = (A_0 - LC)x_{k,\text{nom}} + Bu_k + Ly_k. \tag{7.60}$$

Moreover, the effect of both considered TIU and TVU (by using Lemma B.2) can be bounded as

$$x_{k+1,\text{sup}} = (A_0 - LC)x_{k,\text{sup}} + E_d\left(\frac{\overline{d_k} - \underline{d_k}}{2}\right) + \left(\frac{\overline{\xi_k} - \underline{\xi_k}}{2}\right), \tag{7.61a}$$

$$x_{k+1,\text{inf}} = (A_0 - LC)x_{k,\text{inf}} + E_d\left(\frac{\underline{d_k} - \overline{d_k}}{2}\right) + \left(\frac{\underline{\xi_k} - \overline{\xi_k}}{2}\right), \tag{7.61b}$$

where the gain $L = P^{-1}M$ should be computed using the same LMI in (7.15) to satisfy the H_∞ performance together with the new LMI

$$PA_0 - MC \geq 0, \tag{7.62}$$

to satisfy the monotonicity property of $(A_0 - LC)$.

Proof. Given Proposition 7.6 and assuming that $\overline{L} = \underline{L} = L$, $\overline{d_k} = \underline{d_k}$ and $\overline{\xi_k} = \underline{\xi_k}$, the nominal value of the state estimation can be obtained using the computed center in (7.57) as (7.60). Moreover, using Proposition 7.7, the effect of the uncertainties can be alternatively computed as

$$x_{k+1,\text{sup}} = (A_0 - LC)\left(\frac{\overline{x_k} - \underline{x_k}}{2}\right) + E_d\left(\frac{\overline{d_k} - \underline{d_k}}{2}\right) + \left(\frac{\overline{\xi_k} - \underline{\xi_k}}{2}\right), \tag{7.63a}$$

$$x_{k+1,\text{inf}} = (A_0 - LC)\left(\frac{\underline{x_k} - \overline{x_k}}{2}\right) + E_d\left(\frac{\underline{d_k} - \overline{d_k}}{2}\right) + \left(\frac{\underline{\xi_k} - \overline{\xi_k}}{2}\right). \tag{7.63b}$$

Therefore, (7.61) is obtained by proper manipulation of (7.63). Moreover, the proof

of the mentioned LMIs in (7.15) and (7.62) to compute the observer gain can be obtained following the same manner as Theorems 7.1 and 7.3 to satisfy both H_∞ performance and monotonicity property, respectively. □

Theorem 7.4 shows that both approaches can be merged, generating a new approach where the center and segments of the state-bounding observer are propagated independently (as in zonotopic approach), but obtaining explicit formulas that do not require the use of zonotopes. However, since the observer structure in the set-based IOA is reformulated using the interval hull of the state-bounding zonotope for computing the upper and lower bounds as in the trajectory-based IOA, the integrated scheme will only avoid the wrapping effect and preserve the parameter uncertainty time invariance if the observer gain is designed such that the resulting observer matrix satisfies the monotonicity property. Otherwise, the integrated scheme will not work satisfactorily leading to an unstable interval observer due to the wrapping effect [PSQ05b]. Moreover, the robustness of the observer can be guaranteed considering the H_∞ performance when computing the observer gain using Theorem 7.2.

Corollary 7.1. *Using Theorem 7.4, set-based IOA and trajectory-based IOA can produce the same results when the observer is monotonic.*

Proof. Given a system dynamic as $x_{k+1} = Ax_k + Bu_k$. Using the trajectory-based IOA, the extreme values of upper and lower bounds are computed as

$$\overline{x}_{k+1} = A\overline{x}_k + Bu, \tag{7.64a}$$

$$\underline{x}_{k+1} = A\underline{x}_k + Bu. \tag{7.64b}$$

On the other hand, the main concept of using the set-based IOA to compute the state-bounding observer is to generate both upper and lower bounds using some propagation algorithms (such as the algorithm mentioned in Proposition 7.1) to compute the set $\mathcal{X}_{k+1}$ from $\mathcal{X}_k$. Then, it can be written that

$$x_{k+1} \in \langle c_{k+1},\ R_{k+1} \rangle = \langle Ac_k,\ AR_k \rangle \oplus \langle Bu_k,\ 0 \rangle\,. \tag{7.65}$$

Now, given the relationship obtained in Theorem 7.4, (7.65) can be reformulated using the concept of the interval hull to compute the same result as in (7.64). □

7.6 Case study

Two examples are used for illustrating the effectiveness of the proposed approaches in the previous sections: a numerical example and a real application example (the two-tanks system benchmark). These application examples are selected to show their performance: i) when the system is non-monotonic, i.e., at least one element of system matrix A is negative, ii) when the observer is non-monotonic, i.e., at least one element of observer matrix $(A_0 - LC)$ is negative. In both cases, the proposed observer design is used to overcome the problems using both set-based IOA and trajectory-based IOA.

7.6.1 Numerical example

The first example considered is based on the dynamical model (7.1) with

$$A = \begin{bmatrix} 0.8+\theta_{11} & 0.1+\theta_{12} & 0.3+\theta_{13} \\ 0+\theta_{21} & 0.8+\theta_{22} & 0.2+\theta_{23} \\ 0.01+\theta_{31} & 0+\theta_{32} & 0.8+\theta_{33} \end{bmatrix}, \quad B = \begin{bmatrix} 0 \\ 0 \\ 1 \end{bmatrix}, \quad C = \begin{bmatrix} 0 & 0 & 1 \end{bmatrix}, \tag{7.66}$$

where the TIU parameters are bounded by the interval $\theta_{ij} \in [-0.01, 0.01]$, where the indices i and j refer to the i^{th} row and j^{th} column of $\Delta A(\theta)$, respectively. Moreover, the example includes TVU, i.e., the state disturbance and the measurement noise, E_ω and E_υ are used as in (2.4) with

$$E_\omega = \begin{bmatrix} 0.08 & 0 & 0 \\ 0 & 0.08 & 0 \\ 0 & 0 & 0.08 \end{bmatrix}, \quad E_\upsilon = \begin{bmatrix} 0.2 \end{bmatrix}. \tag{7.67}$$

The input signal u is given by $u = sin(t)$ for $t \in [0, 3\pi]$ with 200 time steps.

Considering the results presented and discussed in this chapter, it is worth comparing the trajectory-based IOA and set-based IOA for the case of a monotonic system. In this regard, matrix A is considered as in (7.66). It can be seen that all the entries of A in (7.66) are positive values. Therefore, the system is monotonic. Then, the set-based interval observer approach gain is computed using Theorem 7.1 to satisfy the H_∞ performance together with Theorem 7.2 to minimize the size of the obtained zonotope at each time instant as $L = \begin{bmatrix} 0.2781 & 0.2855 & 0.7982 \end{bmatrix}^\top$. Furthermore, the gains of upper and lower bounds of the trajectory-based interval observer approach are

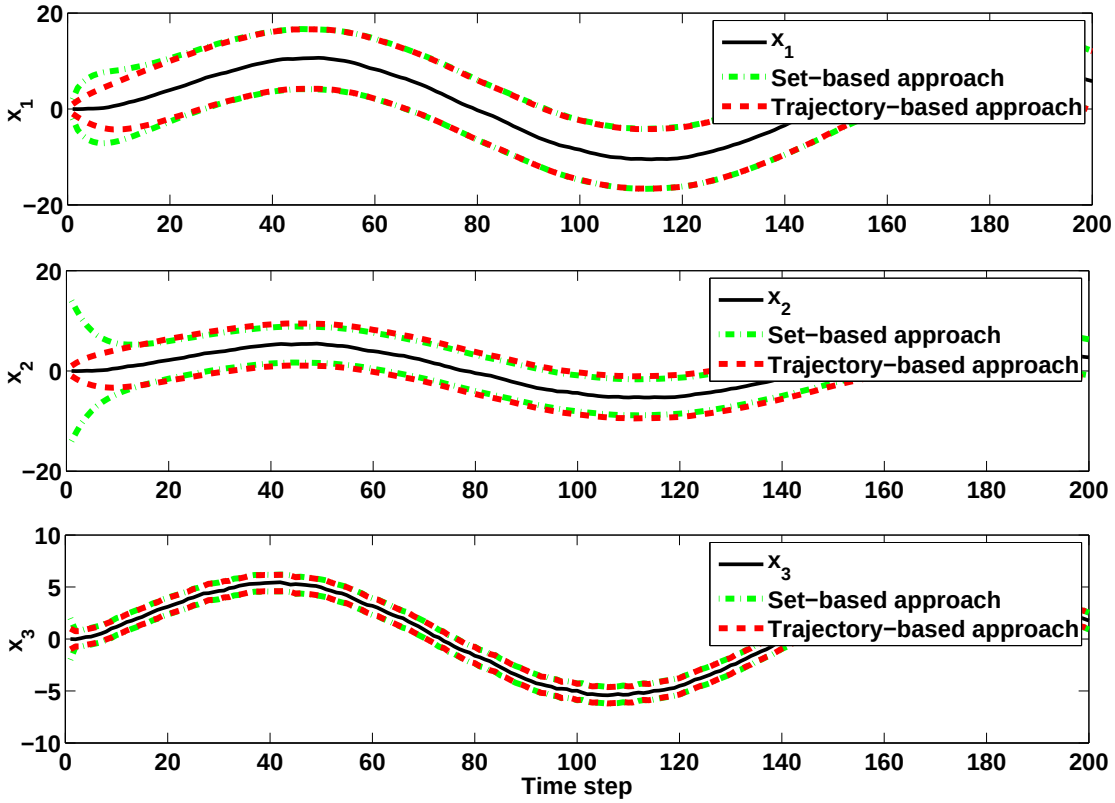

Figure 7.2: Set-based IOA vs. trajectory-based IOA behavior considering monotonic system.

computed using (7.50) and (7.51), respectively as $\overline{L} = \underline{L} = \begin{bmatrix} 0.3 & 0.2 & 0.8 \end{bmatrix}^{\top}$. Figure 7.2 shows the obtained results from the simulation of the monotonic system.

Remark 7.4. *It is worth mentioning that the set-based approach allows to estimate the state set one time instant ahead based on the set estimated in the previous time instant. But, in order to put both approaches into the comparable framework, the state sets are projected into the state space, separately.*

As it can be seen from Figure 7.2, the behavior of the system can be correctly estimated using both set-based IOA and trajectory-based IOA. Moreover, both approaches are producing the same results for the case of a monotonic system.

The problem appears if the system is not monotonic. To illustrate this situation, the scenario to be tested is the case when matrix A contains at least one negative element.

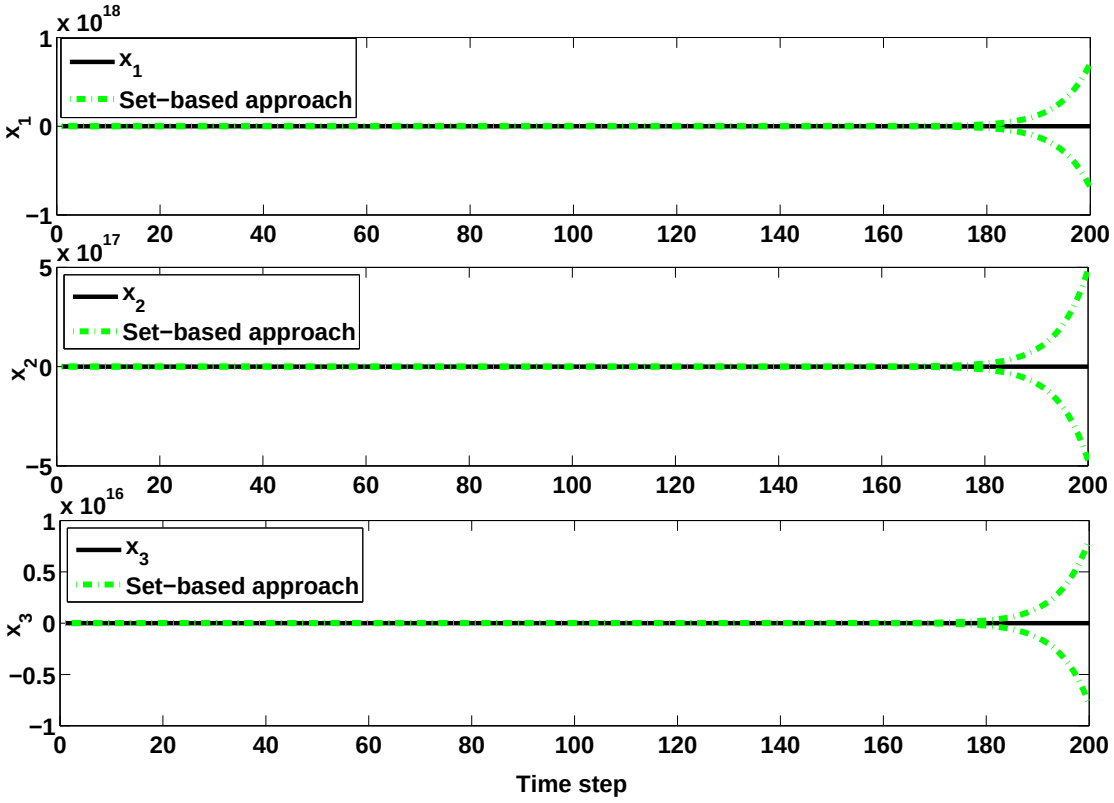

Figure 7.3: Set-based IOA considering a non-monotonic system.

To this aim, A is now considered as

$$A = \begin{bmatrix} 0.8+\theta_{11} & -0.1+\theta_{12} & 0.3+\theta_{13} \\ 0+\theta_{21} & 0.8+\theta_{22} & 0.2+\theta_{23} \\ 0.01+\theta_{31} & 0+\theta_{32} & 0.8+\theta_{33} \end{bmatrix}. \tag{7.68}$$

Having a negative element in matrix A leads to test the case that the system is not monotonic since the positivity condition is not satisfied. The first simulation is the analysis of the behavior of the set-based IOA and trajectory-based IOA when only the stability condition is considered for designing the observer through the obtained LMI in (7.15) for the set-based IOA, and (7.50a) and (7.51a) for the trajectory-based IOA considering the H_∞ technique. Figures 7.3 and 7.4 show the results obtained from the simulation of the non-monotonic system considering set-based IOA and trajectory-based IOA, respectively.

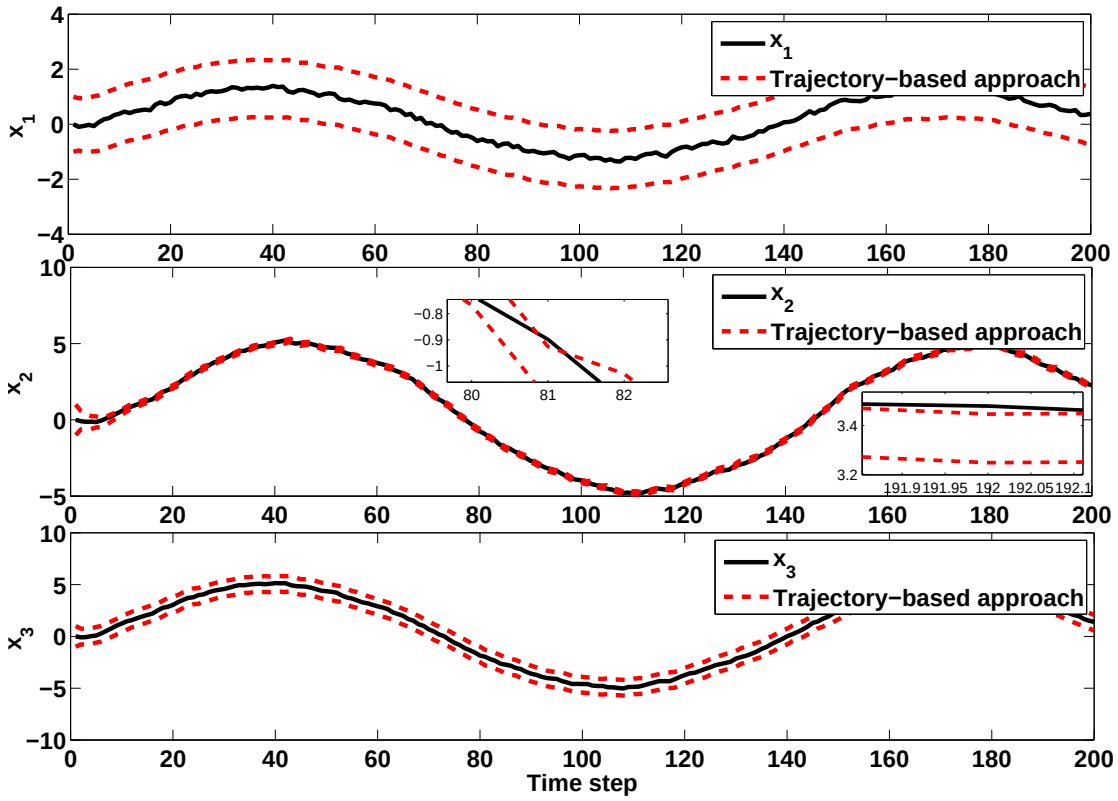

Figure 7.4: Trajectory-based IOA considering a non-monotonic system.

In Figure 7.3, the zonotopic observer is implemented according to Proposition 7.1 and the observer gain is determined using the LMI in (7.15) for the case of set-based interval observer approach as $L = \begin{bmatrix} -1.1376 & -1.9167 & -1.2604 \end{bmatrix}^\top$. It can be observed from Figure 7.3 that, when the system is non-monotonic, the results from the set-based interval observer approach is affected by the problem of wrapping effect and this approach cannot compute the correct state estimation.

On the other hand, in Figure 7.4, the observer in (7.35) is used for implementing trajectory-based interval observer approach and the observer gain is calculated using LMIs in (7.50a) and (7.51a) as $\overline{L} = \underline{L} = \begin{bmatrix} 0.2754 & 1.0571 & 0.7724 \end{bmatrix}^\top$. The idea of considering only (7.50a) and (7.51a) in the case of trajectory-based IOA is to show the problem that appears when the positivity condition is not satisfied for the observer in the case that the dynamics of the system are not monotonic.

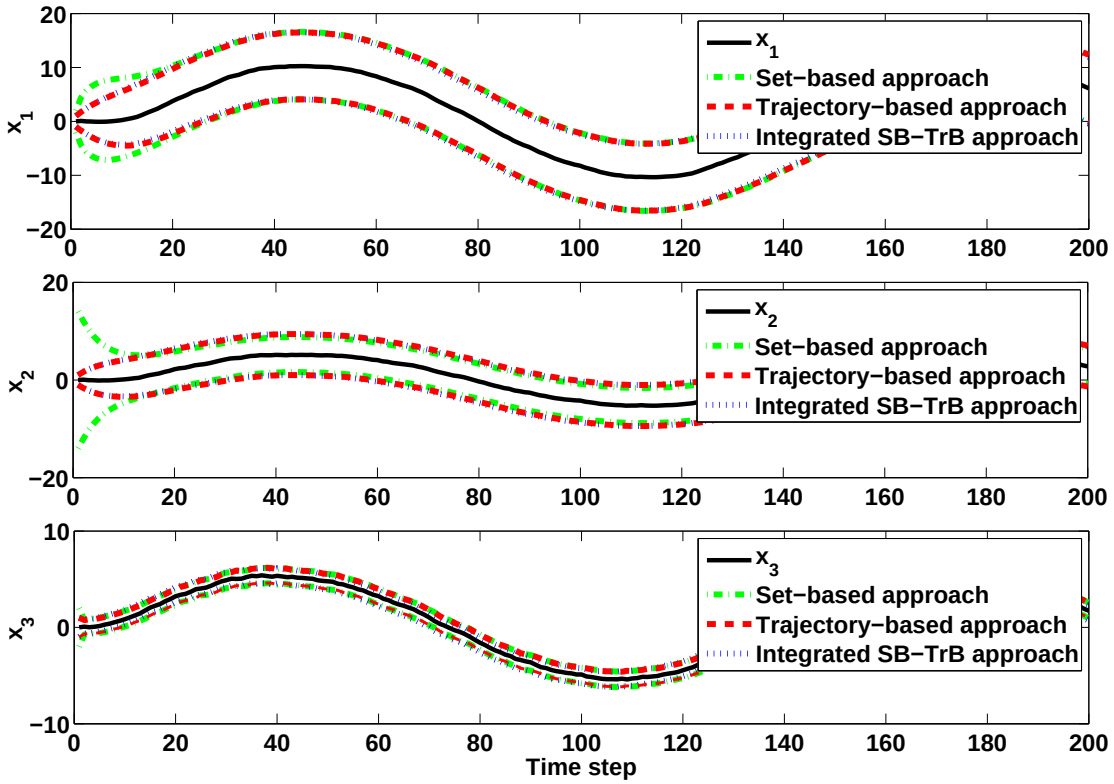

Figure 7.5: Set-based IOA vs. trajectory-based IOA considering non-monotonic system and designing the integrated monotonic observer.

As it can be seen in Figure 7.4, considering only the convergence of the observer to compute the observer gain for a non-monotonic system, the trajectory-based IOA meets a problem to compute the interval for the estimation of the second state of the system x_2 that, according matrix C, is not measured. The only purpose of considering this case is to show the problems of non-satisfaction of the positivity condition to design the observer gain in trajectory-based IOA and presenting the wrapping effect for the same case considering the set-based IOA.

Further analysis is done by implementing the proposed observer design in Section 7.5 to overcome the problems that are presented in Figures 7.3 and 7.4.

As it can be seen in Figure 7.5, the satisfaction of the positivity condition based on the proposed LMIs in (7.50) and (7.51) allows the trajectory-based IOA to estimate correctly the system behavior and to solve the problem of estimating the behaviour of x_2

(see Figure 7.4). Moreover, thanks to the obtained similarity between the set-based IOA and trajectory-based IOA in the case of a monotonic system according to the analysis of the numerical example and also considering the mentioned points in Section 7.5, it can be seen that the interval hull of the state-bounding zonotope computed using the set-based IOA can be converted to the trajectory-based IOA. Having this in mind, Propositions 7.6 and 7.7, and Theorem 7.4 are considered for converting the center and the shape matrix of the state-bounding zonotope obtained from the set-based IOA. This point is also shown in Figure 7.5.

As it is mentioned in Section 7.5 and having the integrated observer structure, the robust observer in Figure 7.5 is obtained by computing the observer gain considering the H_∞ performance and the monotonicity property. It means, in the new proposed structure in Theorem 7.4, the observer gain is computed considering the LMIs in Theorem 7.1 and also the satisfaction of the LMI in (7.62), which guarantees the monotonicity property of the observer as $\begin{bmatrix} 0.2892 & 0.2950 & 0.8001 \end{bmatrix}^\top$. In this regard, the monotonicity property not only can solve the non-inclusion problem of the trajectory-based interval observer approach but also the wrapping effect in the set-based interval observer can be solved. Furthermore, the same results are obtained from both approaches for the case that the system is non-monotonic and the observers are designed to satisfy the monotonicity property having this in mind that both time-varying and time-invariant uncertainties are considered in the simulation.

7.6.2 Two-tank system benchmark

The two-tank system is proposed as the second application example to illustrate the approach proposed in this chapter. The considered tank process is based on Coupled Tanks $33-041$, manufactured by Feedback Instruments company. The general description and the mathematical model of the two tanks system can be found in Section A.2 of Appendix A.

Furthermore, in order to design the process in such a way to be applicable with testing the proposed approach, the TVU, i,e., the state disturbance ω and process noise υ are generated placing a Pump 2 as can be seen in Figure 7.6.

As it is shown in Figure 7.6, inflows of both tanks can also be affected by the additional disturbance ω and noise υ that are generated by the uncertain position of

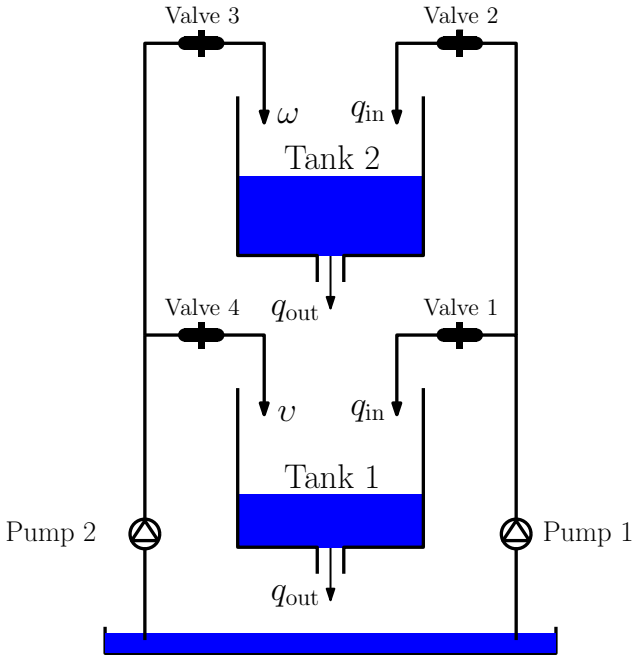

Figure 7.6: Schematic diagram of the tank system affected by the state disturbance and process noise.

Valves 3 and 4, respectively. Moreover, the TIU θ is implemented as an additional inflow using Pump 1. Hence, using the Euler discretization with a sampling time of 1 s, a discrete-time linear model is obtained as in (7.1) with

$$A = \begin{bmatrix} 0.9886 + \theta_{11} & 0 + \theta_{12} \\ 0.0114 + \theta_{21} & 0.9903 + \theta_{22} \end{bmatrix}, \quad B = \begin{bmatrix} 0.2261 \\ 0 \end{bmatrix}, \quad C = \begin{bmatrix} 0 & 1 \end{bmatrix}. \tag{7.69}$$

Moreover, the TIU parameters are bounded by the interval $\theta_{ij} \in [-0.3B, +0.3B]$, and also, time-varying bounded disturbances influencing all the state-space directions and the measurement noise are modeled, respectively, with E_ω and E_υ as

$$E_\omega = \begin{bmatrix} 0.006 & 0 \\ 0 & 0.006 \end{bmatrix}, \quad E_\upsilon = \begin{bmatrix} 0.5 \\ 0.5 \end{bmatrix}.$$

The input signal u is given as it is shown in Figure 7.7. Two scenarios are considered in this section. Both are implemented using the same type of uncertainties. They differ from the observer structure used: set-based IOA vs. trajectory-based IOA as explained

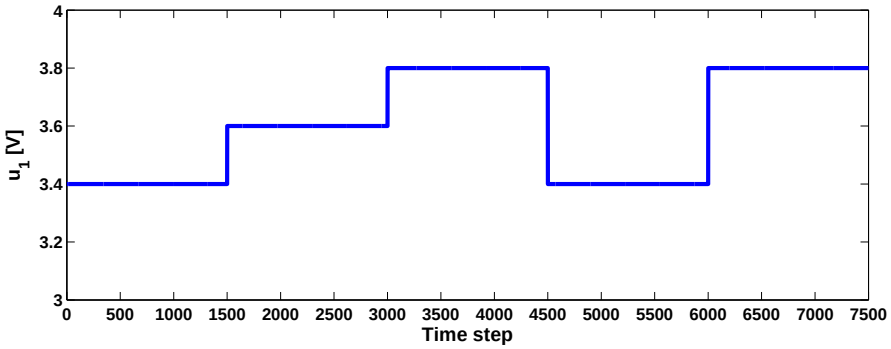

Figure 7.7: Pump signal.

in previous sections. Furthermore, the zonotopic observer structure is considered based on Proposition 7.1 and the observer structure in (7.35) is used as a trajectory-based IOA structure.

As a first scenario, the computation of the observer gain is done using the LMI in (7.15) for the case of set-based interval observer approach as $L = \begin{bmatrix} 0.6647 & 0.6542 \end{bmatrix}^\top$. Additionally, a trajectory-based interval observer approach gain is calculated using LMIs in (7.50a) and (7.51a) as $\overline{L} = \underline{L} = \begin{bmatrix} 0.6542 & 0.6493 \end{bmatrix}^\top$. The main purpose of having this analysis is to check the behavior of the state observation when only the stability condition is satisfied. Figure 7.8 shows the behavior of the set-based and trajectory-based interval observer approaches tracking the height of the water in upper and lower tanks (obtained from the real system).

As it can be seen from Figure 7.8, there is not any problem in lower tank since it is measurable based on matrix C. But, using the trajectory-based IOA, the correct estimation of the unmeasured state h_1 cannot be obtained. A possible explanation for this might be that the observer is not monotonic since the positivity condition is not considered for designing the observer gain. In order to solve this problem, the positivity condition is guaranteed by considering the LMIs in (7.50b) and (7.51b) for computing the observer gain together with (7.50a) and (7.51a) in trajectory-based interval observer approach as $\overline{L} = \underline{L} = \begin{bmatrix} 0.001 & 0.9803 \end{bmatrix}^\top$. Figure 7.9 shows the obtained results from the simulation.

As it can be seen from Figure 7.9, both set-based IOA and trajectory-based IOA are computing the same state estimation. There exists a small difference between the

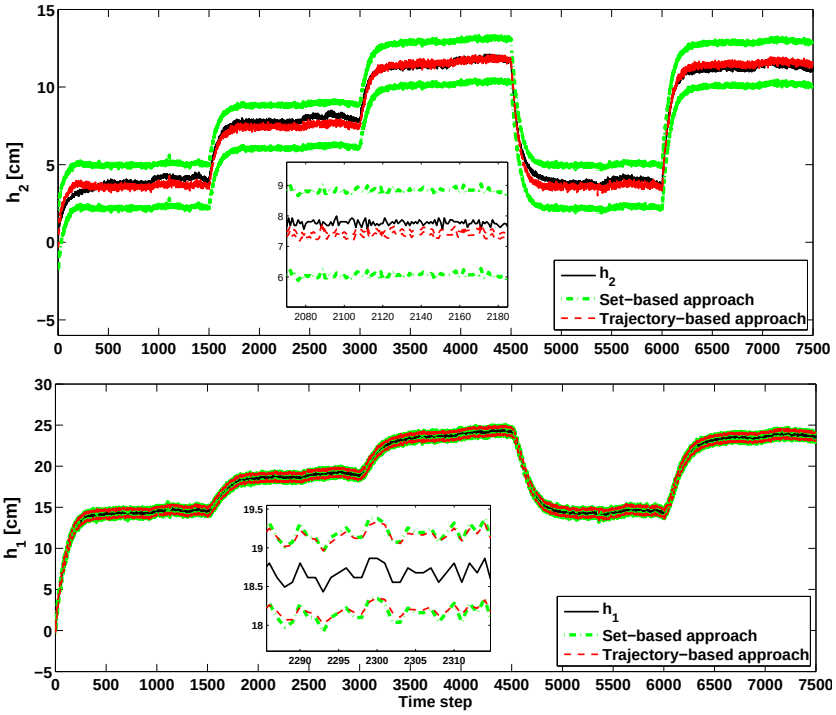

Figure 7.8: Set-based IOA vs. trajectory-based IOA considering monotonic system and non-monotonic observer.

computed bounds. Looking at the simulation, the set-based IOA is a bit more conservative than the trajectory-based IOA since the interval hull of state-bounding zonotope is used instead of the exact zonotope. Moreover, similar to analysis of the example in Section 7.6.1, the new observer structure in Theorem 7.4 is also tested for the real case study. Figure 7.10 shows the obtained results from the simulation.

As it can be seen in Figure 7.10, set-based, trajectory-based IOA and the integrated IOA are compared for the case study. Since the considered case study is monotonic, i.e., all the elements of matrix A are positive, the obtained results from the different observers are the same. It is worth mentioning that the observer gain in the set-based interval observer approach is computed by considering the satisfaction of the LMIs in Theorems 7.1 and 7.2 as $L = \begin{bmatrix} 0.0100 & 0.9903 \end{bmatrix}^\top$. Considering the trajectory-based interval observer approach, the observer gain is designed using the LMIs in (7.50) and (7.51) as $\overline{L} = \underline{L} = \begin{bmatrix} 0.001 & 0.9803 \end{bmatrix}^\top$. Furthermore, observer gain in the proposed integrated observer structure is calculated using Theorem 7.1 to satisfy the H_∞ performance

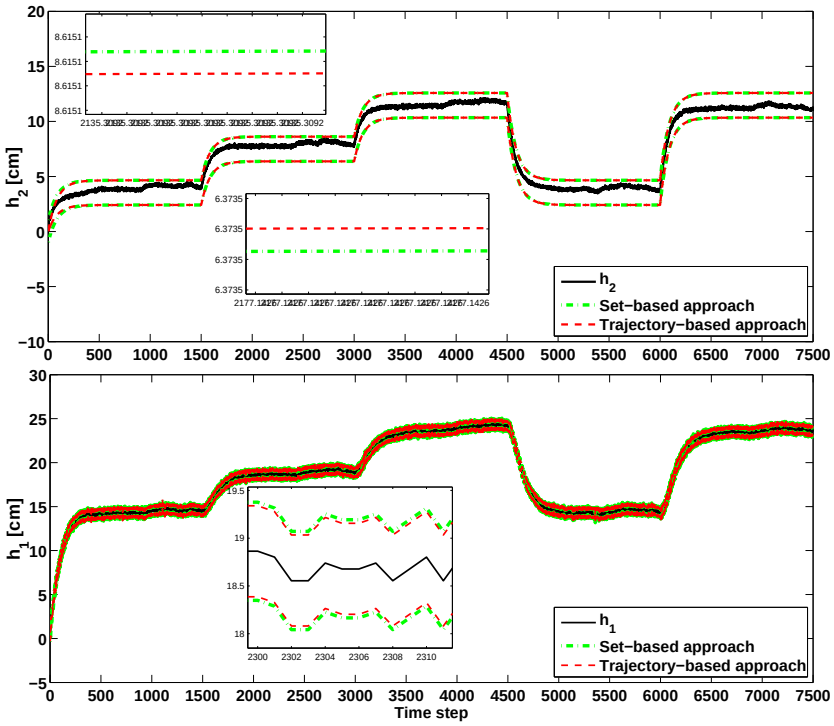

Figure 7.9: Set-based IOA vs. trajectory-based IOA considering monotonic system and monotonic observer.

together with the LMI mentioned in (7.62) to satisfy the monotonicity property of the observer as $L = \begin{bmatrix} 0.001 & 0.9803 \end{bmatrix}^\top$. The results obtained in Figure 7.10 show that the monotonicity and the convergence of the observers can be guaranteed for all different observers and they can compute almost the same results.

Therefore, both application examples illustrate that having a monotonic observer, almost the same results can be obtained by using the proposed LMIs to design the set-based IOA and trajectory-based IOA and it is well suited to also address the TIU and TVU. Furthermore, using the relationship between the set-based IOA and trajectory-based IOA, the new interval observer can be proposed based on the interval hull of the state-bounding zonotope where both problems of the set-based IOA, i.e., preserving time dependency of the uncertain parameter and wrapping effect, are handled in non-monotonic systems.

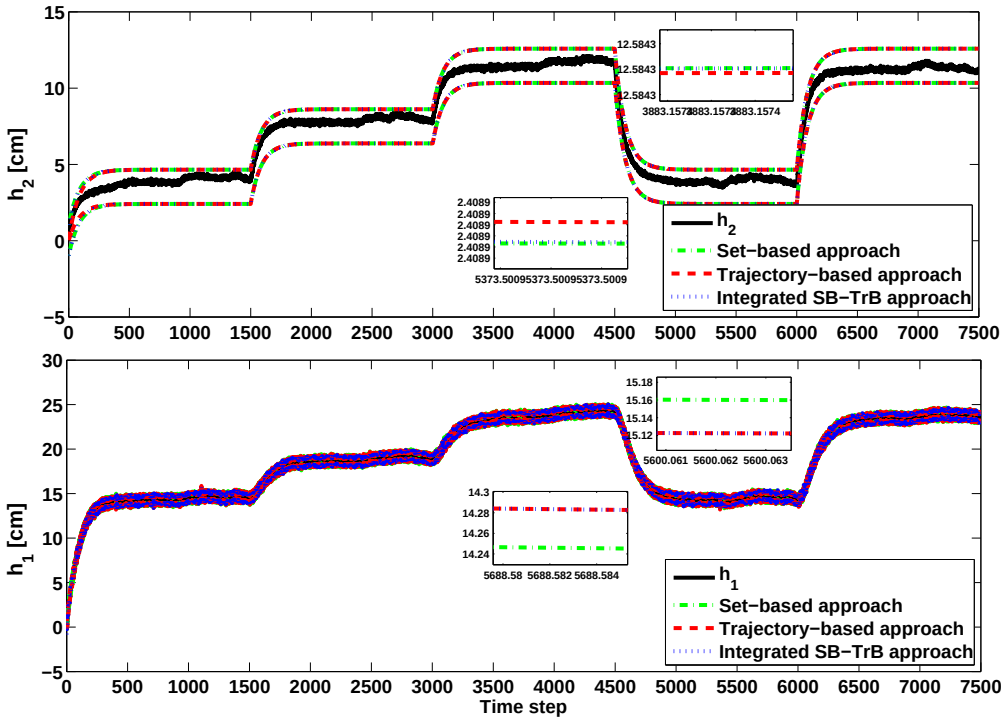

Figure 7.10: Set-based IOA vs. trajectory-based IOA considering monotonic system and designing the integrated monotonic observer.

7.7 Summary

This chapter has proposed the design of an IOA for discrete-time linear systems with both TIU and TVU. First, the time-varying approach, called set-based IOA, is introduced. In the set-based IOA, H_∞ performance and minimization of the size of the obtained state-bounding zonotope are considered to derive the LMI for computing the observer gain. Then, it is shown that in the set-based IOA, the time dependency of the parameter uncertainties cannot be preserved. Furthermore, the wrapping effect problem appears when considering a non-monotonic system for the case of set-based IOA. So far, in order to solve the issues of using the set-based IOA, the time-invariant approach, called trajectory-based IOA, is used. The LMI technique is utilized in trajectory-based IOA to guarantee the computation of the observer gain in order to satisfy both the H_∞ performance and the monotonicity property. As a novelty, based on the comparison of the mentioned interval observation approaches, it is shown that, using the interval hull of

the state-bounding zonotope in set-based IOA, both approaches can be connected when satisfying the monotonicity property. Furthermore, a method for designing the observer that can connect both type of interval observer approaches is proposed. It is shown that the proposed approach, which is based on the set-based IOA, has the same performance of the trajectory-based IOA to preserve the time dependency without having the problem of wrapping effect. The comparison of the set-based IOA, the trajectory-based IOA and the proposed IOA has been conducted on two different case studies, i.e., a numerical example and a real case study based on two-tank system. The obtained results from both case studies are well suited to address the results in the theoretical part of the chapter.

Part III

Conclusions and future research

Chapter 8

Concluding remarks and further extensions

As a concluding remark, the objectives proposed in the beginning of the thesis were fulfilled. Furthermore, during the thesis development new objectives and tasks have appeared that enrich the proposed approaches and have complemented the obtained results. Therefore, this chapter summarizes the main contributions of the thesis. It is worth mentioning that these contributions were reported at each corresponding chapter. Furthermore, the proposal of future ways to continue the research developed in the thesis will be pointed out in this chapter.

8.1 Contributions

In the following, the contributions related to the different proposed objectives are summarized.

- IOA versus SMA
  - The analysis of the IOA and SMA has been done in order to establish the advantages and disadvantages of each approach.
  - The relationship between IOA and SMA has been proposed in a formal mathematical framework.
  - The comparison between IOA and SMA has been performed in the context of FD framework by means of proposing a novel FD test to connect the

approaches.

- The proposed connection between IOA and SMA in FD framework has been used to characterize the MDF.

- IOA versus SIA

  - The relation between the classical IOA and SIA in FD framework has been proposed.
  - The passive robust FD approach has been proposed using IOA in combination with SIA.
  - The sensitivity to both faults and disturbances has been evaluated using a set-based approach enclosing all the possible temporal scenarios of faults and disturbances within specified ranges.
  - The integration of the IOA and SIA in FDI has been proposed.
  - The characterization of the MDF has been proposed by using the classical sensitivity analysis.
  - The characterization of the MDF has been proposed using using SIA.
  - The mathematical expressions of the MDF for different type of sensor and actuator faults have been proposed with the goal of connecting both sensitivity and set-based approaches.
  - The observer-based FDI design that can be used in both transient and steady-state operations of a system has been proposed.
  - The MIF has been characterized based on the combination of the classical sensitivity analysis and the SIA.

- Optimizing FD rather than state estimation

  - An observer-based approach has been proposed in order to enhance the sensitivity to faults with respect to disturbances, rather than only optimizing the precision of the state estimation.
  - The sensitivity to both faults and disturbances has been evaluated using a set-based approach enclosing all the possible fault and disturbance scenarios.
  - The computation of the online time-varying optimal FD observer gains has been proposed without any requirement on the considered frequency ranges.

  - The MDF has been characterized using a classical sensitivity analysis in order to show the effectiveness of the proposed time-varying observer gain on FD performance.

- Set-based IOA versus trajectory-based IOA
  - The design of a robust IOA whose observer gain is computed by using LMI techniques to achieve H_∞ performance has been proposed.
  - The relationship between the set-based IOA and trajectory-based IOA has been investigated in order to connect them under some conditions.
  - The design of an observer taking into account both TVU and TIU has been proposed considering the relationship between the set-based IOA and trajectory IOA.

8.2 Directions for future research

When all the desired tasks were accomplished in order to achieve the planned objectives, some new perspectives were kept out of the scope of this dissertation. However, this set of new ideas for future directions is outlined next:

- IOA versus SMA
  - The comparison can be extended using Linear Matrix Inequalities (LMI)s for computing the observer gain L in IOA and the parameter λ SMA to asses the robustness in state estimation framework.
  - The comparison can be extended to the case of nonlinear systems represented with Takagi-Sugeno or linear parameter-varying (LPV) models to assess the performance of both approaches regarding both FD and FDI.
- IOA versus SIA
  - The influence of the input over the magnitude of the MDF can be further analyzed in order to apply active diagnosis to design the system input such that a better performance is achieved in fault detection and isolation.
  - Different faults can be considered based on their nature in order to characterize the minimum detectable incipient, multiplicative, permanent or intermediate faults.

  - The effect of the observer gain and the influence of the input over the state-bounding observer can be further analyzed in order to improve the algorithm for enhancing the sensitivity to the fault with respect to the influence of disturbance with the goal of improving fault detection and isolation performance.

- Optimizing FD rather than state estimation

  - Different type of faults can be considered separately with the purpose of enhancing the sensitivity of the state estimation to specific kind of faults in orderer to improve both the fault detection and isolation performances.

- Set-based IOA versus trajectory-based IOA

  - The effectiveness of the proposed results can be investigated for enhancing the sensitivity to faults, rather than only the robust state estimation.

Part IV

Appendices

Appendix A

Tank-based benchmarks

For the purpose of illustrating how the FDI algorithms presented in this thesis works, there are several application examples that are used. Among them, the tank system proposed by [Joh00] is one of the most used laboratory process for control and FDI assessment. The main motivation for the use of a tank system in the processes monitoring and fault diagnosis field is related to the following characteristic: in the tank system, a collection of tanks sequentially connected through pipes at the bottom and at the middle part of the tanks is used. Considering these connections and different sets of available sensors allow to test FDI algorithms in both linear and nonlinear frameworks.

A.1 Four-tank system

The quadruple tank is a multi input/multi output process proposed by [Joh00] as a control benchmark. The system contains two pumps and four interconnected tanks. As it can be seen from Figure A.1 and the schematic diagram of the system setup in Figure A.2, the two process inputs are the pump flows that are determined by the voltages v_1 and v_2 (input voltages to the pumps varying between 0 V to 10 V).

Furthermore, the outputs of the process are the water levels in the lower tanks that are obtained as voltages from the measurement devices in the range between 0 V to 10 V. Tanks 3 and 4 are placed on top of Tanks 1 and 2. In addition, the action of pumps is to fill the tanks by extracting the water from the basin. Furthermore, Tanks 1 and 2 receive additional water flow from Tanks 3 and 4 because of the gravity effect.

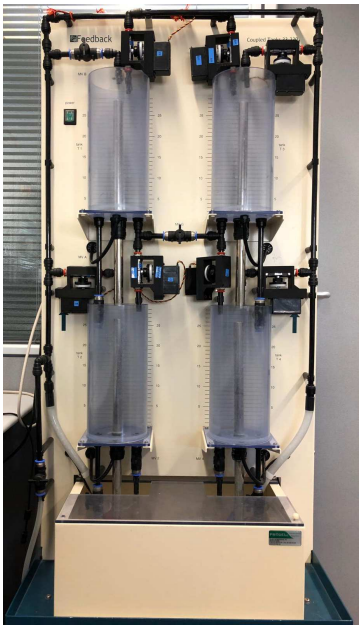

Figure A.1: The quadruple-tank system

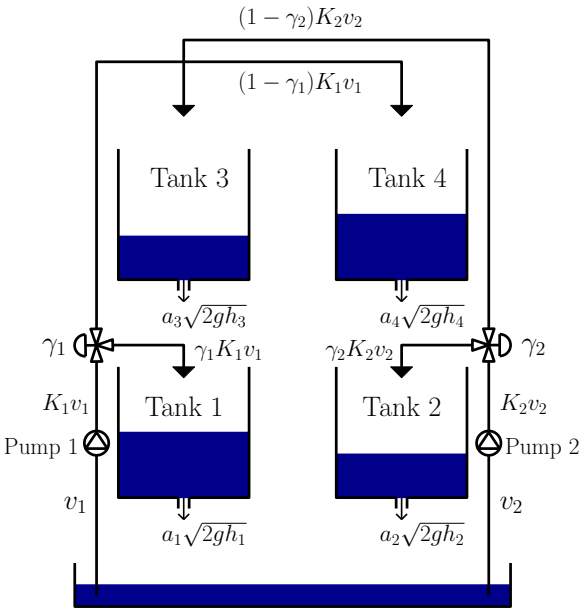

Figure A.2: Schematic diagram of the quadruple-tank system

Table A.1: Model parameters.

Parameter value	**Unit**
$A_1 = A_3 = 28$	cm^2
$A_2 = A_4 = 32$	cm^2
$a_1 = a_3 = 0.071$	cm^2
$a_2 = a_4 = 0.057$	$\text{cm}^{\ 2}$
$g = 981$	$\text{cm} \ / \ \text{s}^2$

The water flow to each tank is controlled by the position of the valves determined by γ_1 and γ_2 in Figure A.2. Furthermore, the position of the valves $\gamma_1,\ \gamma_2 \in (0, 1)$ are the ratios modeling how the output flows of the pumps are divided between the upper and lower tanks. Regarding the physical features, the height of each tank is 20 cm and the connection of the tank and the pump is done using a pipe with a diameter equal to 6 mm.

Considering all the points that are mentioned above, the mathematical model of the process can be determined based on the mass balance relations and Bernoulli's law as

$$\frac{dh_{1,t}}{dt} = -\frac{a_1}{A_1}\sqrt{2gh_{1,t}} + \frac{a_3}{A_1}\sqrt{2gh_{3,t}} + \frac{\gamma_1 K_1}{A_1}v_{1,t}, \tag{A.1a}$$

$$\frac{dh_{2,t}}{dt} = -\frac{a_2}{A_2}\sqrt{2gh_{2,t}} + \frac{a_4}{A_2}\sqrt{2gh_{4,t}} + \frac{\gamma_2 K_2}{A_2}v_{2,t}, \tag{A.1b}$$

$$\frac{dh_{3,t}}{dt} = -\frac{a_3}{A_3}\sqrt{2gh_{3,t}} + \frac{(1-\gamma_2)\,K_2}{A_3}v_{2,t}, \tag{A.1c}$$

$$\frac{dh_{4,t}}{dt} = -\frac{a_4}{A_4}\sqrt{2gh_{4,t}} + \frac{(1-\gamma_1)\,K_1}{A_4}v_{1,t}, \tag{A.1d}$$

where

- h_i with $i = 1, 2, 3, 4$ is the water level in Tank i,
- A_i is the cross section of Tank i with $i = 1, 2, 3, 4$,
- a_i is the cross section of the outlet pipe with $i = 1, 2, 3, 4$,
- K_j is the constant of the Pump j with $j = 1, 2$,
- g is the acceleration due to gravity.

Table A.2: Value of variables.

Operating point	**Parameter value**	**Unit**
$(h_1^\star,\ h_2^\star)$	$(12.4,\ 12.7)$	cm
$(h_3^\star,\ h_4^\star)$	$(1.8,\ 1.4)$	cm
$(v_1^\star,\ v_2^\star)$	$(3,\ 3)$	V
$(K_1^\star,\ K_2^\star)$	$(3.33,\ 3.35)$	cm ^{3}/ Vs
$(\gamma_1^\star,\ \gamma_2^\star)$	$(0.7,\ 0.6)$	-

The value of the parameters of (A.1) is presented in Table A.1. Furthermore, in order to apply the approaches proposed in this thesis, the non-linear model (A.1) is linearized around the working point in Table A.2 and introducing the variables $\tilde{h}_i = h_i - h_i^\star$ and $\tilde{v}_i = v_i - v_i^\star$ as

$$\dot{\tilde{h}}_t = \begin{bmatrix} -\frac{1}{T_1} & 0 & \frac{A_3}{A_1 T_3} & 0 \\ 0 & -\frac{1}{T_2} & 0 & \frac{A_4}{A_2 T_4} \\ 0 & 0 & -\frac{1}{T_3} & 0 \\ 0 & 0 & 0 & -\frac{1}{T_4} \end{bmatrix} \tilde{h}_t + \begin{bmatrix} \frac{\gamma_1 K_1}{A_1} & 0 \\ 0 & \frac{\gamma_2 K_2}{A_2} \\ 0 & \frac{(1-\gamma_1) K_2}{A_3} \\ \frac{(1-\gamma_1) K_1}{A_4} & 0 \end{bmatrix} \tilde{v}_t, \tag{A.2a}$$

$$y_t = \begin{bmatrix} K_c & 0 & 0 & 0 \\ 0 & K_c & 0 & 0 \end{bmatrix} \tilde{h}_t, \tag{A.2b}$$

where the measured level signals are obtained considering that $K_c = 0.5$ V/cm and $T_i = \frac{A_i}{a_i}\sqrt{\frac{2h_i^\star}{g}}$, with $i = 1, 2, 3, 4$ as $T_1 = 62.7034$, $T_2 = 90.3353$, $T_3 = 23.8900$ and $T_4 = 29.9930$.

Finally, using the Euler discretization with a sampling time of 1 s, a discrete-time linear model is obtained as

$$\tilde{h}_{k+1} = A\tilde{h}_k + B\tilde{v}_k + E_\omega \omega_k, \tag{A.3a}$$

$$y_k = C\tilde{h}_k + D\tilde{v}_k + E_\upsilon \upsilon_k, \tag{A.3b}$$

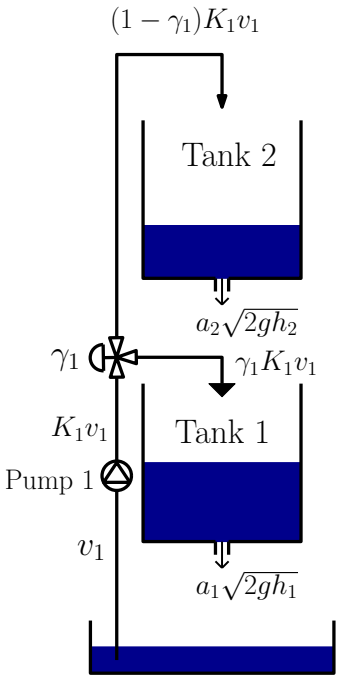

Figure A.3: Schematic diagram of the two-tank system.

with

$$A = \begin{bmatrix} 0.9841 & 0 & 0.0419 & 0 \\ 0 & 0.9889 & 0 & 0.0333 \\ 0 & 0 & 0.9581 & 0 \\ 0 & 0 & 0 & 0.9667 \end{bmatrix}, \quad B = \begin{bmatrix} 0.2102 & 0 \\ 0 & 0.0628 \\ 0 & 0.0479 \\ 0.0094 & 0 \end{bmatrix}, \tag{A.4}$$
$$C = \begin{bmatrix} 0.5 & 0 & 0 & 0 \\ 0 & 0.5 & 0 & 0 \end{bmatrix}, \qquad D = \begin{bmatrix} 0 & 0 \\ 0 & 0 \end{bmatrix}.$$

Moreover, bounded disturbances ω influencing all the state-space directions and the measurement noise υ are modeled respectively with E_ω and E_υ which are known as the associated distribution matrices with appropriate dimensions

A.2 Two-tank system

The four tanks system in Section A.1 can be simplified into two tanks system as it is shown in Figure A.3.

Using the same information as the case of four tanks system, the mathematical model of two tanks system is derived using mass-balance relations and the Bernoulli's law as follows:

$$\frac{dh_{1,t}}{dt} = -\frac{a_1}{A_1}\sqrt{2gh_{1,t}} + \frac{a_2}{A_1}\sqrt{2gh_{2,t}} + \frac{\gamma K_p}{A_1}\omega_t, \tag{A.5a}$$

$$\frac{dh_{2,t}}{dt} = -\frac{a_2}{A_2}\sqrt{2gh_{2,t}} + \frac{(1-\gamma)K_p}{A_2}u_t. \tag{A.5b}$$

Hence, the linearized model of (A.5) around the working point mentioned in Table A.2 can be obtained as

$$\dot{\tilde{h}}_t = \begin{bmatrix} -\frac{1}{T_1} & \frac{A_2}{A_1 T_2} \\ 0 & -\frac{1}{T_2} \end{bmatrix} \dot{\tilde{h}}_t + \begin{bmatrix} \frac{\gamma_1 K_1}{A_1} & 0 \\ 0 & \frac{(1-\gamma_1)K_1}{A_2} \end{bmatrix} \tilde{v}_t, \tag{A.6a}$$

$$y_t = \begin{bmatrix} K_c & 0 \end{bmatrix} \dot{\tilde{h}}_t, \tag{A.6b}$$

where $\tilde{v}_t = \begin{bmatrix} \omega_k \\ v_k \end{bmatrix}$ and K_c is a experimental estimated parameter. Moreover, $T_i = \frac{A_i}{a_i}\sqrt{\frac{2h_i^\star}{g}}$ with $i = 1, 2$. Considering the same parameter as in Section A.1 and using the Euler discretization with a sampling time of 1s, the linearized model of this system can be written in the state-space form as (A.3), where

$$A = \begin{bmatrix} 0.9842 & 0.0407 \\ 0 & 0.9590 \end{bmatrix}, \quad B = \begin{bmatrix} 0.0007 \\ 0.0352 \end{bmatrix}, \quad D = \begin{bmatrix} 0 & 0 \end{bmatrix}, \quad C = \begin{bmatrix} 0.5 & 0 \end{bmatrix}. \tag{A.7}$$

Moreover, the output y is the voltage obtained from the level sensor. Hence, considering the physical features of the two-tank system, the range of the measured output is $[0,\ 10]$ V since the height of the each tank is from 0 cm up to 20 cm and $K_c = 0.5$ V/cm. Moreover, based on the experimental data, the incremental value of the measured output around the working point of the lower tank is from 4 V up to 8 V (or 8 cm to 16 cm).

Appendix B

Mathematical background

B.1 Matrix definitions and properties

In this section, basic matrix definitions and properties are introduced.

Definition B.1. The *Symmetric Positive Definite (SPD)* matrix is a matrix whose eigenvalues are positive. In other words, a square and symmetric matrix A is positive definite if, for all $x \in \mathbb{R}^{n_x}$, $x^\top Ax > 0$. □

Definition B.2. A matrix $A = A^\top \in \mathbb{R}^{n \times n}$ is called a *semipositive-definite matrix*, denoted by $A \geq 0$, if $\tau^\top A\tau \geq 0$ for all non-zero vectors τ with real entries ($\tau \in \mathbb{R}$). □

Definition B.3. A matrix $A = A^\top \in \mathbb{R}^{n \times n}$ is called a *strictly positive-definite matrix*, denoted by $A > 0$, if $\tau^\top A\tau > 0$ for all non-zero vectors τ with real entries ($\tau \in \mathbb{R}$). □

Definition B.4. A matrix $A = A^\top \in \mathbb{R}^{n \times n}$ is called a *seminegative-definite matrix*, denoted by $A < 0$, if $\tau^\top A\tau \leq 0$ for all non-zero vectors τ with real entries ($\tau \in \mathbb{R}$). □

Definition B.5. A matrix $A = A^\top \in \mathbb{R}^{n \times n}$ is called a *strictly negative-definite matrix*, denoted by $A < 0$, if $\tau^\top A\tau < 0$ for all non-zero vectors τ with real entries ($\tau \in \mathbb{R}$). □

Definition B.6. The *Euclidean norm* of a matrix $A \in \mathbb{R}^{n \times n}$ is defined by the quantity $x^\top Ax = \|x\|_A^2$, where $x \in \mathbb{R}^n$ and $A = A^\top > 0$. □

Definition B.7. The *trace* of a square matrix $A \in \mathbb{R}^{n \times n}$ is defined to be the sum of the elements of its main diagonal. It is obtained as $tr(A) = \sum_{i=1}^{n} a_{ii}$. Furthermore, for

a matrix $X = [X_{ij}]$ and, for square matrices A and B, and a scalar α,

$$\begin{aligned} tr(A) &= tr(A^\top), \\ tr(A+B) &= tr(A) + tr(B), \\ tr(\alpha A) &= \alpha tr(A), \\ \partial_X tr(AX^\top B) &= A^\top B^\top, \\ \partial_X tr(AXBX^\top C) &= BX^\top CA + B^\top X^\top A^\top C^\top, \end{aligned}$$

hold. □

Definition B.8. The *Frobenius norm* of a matrix $A \in \mathbb{R}^{n\times m}$ is defined as

$$\|A\|_F = \sqrt{\sum_{i=1}^{n}\sum_{j=1}^{m}|a_{ij}|} = \sqrt{tr(AA^\top)}, \tag{B.1}$$

where a_{ij} are the elements of A. □

Definition B.9. A *Linear Matrix Inequality* (LMI) with the form

$$F(x) \triangleq F_0 + \sum_{i=1}^{m} x_i F_i > 0, \tag{B.2}$$

where $x = \begin{bmatrix} x_1 & x_2 & \dots & x_m \end{bmatrix}^\top \in \mathbb{R}^m$ is the vector of decision variables and the matrices $F_i = F_i^\top \in \mathbb{R}^{n\times n}$, with $i = 0, \dots, m$ are called the scalar decision variables.

The LMI in (B.2) is a convex constraint on x, i.e., the set $\{x \in \mathbb{R}^m : F(x) > 0\}$ is convex. The LMI $F(x) > 0$ will be reduced to a set of scalar linear inequalities, if the matrices F_i with $i = 0, \dots m$, are diagonal. Generally speaking, the matrix decision variables can be used to formulate LMI problems, e.g., the Lyapunov inequality

$$A^\top P + PA < 0, \tag{B.3}$$

where $A \in \mathbb{R}^{n\times n}$ is a given matrix and $P = P^\top \in \mathbb{R}^{n\times n}$ denotes the decision variable [BEGFB94, DY13]. □

Definition B.10. *Schur complement* [BEGFB94, DY13]. Consider the LMI

$$\begin{bmatrix} Q(x) & S(x) \\ S^\top(x) & R(x) \end{bmatrix} > 0, \tag{B.4}$$

where $Q(x)$ and $R(x)$ are symmetric matrices and $Q(x)$, $R(x)$ and $S(x)$ are affine in x. Then, (B.4) is equivalent to

$$\begin{cases} Q(x) > 0, \\ Q(x) - S(x)R^{-1}(x)S^{\top}(x) > 0, \end{cases} \tag{B.5}$$

or

$$\begin{cases} R(x) > 0, \\ R(x) - S(x)^{\top}Q^{-1}(x)S(x) > 0. \end{cases} \tag{B.6}$$

Using this definition, nonlinear matrix inequalities in (B.5) and (B.6) can be transformed into an LMI (B.4). □

B.2 Set definitions and properties

Set-based approaches are used in a large part of this thesis. In this regard, it is necessary to mention their main definitions and properties. In this context, several set representations are used in the set-based approaches, e.g., intervals [JKDW01, MKC09], polytopes [VZ96], parallelotopes [CGZ96], zonotopes [PSQ03, LAC+11, LSA+13c, Com03] and ellipsoids [PNDW04, Com05]. But, the most used sets in this dissertation are intervals, polytopes and zonotopes. Therefore, it is necessary to introduce some basic definitions and operations used in zonotope and interval frameworks.

Before presenting the zonotope and interval, some of the basic set definitions and operations are stated.

Definition B.11. A set $\mathcal{S} \subset \mathbb{R}^n$ is called *convex*, if for any $x_1, x_2, \ldots, x_k \in \mathcal{S}$ with $k \geq 2$, and any $\alpha_1, \alpha_2, \ldots, \alpha_k \in \mathbb{N}$ such that $\sum_{i=1}^{k} \alpha_i = 1$ the element $\sum_{i=1}^{k} \alpha_i x_i$ is in $\mathcal{S}$.

□

Definition B.12. The smallest convex set containing a given set $\mathcal{S}$, denoted by $conv(\mathcal{S})$, is called the *convex hull* of $\mathcal{S}$. □

Definition B.13. The *Minkowski sum* of two sets $\mathcal{S}_1$ and $\mathcal{S}_2$ is defined by $\mathcal{S}_1 \oplus \mathcal{S}_2 = \{s_1 + s_2 : \ s_1 \in \mathcal{S}_1 \text{ and } s_2 \in \mathcal{S}_2\}$. □

Definition B.14. Considering the dynamics $x_{k+1} = f(x_k)$, a set of states $\Omega \subseteq \mathbb{R}^n$ is called *invariant set* if for all $x_0 \in \Omega$ and $k \geq 0$, $x_k \in \Omega$. □

Definition B.15. Considering the dynamics $x_{k+1} = f(x_k, \omega_k)$, a set $\mathcal{S}$ is called *RPI set*, if for all $k \geq 0$, both $x_k \in \mathcal{S}$ and $x_{k+1} \in \mathcal{S}$. □

B.2.1 Interval sets

In this thesis, *intervals* allow enclosing the effect of uncertainties, e.g., state disturbance or measurement noise, into an interval, by introducing upper and lower bounds of these uncertainties. The first study of bounding errors by using intervals was reported by [Moo69]. Some of the most used definitions are stated below.

Definition B.16. An *interval* $[a,\ b]$ is defined as the set $\{x \in \mathbb{R} : a \leq x \leq b\}$. □

Definition B.17. A *strip* is defined as a set $\mathcal{S}(y, d, \sigma) = \left\{x \in \mathbb{R} : \left|y - d^\top x\right| \leq \sigma\right\}$, where $y \in \mathbb{R}$, $d \in \mathbb{R}^n$ and $\sigma \in \mathbb{N}$. □

Definition B.18. Consider two given intervals $[x]$ and $[y]$, the four basic operations of interval analysis are defined as

$$[x] + [y] = [\underline{x} + \underline{y},\ \overline{x} + \overline{y}], \tag{B.7}$$

$$[x] - [y] = [\underline{x} + \overline{y},\ \overline{x} + \underline{y}], \tag{B.8}$$

$$[x].[y] = [\min(\underline{x}.\underline{y},\ \underline{x}.\overline{y},\ \overline{x}.\underline{y},\ \overline{x}.\overline{y}),\ \max(\underline{x}.\underline{y},\ \underline{x}.\overline{y},\ \overline{x}.\underline{y},\ \overline{x}.\overline{y})], \tag{B.9}$$

$$\frac{[x]}{[y]} = [x].\left[\frac{1}{\overline{y}},\ \frac{1}{\underline{y}}\right],\ \text{if } 0 \notin [y]. \tag{B.10}$$

□

Lemma B.1. *Based on [ERP13], if* $\underline{A} \leq A \leq \overline{A}$ *for* $\underline{A},\ A,\ \overline{A} \in \mathbb{R}^{n_x \times n_x}$ *and* $\underline{x} \leq x \leq \overline{x}$ *for* $\underline{x},\ x,\ \overline{x} \in \mathbb{R}^{n_x}$*, then*

$$\underline{A^+}\ \underline{x^+} - \overline{A^+}\underline{x^-} - \underline{A^-}\overline{x^+} + \overline{A^-}\ \overline{x^-} \leq Ax \leq \overline{A^+}\ \overline{x^+} - \underline{A^+}\overline{x^-} - \overline{A^-}\underline{x^+} + \underline{A^-}\ \underline{x^-},$$

where $\overline{A^+} = \max\{0,\ \overline{A}\}$, $\overline{A^-} = \overline{A^+} - \overline{A}$, $\underline{A^+} = \max\{0,\ \underline{A}\}$, $\underline{A^-} = \underline{A^+} - \underline{A}$, $\overline{x^+} = \max\{0,\ \overline{x}\}$, $\overline{x^-} = \overline{x^+} - \overline{x}$, $\underline{x^+} = \max\{0,\ \underline{x}\}$ *and* $\underline{x^-} = \underline{x^+} - \underline{x}$.

Proof. The proof follows from the results presented in [ERP13]. □

Lemma B.2. *Given a system dynamic that is considered to be function of the parameter vectors as*

$$x_{k+1} = A(\theta)x_k + B(\theta)u_k, \tag{B.11}$$

with

$$A(\theta) = A + \Delta A(\theta), \tag{B.12a}$$
$$B(\theta) = B + \Delta B(\theta). \tag{B.12b}$$

Moreover, by assuming that $\Delta A(\theta)$ and $\Delta B(\theta)$ satisfy the following match perturbation condition:

$$\begin{bmatrix}\Delta A(\theta) & \Delta B(\theta)\end{bmatrix} = E_\phi \Xi_k \begin{bmatrix}G_a & G_b\end{bmatrix}, \tag{B.13}$$

where Ξ is a block diagonal matrix which represents the parameter uncertainties. Furthermore, G_a and G_b are known matrices. In this case, if the parameter vector is perturbed around the nominal value $\theta = \theta_0$, the system can be rewritten as

$$x_{k+1} = A(\theta_0)x_k + B(\theta_0)u_k + E_\phi \phi_k, \tag{B.14}$$

where

$$E_\phi = \begin{bmatrix}\dfrac{\partial A}{\partial \theta_1} & | & \dfrac{\partial B}{\partial \theta_1} & | & \dots & | & \dfrac{\partial A}{\partial \theta_i} & | & \dfrac{\partial B}{\partial \theta_i}\end{bmatrix}, \tag{B.15}$$
$$\phi_k = \begin{bmatrix}\delta\theta_1 x^\top & | & \delta\theta_1 u^\top & | & \dots & | & \delta\theta_i x^\top & | & \delta\theta_i u^\top\end{bmatrix}, \tag{B.16}$$

where the index i refers to the dimension of θ.

Proof. According to [CP12], the parameter perturbation can be approximated as

$$\Delta A(\theta) \approx \sum_{i=1}^{N} a_i(\theta) A_i, \tag{B.17a}$$
$$\Delta B(\theta) \approx \sum_{i=1}^{N} b_i(\theta) B_i, \tag{B.17b}$$

where A_i and B_i are the constant matrices and a_i and b_i are unknown scalar vectors. Then, considering (B.12) and (B.17), the uncertain parameter can be approximated only based on the disturbance term as

$$E_{\phi_1}\phi_{1_k} = \Delta A(\theta)x_k + \Delta B(\theta)u_k = \begin{bmatrix} A_1 & \dots & A_N & B_1 & \dots & B_N \end{bmatrix} \begin{bmatrix} a_1(\theta)x_k \\ \dots \\ a_N(\theta)x_k \\ b_1(\theta)u_k \\ \dots \\ b_N(\theta)u_k \end{bmatrix}, \quad \text{(B.18)}$$

where ϕ and E_ϕ show the disturbance term and the disturbance matrix, respectively. Moreover, by assuming (B.13), ϕ_k can be considered as

$$\phi_k = \Xi_k \begin{bmatrix} G_a x_k & G_b u_k \end{bmatrix}. \quad \text{(B.19)}$$

Thus, if the system is considered to be function of the parameter vectors where the parameter vector is perturbed around the nominal value $\theta = \theta_0$ as the dynamical model in (B.11), it can be written that

$$x_{k+1} = A(\theta_0)x_k + B(\theta_0)u_k + \sum_{i=1}^{k} \left\{ \frac{\partial A}{\partial \theta_i}\delta\theta_i x + \frac{\partial B}{\partial \theta_i}\delta\theta_i u \right\}. \quad \text{(B.20)}$$

Therefore, considering (B.20), the dynamical model in (B.11) can be rewritten as it is characterized in (B.14). □

B.2.2 Polytopic sets

A *polytope* is a convex geometrical representation of linear constraints widely used control and optimization. In general, a polytope is a bounded polyhedral set and shaped by gathering a group of half-spaces [BM08]. Mathematically speaking, the polytopic representation of a set can be expressed in two distinct manners: I) half-spaces (H-polyhedron) and II) vertices (V-polyhedron). Both mentioned representations of a polytope are mathematically equivalent and they can convert to each other [Zie94]. Some of the most used definitions are stated below.

Definition B.19. An *Half-space representation or H-polyhedron* $P \subset \mathbb{R}^n$ is an intersection of a finite set of closed half-spaces that can be introduced with the following form:

$$P = \left\{ x \in \mathbb{R}^n : Fx \leq b,\ F \in \mathbb{R}^{n \times m},\ b \in \mathbb{R}^n \right\}, \quad \text{(B.21)}$$

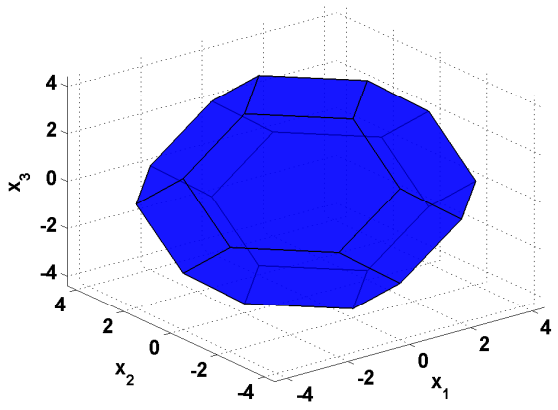

Figure B.1: Zonotope in $\mathbb{R}^3$

where $f_i x \leq b_i$ with $i = 1, 2, \ldots, n$ is the i^{th} half-space, where f_i is the i^{th} row of F and b_i is the i^{th} component of b. □

Definition B.20. A *Vertex representation or V-polyhedron* $P \subset \mathbb{R}^n$ is the Minkowski sum of the convex hull of a set $\mathcal{V} = \{v_1, v_2, \ldots, v_p\} \subset \mathbb{R}^n$ of points and the cone of a finite set $\mathcal{Y} = \{y_1, y_2, \ldots, y_q\} \subset \mathbb{R}^n$ of vectors, where $P = conv(\mathcal{V}) \oplus cone(\mathcal{Y})$ □

B.2.3 Zonotopic sets

Zonotopes are a particular class of convex polytopes, which are symmetric with respect to their center. Some of the most used definitions and propertied are stated below.

Definition B.21. A *zonotope* $\langle c,\ R \rangle \subset \mathbb{R}^n$ with the center $c \in \mathbb{R}^n$ and the generator matrix $R \in \mathbb{R}^{n \times p}$ is a polytopic set defined as a linear image of the unit hypercube $[-1,\ 1]^p$, i.e.,

$$\langle c,\ R \rangle = \{c + Rs, \|s\|_\infty \leq 1\}. \tag{B.22}$$

Moreover, a centered zonotope is denoted by $\langle R \rangle = \langle 0,\ R \rangle$. Any permutation of the columns of R leaves it invariant. For example, Figure B.1 illustrates the sixth-order zonotope in $\mathbb{R}^3$ with $c = \begin{bmatrix} 0 \\ 0 \\ 0 \end{bmatrix}$ and $R = \begin{bmatrix} 1 & 1 & 1 & -1 & 0 & 0 \\ 1 & -1 & 0 & 0 & 1 & -1 \\ 0 & 0 & -1 & -1 & 1 & 1 \end{bmatrix}$.

□

Definition B.22. Consider two given sets $\mathcal{A}$ and $\mathcal{B}$, their *Minkowski sum* is a set defined as $\mathcal{A} \oplus \mathcal{B} = \{a + b |\ a \in \mathcal{A},\ b \in \mathcal{B}\}$. Thus, the Minkowski sum of the zonotopes $\mathcal{Z}_1 = \langle c_1, R_1 \rangle$ and $\mathcal{Z}_2 = \langle c_2, R_2 \rangle$ is $\mathcal{Z}_1 \oplus \mathcal{Z}_2 = \langle c_1 + c_2, \begin{bmatrix} R_1, & R_2 \end{bmatrix} \rangle$. □

Definition B.23. The *interval hull* of a given zonotope $\mathcal{Z} = \langle c,\ R \rangle$, denoted by $\square\mathcal{Z}$, is the smallest interval box that contains $\mathcal{Z}$ and can be evaluated for all $i = 1, 2, \ldots, n$ as

$$\square\mathcal{Z} = \{z : |z_i - c_i| \leq \|R_i\|_1\}, \tag{B.23}$$

where R_i indicates the i^{th} row of matrix R, and z_i and c_i are the i^{th} components of z and c, respectively. □

Definition B.24. The *linear image* of a zonotope $\mathcal{Z} = \langle c, R \rangle$ by a compatible matrix L is $L \odot \langle c, R \rangle = \langle Lc, LR \rangle$. □

Definition B.25. *Zonotope support strip.* Given a zonotope $\mathcal{Z} = \langle c_z,\ R_z \rangle$ and a vector C, the zonotope support strip is introduced by $\mathscr{S} = z : s_d \leq C_i z \leq s_u$, where i denotes the i^{th} row of the vector C. Furthermore, s_d and s_u should satisfy $s_d = \min_{z \in \mathcal{Z}} C_i z$ and $s_u = \max_{z \in \mathcal{Z}} C_i z$ and they can be computed as

$$s_d = C_i c_z + \left\| C_i R_z^\top \right\|_1, \tag{B.24}$$

$$s_u = C_i c_z - \left\| C_i R_z^\top \right\|_1. \tag{B.25}$$

□

Definition B.26. *Covariance of a Zonotope.* Given a zonotope $\mathcal{Z} = \langle c_z,\ R_z \rangle$, the covariance of this zonotope is defined as $cov(\mathcal{Z}) = R_z R_z^\top$. □

Definition B.27. The *F-radius* of a given zonotope $\mathcal{Z} = \langle c_z,\ R_z \rangle \in \mathbb{R}^n$ is the Frobenius norm of that zonotope, i.e., $\|\mathcal{Z}\|_F = \|R_z\|_F$. □

Definition B.28. The *weighted Frobenius radius (F_W-radius)* of a given zonotope $Z = \langle c,\ R \rangle$ is the weighted Frobenius norm of that zonotope, i.e., $\|\mathcal{Z}\|_{F,W} = \|R\|_{F,W}$. □

Definition B.29. Considering a weighting matrix $W \in \mathbb{R}^{n_x \times n_x}$, $W = W^\top$, the *W-radius* of a given zonotope $Z = \langle c,\ R \rangle$ is defined as $\iota_w = \max_z \|z - c\|_{2,W}^2 = \max_b \|Rb\|_{2,W}^2$. □

Property B.1. *A* reduction operator*, denoted $\downarrow_q$, permits to reduce the number of generators of a zonotope $\langle c,\ R \rangle$ to a fixed number q while preserving the inclusion property*

$\langle c,\, R\rangle \subset \langle c,\, \downarrow_q \{R\}\rangle$. *A simple yet efficient solution to compute* $\downarrow_q \{R\}$ *is given in [Com03]. It consists in sorting the columns of* R *on decreasing Euclidean norm and enclosing the influence of the smaller columns only into an easily computable interval hull, so that the resulting matrix* $\downarrow_q \{R\}$ *has no more than* q *columns.* □

Property B.2. *Given a zonotope* $\mathcal{Z} = \langle c,\, R\rangle \subset \mathbb{R}^n$, *a zonotope inclusion (see [ABC05]), indicated by* $\diamond(\mathcal{Z})$, *is defined as* $\diamond(\mathcal{Z}) = \left\langle c, \begin{bmatrix} mid(R) & S \end{bmatrix} \right\rangle$, *where* S *is a diagonal matrix that satisfies* $S_{ii} = \sum_{j=1}^{m} \dfrac{diam(R_{ij})}{2}$, $i = 1, 2, \cdots, n$, *with* $mid(.)$ *and* $diam(.)$ *being the center and diameter of the interval matrix, respectively [Moo66].* □

Property B.3. *[Küh98, GP08]. Given* $\mathcal{X}_{k+1} = A\mathcal{X}_k \oplus Bu_k$, *where* A *and* B *are interval matrices and* u_k *is the input at time instant* k, *considering* $\mathcal{X}_k$ *as a zonotope with the center* $c_{x,k}$ *and the shape matrix* $R_{x,k}$ *such* $\mathcal{X}_k = \langle c_{x,k}, R_{x,k}\rangle$, *the zonotopic state at the next time instant* $k+1$, *defined as* $\mathcal{X}_{k+1}$, *is bounded by a zonotope* $\mathcal{X}^e_{k+1} = \langle c_{x,k+1}, R_{x,k+1}\rangle$, *with*

$$
\begin{aligned}
c_{x,k+1} &= mid(A)\; c_{x,k} + mid(B)\; u_k, \\
R_{x,k+1} &= \begin{bmatrix} \diamond(AR_{x,k}) & \dfrac{diam(A)}{2} c_{x,k} & \dfrac{diam(B)}{2} u_k \end{bmatrix},
\end{aligned}
$$

where $\diamond(AR_{x,k})$ *shows the shape matrix of the state bounding zonotope.* □

Property B.4. *[ABC05, LSA+13b]. Given the zonotope* $\mathcal{Z} = \langle c_z,\, R_z\rangle \in \mathbb{R}^n$, *the strip* $S = \left\{x \in \mathbb{R}^n : \left|C^\top x - d\right| \leq \sigma\right\}$ *and the vector* $\lambda \in \mathbb{R}^n$, *the intersection between the zonotope and the strip is defined as* $\mathcal{Z} \cap S = \langle c,\, R\rangle$, *where* $c = c_z + \lambda\,(d - Cc_z)$ *and* $R\,(\lambda) = \begin{bmatrix} (I - \lambda C)\, R_z & \sigma\lambda \end{bmatrix}$. □

Bibliography

[ABC05] T. Alamo, J. M. Bravo, and E. F. Camacho. Guaranteed state estimation by zonotopes. *Automatica*, 41(6):1035–1043, 2005.

[AR08] Z. Artstein and S. V. Raković. Feedback and invariance under uncertainty via set-iterates. *Automatica*, 44(2):520–525, 2008.

[BAC06] J. M. Bravo, T. Alamo, and E. F. Camacho. Bounded error identification of systems with time-varying parameters. *IEEE Transactions on Automatic Control*, 51(7):1144–1150, 2006.

[BEGFB94] S. Boyd, L. El Ghaoui, E. Feron, and V. Balakrishnan. *Linear matrix inequalities in system and control theory*, volume 15. Society for Industrial and Applied Mathematics, 1994.

[BG04] O. Bernard and J. L. Gouzé. Closed loop observers bundle for uncertain biotechnological models. *Journal of Process Control*, 14(7):765–774, 2004.

[BKL+06] M. Blanke, M. Kinnaert, J. Lunze, M. Staroswiecki, and J. Schröder. *Diagnosis and fault-tolerant control*, volume 2. Springer, 2006.

[Bla99] F. Blanchini. Set invariance in control. *Automatica*, 35(11):1747–1767, 1999.

[BM08] F. Blanchini and S. Miani. *Set-theoretic methods in control*. Springer, 2008.

[BN93] M. Basseville and I. V. Nikiforov. *Detection of abrupt changes: theory and application*, volume 104. Prentice Hall Englewood Cliffs, 1993.

[Bro12] A. Brondsted. *An introduction to convex polytopes*. Springer Science & Business Media, USA, 2012.

[BRPN14] J. Blesa, D. Rotondo, V. Puig, and F. Nejjari. FDI and FTC of wind turbines using the interval observer approach and virtual actuators/sensors. *Control Engineering Practice*, 24:138–155, 2014.

[CFS16] J. Cai, H. Ferdowsi, and J. Sarangapani. Model-based fault detection, estimation, and prediction for a class of linear distributed parameter systems. *Automatica*, 66:122–131, 2016.

[CGZ96] L. Chisci, A. Garulli, and G. Zappa. Recursive state bounding by parallelotopes. *Automatica*, 32(7):1049–1055, 1996.

[Com03] C. Combastel. A state bounding observer based on zonotopes. In *European Control Conference*, pages 2589–2594. IEEE, UK, 2003.

[Com05] C. Combastel. A state bounding observer for uncertain non-linear continuous-time systems based on zonotopes. In *44th IEEE Conference on Decision and Control and European Control Conference.*, pages 7228–7234. IEEE, Spain, 2005.

[Com13] C. Combastel. Stable interval observers in C for linear systems with time-varying input bounds. *IEEE Transactions on Automatic Control*, 58(2):481–487, 2013.

[Com15a] C. Combastel. Merging Kalman filtering and zonotopic state bounding for robust fault detection under noisy environment. *IFAC-PapersOnLine*, 48(21):289–295, 2015.

[Com15b] C. Combastel. Zonotopes and Kalman observers: Gain optimality under distinct uncertainty paradigms and robust convergence. *Automatica*, 55:265–273, 2015.

[Com16] C. Combastel. An Extended Zonotopic and Gaussian Kalman Filter (EZGKF) merging set-membership and stochastic paradigms: Toward non-linear filtering and fault detection. *Annual Reviews in Control*, 42:232–243, 2016.

[CP99] J. Chen and R. J. Patton. *Robust model-based fault diagnosis for dynamic systems*. Kluwer Academic Press, 1999.

[CP12] J. Chen and R. J. Patton. *Robust model-based fault diagnosis for dynamic systems*, volume 3. Springer Science & Business Media, 2012.

[CPZ96] J. Chen, R. J. Patton, and H. Y. Zhang. Design of unknown input observers and robust fault detection filters. *International Journal of control*, 63(1):85–105, 1996.

[CQ14] W. Chai and J. Qiao. Passive robust fault detection using RBF neural modeling based on set membership identification. *Engineering Applications of Artificial Intelligence*, 28:1–12, 2014.

[Din08] S. X. Ding. *Model-based fault diagnosis techniques: design schemes, algorithms, and tools*. Springer Science & Business Media, 2008.

[DJFD00] S. X. Ding, T. Jeinsch, P. M. Frank, and E. L. Ding. A unified approach to the optimization of fault detection systems. *International Journal of Adaptive Control and Signal Processing*, 14(7):725–745, 2000.

[DY13] G. R. Duan and H. H. Yu. *LMIs in control systems: analysis, design and applications*. CRC Press, 2013.

[ERCZ13] D. Efimov, T. Raïssi, S. Chebotarev, and A. Zolghadri. Interval state observer for nonlinear time varying systems. *Automatica*, 49(1):200–205, 2013.

[ERP13] D. Efimov, T. Raïssi, and A. Perruquetti, W.and Zolghadri. Estimation and control of discrete-time LPV systems using interval observers. In *IEEE 52nd Annual Conference on Decision and Control*, pages 5036–5041. IEEE, Italy, 2013.

[ERZ13] D. Efimov, T. Raïssi, and A. Zolghadri. Control of nonlinear and LPV systems: interval observer-based framework. *IEEE Transactions on Automatic Control*, 58(3):773–778, 2013.

[Fav94] C. Favre. Fly-by-wire for commercial aircraft: the airbus experience. *International Journal of Control*, 59(1):139–157, 1994.

[FD94] P. M. Frank and X. Ding. Frequency domain approach to optimally robust residual generation and evaluation for model-based fault diagnosis. *Automatica*, 30(5):789–804, 1994.

[FD97] P. M. Frank and X. Ding. Survey of robust residual generation and evaluation methods in observer-based fault detection systems. *Journal of process control*, 7(6):403–424, 1997.

[FPG04] I. Fagarasan, S. Ploix, and S. Gentil. Causal fault detection and isolation based on a set-membership approach. *Automatica*, 40(12):2099–2110, 2004.

[FTF12] G. Franze, F. Tedesco, and D. Famularo. Actuator fault tolerant control: a set-theoretic approach. In *IEEE 51st Annual Conference on Decision and Control*, pages 1822–1827. IEEE, US, 2012.

[Ger97] J. Gertler. Fault detection and isolation using parity relations. *Control Engineering Practice*, 5(5):653–661, 1997.

[Ger98] J. Gertler. *Fault detection and diagnosis in engineering systems.* CRC Press, US, 1998.

[Ger15] J. Gertler. *Fault Detection and Diagnosis.* Springer, 2015.

[GP08] P. Guerra and M. Puig, V.and Witczak. Robust fault detection with unknown-input interval observers using zonotopes. *IFAC Proceedings Volumes*, 41(2):5557–5562, 2008.

[Hen10] D. Henry. A norm-based point of view for fault diagnosis. application to aerospace missions. In *8th European Workshop on Advanced Control and Diagnosis*, pages 4–16, Italy, 2010.

[HP96] M. Hou and R. J. Patton. An LMI approach to H_-/H_∞ fault detection observers. In *International Conference on Control*, pages 9305–310, UK, 1996.

[IBPA05] A. Ingimundarson, J. M. Bravo, V. Puig, and T. Alamo. Robust fault diagnosis using parallelotope-based set-membership consistency tests. In *44th IEEE Conference on Decision and Control-European Control Conference*, pages 993–998, Spain, 2005.

[Ise05] R. Isermann. Model-based fault-detection and diagnosis-status and applications. *Annual Reviews in Control*, 29(1):71–85, 2005.

[Jau09] L. Jaulin. Robust set-membership state estimation; application to underwater robotics. *Automatica*, 45(1):202–206, 2009.

[JKDW01] L. Jaulin, M. Kieffer, O. Didrit, and E. Walter. *Applied interval analysis: with examples in parameter and state estimation, robust control and robotics*, volume 1. Springer Science & Business Media, 2001.

[JLP06] I. M. Jaimoukha, Z. Li, and V. Papakos. A matrix factorization solution to the H_-/H_∞ fault detection problem. *Automatica*, 42(11):1907–1912, 2006.

[Joh00] K. H. Johansson. The quadruple-tank process: a multivariable laboratory process with an adjustable zero. *IEEE Transactions on Control Systems Technology*, 8(3):456–465, 2000.

[Kal60] R. E. Kalman. A new approach to linear filtering and prediction problems. *Journal of Basic Engineering*, 82(1):35–45, 1960.

[KB61] R. E. Kalman and R. S. Bucy. New results in linear filtering and prediction theory. *Journal of Basic Engineering*, 83(1):95–108, 1961.

[KHS07] E. Kofman, H. Haimovich, and M. M. Seron. A systematic method to obtain ultimate bounds for perturbed systems. *International Journal of Control*, 80(2):167–178, 2007.

[Kof05] E. Kofman. Non-conservative ultimate bound estimation in LTI perturbed systems. *Automatica*, 41(10):1835–1838, 2005.

[KP05] L. Kolev and S. Petrakieva. Assessing the stability of linear time-invariant continuous interval dynamic systems. *IEEE Transactions on Automatic Control*, 50(3):393–397, 2005.

[KPP+17] A. R. Kodakkadan, M. Pourasghar, V. Puig, S. Olaru, C. Ocampo-Martinez, and V. Reppa. Observer-based sensor fault detectability: About robust positive invariance approach and residual sensitivity. In *20th World Congress IFAC*, pages 5041–5046, France, 2017.

[KPPOM17] F. Karimi Pour, V. Puig, and C. Ocampo-Martínez. Comparative assessment of LPV-based predictive control strategies for a pasteurization plant. In *4th International Conference on Control, Decision and Information Technologies*, pages 1–6, Spain, 2017.

[Küh98] W. Kühn. Rigorously computed orbits of dynamical systems without the wrapping effect. *Computing*, 61(1):47–67, 1998.

[LAC+11] V. T. H. Le, T. Alamo, E. F. Camacho, C. Stoica, and D. Dumur. A new approach for guaranteed state estimation by zonotopes. In *18th World Congress IFAC*, pages 9242–9247, Italy, 2011.

[LAC+12] V. T. H. Le, T. Alamo, E. F. Camacho, C. Stoica, and D. Dumur. Zonotopic set-membership estimation for interval dynamic systems. In *American Control Conference*, pages 6787–6792, Canada, 2012.

[LC06a] A. Lalami and C. Combastel. Generation of set membership tests for fault diagnosis and evaluation of their worst case sensitivity. *IFAC Proceedings Volumes*, 39(13):569–574, 2006.

[LC06b] A. Lalami and C. Combastel. Generation of set membership tests for fault diagnosis and evaluation of their worst case sensitivity. In *Fault Detection, Supervision and Safety of Technical Processes*, pages 569–574. Elsevier, China, 2006.

[LSA+13a] V. T. H. Le, C. Stoica, T. Alamo, E. F. Camacho, and D. Dumur. *Zonotopes: From guaranteed state-estimation to control*. John Wiley & Sons, 2013.

[LSA+13b] V. T. H. Le, C. Stoica, T. Alamo, E. F. Camacho, and D. Dumur. Zonotopic guaranteed state estimation for uncertain systems. *Automatica*, 49(11):3418–3424, 2013.

[LSA+13c] V. T. H. Le, C. Stoica, T. Alamo, E. F. Camacho, and D. Dumur. Zonotope-based set-membership estimation for multi-output uncertain systems. In *IEEE International Symposium on Intelligent Control*, pages 212–217. IEEE, India, 2013.

[LWY05] J. Liu, J. L. Wang, and G. H. Yang. An LMI approach to minimum sensitivity analysis with application to fault detection. *Automatica*, 41(11):1995–2004, 2005.

[LZ07] N. Liu and K. Zhou. Optimal solutions to multi-objective robust fault detection problems. In *46th IEEE Conference on Decision and Control*, pages 981–988, US, 2007.

[May82] P. S. Maybeck. *Stochastic models, estimation, and control*, volume 3. Academic Press, USA, 1982.

[MB11] F. Mazenc and O. Bernard. Interval observers for linear time-invariant systems with disturbances. *Automatica*, 47(1):140–147, 2011.

[MdOPB12] S. Montes de Oca, V. Puig, and J. Blesa. Robust fault detection based on adaptive threshold generation using interval LPV observers. *International Journal of Adaptive Control and Signal Processing*, 26(3):258–283, 2012.

[MKC09] R. E Moore, R. B. Kearfott, and M. J. Cloud. *Introduction to interval analysis*, volume 110. Society for Industrial and Applied Mathematics, 2009.

[MNPLW13] M. Milanese, J. Norton, H. Piet-Lahanier, and É. Walter. *Bounding approaches to system identification*. Springer Science & Business Media, US, 2013.

[Moo66] R. E. Moore. Interval Analysis Prentice-Hall Englewood Cliffs. *NJ Google Scholar*, 1966.

[Moo69] R. E. Moore. *Interval analysis*. 1969.

[MPES10] J. Meseguer, V. Puig, T. Escobet, and J. Saludes. Observer gain effect in linear interval observer-based fault detection. *Journal of Process Control*, 20(8):944–956, 2010.

[NPH12] B. Noack, F. Pfaff, and U. D. Hanebeck. Optimal Kalman gains for combined stochastic and set-membership state estimation. In *51st IEEE Conference on Decision and Control*, pages 4035–4040, 2012.

[ODDSS10] S. Olaru, J. A. De Doná, M. M. Seron, and F. Stoican. Positive invariant sets for fault tolerant multisensor control schemes. *International Journal of Control*, 83(12):2622–2640, 2010.

[Oga95] K. Ogata. *Discrete-time control systems*. Englewood Cliffs, N.J., Prentice-Hall, USA, 1995.

[OMDDS10] C. Ocampo-Martinez, J. A. De Doná, and M. M. Seron. Actuator fault-tolerant control based on set separation. *International Journal of Adaptive Control and Signal Processing*, 24(12):1070–1090, 2010.

[PA06] S. Ploix and O. Adrot. Parity relations for linear uncertain dynamic systems. *Automatica*, 42(9):1553–1562, 2006.

[PAR99] S. Ploix, O. Adrot, and J. Ragot. Parameter uncertainty computation in static linear models. In *38th IEEE Conference on Decision and Control*, volume 2, pages 1916–1921. IEEE, US, 1999.

[Pat94] R. J. Patton. Robust model-based fault diagnosis: the state of the art. *IFAC Proceedings Volumes*, 27(5):1–24, 1994.

[PC91] R. J. Patton and J. Chen. A review of parity space approaches to fault diagnosis. In *Fault Detection, Supervision and Safety of Technical Processes*, pages 65–81, Germany, 1991.

[PC97] R. J. Patton and J. Chen. Observer-based fault detection and isolation: Robustness and applications. *Control Engineering Practice*, 5(5):671–682, 1997.

[PCQ01] V. Puig, P. Cugueró, and J. Quevedo. Worst-case state estimation and simulation of uncertain discrete-time systems using zonotopes. *European Control Conference*, pages 1691–1697, 2001.

[PMdOB13] V. Puig, S. Montes de Oca, and J. Blesa. Adaptive threshold generation in robust fault detection using interval models: time-domain and frequency-domain approaches. *International Journal of Adaptive Control and Signal Processing*, 27(10):873–901, 2013.

[PNDW04] B. T. Polyak, S. A. Nazin, C. Durieu, and E. Walter. Ellipsoidal parameter or state estimation under model uncertainty. *Automatica*, 40(7):1171–1179, 2004.

[PPOM16a] M. Pourasghar, V. Puig, and C. Ocampo-Martinez. Comparison of set-membership and interval observer approaches for state estimation of uncertain systems. In *European Control Conference*, pages 1111–1116, Denmark, 2016.

[PPOM16b] M. Pourasghar, V. Puig, and C. Ocampo-Martinez. Characterization of the minimum detectable fault of interval observers by using set-invariance theory. In *3rd Conference on Control and Fault-Tolerant Systems*, pages 79–86, Spain, 2016.

[PPOMZ17] M. Pourasghar, V. Puig, C. Ocampo-Martinez, and Q. Zhang. Reduced-order interval-observer design for dynamic systems with time-invariant uncertainty. *IFAC-PapersOnLine*, 50(1):6271–6276, 2017.

[PQEdlH02] V. Puig, J. Quevedo, T. Escobet, and S. de las Heras. Passive robust fault detection approaches using interval models. *IFAC Proceedings Volumes*, 35(1):443–448, 2002.

[PQES03] V. Puig, J. Quevedo, T. Escobet, and A. Stancu. Robust fault detection using linear interval observers. *IFAC Proceedings Volumes*, 36(5):579–584, 2003.

[PSE+06] V. Puig, A. Stancu, T. Escobet, F. Nejjari, J. Quevedo, and R. J. Patton. Passive robust fault detection using interval observers: Application to the damadics benchmark problem. *Control engineering practice*, 14(6):621–633, 2006.

[PSQ03] V. Puig, J. Saludes, and J. Quevedo. Worst-case simulation of discrete linear time-invariant interval dynamic systems. *Reliable Computing*, 9(4):251–290, 2003.

[PSQ05a] V. Puig, A. Stancu, and J. Quevedo. Simulation of uncertain dynamic systems described by interval models: A survey. In *16th IFAC World Congress*, volume 16, pages 207–218, Czech Republic, 2005.

[PSQ05b] V. Puig, A. Stancu, and J. Quevedo. Observers for interval systems using set and trajectory-based approaches. In *44th IEEE Conference on Decision and Control and European Control Conference*, pages 6567–6572, Spain, 2005.

[Pui10] V. Puig. Fault diagnosis and fault tolerant control using set-membership approaches: Application to real case studies. *International Journal of Applied Mathematics and Computer Science*, 20(4):619–635, 2010.

[PY17] Y. Pan and G. H. Yang. Event-triggered fault detection filter design for nonlinear networked systems. *IEEE Transactions on Systems, Man, and Cybernetics: Systems*, 2017.

[RC13] S. A. Raka and C. Combastel. Fault detection based on robust adaptive thresholds: A dynamic interval approach. *Annual Reviews in Control*, 37(1):119–128, 2013.

[REZ12] T. Raïssi, D. Efimov, and A. Zolghadri. Interval state estimation for a class of nonlinear systems. *IEEE Transactions on Automatic Control*, 57(1):260–265, 2012.

[RKKM05] S. V Rakovic, E. C. Kerrigan, K. I. Kouramas, and D. Q. Mayne. Invariant approximations of the minimal robust positively invariant set. *IEEE Transactions on Automatic Control*, 50(3):406–410, 2005.

[Sch68] F. Schweppe. Recursive state estimation: Unknown but bounded errors and system inputs. *IEEE Transactions on Automatic Control*, 13(1):22–28, 1968.

[SCP96] M. A. Sadrnia, J. Chen, and R. J. Patton. Robust fault diagnosis observer design using H_∞ optimisation and μ synthesis. *IEE Colloquium on Modelling and Signal Processing for Fault Diagnosis*, pages 1–9, 1996.

[SDD10] M. M. Seron and J. A. De Doná. Actuator fault tolerant multi-controller scheme using set separation based diagnosis. *International Journal of Control*, 83(11):2328–2339, 2010.

[SDW13] B. Shen, S. X. Ding, and Z. Wang. Finite-horizon H_∞ fault estimation for linear discrete time-varying systems with delayed measurements. *Automatica*, 49(1):293–296, 2013.

[SHO13] F. Stoican, M. Hovd, and S. Olaru. Explicit invariant approximation of the mRPI set for LTI dynamics with zonotopic disturbances. In *52nd Annual Conference on Decision and Control*, pages 3237–3242, Italy, 2013.

[SODDS11] F. Stoican, S. Olaru, J. A. De Doná, and M. M. Seron. Zonotopic ultimate bounds for linear systems with bounded disturbances. *IFAC Proceedings Volumes*, 44(1):9224–9229, 2011.

[SRHS17] D. Silvestre, P. Rosa, J. P Hespanha, and C. Silvestre. Fault detection for LPV systems using set-valued observers: A coprime factorization approach. *Systems & Control Letters*, 106:32–39, 2017.

[Sto11] F. Stoican. *Fault tolerant control based on set-theoretic methods.* PhD thesis, Supélec, 2011.

[SZDDM08] M. M. Seron, X. W. Zhuo, J. A. De Doná, and J. J. Martinez. Multisensor switching control strategy with fault tolerance guarantees. *Automatica*, 44(1):88–97, 2008.

[Tab15] S. M. Tabatabaeipour. Active fault detection and isolation of discrete-time linear time-varying systems: a set-membership approach. *International Journal of Systems Science*, 46(11):1917–1933, 2015.

[TB14] S. M. Tabatabaeipour and T. Bak. Robust observer-based fault estimation and accommodation of discrete-time piecewise linear systems. *Journal of the Franklin Institute*, 351(1):277–295, 2014.

[TCRZ15] R. E. H. Thabet, C. Combastel, T. Raïssi, and A. Zolghadri. Set-membership fault detection under noisy environment with application to the detection of abnormal aircraft control surface positions. *International Journal of Control*, 88(9):1878–1894, 2015.

[Tib93] B. Tibken. A new simulation tool for uncertain discrete time systems. In *European Control Conference*, Netherlands, 1993.

[TSOMPE12] S. Tornil-Sin, C. Ocampo-Martinez, V. Puig, and T. Escobet. Robust fault detection of non-linear systems using set-membership state estimation based on constraint satisfaction. *Engineering Applications of Artificial Intelligence*, 25(1):1–10, 2012.

[TTQ13] C. Tan, G. Tao, and R. Qi. A discrete-time parameter estimation based adaptive actuator failure compensation control scheme. *International Journal of Control*, 86(2):276–289, 2013.

[ULHM15] L. Uusitalo, A. Lehikoinen, I. Helle, and K. Myrberg. An overview of methods to evaluate uncertainty of deterministic models in decision support. *Environmental Modelling & Software*, 63:24–31, 2015.

[VZ96] A. Vicino and G. Zappa. Sequential approximation of feasible parameter sets for identification with set membership uncertainty. *IEEE Transactions on Automatic Control*, 41(6):774–785, 1996.

[WLSL15] G. Wei, S. Liu, Y. Song, and Y. Liu. Probability-guaranteed set-membership filtering for systems with incomplete measurements. *Automatica*, 60:12–16, 2015.

[WYL07] J. L. Wang, G. H. Yang, and J. Liu. An LMI approach to H_- index and mixed H_-/H_∞ fault detection observer design. *Automatica*, 43(9):1656–1665, 2007.

[XPOM+15] F. Xu, V. Puig, C. Ocampo-Martinez, S. Olaru, and F. Stoican. Set-theoretic methods in robust detection and isolation of sensor faults. *International Journal of Systems Science*, 46(13):2317–2334, 2015.

[XSP+13] F. Xu, F. Stoican, V. Puig, C. Ocampo-Martinez, and S. Olaru. On the relationship between interval observers and invariant sets in fault detection. In *Conference on Control and Fault-Tolerant Systems*, pages 49–54, France, 2013.

[XTW+17] F. Xu, J. Tan, X. Wang, B. Puig, V.and Liang, B. Yuan, and H. Liu. Generalized set-theoretic unknown input observer for LPV systems with application to state estimation and robust fault detection. *International Journal of Robust and Nonlinear Control*, 27(17):3812–3832, 2017.

[YL12] F. Yang and Y. Li. Robust set-membership filtering for systems with missing measurement: a linear matrix inequality approach. *Signal Processing*, 6(4):341–347, 2012.

[ZDLW03] M. Zhong, S. X. Ding, J. Lam, and H. Wang. An LMI approach to design robust fault detection filter for uncertain LTI systems. *Automatica*, 39(3):543–550, 2003.

[Zie94] G. M. Ziegler. *Lectures on polytopes (graduate texts in mathematics)*. Springer, 1994.

[ZJ08] Y. Zhang and J. Jiang. Bibliographical review on reconfigurable fault-tolerant control systems. *Annual Reviews in Control*, 32(2):229–252, 2008.

[ZLX14] B. Zhang, J. Lam, and S. Xu. Reachable set estimation and controller design for distributed delay systems with bounded disturbances. *Journal of the Franklin Institute*, 351(6):3068–3088, 2014.